



UNCERTAINTY AND SENSITIVITY ANALYSIS OF
DISCRETE MODEL INPUTS IN ECO-HYDROLOGICAL
MODELING

Dissertation to obtain the academic degree

DOCTOR NATURALIUM TECHNICARUM
(Dr.nat.techn.)

at the University of Natural Resources and Life Sciences, Vienna

Submitted by

DIPL.-ING. CHRISTOPH SCHÜRZ

Supervised by

UNIV.PROF. DIPL.GEOÖKOL. DR.RER.NAT. KARSTEN SCHULZ

Co-supervisors

BANO MEHDI, MSc. PH.D.

DIPL.-ING. DR.NAT.TECHN. MATHEW HERRNEGGER

Vienna, April 2020

ACKNOWLEDGEMENTS

Reaching this point where the long and winding path of my PhD finally comes to an end is not an accomplishment that I achieved on my own. Gratitude and appreciation belong to the many people who supported, guided, and accompanied me on this journey.

First, I want to thank Prof. Karsten Schulz for supervising my thesis. Prof. Schulz sowed the initial idea that over time grew and developed to what now forms the foundation of this thesis. I appreciate that he placed great trust in my work and gave me the freedom to explore my own ideas. Trial and failure are essential experiences to make in research. I am grateful for his professional and personal guidance.

I want to thank my co-supervisors Bano Mehdi and Mathew Herrnegger. The constant exchange of ideas with Bano and Mathew guided me and greatly supported me to improve the quality of my research and my writing. Thank you for your great inputs, your time and your patience.

There is no research without financial support. Therefore, I am grateful that I was provided with continuous financial support through the two projects "*UnLoadC³: Uncertainty assessment of water flow and nutrient loads under future climate change conditions*" (KR13AC6K11021) funded by the Austrian Climate Research Program (ACRP) and "*Capacity building on the water-energy-foodsecurity Nexus through research and training in Kenya and Uganda (CapNex)*" (Proj.-Nr. 158) funded by the Austrian Partnership Program in Higher Education and Research for Development (Appear).

I want to thank all of my colleagues at HyWa. Together we created a working environment that was enjoyable and unique. The worlds slowest coffee brewing and our common cooking brought so much joy into every single working day. Particularly, I want to thank Benni, Carolina, Claire, Claude, Cong, Daniel, Elizabeth, Franzi, Freddy, Gabriel, Hanna, Hope, Ignacio, Johannes, Kathi, Mathew, Moritz, Morteza, Paul, and Simon for the numerous hours we spent in the institute kitchen having our "nerd talk".

Even if I might for ever fail to explain what I am actually doing here, I want to thank my family for their unconditional love and support. I am very grateful to my parents for their patience and their emotional and financial support throughout my many years of studying. Wholeheartedly, I want to thank my mother who always believed in what I have been doing and trusted me in making my own choices.

Finally, Marlene, I am forever grateful for your unconditional love and support. Thank you for your patience and good nature, particularly in times when I am insufferable. Thank you for all the wonderful time and experiences we shared and will share together. Thank you for being there.

ABSTRACT

Eco-hydrological modeling is essential in studying the complex interactions of ecosystems and their responses to anthropogenic impacts. Environmental modeling studies typically analyze environmental systems under changing conditions, such as climate change, or land use change. The characterization of environmental systems under change requires to draw assumptions on the development of one or several components of the environmental system that is analyzed. The model description of the environmental system and the implementation of change processes in the eco-hydrological model typically strongly simplify the actual system processes. The drawn assumptions in the characterization of the model inputs and the simplifications of the modeled system can be summarized as potential sources of uncertainties in a simulation.

In environmental modeling, plausible representations of a system (component) under future change are often expressed by a set of discrete realizations of that system (component), that account for uncertainties in the development of an input realizations and the assumptions that were drawn for the characterized system change. In the eco-hydrological model setup usually multiple model setups and parametrizations can be identified that depict the simulated environmental system equally well, eventually resulting in discrete sets of acceptable model parametrizations and model setups. Eventually, the entire chain of input and model uncertainties must be account for to appropriately depict the simulation uncertainties of an environmental variable.

The goal of this thesis was to develop a comprehensive uncertainty (UA) and sensitivity analysis (SA) framework for eco-hydrological modeling that facilitates an analysis of the entire chain of uncertainties in eco-hydrological modeling. The framework development particularly focused on the analysis of discrete and composite model inputs, such as model input scenarios or different model representations and parametrizations.

The application of the outlined UA and SA framework is presented in two case studies, where in the first case study a comprehensive UA and SA for simulations of long-term annual soil loss simulated with the empirical USLE model was performed. The second study investigates discharge and nitrate-nitrogen loads under future changing conditions simulated with the process based eco-hydrological model SWAT.

In both studies a wide range of potential sources of uncertainties was considered in the analysis. Propagating through the established chains of uncertainties, both studies resulted in large simulation uncertainties for the respective simulated eco-hydrological variables. The two case studies further highlighted the great potential of SA to investigate the dominant sources of simulation uncertainties.

Standard environmental modeling frameworks include a single model setup to simulate environmental variables (under change). Yet, the presented results

clearly highlight that the selected representation of the simulated system and the selected model parametrizations are highly relevant for the simulation of the respective environmental variable. Thus, both presented studies stress the importance of a comprehensive consideration of the uncertainties in environmental modeling studies.

Finally, this thesis discusses the limitations of a comprehensive UA and SA analysis approach. Limitations might be present because of the subjectivity that is inherent in the uncertainty definition, but also through limited computational resources to perform a large number of simulations or to process large data. Eventually, a clear communication of the predictive power and the limitations of study results is essential.

ZUSAMMENFASSUNG

Die öko-hydrologische Modellierung ist ein wichtiges Werkzeug zur Analyse von komplexen Interaktionen zwischen Ökosystemprozessen und deren Reaktion auf anthropogene Einflüsse. Häufig, analysieren öko-hydrologische Modellstudien die Entwicklung von Systemen die sich in Wandlungsprozessen befinden und etwa durch den Klimawandel, oder durch Landnutzungsänderungen beeinflusst sind. Um Wandlungsprozesse abbilden zu können müssen Annahmen über Prozesse die diese Entwicklung beeinflussen getroffen werden. Die modellhafte Beschreibung eines sich ändernden Umweltsystems und die adequate Berücksichtigung von Änderungsprozessen in öko-hydrologischen Modellen geht mit Vereinfachungen in der Betrachtung des modellierten Systems einher. Die getroffenen Annahmen über die analysierten Änderungen sowie die modellhaften Vereinfachungen stellen potentielle Unsicherheitsquellen in der Modellierung dar.

In der Umweltsystemmodellierung werden Änderungsprozesse typischerweise mittels einer diskreten Anzahl an Szenarien dargestellt, welche mögliche Entwicklungen einer Systemkomponente plausibel abbilden. Ein Set an Szenarien beinhaltet daher alle Annahmen die für die Entwicklung dieser Systemkomponente getroffen wurden sowie die Unsicherheiten die bei der Entwicklung eines Szenarios entstehen. Bei der Entwicklung eines öko-hydrologischen Modells welches das betrachtete System beschreiben soll können in der Regel ein Vielzahl an (räumlichen, zeitlichen und mathematischen) Modellkonfigurationen, sowie Modellparametrisierungen gefunden werden, die das betrachtete System mit ähnlicher Güte beschreiben können. Um schlussendlich die Unsicherheiten in Modellierung einer Umweltsystemvariable ausreichend beschreiben zu können muss die gesamte Kette an Unsicherheiten welche durch Unsicherheiten in den Eingangsgrößen sowie in der modellhaften Beschreibung entstehen berücksichtigt und analysiert werden.

Ziel dieser Arbeit war es einen umfassenden Rahmen für die Analyse der gesamten Kette an Unsicherheiten in der öko-hydrologischen Modellierung sowie der Analyse der Eingangsgrößen hinsichtlich ihres Beitrags an den Unsicherheiten zu schaffen. Da Unsicherheiten in den Modelleingangsgrößen, sowie in der Modellbeschreibung und -parametrisierung typischerweise durch diskrete Sets an Realisierungen der betrachteten Größe beschrieben werden, lag der Fokus bei der Entwicklung des Rahmenwerks auf der Analyse von diskreten Eingangsgrößen. Das Konzept zur Unsicherheits- und Sensitivitätsanalyse wurde im Rahmen von zwei Fallstudien angewandt. Hierbei wurden zwei unterschiedlich komplexe Modelle zur Modellierung öko-hydrologischer Variablen eingesetzt, wobei die USLE einen Vertreter der Gruppe empirischer Modelle darstellt und das verwendete SWAT Modell ein komplexeres prozessbasiertes Modell ist.

Das Ziel beider Studien war es eine große Bandbreite potentieller Unsicherheitsquellen zu beschreiben, diese in eine umfassende Unsicherheits- und Sensitivitätsanalyse einzubinden und den Einfluss der analysierten unsicheren Modelleingangsgrößen auf die Simulation verschiedener öko-hydrologischer Variablen zu analysieren. Beide Studien zeigten ein deutliches Potential für Sensitivitätsanalysen als Werkzeug um die dominanten Unsicherheitsquellen in der Modellierung zu identifizieren.

In der Regel werden in der öko-hydrologischen Modellstudien keine Modelensembles, sondern einzelne Modellsetups zur Simulation eingesetzt. Die beiden präsentierten Studien zeigen jedoch klar, dass die Wahl der Modellkonfiguration, bzw. die Parametrisierung eines Modells einen starken Einfluss auf die Ergebnisse einer Modellierungsstudie haben können. Dies verdeutlicht die Wichtigkeit einer umfassenden Unsicherheitsanalyse um die Aussagekraft von Umweltsystemstudien zu untermauern.

Die präsentierte Arbeit behandelt darüber hinaus die Einschränkungen einer umfassenden Unsicherheits- und Sensitivitätsanalyse in der öko-hydrologischen Modellierung. Die Beschreibung der betrachteten Unsicherheiten ist immer auch durch eine subjektive Betrachtung durch den Modellierer beeinflusst. Rechenkapazitäten und zeitliche Ressourcen können den Umfang einer umfassenden Studie stark einschränken. Daher müssen die gesteckten Rahmenbedingungen, d.h. welche Unsicherheiten in einer Studie beschrieben werden, bzw. welche Vereinfachungen in einer Studie getroffen werden mussten immer klar kommuniziert werden.

CONTENTS

1	INTRODUCTION	1
1.1	Research goal	4
1.2	Outline	6
1.3	Scientific contributions	7
I	GENERAL FRAMEWORK	9
2	ECO-HYDROLOGICAL MODELING	11
2.1	A brief systematic view on eco-hydrological modeling	11
2.2	The Universal Soil Loss Equation (USLE)	14
2.3	The Soil and Water Assessment Tool (SWAT)	16
3	UNCERTAINTY AND SENSITIVITY ANALYSIS	19
3.1	Uncertainty Analysis (UA)	19
3.2	Sensitivity Analysis (SA)	21
3.2.1	A systematic review of SA methods	22
3.3	Framework for UA and SA with discrete, composite inputs	27
3.3.1	Analytical uncertainty propagation	29
3.3.2	The PAWN sensitivity index	30
3.3.3	Workflow for UA and SA with discrete composite inputs	33
II	CASE STUDIES	37
4	SOIL LOSS ESTIMATION WITH DIFFERENT USLE REALIZATIONS	39
4.1	Introduction and objectives	39
4.2	Study region	42
4.3	Estimation of USLE model inputs	43
4.3.1	Rainfall erosivity factor R	45
4.3.2	Soil erodibility factor K	45
4.3.3	Slope length and slope steepness factor LS	49
4.3.4	Cover management factor C	51
4.4	Soil loss estimation and analysis	53
4.4.1	Estimation of soil loss	53
4.4.2	Analysis of spatially distributed soil loss estimates	54
4.4.3	Analysis of the USLE input factors	56
4.4.4	Analysis of soil loss on administrative level	56
4.4.5	Comparison of soil loss estimates to in field assessments	56
4.5	Results	57
4.5.1	Soil loss from USLE ensemble simulations	57
4.5.2	Influence of USLE inputs on soil loss estimates	61
4.5.3	Soil loss at the administrative level	65
4.5.4	Comparison of soil loss estimates to in field assessments	66
4.6	Discussion	68
4.6.1	What can we learn from such an analysis	68
4.6.2	Are in-field data a valid reference for USLE model evaluation	69

4.6.3	Further considerations and limitations	70
4.7	Conclusion	71
5	DISCHARGE AND NITRATE-NITROGEN LOADS UNDER CHANGE	73
5.1	Introduction and objectives	73
5.2	Study sites	76
5.3	The baseline SWAT model setup	78
5.3.1	Model input data and preparation	78
5.3.2	Model setup, parameter selection and identification of non-unique parameter sets	81
5.4	Scenario definition - Preparation of discrete inputs	89
5.5	Simulations under future change and analysis	92
5.5.1	Global sensitivity analysis	92
5.5.2	Visual analysis of the simulation uncertainties	95
5.6	Results	95
5.6.1	Identification of the most influential model inputs	95
5.6.2	Simulation uncertainties of discharge and NO ₃ ⁻ -N loads	98
5.7	Discussion	102
5.7.1	What can we as modelers learn from such analysis	102
5.7.2	How to attribute subjectivity inherent in the scenarios	108
5.7.3	Sensitivity analysis or hydrologic storylines	108
5.8	Conclusion	109
III	SYNTHESIS	111
6	SYNTHESIS AND CONCLUSIONS	113
6.1	Scientific context	113
6.2	Generalized UA and SA framework	114
6.3	Comprehensive UA, overlooked necessity?	116
6.4	Comprehensive UA, an uncertain affair?	117
6.5	Significance of impact studies, a chimera?	119
7	OUTLOOK AND POTENTIAL RESEARCH	123
A	APPENDIX	125
A.1	Used software	125
A.2	Supplementary materials for the USLE input generation	125
A.3	USLE results for administrative units	133
A.4	Efficiency criteria and signature measures	137
	BIBLIOGRAPHY	141

LIST OF FIGURES

Figure 2.1	Systematic classification of established eco-hydrological models.	12
Figure 3.1	Systematic classification of standard methods for sensitivity analysis adopted from Pianosi et al. (2016) and Yuan et al. (2015).	24
Figure 3.2	Example for the analysis of a two dimensional input response surface using PAWN.	31
Figure 3.3	Example for sampling and subsetting of discrete model inputs for the implementation of PAWN for GSA.	33
Figure 3.4	General workflow for the implementation of discrete composite model inputs in UA and SA.	35
Figure 4.1	Study area covering the countries of Kenya and Uganda.	42
Figure 4.2	Methodological framework to generate the realizations of the USLE model input factors R , K , LS , and C	46
Figure 4.3	Descriptive statistics calculated for each grid cell based on the 756 USLE model realizations.	58
Figure 4.4	Frequency of USLE model ensemble members to predict one of the four soil loss classes <i>tolerable</i> , <i>moderate</i> , <i>high</i> , and <i>severe</i>	59
Figure 4.5	Dominant soil loss levels in the study region of Kenya and Uganda and specifically erosion prone regions.	60
Figure 4.6	Most influential USLE model input factors for the calculation of the soil loss A	62
Figure 4.7	Variability between the realizations of the most important USLE model input factors.	64
Figure 4.8	Mean soil loss in selected erosion prone administrative units of Uganda and Kenya.	66
Figure 4.9	Comparison of soil loss simulations from the USLE model ensemble to in field soil loss assessments.	67
Figure 5.1	The study sites Schwechat and Raab	76
Figure 5.2	Identification of the influential SWAT model parameters for the Schwechat and the Raab.	86
Figure 5.3	Simulated discharge and NO_3^- -N loads using the behavioral parameter sets for the Schwechat and the Raab.	87
Figure 5.4	Parallel coordinate plot of the 43 and 52 behavioral model parameter combinations that were used in the SWAT model setups.	88
Figure 5.5	Influence of discrete SWAT inputs on simulated signature measures of discharge and NO_3^- -N loads in the Schwechat and the Raab.	97

Figure 5.6	Simulated uncertainties resulting from the 7000 model input combinations for the Schwechat and the Raab . . .	99
Figure 5.7	The influence of land use change and the development of point source emissions on the simulation uncertainties of discharge and NO_3^- -N loads	100
Figure 5.8	The influence of deviations in precipitation on the uncertainties on the simulation uncertainties of discharge and NO_3^- -N loads	101
Figure 5.9	The influence of deviations in precipitation on the uncertainties on the simulation uncertainties of discharge and NO_3^- -N loads	103
Figure 5.10	The influence of the model setup on the uncertainties on the simulation uncertainties of discharge and NO_3^- -N loads	104
Figure 5.11	The influence of model parametrization on the uncertainties on the simulation uncertainties of discharge and NO_3^- -N loads	105
Figure A.1	Schematic example of a Flow Duration Curve (FDC).	140

LIST OF TABLES

Table 4.1	Terrain properties for administrative units that were analyzed in more detail.	44
Table 4.2	Methods to calculate the rainfall erosivity factor R	47
Table 4.3	Realizations for the soil erodibility factor K	48
Table 4.4	Methods to calculate the soil erodibility factor K	49
Table 4.5	Realizations for the slope length and slope steepness factor LS	50
Table 4.6	C factor literature values from Panagos et al. (2015c) and Angima et al. (2003) for crop groups.	53
Table 4.7	C factor value ranges for non agricultural land uses from Panagos et al. (2015c).	54
Table 4.8	C factor value values and weights for agricultural and non agricultural land uses for the use with the ESA CCI LC Map v2.0.7.	55
Table 5.1	Area and percentage of the land uses in the Schwechat catchment.	77
Table 5.2	Area and percentage of the land uses in the Raab catchment.	79
Table 5.3	SWAT model input data, data sources, and data processing steps	81
Table 5.4	SWAT model setups for the Schwechat and the Raab catchments	82
Table 5.5	Influential and non-influential SWAT model parameters	84
Table 5.6	Ranges of parameter changes for the behavioral SWAT model parameter sets.	89
Table 5.7	Transformations of land uses implemented in the land use scenarios for the Schwechat and the Raab.	90
Table 5.8	Municipal point source emissions and emission changes at Schwechat and Raab	90
Table 5.9	Industrial point source emissions and implemented emission changes of the dominant leather producer at the Raab	91
Table 5.10	Implemented GCM–RCM combinations in the Schwechat and the Raab catchment	93
Table 5.11	SWAT model inputs and their numbers of realizations that were implemented in the analyses for the Schwechat and the Raab.	94
Table A.1	Lookup table to derive the soil permeability p from the USDA soil texture classification.	126
Table A.2	Lookup table to derive the soil structure s from the soil taxonomy classification according to the WRB	126

Table A.3	Grouping of crops available from Monfreda et al. (2008) based on Borrelli et al. (2017).	129
Table A.4	Quantiles of mean soil loss estimates for all Kenyan counties based on the 756 USLE model setups in tons ha ⁻¹ yr ⁻¹ .133	
Table A.5	Quantiles of mean soil loss estimates for all Ugandan districts based on the 756 USLE model setups in tons ha ⁻¹ yr ⁻¹ .135	

ACRONYMS

A	Long-term average annual soil loss calculated with the USLE model in $\text{tons ha}^{-1} \text{yr}^{-1}$
AAT	All-at-a-time Sensitivity Analysis
AGNPS	Agricultural Non-point Source model
AnnAGNPS	Annualized Agricultural Non-point Source model
ANSWERS	Areal Non-point Source Watershed Environment Response Simulation
APEX	Agricultural Policy/Environmental eXtender
ArcSWAT	ArcGIS interface for SWAT to set up and execute SWAT projects
C	USLE cover management factor (unitless)
CART	Correlation and Regression Trees
CDF	Cumulative Distribution Function
CEC	Cation Exchange Capacity of soil in cmol kg^{-1}
Cl	Clay content mass fraction in 100 % ·g clay per g soil
CI	Confidence interval
CREAMS	Chemicals, Runoff, and Erosion from Agricultural Management Systems
CRF	Volumetric fraction of coarse fragments in the soil in %
DEM	Digital Elevation Model
d_r	Refined index of agreement (Willmott et al., 2012)
DREAM	Differential Evolution Adaptive Metropolis (Vrugt et al., 2008)
EET	Elementary Effects Test
EPIC	Erosion-Productivity Impact Calculator
FDC	Flow Duration Curve
GCM	Global Climate Models
GIS	Geographic Information System
GLEAMS	Groundwater Loading Effects on Agricultural Management Systems

GLUE	Generalized Likelihood Uncertainty Estimation
GSA	Global Sensitivity Analysis
GSDE	Global Soil Dataset for use in Earth System Models
GWLF	Generalized Watershed Loading Functions
HRU	Hydrologic Response Unit
INCA	Integrated Nowcasting through Comprehensive Analysis
IVARS	Integral of the VARS sensitivity measure over percentages of distances in a parameter direction in the parameter space (see Razavi and Gupta (2016a))
K	USLE soil erodibility factor in $\text{tons h MJ}^{-1} \text{mm}^{-1}$
KGE	Kling Gupta Efficiency criterion (Gupta et al., 2009)
L	USLE slope length factor (unitless)
LAI	Leaf Area Index
LHS	Latin Hypercube Sampling
LS	USLE slope length and steepness factor (unitless)
LSA	Local Sensitivity Analysis
MAROV	Maximum Absolute Ratio Of Variation (Dubus and Brown, 2002)
MC	Monte Carlo
MCF	Monte Carlo Filtering
MCMC	Monte Carlo Markov Chain
MIKE SHE	MIKE coupling with the Systeme Hydrologique Europeen
MODIS	Moderate Resolution Imaging Spectroradiometer
MONERIS	MOdelling Nutrient Emissions in RIVER Systems
MUSLE	Modified Universal Soil Loss Equation
NDVI	Normalized Difference Vegetation Index
NO_3^- -N	Nitrate-nitrogen
NSE	Nash Sutcliffe Efficiency criterion (Nash and Sutcliffe, 1970)
OAT	One-at-a-time SA
OM	Soil organic matter content in 100 % ·g OM per g soil
orgC	Soil organic carbon content in g orgC per kg soil

<i>P</i>	USLE support practice factor (unitless)
<i>p</i>	unitless soil permeability coefficient (Wischmeier and Smith, 1978)
PAWN	Global Sensitivity Analysis after Pianosi and Wagener (2015)
<i>pbias</i>	Percentage bias criterion (Gupta et al., 1999)
PDF	Probability Density Function
PE	Population Equivalent
<i>pH</i>	Soil pH $\times 10^1$ in Water
QSWAT	QGIS interface for SWAT to set up and execute SWAT projects
<i>R</i>	USLE rainfall erosivity factor in $\text{MJ mm ha}^{-1} \text{h}^{-1} \text{yr}^{-1}$
ρ_d	Bulk density (fine earth) in kg cm^{-3}
RCM	Regional Climate Model
RCP	Representative Concentration Pathway
RCP4.5	RCP that describes a positive change in radiative forcing of 4.5 W m^{-2} in the 21 st century
RCP8.5	RCP that describes a positive change in radiative forcing of 8.5 W m^{-2} in the 21 st century
RSA	Regional Sensitivity Analysis
RSR	Ratio of the root mean square error and standard deviation (Moriasi et al., 2007)
RUSLE	Revised Universal Soil Loss Equation
<i>S</i>	USLE slope steepness factor (unitless)
<i>s</i>	unitless soil structure coefficient (Wischmeier and Smith, 1978)
SA	Sensitivity Analysis
<i>Sa</i>	Sand content mass fraction in 100% ·g sand per g soil
SDR	Sediment Delivery Ratio
<i>Si</i>	Silt content mass fraction in 100% ·g silt per g soil
SoilGrids250m	Globally consistent, data-driven system that predicts soil properties on a 250m grid soilgrids.org
SPARROW	SPATIally Referenced Regression On Watershed attributes

STAR	Transectorial parameter sampling design for GSA after Razavi and Gupta (2016b)
SWAT	Soil and Water Assessment Tool
SWAT ₂₀₁₂	Soil and Water Assessment Tool Version 2012
SWM/HSPF	Stanford Water Model/Hydrological Simulation Program-Fortran
SWRRB	Simulator for Water Resources in Rural Basins
TMPA	TRMM Multi-satellite Precipitation Analysis
TRMM	Tropical Rainfall Measuring Mission
UA	Uncertainty Analysis
USDA-ARS	US Department of Agriculture Agricultural Research Service
USA	United States of America
USLE	Universal Soil Loss Equation
VARs	Variogram approach for Global Sensitivity Analysis after Razavi and Gupta (2016a)
VBSA	Variance-based SA
VCF	MODIS vegetation continuous fields
WEPP	Water Erosion Prediction Project
WRB	World Reference Base for Soil Resources
WWTP	Waste Water Treatment Plant
ZAMG	Zentralanstalt für Meteorologie und Geodynamik (<i>Central Institute for Meteorology and Geodynamics of Austria</i>)

INTRODUCTION

"All models are wrong but some are useful" (Box, 1979). This aphorism is very likely an overused one in the scientific modeling community. Yet, George Box addressed a central issue in scientific modeling that is still relevant today as it was 40 years ago. A model is always a simplification of the "real" system that the model describes (e.g., Box, 1976; Box, 1979; Beven, 2006). The simplifying nature of empirical and conceptual input-output relationships may be obvious. Yet, it is a commonly held misconception that physically based model input measured physical (or chemical) properties as parameters. The effective model parameters are always lumped at the scale at which models operate and cannot account for heterogeneity at smaller scales and thus may differ to any measured physical or chemical property (Beven, 1989; Beven et al., 2015). At small scales and under controlled conditions we are able to describe many physical and chemical processes, we still lack the understanding to implement these processes in complex systems and transfer the processes to larger scales (Beven, 2019; Gupta et al., 2014; Kirchner, 2006). Considerable uncertainties lie in the mapping of the landscape into the *"feasible model space"* (Beven, 2000). The main challenge is to capture the relevant processes in the landscape to be included in as simple as necessary models (Grayson and Blöschl, 2000; Blöschl and Montanari, 2010) and get the right system responses for the right reasons rather than to employ overly complex models to perform curve-fitting (Klemeš, 1986; Kirchner, 2006; Hrachowitz and Clark, 2017), or as Kirchner (2006) puts it: *"Such models are often good mathematical marionettes; they often can dance to the tune of the calibration data"*. Model parsimony, establishing simple models with great explanatory power, should be desired in model development. While parsimonious models can provide expedient approximations of a system while retaining simplicity (Box, 1979), overly complex models may find a multitude of configurations to fit a data set and thus *"misconceptions find it progressively easier to hide and flourish in the thickets of mathematistry of their hydrologic models"* (Klemeš, 1986). In other words, our highly parameterized models might even hinder us to identify the relevant processes and understand the dominant patterns in the systems we analyze in a meaningful way (Kirchner, 2006; Hrachowitz and Clark, 2017). Yet, hydrological (or any other environmental) models are established by defining and including potentially relevant processes apriori, where eventually many processes might not be relevant in any situation. This is a fundamental argument for recent advancements to employ purely data driven machine learning methods in hydrology, that identify and implement input-output relationships that can be explained by patterns in the available data (see e.g. Nearing et al., 2020; Kratzert et al., 2019; Kratzert et al., 2018; Shen et al., 2018; Shen, 2018).

Eco-hydrology studies the complex interactions of ecosystems and the atmosphere with the water cycle (Zalewski, 2013). To fully describe the inter-

actions of several complex systems requires to characterize a large number of interconnected processes on multiple spatial and temporal scales. As a consequence, the majority of (eco-)hydrological models tend to be overly complex "models of everything" (Blöschl and Montanari, 2010). The extent of processes detail in such a comprehensive modeling approach is in fact limited and the capability of a model to describe the entire range of large scale fluxes down to microbial activities in a holistic framework must be questioned (Blöschl and Zehe, 2005). Chapter 2 provides a brief summary of frequently applied eco-hydrological models where also the models' complexities are addressed. Indeed, adding process realism and introducing further process relationships into a model might take the noble intention of a comprehensive system representation ad absurdum when the implemented parameters (although represented as physical properties in a model) do not adequately describe the underlying processes, or the data to parameterize the described processes are absent at all (Blöschl and Montanari, 2010). A larger number of degrees of freedom of the model introduces larger uncertainties in the model simulations (Beven, 1989). Eventually, a large number of parameter combinations can almost identically fit observations equally well (Kirchner, 2006; Beven and Binley, 1992).

Other concepts in eco-hydrology approach data limitations and the limited capabilities to describe a complex system by deriving empirical relationships between the environmental variable of interest with system properties that are readily acquirable (Grayson and Blöschl, 2000; Beven and Brazier, 2011). While empirical approaches are usually easy to implement, the boundary conditions for which an empirical relationship was developed must be considered. An empirical model may give good results under conditions that are similar to the conditions the model was established for. Yet, any application of an empirical model to different conditions must be treated as a model extrapolation and is thus not supported by the data that were employed in the model development (Bosco et al., 2015; Favis-Mortlock, 1998). In the case of a model extrapolation there is a risk that the empirical model results in implausible model predictions. To facilitate a wide range of conditions to which an empirical concept should be applicable, generalization of the concept is indispensable (see e.g. the development of the USLE (Wischmeier and Smith, 1978) briefly summarized in section 2.2). Yet, a highly general concept might not be capable to account for complex conditions. Thus, the mapping of complex landscape properties into empirical concepts will, eventually, involve large uncertainties (Beven, 2000; Beven, 2001; Gupta et al., 2014).

Eco-hydrological models are essential tools to analyze a wide range of environmental problems. Environmental modeling tasks often involve discrete scenarios of one or several system components (such as the climate, or land cover) under change to model the system under changed conditions (Hrachowitz and Clark, 2017). Such modeling tasks typically employ a parameterized (calibrated) eco-hydrological model setup that sufficiently fits historic observations. The impact assessment, however, bases on the strong assumption that the calibrated model also represents the system under change. The changed conditions defined by scenarios are implemented into the model while the remaining parts

of the model are kept unchanged. The simulations for the changed system conditions are usually compared to historic conditions to assess the impact of a change (Merz et al., 2011). Yet, the implicit assumption that a model which is considered to be a valid representation of historic conditions is also an adequate representation of the system under future change is likely to be deficient due to two main reasons: i) Simulated output variables (e.g. river discharge) typically result from superimposing several sub-process variables. Multiple configurations of the included sub-processes (e.g. parametrizations or structures) can result in simulations that, when summed up, fit historic observation data equally well (Beven, 1996). The sub-process configurations (and possibly entire sub-processes) must not necessarily represent the actual processes in the modeled system (Kirchner, 2006). Thus, a sub-process configuration that adequately reproduced historic observations might poorly reflect a system change and yield in simulations that strongly differ from the actual behavior that the system would show under changed conditions (Klemeš, 1986; Kirchner, 2006). ii) Even if the parameterized model is a good representation of the underlying processes under historic conditions there is a risk that the system changes do not only affect the driving forces of the system but also alter the underlying processes and consequently require to update the simulated sub-processes in the model (Merz et al., 2011). Admittedly, it is virtually impossible to adequately account for these limitations when modeling changed conditions. Albeit, the consequences for a simulation under change that result from these limitations are far too often neglected or not well examined.

In fact, we as model users tend to be overly optimistic when it comes to evaluate the reliability of our model simulations under change (Blöschl and Montanari, 2010). To get an improved picture of the entire chain of uncertainties in a modeling workflow, inevitably, requires to analyze the scenarios that represent system changes together with the model uncertainties (Clark et al., 2016). We have to acknowledge that the current eco-hydrological model concepts greatly fail to be adequate representations of any environmental system and thus their simulations are uncertain. These uncertainties are not something that must be avoided, but are an attribute of the simulations that must be accepted (Blöschl and Montanari, 2010). Yet, for the model users who perform impact assessments, the immanent question arises how to consider the entire chain of uncertainties in modeling. While the hydrologist may consider a hydrological model (structure) to be a hypothesis that must be tested and eventually be rejected if a model fails to be fit-for-purpose (Savenije, 2009; Beven, 2007; Beven, 2019) such a perception of the model is by far outside the model users' scope. The environmental modelers' perspective on the model is rather the one of an engineer using a tool that is the best available representation of a system (Hrachowitz and Clark, 2017; Savenije, 2009).

Thus, along with improving the model representations we have to improve the ways to estimate and communicate simulation uncertainties. Moreover, it is important that the model community improves their understanding of how highly uncertain model predictions are under given conditions (Blöschl and Montanari, 2010). Hence, uncertainty and sensitivity analysis must become stan-

standard procedures in environmental modeling studies (Hrachowitz and Clark, 2017). Although methods for uncertainty and sensitivity analysis are progressively finding their way into environmental modeling studies to evaluate the model parametrization (Saltelli et al., 2019; Razavi and Gupta, 2015; Pappenberger and Beven, 2006), their utilization to evaluate system changes and different system representations remains challenging (Baroni and Tarantola, 2014). Yet, it is an indispensable process to cover the full range of uncertainties that are inherent in eco-hydrological simulations.

1.1 RESEARCH GOAL

In this context, the goal of this thesis was to develop a comprehensive uncertainty (UA) and sensitivity analysis (SA) framework for eco-hydrological modeling that facilitates an analysis of the entire chain of uncertainties in eco-hydrological modeling workflows. With a focus on the UA and SA of discrete input scenarios and different system representations, great attention was given to the implementation of discrete, composite model inputs into UA and SA. A central goal of the developed framework was to provide a generalized concept that allows to systematically establish eco-hydrological modeling workflows that aim to illustrate a comprehensive picture of the total simulation uncertainties and pinpoint the dominant sources of the uncertainties in a wide range of applications in environmental modeling.

The generalized framework follows a modular procedure, including i) the selection of inputs that potentially have a relevant impact on the simulation uncertainties, ii) the delineation of the input uncertainties for each of the selected inputs, iii) the choice of methods for UA and SA and their implementation in the modeling framework, and iv) the analysis and appropriate communication of the total simulation uncertainties and the influences of the considered inputs on the simulation results. Each step in the framework development requires certain decisions to be made and to draw assumptions that eventually affect the significance of the UA and SA results.

This thesis systematically studies the relevant steps in the development of such an UA and SA framework for eco-hydrological modeling. In the given frame of this work several general and specific questions arise that are covered:

- i. *Application of an UA and SA framework in environmental modeling studies. Extravagance or requisite?*

Without doubt the implementation of a detailed UA and SA framework to perform model diagnostics comes with a substantial increase in analysis and computational costs. Yet, the significance of the current modeling approaches is clearly limited when simulating systems under change, or implementing highly generalized empirical concepts to simulate complex processes, as outlined in the introduction. Thus, the central question in this context is whether detailed UA and SA require a substantial effort in simulating environmental impacts (although the results might provide illuminating insights), or whether a comprehensive UA that considers both,

uncertainties in model inputs and uncertainties in the systems representation, is in fact necessary to realistically depict the uncertainties that are inherent in the simulation results (Clark et al., 2016). The relevance of the implementation of a comprehensive UA and SA approach is evaluated by an assessment of the influence of the implemented inputs, but also by comparing the comprehensive approach to studies that implemented a typical "single model" approach.

- ii. *What are the uncertainties in the delineation of input uncertainties? Scope, subjectivity, and many unknowns.*

The discrete realizations of a model input developed for UA and SA ideally reflect the full range of uncertainties that the respective input contributes in the simulation of the output variables (Clark et al., 2016). Although this step sounds very plausible in theory, the definition of the full range of input uncertainties is limited by large unknowns, subjective assumptions that are drawn for an input, or simply by focusing on one specific scope in a study while neglecting other aspects that might introduce additional uncertainties (Beven et al., 2018). There is no guaranty to cover all possibilities by which an input can affect the simulation of an output variable. Taking that into consideration any additional information that attributes the simulation uncertainties is beneficial and uncertain information should be preferred over wrong certainty (Blöschl and Montanari, 2010). Eventually a rigorous specification of the considered sources of uncertainties and the awareness of potential sources of uncertainties that remained unnoted is vital.

- iii. *What are the limitations and requirements for UA and SA methods when they are implemented in a modeling framework with discrete, composite model inputs?*

The vast majority of applications of UA and SA were implemented with continuous model inputs. An implementation of UA and SA with discrete, nominal input variables limits the application of certain groups of SA methods. Characteristics such large differences in the numbers of realizations of the analyzed model inputs and output distribution characteristics, that can be highly skewed and multi model might introduce additional limitations and specifics that have to be accounted for in the analysis.

- iv. *Significance, interpretability, and plausibility of comprehensive uncertainty analyses. Lessons to be learned from uncertain model results and potentials for uncertainty reduction?*

A comprehensive consideration of uncertainties in eco-hydrological modeling ultimately raises doubts concerning the significance of simulation results. Can conclusions for the research questions of a modeling study be drawn from the simulation results, when substantial uncertainties are present? Is an interpretability of the simulation results (e.g. trends in an environmental variable) even given with possible large uncertainties? Further, the question arises whether all combinations of model inputs that are implemented in such a modeling framework are not only feasible from a

modeling perspective, but also plausible from a system's perspective. The plausibility of input combinations arises the question of potential possibilities for uncertainty reduction, by falsifying input combinations of model input realizations that are not fit-for-purpose to represent an output variable (Beven, 2018). Though, in the context of environmental modeling studies uncertainty reduction can be limited due to the lack of any reference for a future development (Merz et al., 2011), or a general data scarcity.

1.2 OUTLINE

The thesis comprises of three major parts, where Part I renders the theoretical foundation of this work, the central Part II presents two comprehensive case studies that demonstrate the application of UA and SA modeling frameworks as diagnostic tools, and a synthesis of this work in Part III that revisits the formulated research questions from Section 1.1 considering the findings of the case studies from Part II.

In Part I Chapter 2, a general overview on eco-hydrological modeling is provided. The two models that are implemented in the individual case studies are described with more detail. The following Chapter 3 gives a brief outline of uncertainty analysis and systematically reviews different groups of methods for sensitivity analysis. Strengths and limitations of specific methods are discussed to underpin the decisions for the selected methods of SA that were eventually implemented in the case studies and that are explained with more detail in this chapter.

The two case studies that are presented in Part II show a wide spectrum of eco-hydrological model applications, as well as implementation of UA and SA for model diagnostics of systems under change and different model representations of the analyzed systems. Chapter 4 implements the USLE model which can be considered as a simple empirical model to compute spatial estimates of soil loss on a large scale. In the shown setting the uncertainties that is introduced through different system representations was the central focus. The case study in Chapter 5 implemented the more complex model SWAT to simulate time series of discharge and NO_3^- -N loads under system change and with different system representations at the catchment scale.

Part III summarizes the general findings that can be delineated from the two case studies and discusses potentials and limitations of the presented approaches. At the end a brief outlook for possible future research is provided.

1.3 SCIENTIFIC CONTRIBUTIONS

This thesis summarizes contributions to UA and SA in eco-hydrological modeling as analysis tools for discrete composite model inputs. Edited versions of the two case studies that are illustrated in Part II in the Chapters 4 and 5 of this dissertation were submitted to the peer reviewed journal Hydrology and Earth System Sciences (HESS) and published as:

Schürz, C., B. Mehdi, J. Kiesel, K. Schulz, and M. Herrnegger (*in review*, 2019) *A systematic assessment of uncertainties in large scale soil loss estimation from different representations of USLE input factors - A case study for Kenya and Uganda*, In: Hydrol. Earth Syst. Sci. Discuss., doi: 10.5194/hess-2019-602

Schürz, C., B. Hollosi, C. Matulla, A. Pressl, T. Ertl, K. Schulz, and B. Mehdi (2019) *A comprehensive sensitivity and uncertainty analysis for discharge and nitrate-nitrogen loads involving multiple discrete model inputs under future changing conditions*, In: Hydrol. Earth Syst. Sci., 23, 1211–1244, doi: 10.5194/hess-23-1211-2019

In the course of the case studies outlined in this thesis several data processing and data analysis tools were developed, that substantially supported the progress of these studies. Several of these contributions were generalized and implemented in R packages. These R packages found great acceptance and applications in the respective modeling communities. Although these tools are essential for the presented studies they are not discussed in detail in the present thesis. Selected openly accessible R packages are listed below:

Schürz C. (2020) *SWATplusR: Running SWAT2012 and SWAT+ Projects in R*, R package version 0.2.8, available at: <https://github.com/chrisschuerz/SWATplusR>, doi: 10.5281/zenodo.3373859

Schürz C. (2020) *soilgridr: Working with Soilgrids data in R*, R package version 0.2.0, available at: <https://github.com/chrisschuerz/soilgridr>

Schürz C. (2017) *SWATfarmR: Simple rule based scheduling of management operations in SWAT2012*, R package version 0.2.2, available at: <https://github.com/chrisschuerz/SWATfarmR>

Strauch, M., R. Schweppe, and C. Schürz (2016) *TopHRU: Threshold optimization for HRUs in SWAT*, R package version 1.2.3, available at: https://github.com/mic_hstrauch/TopHRU, doi: 10.5281/zenodo.154379

Part I

GENERAL FRAMEWORK

"Is the model true?".

If "truth" is to be the "whole truth" the answer must be "No".

The only question of interest is

"Is the model illuminating and useful?".

— George Box (1979)

ECO-HYDROLOGICAL MODELING

2.1 A BRIEF SYSTEMATIC VIEW ON ECO-HYDROLOGICAL MODELING

Eco-hydrology subsumes the complex interactions between the hydrological water cycle, our ecosystems, and the anthropogenic impacts on natural resources (Zalewski et al., 1997; Zalewski, 2013). A wide choice of computer models is available to simulate the complex interaction between hydrological variables and ecological responses. However, the mathematical representation of eco-hydrological processes, the representation of their interactions, the model input requirements, or the spatial and temporal scale on which a model operates can strongly differ between models that eventually simulate the same output variables (Pandey et al., 2016). In a model application, the research questions that a simulation should support to answer and consequently the complexity of the modeling task and the data availability should determine the selection of the appropriate modeling approach (Mannschatz et al., 2016; Pandey et al., 2016). Yet, the model selection is a challenging task.

The brief systematic overview below provides a summary of relevant specifications of eco-hydrological models. The presented list of models is incomplete and summarizes only a selection of well established eco-hydrological models with a specific focus on the simulation of the interactions between land cover and the management of the land use (with agriculture as its main driver) and the environmental variables soil erosion and nutrient transport (Fig. 2.1). Model specifications that are relevant for the model selection and the evaluation of the model results were classified summarizing previous model reviews (e.g. Pandey et al., 2016; Tuo et al., 2015; Borah and Bera, 2003; Merritt et al., 2003; Singh and Woolhiser, 2002). More exhaustive reviews of eco-hydrological models can be found in Pandey et al. (2016), Borah and Bera (2003), or Singh and Woolhiser (2002). Additionally, the Nexus Tools Platform (Mannschatz et al., 2016) provides a detailed online model inventory to interactively compare and evaluate a wide range of (also but not exclusively) eco-hydrological models, to offer support in the model selection. In the following the reviewed models are referred to by their model acronyms and their full names can be found in the Acronyms section.

Processes, such as soil erosion, sediment and nutrient transport are affected by a large number of environmental processes and spatially distributed properties of the landscape. Their adequate representation in a model requires an implementation of the relevant processes and interactions between the processes and the environment. Thus, models that were developed for the simulation of sediment and nutrient transport follow a comprehensive modeling approach and include concepts and model parametrizations to describe processes such as plant growth, agricultural practices and field management, point sources and

water abstraction, structural measures that affect the hydrology, and changes in land use or climate, among other relevant processes. Well established members of this class of models are the AGNPS (Young et al., 1989), AnnAGNPS (Bingner et al., 2017), APEX (Williams and Izaurre, 2006), SWM/HSPF (Bicknell et al., 1993), MIKE SHE (Refsgaard and Storm, 1995), or SWAT (Arnold et al., 1998) (see large squares in Fig. 2.1). These models simulate the major environmental processes of the hydrological cycle, sediment transport and deposition, and the trajectories of a wide range of chemical components in a combined framework (Pandey et al., 2016). Models, such as ANSWERS (Beasley et al., 1980), GLEAMS (Leonard et al., 1987), GWLF (Haith and Shoemaker, 1987), MONERIS (Venohr et al., 2011), SPARROW (Smith et al., 1997), or (Geo)WEPP (Laflen et al., 1997; Renschler, 2003) simulate selected processes such as erosion, or nutrient transport. Most of the models simulate hydrology as a driving component as a driver for the simulation of sediment or nutrient transport. Other models such as MONERIS require the hydrologic component as an input to evaluate in-stream nutrient fluxes. The USLE (Wischmeier and Smith, 1978) is considered in this overview as a member of models that simulate one particular process. The USLE is particularly interesting as the USLE or any of its derivatives forms the basis for soil loss estimation in many of the more complex models that are listed here, but also as the USLE is frequently used for soil loss estimation in a stand-alone approach.

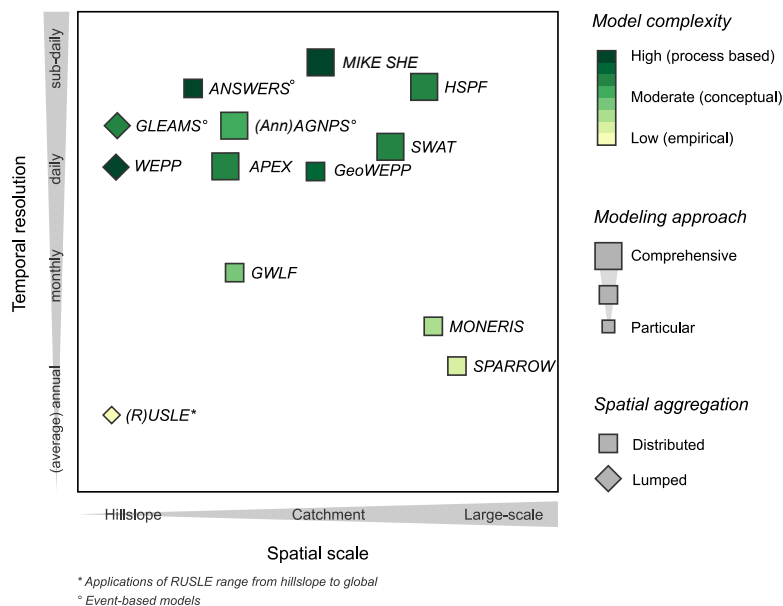


Figure 2.1: Systematic but incomprehensive classification of established eco-hydrological models. The visualized classification of model specifications is based on model reviews of Singh and Woolhiser (2002), Merritt et al. (2003), Borah and Bera (2003), and Pandey et al. (2016). The classification of the models represents the "standard" case for the application of a specific model. Many models however find application on wider spatial and temporal ranges.

Although different models may simulate the same set of output variables, their process representation can greatly differ. The USLE, or the SPARROW model mostly follow an empirical regression approach (light green in Fig. 2.1) to simulate soil loss and nutrient/contaminant fluxes, respectively (Kinnell, 2010;

Schwarz et al., 2006). Thus, the input-output relationship is primarily derived from observation data (Pandey et al., 2016). While such approaches are less input data demanding it is highly relevant to consider the data basis on which the regression was established (Jetten and Favis-Mortlock, 2006). The greater majority of eco-hydrological models can be considered as a mix of different model complexities. While the simulation of some processes employ physically based concepts, other processes are represented by conceptual models, and another group of processes is based on empirical relationships. Spuriously, this group of models is typically referred to as process-based models, although much simpler model concepts are also involved (Hrachowitz and Clark, 2017). Typical members of this group of models are AGNPS, APEX, GLEAMS, SWAT, or SWM/HSPF. Most of these models represent the hydrologic cycle by a conceptual cascade of linear storages. Runoff separation, however, is represented by the empirical SCS-CN (Curve Number) approach (Mockus, 1964) (e.g. AGNPS, APEX, or SWAT) other models employ physical concepts to simulate infiltration, such as the Green-Ampt model (e.g. ANSWERS) or the Richards (1931) equation (e.g. MIKE SHE) (Borah and Bera, 2003). Another example is the simulation of soil erosion where a large majority of the "mixed-type" models employ a derivative of the empirical USLE (e.g. AGNPS, ANSWERS, APEX, GLEAMS, or SWAT). In contrast, soil erosion is simulated with the Exner equation of sediment continuity in MIKE SHE, or WEPP. Overall, only MIKE SHE and WEPP can be considered as "truly" process based models from the presented model selection, as only these models employ physical concepts for the majority of the simulated processes (illustrated in dark green in Fig. 2.1). Generally, a higher degree of a process based process representation requires a higher detail in the required model inputs and thus more complex models are usually more data intensive (Tuo et al., 2015). Well structured summaries on the simulated processes, the employed relationships and the simulated output variables can be found in Borah and Bera (2003) and Quilbé et al. (2006).

The spatial representation of a model differentiates two aspects, the spatial aggregation of the study domain and the spatial scale of the study domain for which a model is usually implemented. Models that were developed to simulate processes on a single plot or a hillslope often represent the small scale domain in a lumped form (GLEAMS, WEPP, or the USLE in Fig. 2.1). Catchment scale models usually allow a spatial separation of the modeled study domain. Models such as AGNPS, ANSWERS, or MIKE SHE disaggregate the spatial domain by grids (Borah and Bera, 2003). SWAT for example by default separates the study domain into spatially referenced subbasins that follow the catchment delineation based on elevation and flow accumulation (Neitsch et al., 2011). Further developments also allow a gridded separation (Rathjens et al., 2015; Arnold et al., 2010), or a separation into landscape units (Bieger et al., 2017). Models such as MONERIS allow a user defined separation of the study domain into sub units (Venohr et al., 2011). On the x-axis the Fig. 2.1 illustrates typical spatial domain on which the respective model is usually implemented. Although the models are assigned to a spatial scale, model applications show much wider ranges of spatial scales. The USLE for example was developed on the plot scale. Yet, the USLE has been im-

plemented in studies that range from plot scale experiments, to catchments (e.g. Angima et al., 2003), to a national scale (e.g. Karamage et al., 2017), to global applications (e.g. Yang et al., 2003; Borrelli et al., 2017). The SWAT model for example was developed at the catchment scale. The majority of published studies applied SWAT to catchments of a few km² to several thousand km² (Gassman et al., 2007). A few studies also show large scale applications on the continental-scale (Abbaspour, 2015), or for trans-national basins (e.g. Malagó et al., 2017; Rouholahnejad et al., 2014).

The temporal scale on which a model can operate is illustrated on the y-axis in Fig. 2.1. While the two empirical modeling approaches of SPARROW, or the USLE provide annual and long-term annual estimates for the output variables, the majority of the conceptual and process-based models can operate on a daily, or sub-daily time scale. Although with a high temporal resolution, AGNPS, or ANSWERS for example only allow an event based simulation, while all other models can perform multi-annual time continuous simulations (Pandey et al., 2016; Singh and Woolhiser, 2002).

In summary, the specifications of the selected and compared models differ in their process representation and in other basic configurations such as the spatial representation, or the minimum temporal time step on which a model simulates the respective processes. These specifications are relevant when it comes to select an appropriate model to approach a given research question. The two case studies presented in Part II exemplify different requirements for the simulated processes and the spatial and temporal resolutions that result from the stated research questions and consequently define the model selection. In the chapters 4 and 5 the two models, the Universal Soil Loss Equation (USLE) and the Soil and Water Assessment Tool (SWAT) were selected. Both models are representatives of either side of the spectrum in terms of complexity and spatio-temporal process representation. Below brief model descriptions for the USLE and SWAT are provided.

2.2 THE UNIVERSAL SOIL LOSS EQUATION (USLE)

The Universal Soil Loss Equation (USLE, Wischmeier and Smith, 1965; Wischmeier and Smith, 1978) formulates the most commonly applied concept to assess soil loss by water erosion (Alewell et al., 2019; Borrelli et al., 2017; Panagos et al., 2015e; Kinnell, 2010). The USLE is an empirical relationship that computes long-term average annual soil loss as a product of six input factors that characterize the erosive force of the rainfall, the soil erodibility, topographic properties, plant cover, and support practices to mitigate erosion. Historically, the USLE succeeded earlier attempts to quantify soil erosion by water developed for the Corn Belt region of the United States of America (USA) in the 1940s. First relationships between soil loss on cropland and topography (Zingg, 1940), factors for crops and conservation practices (Smith, 1941), soil erodibility (Browning et al., 1947), and rainfall (Musgrave, 1947) were developed and reported by Wischmeier and Smith (1965). Over several decades extensive soil erosion data were collected in many locations on field plot scale in the USA. Eventually more than 10 000

plot-years of field data were analyzed, mostly derived from experiments on the "unit plot", a 6.0 ft (1.8 m) wide and 72.6 ft (21.1 m) long farm plot (Renard et al., 1997). A regression of the plot properties to the observed soil loss formulated a generally applicable approach for soil loss estimation in the USA (Wischmeier and Smith, 1965; Kinnell, 2010; Renard et al., 2011). The new approach overcame restrictions of previous methods for soil loss estimation to specific regions in the USA and thus was termed "universal" in the literature (Wischmeier and Smith, 1965). Additional data were collected over the following decades and the methods to calculate the USLE input factors were substantially revised (Renard et al., 1991; Renard et al., 1997; Govers, 2011). The revised model was termed as the Revised USLE (RUSLE, Renard et al., 1991). Yet, the general structure of the equation remained unchanged. The different revisions of the USLE were summarized in Agriculture Handbooks (Wischmeier and Smith, 1965; Wischmeier and Smith, 1978; Renard et al., 1997) that proved to be pragmatic and effective tools for soil conservation planning in the USA (Renard et al., 1991; Renard et al., 2011). For simplicity USLE or RUSLE type models are referred to as USLE in this work. The general form of USLE-type equation is as follows:

$$A = R \times K \times LS \times C \times P \quad (2.1)$$

where A is the long-term mean annual soil loss in $\text{tons ha}^{-1} \text{yr}^{-1}$, R is the rainfall erosivity in $\text{MJ mm ha}^{-1} \text{h}^{-1} \text{yr}^{-1}$, K is the soil erodibility factor in $\text{tons h MJ}^{-1} \text{mm}^{-1}$, L and S are the unitless slope length factor and the slope steepness factor (often combined as the slope length and steepness factor LS), C is the unitless cover management factor, and P is the unitless support practice factor.

Although the USLE was developed to estimate long-term average annual soil loss from farm plots in the USA the model is widely implemented in settings that strongly differ to the initial setting in which it was developed, mainly due to its highly pragmatic approach and its principally simple implementation. Since the USLE was developed, it has been implemented in erosion studies in more than 100 countries (Alewell et al., 2019), at various spatial scales and in various geo-climatic regions (Benavidez et al., 2018). The applications of the USLE model were extended to land uses other than cropland (Renard et al., 1991; Alewell et al., 2019), such as rangeland (Spaeth et al., 2003; Weltz et al., 1998), or woodland (Dissmeyer and Foster, 1980). Several studies adopted the methods to calculate the USLE input factors to meet local or regional conditions (e.g., Roose, 1975; Moore, 1979; Bollinne, 1985; Favis-Mortlock, 1998; Angima et al., 2003). Further development of the USLE was undertaken to employ the empirical model concept to compute event based soil loss (USLE-M, Kinnell, 2010) and event based sediment yield (MUSLE, Williams, 1995). The case study presented in chapter 4 employs different representations of the USLE to estimate long-term annual soil loss in a large scale application.

2.3 THE SOIL AND WATER ASSESSMENT TOOL (SWAT)

The Soil and Water Assessment Tool (SWAT, Arnold et al., 1998) is a conceptual, process based, continuous time, semi-distributed eco-hydrological model. Its development started in the 1990s within the US Department of Agriculture Agricultural Research Service (USDA-ARS) with the goal to provide a tool to analyze the water cycle and non-point sources of pollution on the catchment scale. The conceptual idea of SWAT was to scale up processes that were initially simulated on the field scale to the scale of large river basins (Arnold and Fohrer, 2005). The SWAT model predeceases the Simulator for Water Resources in Rural Basins (SWRRB, Williams et al., 1985) and involves concepts and process representations adopted from field scale models also developed within the USDA-ARS, such as the Chemicals, Runoff, and Erosion from Agricultural Management Systems (CREAMS, Knisel, 1980) to compute the upland hydrology, the Groundwater Loading Effects on Agricultural Management Systems (GLEAMS, Leonard et al., 1987) to simulate pesticide fate, the Erosion-Productivity Impact Calculator (EPIC, Williams et al., 1983) to implement crop growth, or the Modified Universal Soil Loss Equation (MUSLE, Williams, 1995) to simulate sediment yield (Arnold and Fohrer, 2005; Gassman et al., 2007; Krysanova and Arnold, 2008; Williams et al., 2008).

The spatial reference of SWAT to a catchment is given by a subdivision of the basin into subbasins. The number of subbasins and thus the spatial discretization of the analyzed basin is manually defined in the watershed delineation, that can be performed with available tools such as ArcSWAT (Winchell et al., 2015) or QSWAT (Dile et al., 2016). Areas containing the same land use, soil type and lying in the same slope range are lumped together in each subbasin to form Hydrologic Response Units (HRUs). All processes on the land phase of each subbasin are calculated at the HRU scale and are further propagated into the water phase of each subbasin. The processes calculated on the land phase include water balance components such as interception, infiltration, shallow and deep percolation, surface runoff, lateral flow, groundwater flow, plant uptake and evapotranspiration, or the pathways of nutrients such as the input through atmospheric deposition, or fertilizer application, the transformation into other forms of a nutrient and the transport through surface runoff, percolation, lateral flow and return flow in the groundwater (Neitsch et al., 2011). In the water phase, the nutrients budgets are calculated. Following the calculation of the water balance and the nutrient budgets, the discharge, the nutrient loads and other substances are routed through the linked subbasins to the defined catchment outlet (Neitsch et al., 2011).

Although SWAT has been developed for application on the catchment scale in the USA (e.g. within the Hydrologic Unit Model of the U.S. (HUMUS) modeling system (Arnold et al., 1999)), up today it has been applied worldwide on a wide range of spatial scales from the field scale, to small catchments, and continental studies (Gassman et al., 2007). In a meta-analysis on the popularity of water quality models Mannschatz et al. (2016) identified the SWAT model to be by far the most frequently applied model to simulate water and nutrient fluxes. SWAT

is a comprehensive framework of conceptual and empirical models to simulate a large variety of environmental processes. Thus, the model description above is very general. Neitsch et al. (2011) provides a detailed description of all the simulated processes and the exact process equations. SWAT is continuously updated and revised. In the case study presented in chapter 5 the SWAT model in the version SWAT₂₀₁₂ and the revision number 622 was implemented to simulate daily time series of discharge and NO_3^- -N loads at the catchment outlets.

Uncertainty Analysis (UA) and Sensitivity Analysis (SA) are two strongly linked procedures in modeling. While UA quantifies the uncertainties of a simulated model output that results from uncertainties in the inputs, SA focuses on identifying the dominant sources for the output uncertainties or tries to apportion the output uncertainties to the different uncertain inputs (Saltelli et al., 2008; Saltelli et al., 2004). At best, UA and SA are combined in the analysis of a system to obtain an understanding of the amplitude of the output uncertainties but also to identify the dominant sources of uncertainties of a model application (Saltelli et al., 2008). UA and SA often employ similar methods and therefore allow a combined assessment. Monte Carlo (MC) sampling, for instance, is commonly implemented for uncertainty estimation. Bayesian methods such as the Generalized Likelihood Uncertainty Estimation algorithm (GLUE, Beven and Binley, 1992) or procedures that implement Monte Carlo Markov Chain (MCMC) processes (e.g. Kuczera and Parent (1998), or Vrugt et al. (2008) and Vrugt et al. (2009) with the DREAM algorithm) employ a MC sampling scheme. MC sampling, further allows the implementation of different SA methods (e.g. Pianosi and Wagener, 2018; Ratto et al., 2001; Sobol, 1993, see more detail in section below). Particularly in eco-hydrological modeling where the number of simulation runs contribute the largest part of the computational costs and are therefore a limiting factor, an efficient use of the performed simulations is valuable. Thus, it is highly beneficial to complement UA and SA in the analysis of environmental systems (Pianosi et al., 2016) to gain additional insights in the complementing analyses (see good practice examples in Borgonovo et al., 2017; Pappenberger et al., 2008). The following chapter gives a brief overview of UA and SA in eco-hydrological modeling. The review of UA methods is kept concise as the following case studies employ standard methods to express uncertainties in the simulation outputs. The review of SA methods was performed more systematically and with greater detail to highlight the specifications and limitations of the current methods for SA and to distinguish the methods that are suitable for an implementation with discrete, nominal, composite inputs. Finally a general workflow for the implementation of UA and SA with discrete, composite model inputs is presented.

3.1 UNCERTAINTY ANALYSIS (UA)

Uncertainty is often framed as a negative property that has to be prevented or avoided. Yet, in a very general sense uncertainty is simply an *"attribute of information"* (Zadeh, 2005; Blöschl and Montanari, 2010) that must be rather acknowledged than ignored. A very broad definition of uncertainty distinguishes between two types of uncertainties. Aleatory (*alea* = rolling of a dice) uncertain-

ties represent randomness, or variability and are typically treated as a statistical property. Epistemic ($\epsilon\pi\iota\sigma\tau\eta\mu\eta$ = knowledge) uncertainties define systematic uncertainties due to a lack of knowledge (Beven et al., 2018; Kiureghian and Ditlevsen, 2009). Refsgaard et al. (2007) state that only epistemic uncertainty is reducible by acquiring additional information, while true random aleatory uncertainty is not reducible. In a modeling context Beven (2016) and Beven et al. (2018) argue that all considered sources of uncertainty are a result of missing knowledge. Yet, some types of uncertainties are widely accepted to be treated as random aleatory uncertainties while their nature is epistemic. Consequently, in hydrology and many other disciplines it is common to employ probability theory to express uncertainties in hydrological variables (Montanari, 2007). A textbook example for the implementation of probability theory to express the uncertainties in model outputs is to propagate the input variabilities through the model employing Taylor series expansion.

$$s_y = \sqrt{\sum_{i=1}^n s_{x_i}^2 \left(\frac{\partial f}{\partial x_i}\right)^2} \quad (3.1)$$

where s_y is the standard deviation of the model output y , $\frac{\partial f}{\partial x_i}$ is the first partial derivative of the model f for the n inputs x_i , and s_{x_i} is the standard deviation of the input x_i . While such an approach can be valid to propagate measurement errors of the inputs that are assumed to be independent and identically distributed random variables through a known derivable function, such strict requirements for the inputs and the input-output relationship hardly hold for any eco-hydrological model. Yet, authors such as Mantovan and Todini (2006) argue that only formal statistics allow an objective estimation of uncertainty in terms of probabilities. Bayesian approaches (such as the above mentioned ones) overcome the limitations of "traditional" error propagation as they allow any shapes of the posterior distribution functions of the analyzed inputs (Yang et al., 2007). Yet, to infer the posterior distributions for the model parameters of a deterministic eco-hydrological employing Bayesian inference as well requires strong statistical assumptions for the error term, the definition of a Likelihood function and a prior distribution of the model inputs (model parameters in most cases, see e.g., Ammann et al., 2019; McInerney et al., 2019; Yang et al., 2007; Reichert, 2006). Nearing (2013) and Gupta and Nearing (2014) call the implementation of Bayesian inference in computational modeling an "imperfect implementations of Bayes law", due to strong imperfect assumptions for the Prior distributions of the parameters and the Likelihood functions that are necessary to estimate the posterior parameter distributions.

Besides a probabilistic perception of uncertainties, model input uncertainties can originate from a wide range of sources and follow other concepts that cannot be expressed in a probabilistic way. Assumptions in the model input definition can express ambiguity, formulations can be vague, and information can be fuzzy, or inconsistent (Beven et al., 2018). The description of such model and input qualities with a probabilistic approach very likely fails and a more

flexible possibilistic characterization is necessary (Montanari, 2007). A practical example for these types of uncertainties is to describe how a system develops in the future. Typically, scenarios are developed that express how the future could evolve from historic conditions (Refsgaard et al., 2007). These scenarios are based on assumptions that reflect the current state of knowledge and thus all scenarios are usually considered as equally plausible possibilities. Such a perception of uncertainty can be extended to other inputs where different representations of an input are equally plausible and no representation can be rejected, such as equifinal model parameter combinations (Beven, 1996), or different model structures (Clark et al., 2008) among many other examples. The combination of all plausible representations of the inputs eventually result in the total output uncertainty. To describe the range of the output uncertainties different communities established different concepts. The dominating concept to express the simulation outputs of a SWAT model simulation is to derive the 95 % uncertainty bands that cover 95 % of the behavioral simulations (Abbaspour, 2015).

The two case studies presented in this thesis clearly follow the latter epistemic concept to describe uncertainties in modeling studies. In both studies uncertainties in the analyzed model inputs are defined by equally valid realizations of that input. The output uncertainties are described by the total simulated uncertainties that result from all combinations of the uncertain inputs or a sample of the input combinations, if a computation of all input combinations is infeasible. Although the technical implementation to express the simulation uncertainties is relatively straightforward, the actual challenge lies in the communication of the resulting uncertainties. The two case studies outline and present ways for the communication of the simulation uncertainties that fit the individual requirements of both studies. The individual methods that were used for the analysis and presentation of the output uncertainties of both studies are outlined in the sections 4.4.3 and 5.5.2.

3.2 SENSITIVITY ANALYSIS (SA)

Sensitivity Analysis (SA) studies the response of a target variable to the variation of input variables (Saltelli, 2009; Saltelli et al., 2008). In a modeling context, the target variable is either a simulated output or any system state that is investigated. Most methods for SA require scalar quantities to evaluate, and the target variable is usually summarized by a summary statistics. An input variable can be any attribute of a model that might influence the target variable when that input is altered. Input variables can represent single model parameters, external model forcings, but also the entire model composition (i.e. the set of equations that is implemented, the spatial or temporal system representation, or the system boundary conditions) (Gupta and Razavi, 2018).

The SA literature generally defines two main settings in which an SA is typically employed. A *diagnostic* setting of SA aims to enable a better understanding of a system and its input-output relationship. The typical application for model diagnostics is to vary continuous model parameters of interest in their feasible

range and analyze the influence of these changes on the model outputs (see e.g., Sarrazin et al., 2016; Pianosi and Wagener, 2015; Razavi and Gupta, 2016b, and many others). More uncommon, but interesting in a model diagnostics context is to define a set of model configurations or equations that describe the input output relationship, or the representation of uncertainties inherent in the external forcings and the observation data as input variables to investigate (see e.g., Baroni and Tarantola, 2014; Savage et al., 2016; Dai and Ye, 2015; Dai et al., 2017). In a *prognostic* setting SA can be employed to assess the importance of input variables for the (future) simulation of a target variable (see e.g., Schürz et al., 2019; Anderson et al., 2014; Butler et al., 2014). Often, the variation of an input is represented by a set of possible future representations (e.g. climate model simulations, or land use scenarios), or a possible range of an input, in such a setting. The variability of an input, that is considered in a prognostic setting, should encompass all possible (future) settings and/or uncertainties associated with that input (Clark et al., 2016).

Today a wide range of methods for SA exists. Although many of the published methods for SA follow similar concepts, some methods excel for specific purposes of SA. Apart from the modelers' personal preference a few parameters of a study setting eventually define an appropriate choice of an SA method. In the following a brief overview of widely implemented SA methods is given. Based on a few relevant parameters for the selection of an SA method selected methods are systematically classified and analyzed. The two SA methods that were implemented in the case studies in Part II are outlined in greater detail.

3.2.1 A systematic review of SA methods

The setting of a study that employs a SA, determines the main purpose of the implemented SA method. The SA literature defines different purposes for SA (e.g., Saltelli et al., 2004; Saltelli et al., 2008; Campolongo et al., 2009; Razavi and Gupta, 2015; Pianosi et al., 2016). Although an equivocal terminology is used (often interchangeably with the extent of an SA, or from an Uncertainty Analysis (UA) perspective) three main purposes of SA are commonly defined in the literature. The systematic classification of SA purposes that is presented here (see Fig. Figure 3.1) is based on Pianosi et al. (2016) but also refers to other common terminology, such as Razavi and Gupta (2015), or Saltelli et al. (2008). The three main purposes are outlined here: The aim of *screening* (analogue to *factor fixing*, or *identification* of non-influential inputs) is to identify inputs that influence the target variable, or to fix the inputs that have no significant impact on the target variable (Pianosi et al., 2016; Razavi and Gupta, 2015; Saltelli et al., 2008; Campolongo et al., 2009; Saltelli et al., 2004). *Ranking* (*factor prioritization*, or the analogue pendant of *uncertainty apportionment*) the input factors according to their calculated sensitivity index values helps to identify the inputs that have the strongest contributions to variability of the target variable, or output uncertainty (Pianosi et al., 2016; Razavi and Gupta, 2015; Saltelli et al., 2008; Saltelli et al., 2004). *Mapping* (related to the identification of *factor interdependence* and *model calibration*) aims to identify regions in the input space where

the input combinations lead to defined ranges of the target variable (Pianosi et al., 2016; Razavi and Gupta, 2015; Saltelli et al., 2008; Saltelli et al., 2004; Rakovec et al., 2014; Ratto et al., 2001).

The purpose of an SA steers the selection of the SA method that is implemented. Generally, the three outlined purposes of SA that were defined above differ in the degree of information that is required on the input response surface to achieve a robust result for that purpose. The response surface describes how changes in the inputs result in changes of the target variable (comparable to an elevation map where "walking" into a direction causes a change in altitude). More information on the response surface, however, comes with an increase in computational costs (see Fig. 3.1). While a *screening* can identify the influence of an input on a target variable at a cost of a few hundred model evaluations, a *mapping* might require several hundred thousand model evaluations to find regions in the input space where input combinations result in acceptable values for the target variable (Pianosi and Wagener, 2015; Razavi and Gupta, 2015). In most SA applications the number of model evaluations that is required to implement a specific SA method is the major limiting factor for its implementation (Razavi and Gupta, 2015; Pianosi and Wagener, 2015). While simple model applications allow a large number of model evaluations (e.g. Sarrazin et al., 2016; Razavi and Gupta, 2016b), large scale model applications such as global climate simulations can only afford a few simulation runs and are therefore limited to basic analyses of the model inputs (Gupta and Razavi, 2017; Pianosi et al., 2016), such as a one-at-a-time (OAT) analysis of the model inputs (e.g. Murphy et al., 2004). Environmental model applications are usually less computationally expensive and allow a more extensive SA, illustrated in many environmental modeling studies (e.g. Guse et al., 2016; Haghnegahdar et al., 2017; Massmann and Holzmann, 2015; Razavi and Gupta, 2016b; Sarrazin et al., 2016).

Fig. 3.1 illustrates a systematic classification of frequently implemented methods for SA based on the five attributes that characterize the SA methods and eventually determine their applicability. The considered attributes are the mathematical concept of a method, the extent of the input response surface that is analyzed, the types of inputs that can be analyzed with a certain method, the sampling approach of a method, and its sampling design strategy. Based on the main purpose and the typical computational costs of the classified SA methods three main groups are identifiable. In terms of computational costs at the lower end of the spectrum the group of derivative based methods are located. Derivative based methods for SA evaluate the partial derivatives $\frac{\partial y}{\partial x_i}$ to assess the influence of the input x_i on the target variable y (Pianosi et al., 2016). All derivative based methods have in common that they perturb one input at a time (OAT) from a starting value to assess the amplitude of change in the target variable when changing the input by a certain value (Norton, 2015). Derivative based methods require the definition of a change interval Δ_i and thus can only employ continuous input variables in the analysis. The main differences between the individual derivative based methods can be found in the extent of the input space they analyze and the required sampling design that eventually define their computational costs. The most basic approach is a local OAT

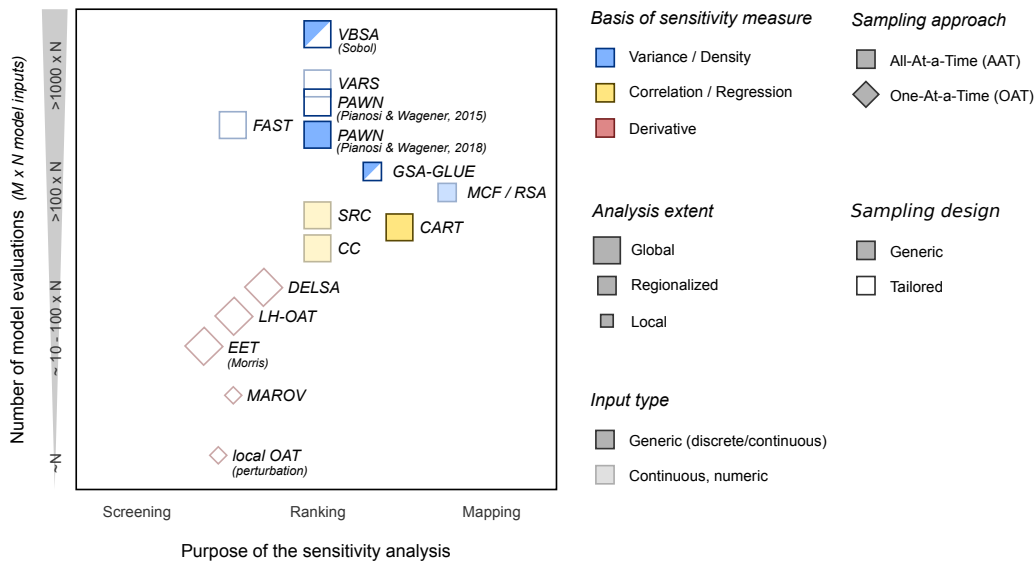


Figure 3.1: Systematic classification of standard methods for sensitivity analysis adopted from Pianosi et al. (2016) and Yuan et al. (2015). The methods are plotted with respect to their main purpose and the computational costs (The approximate number of required model evaluations depending on the number of analyzed input variables). The methods are further classified according to the statistical/mathematical concept that is applied to derive the sensitivity measure, the extent of the analysis in the input space, the assumptions for model inputs to be implemented in the analysis, the sampling approach, and the sampling design.

analysis where each input is perturbed one time in a nominal point (often the "optimum" input set that results from a model optimization). Such an approach only provides the sensitivity of the target variable to the analyzed inputs in that local point and is highly dependent on the selected change interval Δ_i and the variability of the response surface around the analyzed point on the response surface (Yuan et al., 2015). At slightly higher computational costs the MAROV method (Dubus and Brown, 2002) for instance tries to overcome the effect of the change interval by performing multiple perturbations using different change intervals and assessing the maximum influence on the target variable (Yuan et al., 2015). Yet an analysis with MAROV is a local one. Local perturbation methods, however, are incapable of depicting a general picture of the influence of a model input on a target variable (Saltelli and Annoni, 2010). Performing perturbation experiments from multiple starting points and aggregating an inputs' influence in all of these points extends the perturbation concept for GSA (Pianosi et al., 2016). Such an approach is generally known as Elementary Effects Test (EET) (Saltelli et al., 2008) and became established methods with tailored sampling designs and analysis approaches, such as the method of Morris (Morris, 1991), the staircase approach (Jansen, 1999), LH-OAT (Griensven et al., 2006) that uses a Latin Hypercube Sampling (LHS) approach for the sampling of the starting points, or DELSA (Distributed Evaluation of Local Sensitivity Analysis, Rakovec et al., 2014). Although computationally inexpensive these type of methods are mostly applicable in input factor screening, or when more intensively sampled for an input ranking. A straight forward and efficient im-

plementation of EET for screening and ranking in higher dimensional problems can be found for example in Cuntz et al. (2015).

A second group of methods employs the correlation between the inputs and the target variable or methods for regression analysis to infer the influence of model inputs on a target variable (Pianosi et al., 2016). A benefit of these types of methods is that generic sampling designs such as Monte Carlo sampling can be applied to sample the inputs (Kleijnen and Helton, 1999; Pianosi et al., 2016), where all inputs are perturbed at a time AAT. These methods provide a global picture of sensitivities of the input output relationship to allow a ranking of the inputs at generally slightly higher computational costs compared to the EET methods (see Fig. 3.1). Depending on the implemented method to compute the correlation coefficient or the type regression analysis the input output relationship must meet certain requirements. Pearson correlation, or linear regression assume a linear relationship between the model inputs and the target variable, while Spearman rank correlation can be applied to non-linear but monotonic relationships (Kleijnen and Helton, 1999; Saltelli et al., 2008). All of these methods, however, require continuous, numeric model inputs. In terms of the requirements for the model inputs and the mathematical relationship between inputs and the target variable correlation and regression trees (CART, Breiman et al., 1984) are a very flexible approach to infer sensitivities. A key advantage of CARTs is that they allow discrete inputs and outputs in the analyses (see e.g. Singh et al., 2014).

A large group of SA methods includes approaches that employ the variance or the density of the target variable to infer sensitivity. The two main groups of this type of SA follow either a global or a regionalized approach for the analysis of the input response surface. The main purposes of a Regional Sensitivity Analysis (RSA) are the mapping of input factors and the identification of the dominant inputs in the analyzed system. Generally, the concept of RSA methods is to identify regions of the input response surface where the values of the target variable meet a criterion, typically having a value above or below a certain threshold (Saltelli et al., 2008; Pianosi et al., 2016). An early approach for RSA was proposed by Spear and Hornberger (1980). This method is often found as Monte Carlo Filtering (MCF) in the literature and is the conceptual foundation of several newer SA methods. In Spear and Hornberger (1980) simulation results are separated in behavioral B and non-behavioral \bar{B} sets. Cumulative Distribution Functions (CDFs) of the analyzed inputs for the behavioral set $F(x_i|B)$ and the non-behavioral set $F(x_i|\bar{B})$ are calculated and investigated for differences, where $F(x_i) = F(x_i|B) = F(x_i|\bar{B})$ indicates a non influential input x_i and $F(x_i) \neq F(x_i|B) \neq F(x_i|\bar{B})$ identifies an input to be influential. To quantify the sensitivity of the target variable to an input Spear and Hornberger (1980) suggested to calculate the Kolmogorov-Smirnov distance for the two CDFs:

$$KS_i = \|F(x_i|B) - F(x_i|\bar{B})\| \quad (3.2)$$

MCF allows to implement any generic sampling design to sample the analyzed inputs. The formulation of the CDF, however, requires continuous vari-

ables and therefore MCF can only be applied to continuous inputs. Yet, MCF is applicable to any type of target variable, for which a criterion can be defined to split the simulation results into behavioral and non-behavioral sets (Pianosi et al., 2016). If a target variable allows a separation into multiple classes MCF can be extended to perform an SA for multiple classes, as it is demonstrated in Schulz et al. (1999) for a continuous target variable that was separated into 10 performance levels.

A method that is frequently applied in the hydrological modeling community and that follows the same concept as Spear and Hornberger (1980) is the GLUE method (Beven and Binley, 1992). GLUE separates the input response surface in behavioral (B) regions that meet the criterion of the target variable and non-behavioral (\bar{B}) which do not meet that criterion. Ratto et al. (2001) employed the glue concept for the use in global sensitivity analysis (GSA-GLUE). GSA-GLUE specifically analyzes the behavioral regions of the input response surface and applies Variance-based SA (VB-SA) to these regions (methods for VB-SA will be outlined in the following).

Variance-based SA (VB-SA) employs the variance of the target variables' distribution as measure for the target variables' sensitivity to changes in the model inputs (Saltelli et al., 2008). VB-SA is frequently implemented in environmental modeling as it is easy to implement. The main benefit of VB-SA, however, is that at no additional computational costs the *main effect* of an input (the individual influence that input has on the target variable) and the *total effect* (the influence of an input considering all interactions with the other inputs) can be computed (Pianosi et al., 2016; Saltelli et al., 2010):

$$S_i = \frac{V[E(y|x_i)]}{V(y)} \quad (3.3)$$

$$S_{Ti} = 1 - \frac{V[E(y|x_{\sim i})]}{V(y)} \quad (3.4)$$

where S_i and S_{Ti} are the main order and total order sensitivities of the target variable y for the input x_i , $V(y)$ is the unconditional variance of y , and $V[E(y|x_i)]$ and $V[E(y|x_{\sim i})]$ are the variances of y under the conditions of $x = x_i$ and $x = x_{\sim i}$ (all but x_i). Yet, the use of the variance as a measure for sensitivity assumes properties such as a low skewness and unimodality of the target variables' distribution (Pianosi et al., 2016). Generally, variance-based methods proved to be robust methods for high dimensional problems (e.g., Sarrazin et al., 2016; Razavi and Gupta, 2016b; Haghnegahdar et al., 2017; Sheikholeslami et al., 2019; Haghnegahdar and Razavi, 2017), although at higher computational costs compared to correlation or derivative based methods (see Fig. 3.1). The variance decomposition approach shown with Eq. 3.3 was first proposed by (Sobol, 1993) (later extended to total order effects by Homma and Saltelli, 1996 shown with Eq. 3.4) and is still the reference method for GSA studies nowadays. Other variance-based approaches employ the Fourier series expansion of the target variable, such as the Fourier Amplitude Sensitivity Test (FAST, Cukier et al.,

1973) (extended for total order sensitivities by Saltelli et al. (eFAST, 1999)), or the variogram based approach (VARS) proposed by Razavi and Gupta (2016a). In order to implement the proposed variance-based measures for SA, most of these methods require specifically tailored sampling designs, such as the STAR sampling (Razavi and Gupta, 2016b) for VARS, or sampling the inputs with varying frequencies and amplitudes for the Fourier series expansion with FAST. The Sobol method was initially proposed to implement generic input sample. Although tailored sampling designs were developed that increased the computational efficiency and the robustness of the method (e.g. Jansen, 1999; Saltelli, 2002; Saltelli et al., 2010).

Density-based methods employ changes in the target variables' conditional empirical density function compared to the unconditional case as a measure for sensitivity instead of using any statistical moments as a measure (Pianosi et al., 2016). The implementation of the target variables' distribution is particularly useful when dealing with skewed and multi-modal distributions that pose an issue for the use of variance-based methods (Mora et al., 2019). The major differences between the density-based methods is whether they implement the target variables' Probability Density Function (PDF) (e.g. Borgonovo, 2007; Liu et al., 2006) or the Cumulative Distribution Function (CDF) (e.g. Chun et al., 2000; Pianosi and Wagener, 2015) and the measure that is employed to evaluate the difference between the conditional and the unconditional distribution function, such as entropy measures (e.g. Liu et al., 2006; Park and Ahn, 1994), the enclosed area between the curves (e.g. Chun et al., 2000; Borgonovo, 2007), or the maximum distance between the curves (e.g. Pianosi and Wagener, 2015). Although these methods are very flexible in terms of the shape of the target variables' distribution only numeric, continuous outputs can be analyzed that have a distribution. Yet, the major benefit of density-based methods is that any type of inputs can be employed in an SA since only the output distributions are considered for the analysis. In the following, the density-based SA method PAWN (Pianosi and Wagener, 2015; Pianosi and Wagener, 2018) is described with greater detail, as it was implemented in the case study in chapter 5.

3.3 FRAMEWORK FOR UA AND SA WITH DISCRETE, COMPOSITE INPUTS

In the two case studies that are presented in Part II the focus of the implemented UA and SA was to analyze the influence of discrete, composite model inputs on the simulation of different eco-hydrological variables. A composite model input is very broadly defined in the present context as any part or component of a model simulation that when modified can impact the simulation results of that model setup. Composite model inputs can be single model parameters that when modified impact any state variable in the model and thus alter the simulation results, but also sets of parameter combinations, the method to derive a model parameter, the entire spatial model representation of the simulated system, or different scenarios for a model component such as the land use or the hydro-climatic inputs. In contrast to continuous model parameters that are typically analyzed with SA, composite model inputs are represented by a

finite number of discrete realizations and must be treated as nominal measures (Stevens, 1946). Nominal variables can generally only be classified as members of a groups and disallow any sorting of the members or the definition of intervals between the members. An example in a modeling context could be that a discrete set of scenarios of a model input must not necessarily allow the sorting of the individual scenarios, nor to define any distance measure between the realizations. Such quality of the inputs induces limitations for the UA and SA methods that are implemented in an analysis. For the SA applications in the two case studies, the following requirements were relevant for the implemented SA methods:

- i. The implemented SA methods should provide information on the overall impact of the considered inputs on the analyzed target variables. Hence, GSA methods were employed in both case studies to analyze the entire input space.
- ii. The analyzed inputs were represented by discrete, nominal sets of realizations for each input. Thus, only SA methods can be considered that allow non-continuous inputs where no sorting or any interval measures are applicable.
- iii. The numbers of the members of the discrete model input sets differed for the individual model inputs. Therefore, the selected statistical measure that was implemented as the sensitivity measure must be independent of the number of members of each input set.
- iv. Although the analyzed target variables were scalar and continuous, their output distributions were assumed to be highly skewed, multi-modal and non-normally distributed. This is as well a limitation for the statistical sensitivity measure.
- v. The selected SA methods must be robust and computationally efficient. For the two presented case studies the the two attributes robustness and efficiency were limited by entirely different configurations in the individual study settings. While in one case study the total number of possible model combinations and the computational costs of a simulation were very low and thus all possible combinations could be run with ease, for the other case study the simulation time and the number of possible model combinations were the limiting factor and only a small set of model combinations could be sampled for the analysis. The design of the SA analysis was however strongly affected by large amounts of output data and limited storage capacities in the first case study. Such technical boundary conditions of a study also influence the selection of the employed SA method.

The systematic review of SA methods above provides a broad overview of the requirements, strengths and limitations of different groups of methods for SA. Below the two approaches for SA are described in detail that were implemented

in the case studies in Part II . Any extensions and alterations of established methods that were necessary to fulfill all defined requirements above are outlined in the following.

3.3.1 Analytical uncertainty propagation

The first case study implements the USLE model to calculate spatially distributed estimates of the long-term average annual soil loss, based on an entire ensemble of USLE model setups. The aim of the SA in this study was to identify the most relevant USLE model inputs for each spatially distributed soil loss estimate. Although the generation of the USLE model input factors is a non-trivial step in the erosion model setup and is thus prone to large uncertainties that are inherent the model input realizations, the USLE model itself has a very simple model structure from an SA perspective (see model structure in Eq. 2.1). In the case of such a simple model, uncertainties in the inputs can be analytically propagated through the model to infer the uncertainties in the simulation outputs (Beven and Brazier, 2011). Thus, the sensitivity of the calculated soil loss to the ranges of the input factors can be analyzed analytically as well. However, the structure of the USLE model results in two important considerations for the development of the measure that was implemented to express sensitivity:

- i. The soil loss estimate calculated with the USLE is the product of the individual model inputs. Thus, any measure that describes the influence of an input on the simulation outputs is highly sensitive to inputs with values close to zero or exactly zero. The implemented measure must be able to cope with such effects.
- ii. The value ranges of the USLE model inputs strongly differ by several orders of magnitude. A normalized sensitivity measure is beneficial that is independent from large differences in the input ranges.

The developed sensitivity measure expresses the importance of the USLE input factors on the simulation of the soil loss in each grid cell (m, n) by calculating the fraction between the range in soil loss that is caused by an input factor I_j and the total range of A that results from the entire model ensemble in a location (m, n) :

$$s_{j,m,n} = \frac{(\max(I_{j,m,n}) - \min(I_{j,m,n})) \cdot \prod_{k \neq j} \max(I_{k,m,n})}{\left(\prod_k \max(I_{k,m,n}) - \prod_k \min(I_{k,m,n}) \right)} \quad (3.5)$$

where $s_{j,m,n}$ is the sensitivity of the input factor I_j in the location (m, n) , I is the set of the analyzed input factors R , K , LS , and C and k is the index of the respective input factor. The resulting sensitivity measure is normalized between 0 and 1, where a sensitivity $s_{j,m,n} = 1$ means that the total range of the calculated soil loss can result from varying the input I_j and 0 means that this input shows no variation between its realizations in the location (m, n) .

3.3.2 The PAWN sensitivity index

In the second case study the more complex eco-hydrological model SWAT was implemented to simulate daily time series of discharge and NO_3^- -N loads. From these simulated time series several scalar, continuous signature measures were computed that were implemented in an SA. In contrast to the first case study, a SWAT model setup cannot be analyzed analytically. Thus the input-output relationship is considered to be a "black box" in the SA. The continuous, but non-normal distribution of the analyzed target variables and the discrete and nominal inputs strongly limited the number of suitable SA methods for the application in this case study. Eventually the PAWN sensitivity measure was identified as an appropriate method. PAWN was found to be a robust measure for sensitivity of non-symmetrically distributed outputs of environmental models (e.g. Pianosi and Wagener, 2015; Zadeh et al., 2017; Hosseini et al., 2017). Yet, benchmarking tests showed limitations for parameter ranking with PAWN in synthetic test examples (Puy et al., 2019; Mora et al., 2019).

The PAWN sensitivity index is a member of the group of density-based moment independent methods for GSA. As it is a global method it explores the entire input space to evaluate the target variables sensitivity to the considered model inputs. It is model and moment independent and thus the implementation of PAWN is independent from the type of input-output relationship as well as independent from the output distribution. PAWN employs the empirical CDF of a target variable to infer the model input impacts on the simulation of the target variable (Pianosi and Wagener, 2015). A minimal example in Fig. 3.2 demonstrates the implementation of the CDF for SA applied for two continuous model inputs. Fig. 3.2 a) shows the input response surface of a target variable y for the entire feasible input space of two uncorrelated continuous model inputs x_1 and x_2 , where y shows a low sensitivity for the input x_1 and a high sensitivity for x_2 . The dashed iso-lines indicate curves along which the target variable y results in the same value for pairs of (x_1, x_2) . The three colored lines along the two input dimensions indicate transects along which input combinations are sampled and $y(x_1, x_2)$ is evaluated where either one of the inputs is kept constant and the other input is perturbed. For the entire input space and for the individual transects the unconditional CDF $F_y(y)$ and the conditional CDFs $F_{(y|x_i)}(y)$ are calculated, respectively. Fig. 3.2 b) and c) show the resulting CDFs for the inputs x_1 and x_2 , respectively. The black solid curves in both plots show the unconditional CDF $F_y(y)$ where both inputs x_1 and x_2 were altered simultaneously. The colored curves show the conditional CDFs for the transects drawn along the input dimensions in Fig. 3.2 a). When fixing the input x_1 at constant values (horizontal transects in Fig. 3.2 a)) the densities along the transects show very similar distributions compared to density of the entire input space. Thus, their CDFs closely follow the unconditional CDF in Fig. 3.2 b). The blue and the red curves show minor shifts towards lower values, as those transects do not cross areas with the largest values for y in the input space. The transects with constant values for input x_2 (vertical transects in Fig. 3.2 a)) result in conditional CDFs that strongly differ from the unconditional CDF. Particularly the blue and

the yellow CDFs in Fig. 3.2 c) are steep with values that are substantially lower than the density distribution of the unconditional CDF. The blue and yellow transects in Fig. 3.2 a) are almost parallel to the low iso-lines and thus result in the strong differences in the CDFs. This minimal example illustrates that the comparison of conditional CDFs to the unconditional CDF can potentially measure sensitivity.

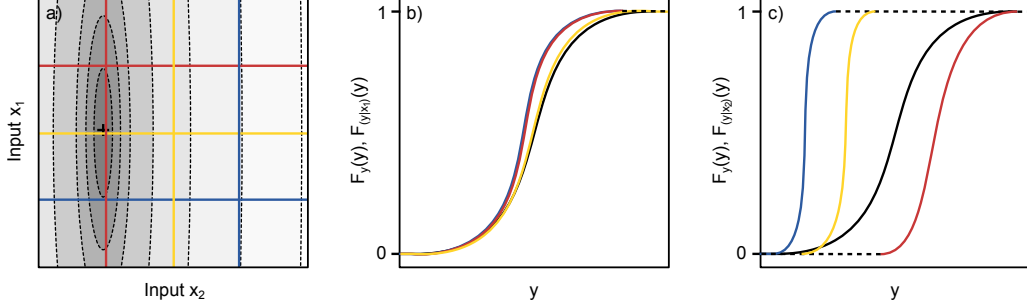


Figure 3.2: Example for the analysis of a two dimensional input response surface using PAWN. Panel a) shows a two dimensional input response surface of two uncorrelated model inputs, where the input x_1 has a low influence and input x_2 has a high influence on the target variable shown by the iso-lines. The colored lines along the two input dimensions are transects along which the conditional CDFs are assessed for the two inputs x_1 and x_2 . The panels b) and c) show the comparison of the conditional CDFs $F_{(y|x_i)}(y)$ to the unconditional CDF $F_y(y)$ (black line) for the inputs x_1 and x_2 , respectively.

PAWN expresses the sensitivity of the target variable y to the model inputs x_i by computing a distance measure between the unconditional CDF $F_y(y)$ where all model inputs are perturbed and the conditional CDF $F_{(y|x_i)}(y)$ where the model input of interest is fixed and all others are perturbed. Pianosi and Wagener (2015) proposed is the Kolmogorov-Smirnov test statistics as a distance measure. The distance $KS_j(x_i^j)$ between the CDFs for the model input x_i fixed at a value $x_i = x_i^j$ is defined as:

$$KS_j(x_i^j) = \left\| F_y(y) - F_{y|x_i, x_i=x_i^j}(y) \right\|_y \quad (3.6)$$

In the example of Fig. 3.2 the Eq. 3.6 results in three values of $KS_j(x_i^j)$ for the transects $j = 1 \dots 3$ along each of the two parameter dimensions of x_1 and x_2 . To assess the overall sensitivity considering all fixed values of x_i , the values of $KS_j(x_i^j)$ are summarized for all j sampling points to compute the PAWN index T_i for the model input x_i . Pianosi and Wagener (2015) suggested to employ the median or the maximum as a summary statistics.

$$T_i = \text{stat}_{x_i=x_i^1 \dots x_i^n} (KS_j(x_i^j)) \quad (3.7)$$

where stat is replaced by the employed summary statistics (e.g. median or max). Pianosi and Wagener (2015) introduced the PAWN sensitivity method using a specifically tailored sampling design to infer the PAWN indices T_i for continuous model inputs x_i . The proposed sampling scheme suggests to draw N_c

conditional samples at n randomly sampled points of each input variable x_i , where x_i is fixed at a value $x_i = x_i^j$ while all others are perturbed. Pianosi and Wagener (2018) extended the applicability of the PAWN sensitivity method to estimate T_i from a generic random sample of continuous model inputs. To approximate T_i the generic sample N is split into n segments along each model input dimension resulting in conditional samples N_c with an approximate size of N/n . The approximation of T_i presented in Pianosi and Wagener (2018) facilitates a comparison to other methods that allow generic sampling strategies and increases the computational efficiency of PAWN, as the generic sample can also be employed to compute the unconditional CDF, whereas Pianosi and Wagener (2015) requires an additional sample to compute the unconditional CDF.

Both, Pianosi and Wagener (2015) and Pianosi and Wagener (2018) considered continuous model inputs in a GSA. Yet, the implementation in the case study in chapter 5 requires an implementation of discrete inputs. With PAWN the sensitivity of a target variable to an input is assessed entirely based on the target variables' density distribution. Thus, PAWN facilitates to extend the method to an application with discrete model inputs. Fig. 3.3 provides a minimal toy example for sampling and subsetting of discrete model inputs to employ PAWN for SA. Fig. 3.3 a) illustrates three discrete nominal model inputs with different numbers of realizations for each input. The illustrated toy blocks act as individual model inputs in this example that can be assembled to a house. The colors of each toy block shape represent the individual representations for that input.

In the minimal example a random sample of $N = 8$ input combinations was drawn from the discrete input realizations and assembled to realizations of the system that is analyzed (different configurations of a toy house in Fig. 3.3 b)). To infer $KS_j(x_i)$ for all discrete values x_i^j of a model input x_i the sample N is split into subsets for all n_i discrete values, resulting in subsets of the size N/n_i on average (Fig. 3.3 c)). It is important to notice, that the subset size for discrete inputs with different numbers of realizations depends on the number of realizations n_i of a model input x_i , while the subsets resulting from the sampling scheme proposed by Pianosi and Wagener (2018) had an average size of N/n for all model inputs x_i .

The minimal example illustrated in Fig. 3.3 included a low number of possible input combinations and a small sample size of $N = 8$. The impact of n_i on the number of realizations in each subset $y|x_i, x_i = x_i^j$ becomes evident by looking at the example of input x_3 in Fig. 3.3. The input x_3 includes a set of $n_3 = 4$ realizations. Thus, each subset of x_3 contains on average $N/n_3 = 2$ input combinations (assembled houses). Yet, due to the low total number of samples $N = 8$, there is a high chance that a subset includes only one system representation, as it is illustrated for the third subset of x_3 in Fig. 3.3 c). Very low subset sizes eventually limit the analysis of that input with PAWN. In a practical application, the sample size must be therefore substantially larger than the largest number of realizations of the analyzed model inputs to reduce the impact of different input set sizes.

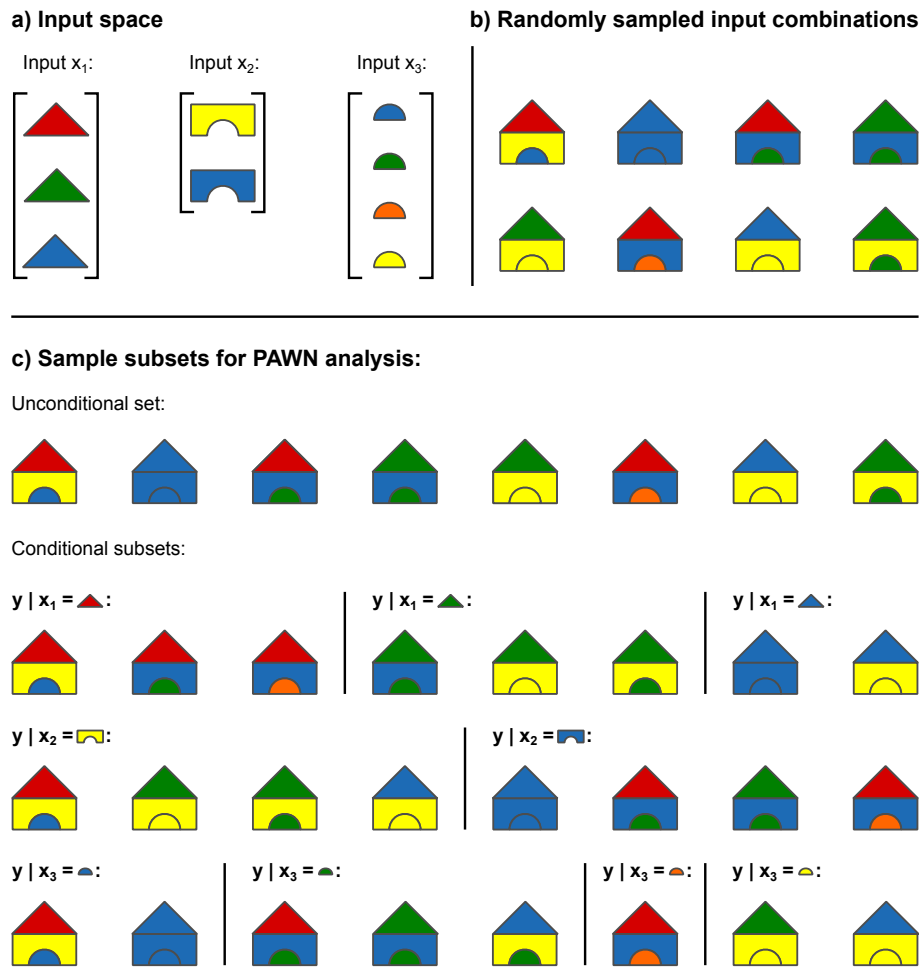


Figure 3.3: Example for sampling and subsetting of discrete model inputs for the implementation of PAWN for GSA. The illustrated toy blocks in panel a) act as individual model inputs that can be assembled to a house. The colors of each toy block shape represent the individual representations for that input. A random sample of input combinations is drawn and assembled to realizations of the analyzed system (toy houses) in panel b). Panel c) shows the unconditional set of the entire sample and the conditional sets for the realizations of all three inputs for an analysis with PAWN.

3.3.3 Workflow for UA and SA with discrete composite inputs

Although the two case studies greatly differ in attributes of the study setups, such as the complexity of the implemented model, or the analyzed target variables a general framework can be outlined for the analysis of the discrete composite model inputs that were performed in both studies. Fig. 3.4 provides a general overview of the workflow that was processed to analyze the uncertainties in the simulated model outputs and the influences of the model input realizations on the defined target variables in each study. Overall, the workflow can be separated into two main steps, a data pre-processing step, and the actual UA and SA framework.

The data pre-processing includes the data acquisition and the setup of one or several baseline models. In this step all data are collected that are necessary

to define the model structure that describes the simulated system. While the USLE model structure is predefined by the product of its six model inputs and thus does not require any further processing in this step, a SWAT model setup requires the input of layers for terrain, soil and land cover to define the models' HRU configuration and to determine the baseline model structure. In the case that a spatially distributed or semi-distributed model (as it is the case for SWAT) is employed and the model structure should be considered as an input in the SA analysis, the setup of multiple baseline models is required. In the following step the inputs are defined that are considered for the analysis in the UA and SA framework. The main challenge here is to clearly separate parts of a model that fully represent the respective input that is analyzed. For a model such as the USLE this separation of the individual parts of the model that define the respective inputs is a straight forward procedure as the model components are considered as independent linearly combined inputs. With more complex models, however, the separation of the model components into the individual model inputs can be non-trivial, as several defined inputs can affect same model components. Land cover change can affect the land cover that is assigned to an HRU, but can also affect the structural model setup and thus cause a conflict if both, land cover change and model structure are considered as inputs in the analysis. After a successful definition of the model inputs and the separation of model components, realizations for the defined inputs are generated. The realizations can for instance be generated based on different scenarios or by assigning uncertainties to the inputs.

For the implementation of the generated input realizations in the UA and SA framework, the input realizations are arranged in discrete input sets x_i with n_i realizations (as already illustrated in the minimal example in Fig. 3.3). Depending on the SA method that is implemented, N input combinations are sampled from the input sets by employing either a specifically tailored, or a random sampling design. The total number of required samples N is highly dependent on the selected SA method, the number of model inputs, and can also be dependent on the numbers of realizations n_i of the inputs x_i in the case of discrete inputs. The N sampled input combinations $x^{1\dots N}$ are assembled to N executable model setups $M^{1\dots N}$, that describe the system that should be analyzed (possibly under changed conditions from the baseline configuration). All assembled model realizations $M^{1\dots N}$ are used to simulate the output of interest $y(x)$, where the differences in the simulation results directly result from the impacts of the sampled input combinations $x^{1\dots N}$. The simulation outputs are used to calculate a defined target variable $crit = f(y)$ (or several target variables. The simulation output itself can also be considered as the target variable). Based on the simulation outputs $y^{1\dots N}(x)$ and/or the calculated target variables the simulation uncertainties that result from the model ensemble and the influences of the defined model inputs x_i on the simulated outputs and the target variables are evaluated.

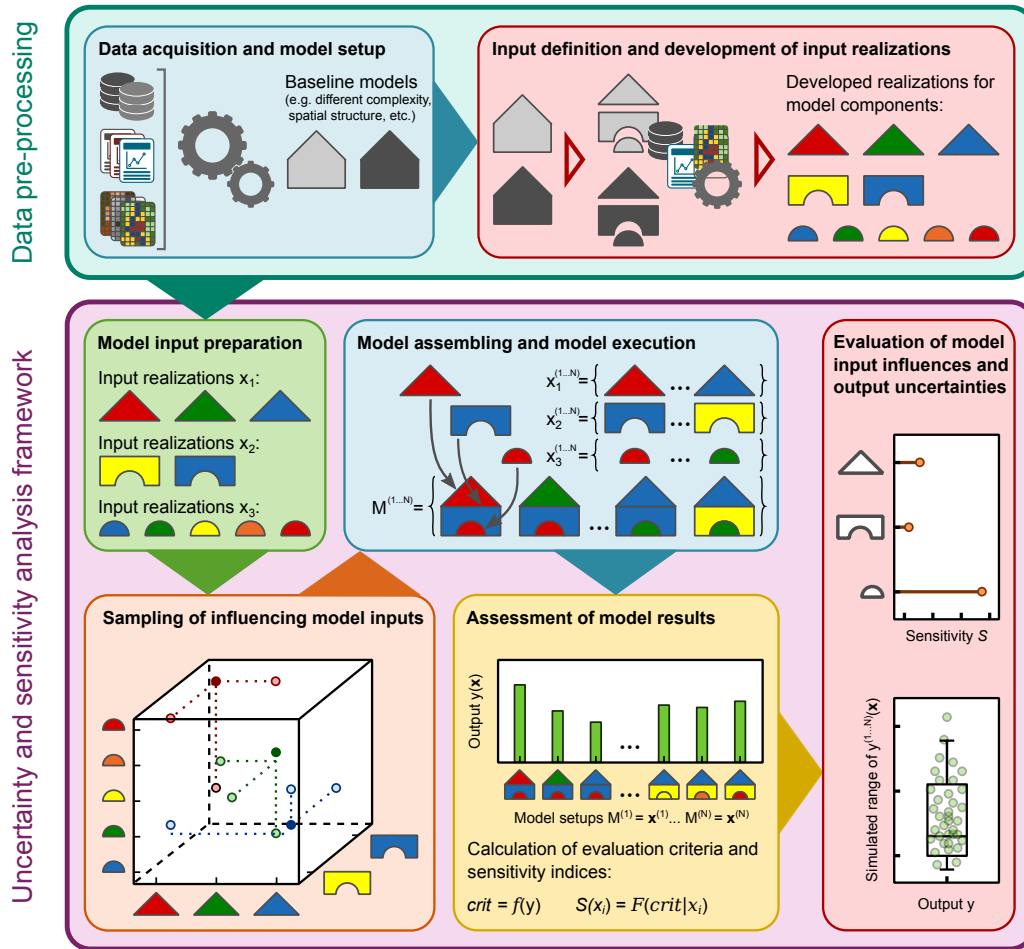


Figure 3.4: General workflow for the implementation of discrete composite model inputs in UA and SA.

Part II

CASE STUDIES

...in hydrologic modelling we concentrate on refining the computation of various hydrologically trivia while evading the difficult problems, "...our technological successes have simply made us more efficient at being stupid" (Welles, 1984).

— Vit Klemeš (1986)

SOIL LOSS ESTIMATION WITH DIFFERENT USLE REALIZATIONS

4.1 INTRODUCTION AND OBJECTIVES

Kinnell (2010) used a very provocative wording when he described the USLE as "*the most widely used, and misused, soil loss estimation equation in the world*". Though, the entirely empirical nature of the USLE model and its principally simple implementation facilitates a model application outside of the USLEs' predictive capability and makes the interpretation of how representative the developed USLE input factors are for a certain study setting infeasible. To repeat a central issue inherent in the USLE, it is relevant to note that the USLE model structure and the model parameters have been developed for conditions in the USA and entirely based on experimental data collected in the USA. Any adaptations of the USLE model inputs to regional conditions adopt the initial USLE model structure and neglect other empirical relationships that might meet any regional conditions better. Many published adaptations of USLE are well accepted due to their simple use. Yet, several published adaptations were not evaluated (see e.g. the method for the C factor calculation in Van der Knijff et al. (2000)). Eventually, any application of the USLE to conditions that is different from the plot experiments must be treated as a model extrapolation that is not supported by field data (Bosco et al., 2015; Favis-Mortlock, 1998).

It is well accepted that the USLE does not at all attempt to represent the physical processes to erode and transport soil particles, but empirically relates field properties to long term soil loss (Beven and Brazier, 2011; Kinnell, 2010). The USLEs' wide application does not distinguish it to be the best, or only option for soil loss estimation (Evans and Boardman, 2016b). Limitations of the USLE (but also other soil erosion models) have been well documented in the literature (see e.g. Boardman, 1996; Boardman, 2006). Jetten and Favis-Mortlock (2006), for example, summarize applications of the USLE in Europe, where the validation of calculated soil losses with observed data showed poor results (e.g., Favis-Mortlock, 1998; Bollinne, 1985). Kinnell (2010) reports a good performance of a locally adapted variant of the USLE in New South Wales, Australia, but documents the over-prediction of small soil losses and under-prediction of large soil losses when applied to larger domains with a higher variability in agricultural systems (Tiwari et al., 2000; Risse et al., 1993). A recent pan-European soil loss assessment started a broad discussion of the validity of the estimates when compared to in-field soil loss assessments in Great Britain (see the discussion in Panagos et al., 2015e; Evans and Boardman, 2016b; Panagos et al., 2016; Evans and Boardman, 2016a). Several authors question the applicability of the plot scale based USLE to the landscape scale (e.g., Boardman, 2006; Evans, 1995; Govers, 2011), particularly as in large domains other processes such as

gully erosion, bank erosion, or sediment deposition can dominate the erosion response (Govers, 2011). Evans (2013) concludes that the USLE can be helpful to identify the erosion potential or erosion hot spots, but fails to predict the exact magnitude of erosion.

The above criticism does not impede the wide application of the USLE. For large scale erosion assessments, the availability of large scale spatial data and methods to infer the USLE inputs facilitate its implementation in GIS (Govers, 2011) and therefore is an attractive option to assess soil erosion. The implementation of remote sensing (satellite) products advances large scale soil loss assessments, particularly in data scarce regions where observations are limited as well as in large domains where in-field data acquisition is infeasible (Alewell et al., 2019; Bosco et al., 2015). This procedure yielded several continental and global estimates of USLE input factors (e.g., Panagos et al., 2017; Panagos et al., 2015a; Panagos et al., 2015b; Panagos et al., 2015c; Vrieling et al., 2010) and soil loss assessments (e.g., Borrelli et al., 2017; Panagos et al., 2015e; Naipal et al., 2015; Yang et al., 2003; Van der Knijff et al., 2000) that were primarily derived from large scale (remote sensing) data products. The methods to compute realizations for the USLE inputs that were proposed in these (and other) large scale assessments attempt to employ data products that describe or are a proxy for features in the landscape (such as topography, or vegetation cover) to infer spatially distributed estimates for the USLE inputs. For each USLE input, various methods exist to generate the spatially distributed estimates for the USLE inputs that use different data sources (see e.g. the review of Benavidez et al., 2018). Thus, differing results in the realizations of a USLE input factor can follow from the different computational approaches. However, a typical setup of the USLE combines only one representation of each USLE input in a single model setup and therefore does not depict the variations in the soil loss calculations that may arise from different representations of the USLE input factors. Very few studies consider the impact of the different representations of the USLE inputs (e.g., Bosco et al., 2015) to account for the resulting ranges in calculated soil loss. Because of the multiplicative structure of the USLE, uncertainties in the input factors are decisive for the computation of the soil loss as they are also propagated by multiplication.

Model validation is a widely applied procedure in environmental modeling to gain confidence in a model setup. In a model validation calculated model outputs are compared and evaluated against observed data that was not used in any step of the model setup (Beven and Young, 2013; Young, 2001). Beven and Young (2013) further stress the importance of model falsification when a model fails to reproduce observations. For large scale soil loss assessments the possibilities to evaluate calculated soil losses, or spatially distributed estimates of the USLE inputs are very limited (Bosco et al., 2015; Van der Knijff et al., 2000). Typically, studies that monitored soil loss within the study domain rarely exist. Existing in-field data, however, entail issues of their spatial and temporal representativeness (Evans, 2013; Govers, 2011). Boardman (2006) questions the comparability of erosion plot data or in-stream sediment yields with soil losses at the catchment scale. Govers (2011) highlights that USLE estimates reflect long

time periods (Wischmeier and Smith (1965) e.g. recommended 20 years). Such time periods are usually not covered by a soil loss monitoring campaign. Eventually, USLE input factor estimates and large scale soil loss assessments are compared to very limited observation data (e.g., Borrelli et al., 2017; Vrieling et al., 2010; Moore, 1979) and in many cases no validation was carried out at all (e.g., Karamage et al., 2017; Van der Knijff et al., 2000).

As modelers we must acknowledge that any soil loss assessments that implements the USLE is highly uncertain and that the evaluation of soil loss estimates in large scale assessments face the limitations that were described above. This case study presents a systematic analysis of the uncertainties that result from different representations of USLE model inputs. Given the uncertain simulated soil losses on a large scale this case study addresses the capabilities and limitations of a model evaluation employing measured soil loss data. To approach the stated issues the following objectives were formulated and systematically addressed that are covered in the following sections of this chapter:

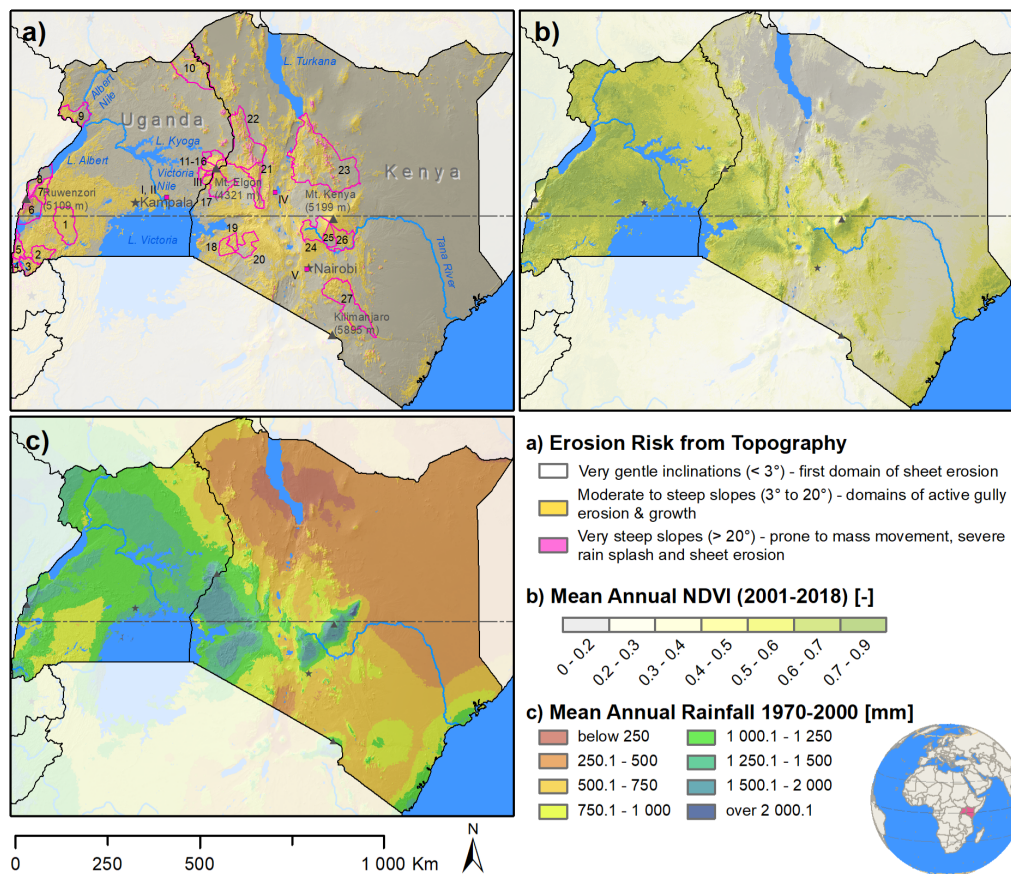
- i. What are the uncertainties in soil loss estimates that we can expect from the implementation of different model input realizations in the USLE model? How can we interpret uncertain soil loss estimates?
- ii. Which USLE model inputs contribute the most to the uncertainties of the soil loss estimates?
- iii. Can we compare the calculated soil loss estimates to in-field soil loss data? Does the evaluation enable us to reduce the uncertainties in the estimated soil losses?

The research questions are covered in a large scale soil loss assessment for Kenya and Uganda. The case study is structured in the following way: Methods to calculate USLE inputs that were widely used in previous large scale soil loss assessments were reviewed. In section 4.3 a set of standard methods for the generation of USLE inputs were selected and employed to generate spatially distributed estimates for the study domain. All combinations of the input factor realizations delineate a USLE model ensemble. The analysis of the USLE ensemble results is outlined in the sections 4.4.2, 4.5.1, and 4.6.1. In the sections 4.4.3, 4.5.2, and 4.6.1 the impact of the USLE input factors R , LS , K , and C on the calculated ranges of the soil loss estimates were analyzed in a spatial analysis. For selected erosion prone counties of Kenya and districts of Uganda, spatially aggregated mean soil loss estimates were analyzed and compared to the results on the administrative level for Uganda as presented in Karamage et al. (2017). The analysis and the comparison is presented and discussed in the sections 4.5.3 and 4.6.1. In the sections 4.5.4 and 4.6.2 the reported in-field erosion data from selected in-field erosion studies that were conducted in Kenya and Uganda were compared to the ensemble soil loss estimates derived with the USLE model ensemble.

4.2 STUDY REGION

The study area covers the countries of Kenya and Uganda, located in East Africa (Fig. 4.1). Overall the Sub-Saharan countries experienced drastic land degradation and a decrease in net-primary productivity of the land over the last decades (Bai et al., 2008). The dominant driver for land degradation in the horn of Africa is soil erosion by water (Jones et al., 2013). Large parts of Kenya and Uganda are generally prone to soil loss by water induced erosion.

In total, the study region covers an area of 821 405 km², of which 729 622 km² or 89% of the surface are analyzed, since lakes and other water bodies are excluded from the analysis. Additionally, 27 administrative units in both countries (Fig. 4.1a), Table 4.1) are analyzed in detail. The selection of the erosion prone administrative units is based on a visual analysis of Fig. 4.1a) and on local knowledge and on-site experience.



Data sources: DEM & hillshade: SRTM90m (Jarvis et al., 2008), NDVI: MODIS MOD13Q1 (Didan, 2015), Precipitation: WorldClim V2 (Fick and Hijmans, 2017)
Country boundaries, Cities, Mountains & Rivers: © Natural earth dataset, Administrative units: © Ugandan Bureau of Statistics & © Kenya National Bureau of Statistics,
Water surfaces: Carroll et al. (2009)

Figure 4.1: Study area covering the countries of Kenya and Uganda. A classification of the soil erosion risk after Ebisemiju (1988) (a), the mean annual MODIS NDVI as a proxy for vegetation cover (b), and mean annual rainfall (c) are plotted to characterize spatial properties of the study region. The boundaries for administrative units where the mean soil loss was assessed are shown with pink outlines in panel a). Locations of soil loss assessments from previous studies that were used for comparison are shown as pink squares.

The study region covers a wide range of factors influencing soil erosion. Fig. 4.1a) shows the potential erosion risk solely stemming from topography, based on thresholds by Ebisemiju (1988). Large areas with moderate to steep slopes ("moderate risk") are evident in the South-West of Uganda and in a north-to-south band in Kenya, where the Western or Gregory Rift as part of the Great Rift Valley transects the country. The area in Uganda is characterized by a hilly topography with low elevation differences. In contrast, the erosion prone regions in Kenya are mostly characterized by larger elevation differences, e.g. escarpments. Very steep slopes that exhibit a high risk of erosion from topography are evident around mountain massifs, e.g. Ruwenzori (5109 m a.s.l., Uganda), Mt. Elgon (4321 m a.s.l., Uganda and Kenya) or Mt. Kenya (5199 m a.s.l., Kenya). Additionally, high erosion risk prone areas are evident in the south-western corner of Uganda and along the Rift Valley in the northern part of Kenya. Fig. 4.1b) shows the mean annual MODIS NDVI (Didan, 2015) for the period 2001 to 2018 as a proxy for the vegetation cover. Higher values in NDVI show pixels with high vegetation cover, where a lower risk of water erosion due to ground cover can be assumed, and vice-versa. Kenya exhibits a large variability in NDVI with low values in the arid to semi-arid northern and south-eastern parts. Higher vegetation cover is present at the coast towards the Indian Ocean, around Mt. Kenya, but also around Lake Victoria in the western part of the country. Uganda shows a rather homogeneous vegetation distribution, with some semi-arid areas in the north-east showing a lower vegetation cover.

Fig. 4.1c) shows the long-term mean annual rainfall (based on WorldClim Version2 for the period 1970 to 2000, Fick and Hijmans, 2017) as a proxy for the erosivity by rainfall. This assumes that larger annual rainfall values lead to higher erosion rates. Rainfall and vegetation cover are clearly connected. Hence, a more homogeneous rainfall pattern is visible for Uganda. Drier areas in the south-west and north-east receive around 750 to 1000 mm yr⁻¹ of precipitation. The center of the country is wetter with around 1000 to 1500 mm yr⁻¹. In Kenya, wetter areas are evident around Lake Victoria and Mt. Kenya, receiving 1500 to 2000 mm yr⁻¹ or even higher. The northern part of the country only receives 250 to 500 mm yr⁻¹. Here, areas around Lake Turkana are very dry, with an annual precipitation of less than 250 mm yr⁻¹. In accordance with vegetation cover, the coast is wetter (1000 to 1250 mm yr⁻¹). Between the coast and the central highlands, a dry belt is visible (500 to 750 mm yr⁻¹).

4.3 ESTIMATION OF USLE MODEL INPUTS

To address the impact of different USLE input factor realizations on the simulation of the soil loss A , a set of realizations for each of the four USLE input factors R , K , LS , and C was generated. Methods to calculate the inputs were considered that were either used in previous large scale applications or that were specifically developed for Eastern Africa (or regions with similar climatic, topographic, and vegetation conditions). The implemented methods are described below. Further details to the input factor generation is provided in the supplementary materials section S.1. The support practice factor P was excluded from

Table 4.1: Terrain properties for administrative units analyzed in more detail. The locations are shown in Fig. 4.1a). The slope and elevation statistics are based on SRTM v4.1 90m DEM (Jarvis et al., 2008).

Nr.	Greater Region	Administrative unit	Area (km ²)	Slope		Elevation		
				min (°)	max (°)	mean (m)	min (m)	max (m)
Uganda								
1	-	Kiruhura	4636	4.39	28.96	1310	1178	1670
2	Lake Bunyoni	Ntungamo	2062	7.57	43.61	1497	1279	2224
3	Lake Bunyoni	Kabale	1740	14.79	46.15	1990	1355	2601
4	Lake Bunyoni	Kisoro	733	11.95	49.44	1983	1338	3861
5	Lake Bunyoni	Kanungu	1335	8.61	46.52	1388	912	2499
6	Ruwenzori	Kasese	3402	8.81	60.54	1493	878	5034
7	Ruwenzori	Kabarole	1825	8.01	48.94	1515	626	3996
8	Ruwenzori	Bundibugyo	2265	5.65	52.24	1002	612	4659
9	-	Nebbi	2922	3.71	34.70	1039	612	1873
10	-	Kaabong	7301	5.87	61.41	1416	834	2720
11	Mt. Elgon	Bukwo	529	12.28	53.35	2420	1253	4204
12	Mt. Elgon	Kapchorwa	1215	8.00	53.39	1823	1062	4265
13	Mt. Elgon	Sironko	1106	7.15	60.43	1619	1045	4280
14	Mt. Elgon	Bududa	253	16.99	61.70	2103	1216	4314
15	Mt. Elgon	Mbale	522	5.50	71.23	1288	1083	2351
16	Mt. Elgon	Manafwa	606	8.34	57.77	1608	1139	3319
Kenya								
17	Mt. Elgon	Bungoma	3036	5.15	45.12	1859	1213	4304
18	S-W Kenya	Kisii	1353	6.24	32.83	1750	1394	2190
19	S-W Kenya	Nyamira	897	6.70	31.99	1888	1509	2214
20	S-W Kenya	Bomet	2384	5.14	30.29	1997	1693	2465
21	Cherangani Hills	Elgeyo-Marakwet	3058	9.97	60.70	2122	920	3517
22	Cherangani Hills	West Pokot	9328	8.70	67.15	1443	691	3524
23	-	Samburu	21 250	6.81	66.83	1185	296	2834
24	Mt. Kenya	Nyeri	3380	7.39	54.88	2284	1210	5035
25	Mt. Kenya	Kirinyaga	1491	4.41	45.27	1619	1057	4747
26	Mt. Kenya	Embu	2780	4.89	38.56	1191	520	4760
27	-	Makueni	8297	3.84	58.42	1065	404	2120

the analysis, as large scale data to derive estimates for P are very limited. Previous large scale studies, for example, inferred the P factor from relationships with the land use (e.g., Yang et al., 2003), or implemented a global estimate of

P for the entire study region (e.g., Karamage et al., 2017), or did not consider the P factor (e.g., Borrelli et al., 2017).

4.3.1 Rainfall erosivity factor R

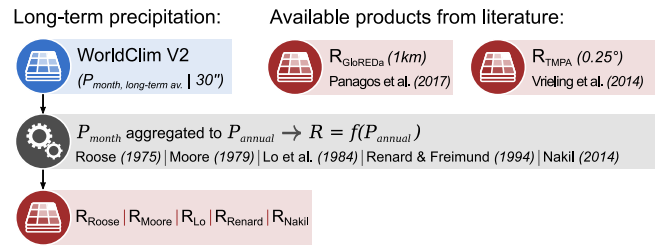
The rainfall erosivity factor R relates the intensity of rainfall events to the kinetic energy that is available to erode soil particles (Wischmeier and Smith, 1978; Panagos et al., 2015a). Rainfall intensity records are hardly available for large domains. Thus, large scale erosion studies usually employ long-term annual average precipitation sums to infer R . Several large scale precipitation data products are available that provide precipitation sums for different time intervals and on different spatial scales. WorldClim Version2 (Fick and Hijmans, 2017) for example provides long-term monthly precipitation sums with a spatial resolution of $30''$. Other products such as TRMM are available with a high temporal resolution of 3 h, but are provided with a much coarser resolution of 0.25° . Several methods that require long-term annual precipitation as input. Thus long-term monthly precipitation sums from WorldClim Version2 were implemented and aggregated to long-term annual precipitation sums. The following five methods that relate long-term mean annual precipitation (P_{annual}) to R were considered, that differ in their type of mathematical relationship. Each pixel value from the aggregated WorldClim Version2 data set for the region of Kenya and Uganda was implemented in each of the selected methods to compute R factor estimates. The workflow to derive the realizations is shown in Fig. 4.2a). Table 4.2 summarizes the mathematical relationships proposed with the respective methods.

Roose (1975) and Moore (1979) developed relationships between mean annual rainfall sums and R based on station data in Western and Eastern Africa, respectively. Karamage et al. (2017) used the method developed by Lo et al. (1985) to calculate R for Uganda. The method of Renard and Freimund (1994) was developed for USA precipitation station data and has been employed in global applications (e.g., Naipal et al., 2015; Yang et al., 2003). Nakil (2014) developed a relationship between precipitation and R for the highly variable rainfall patterns of the west coast of India. Additionally, recent products by Panagos et al. (2017) and Vrieling et al. (2014) were considered that inferred R estimates from high temporal precipitation data. While Panagos et al. (2017) derived global estimates for R on a 1 km grid based on a large global rainfall intensity data set to assemble the GloREDA data base, Vrieling et al. (2014) used the 3 hourly TRMM Multi-satellite Precipitation Analysis (TMPA) product (Huffman et al., 2007) to infer R estimates for the African continent in a 0.25° spatial resolution. In total seven realizations for R were included in this study (Fig. 4.2 a)).

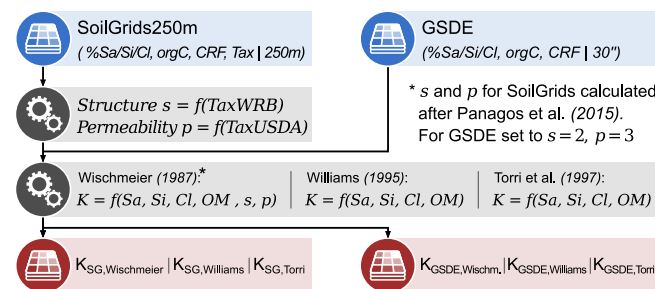
4.3.2 Soil erodibility factor K

The soil erodibility factor K describes the tendency of a soil to erode due to the erosive force of precipitation or surface runoff and can be related to soil physical and chemical properties (Panagos et al., 2014). Direct assessments of the soil

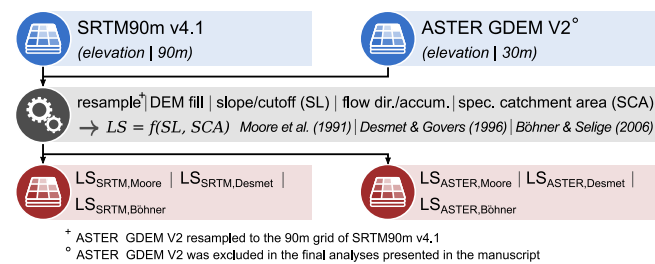
a) Rainfall erosivity factor (R): 7 realizations



b) Soil erodibility factor (K): 6 realizations



c) Slope-length factor (LS): 6 (3)^o realizations



d) Cover Management factor (C): 6 realizations

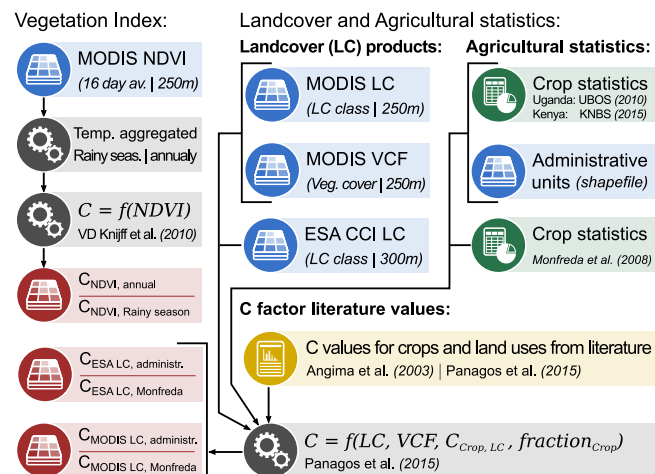


Figure 4.2: Methodological framework to generate the realizations of the USLE model input factors R, K, LS, and C.

Table 4.2: Methods to calculate the rainfall erosivity factor R that were implemented in the study.

Realization	Definition	References
R_{Roose}	$R = 0.5 \cdot P_{annual} \cdot 17.3$, (value 17.3 conversion factor from imperial to SI units)	Roose (1975), Morgan (2009)
R_{Moore}	$KE_{15} = 11.46 \cdot P_{annual} - 2226$, $R = 0.0029 \cdot KE - 26.0$, $R_{SI} = 17.02 \cdot R$, (value 17.02 conversion factor from imperial to SI units)	Moore (1979)
R_{Lo}	$R = 3.48 \cdot P_{annual} + 38.46$	Lo et al. (1985), Karamage et al. (2017)
R_{Renard}	$R = 0.0483 \cdot P_{annual}^{1.61}$, $P_{annual} \leq 850\text{mm}$, $R = 587.8 - 1.219 \cdot P_{annual} + 0.004105 \cdot P_{annual}$, $P_{annual} \geq 850\text{mm}$	Renard and Freimund (1994), Ferro et al. (1991), Yu and Rosewell (1996), Naipal et al. (2015), Yang et al. (2003)
R_{Nakil}	$R = 839.15 \cdot \exp(P_{annual})$	Nakil (2014)
R_{TMPA}	R Estimates for Africa derived from 3-hourly rainfall TRMM-TMPA data with 0.25 ° spatial resolution employing the procedure described in Renard and Freimund (1994)	Vrieling et al. (2014)
$R_{GloREDA}$	R estimates from 3540 stations records worldwide using RBF and multiple global input features for global interpolation on a 1 km grid	Panagos et al. (2017)

erodibility are only available at a plot scale. Typically, these values were derived from bare soil plot experiments, where the rainfall intensity was measured and the topographic properties are known (Kinnell, 2010). Large scale erosion studies employ transfer functions that infer the soil erodibility from soil properties that are easier to acquire. Several global soil data products are available that provide physical and chemical soil properties with different spatial resolution. Two recently compiled and updated soil information products with a high spatial resolution are SoilGrids250m (Hengl et al., 2017) and the Global Soil Dataset for use in Earth System Models (GSDE, Shangguan et al., 2014) that were implemented in this study. SoilGrids250m is a soil information system that employs a large data base of global soil profile data providing physical and chemical parameters for over 150 000 soil profiles worldwide. Employing global spatial features, such as global terrain information, or global satellite products, physical and chemical soil parameters were estimated on a 250 m grid for the entire land mass of the world. The GSDE harmonizes the Soil Map of the World together with national and regional soil databases and soil mapping data in a comprehensive global soil data product providing estimates for physical and chemical soil parameters in several depths with a spatial resolution of 30''.

Table 4.3: Realizations for the soil erodibility factor K that were developed based on different soil data bases and methods for the computation of K .

Realization	Definition	References
$K_{SoilGrids,Wischmeier}$	Mean values of sand, silt, and clay fractions for the soil depths 0 to 10 cm derived from SoilGrids250m layers employed in the equation of Wischmeier and Smith (1978) and applying the corrections described in Panagos et al. (2014) (additionally employing the coarse fractions layer from SoilGrids250m). The soil structure s was derived from the World Reference Base for Soil Resources (WRB) soil classification layer available from SoilGrids250m and a corresponding structure classification based on Baruth et al. (2006) as described in Panagos et al. (2014) or Borrelli et al. (2017)	Panagos et al. (2014), Panagos et al. (2015e), Borrelli et al. (2017)
$K_{SoilGrids,Williams}$	Mean values of sand, silt, clay, and organic carbon percentages for the soil depths 0 to 10 cm derived from SoilGrids250m layers employed in the equation of Williams (1995)	Karamage et al. (2017), Yang et al. (2003)
$K_{SoilGrids,Torri}$	Mean values of sand, silt, clay, and organic carbon fractions for the soil depths 0 to 10 cm derived from SoilGrids250m layers employed in the equation of Torri et al. (1997)	Yang et al. (2003), Naipal et al. (2015), Torri et al. (1997)
$K_{GSDE,Wischmeier}$	Mean values of sand, silt, and clay fractions for the soil depths 0 to 10 cm derived from SoilGrids250m layers employed in the equation of Wischmeier and Smith (1978) and applying the corrections described in Panagos et al. (2014) (additionally employing the coarse fractions layer from GSDE). The soil structure s and permeability p were set to 2 and 3 as default values, respectively, as shown in Tamene and Le (2015)	Tamene and Le (2015)
$K_{GSDE,Williams}$	Mean values of sand, silt, and clay fractions for the soil depths 0 to 10 cm derived from GSDE layers employed in the equation of Williams (1995)	
$K_{GSDE,Torri}$	Mean values of sand, silt, clay, and organic carbon fractions for the soil depths 0 to 10 cm derived from GSDE layers employed in the equation of Torri et al. (1997)	Yang et al. (2003), Naipal et al. (2015), Torri et al. (1997)

Layers of mass fractions of sand S_a , silt S_i , and clay C_l , the soil organic carbon content $orgC$ and the fraction of coarse fragments CRF were acquired for the available soil depths and weighted average values for 0 to 10 cm were calculated. The layer acquisition and the computation with the SoilGrids250m layers was performed using the R package `soilgridr` (Schürz, 2020a). The aggregated soil layers were used in three transfer functions that were employed in previous large scale studies to compute K . Table 4.4 lists the three methods and their equations for the computation of K . The method of Wischmeier and Smith (1978) was implemented while following the procedure suggested by Panagos

et al. (2014) and Borrelli et al. (2017) to compute K from the SoilGrids250m layers. The method of Wischmeier and Smith (1978) requires S_a , S_i , Cl and organic matter content OM as inputs. Additionally, information on soil structure s and soil permeability p is relevant. Borrelli et al. (2017) derived these properties from soil classes according to the World Reference Base for Soil Resources (WRB) and the USDA soil texture classification systems which are available for SoilGrids250m. The values for s and p according to Borrelli et al. (2017) are summarized in the Appendix Section A.2 in the Tables A.1 and A.2. The GSDE does not provide soil class layers, nor does it give any information on the soil structure. Thus, the parameters s and p were kept constant when using the GSDE as input, following a procedure by Tamene and Le (2015). The other two methods that were implemented to infer K from soil properties were the methods of Williams (1995) and Torri et al. (1997). Both methods require values of S_a , S_i , Cl and OM as inputs. The soil products SoilGrids250m and GSDE in combination with three transfer functions resulted in six realizations of the K factor. Table 4.3 summarizes the six developed realizations for the K factor and Fig. 4.2b) illustrates the workflows for the computation of K .

Table 4.4: Methods to calculate the soil erodibility factor K that were implemented in the study.

Author	Equations
Wischmeier and Smith (1978)	$K = 0.1317 \cdot \frac{0.00021 \cdot M^{1.14} \cdot (12 - orgC) + 3.25 \cdot (s - 2) + 2.5 \cdot (p - 3)}{100}$ $M = (m_{Silt} + m_{vfSand}) * (100 - m_{Clay})$
Williams (1995)	$K = 0.1317 \cdot f_{cSand} \cdot f_{Cl-Si} \cdot f_{orgC} \cdot f_{hiSand}$ $f_{cSand} = 0.2 \cdot 0.3e^{-0.0256 \cdot m_{Sa} \cdot (1 - \frac{m_{Silt}}{100})}$ $f_{Cl-Si} = \frac{m_{Silt}}{m_{Clay} + m_{Silt}}$ $f_{orgC} = 1 - \frac{0.0256 \cdot orgC}{orgC + e^{3.72 - 2.95 \cdot orgC}}$ $f_{hiSand} = 1 - \frac{0.7 \cdot SN}{SN + e^{-5.51 + 22.9 \cdot SN}}$ $SN = 1 - \frac{m_{Sand}}{100}$
Torri et al. (1997)	$0.0293 \cdot (0.65 - D_g + 0.24 \cdot D_g^2) \cdot f_{orgC,Clay}$ $D_g = 0.01 \cdot (-3.5 \cdot m_{Sand} - 2.0 \cdot m_{Silt} - 0.5 \cdot m_{Clay})$ $f_{orgC,Clay} = e^{-0.0021 \cdot \frac{orgC}{m_{Clay}/100} - 0.00037 \cdot (\frac{orgC}{m_{Clay}/100})^2 - 4.02 \cdot \frac{m_{Clay}}{100} + 1.71 \cdot (\frac{m_{Clay}}{100})^2}$

4.3.3 Slope length and slope steepness factor LS

The slope length and slope steepness factor LS represents the influence of the terrain topography on soil erosion, where L accounts for impacts of the slope length and S accounts for the steepness of a slope (Panagos et al., 2015b). L and S are unitless inputs that can have values equal to and greater than 0. Values different to 1 imply conditions that are different to the unit plot (Kinnell, 2010). Although, initially treated as two separate model inputs, L and S are treated as one combined terrain parameter in newer approaches.

A Digital Elevation Model (DEM) is the basis to derive the LS factor. Several global DEM products exist, whereby many products are derived from the use of satellite based sensors that provide elevation with different spatial resolutions.

In this study the two satellite mission products SRTM v4.1 90m DEM (Jarvis et al., 2008) with a 90 m resolution and ASTER GDEM V2 (NASA/METI/AIST/Japan Spacesystems, and US/Japan ASTER Science Team, 2009) with a 30 m resolution were implemented. ASTER GDEM V2 data was aggregated and projected to the 90 m grid of SRTM v4.1 for comparability, but also because the computation capacities were insufficient to calculate soil erosion rates on a 30 m grid for the study extent. Three methods were applied from Moore et al. (1991), Desmet and Govers (1996), and Böhner and Selige (2006). All three methods are available as routines from the System for Automated Geoscientific Analyses (SAGA) v. 2.1.4 (Conrad et al., 2015).

Table 4.5: Realizations for the slope length and slope steepness factor LS that were developed based on different DEM products and methods for the computation of LS .

Realization	Definition	References
$LS_{SRTM,Moore}$	Slope and Catchment Area derived from SRTM90m V4.1 implemented in the method of Moore et al. (1991)	Bosco et al. (2015)
$LS_{SRTM,Desmet}$	Slope and Catchment Area derived from SRTM90m V4.1 implemented in the method of Desmet and Govers (1996)	Borrelli et al. (2017)
$LS_{SRTM,Boehner}$	Slope and Catchment Area derived from SRTM90m V4.1 implemented in the method of Böhner and Selige (2006)	-
$LS_{ASTER,Moore}$	Slope and Catchment Area derived from ASTER GDEM V4 implemented in the method of Moore et al. (1991)	Bosco et al. (2015)
$LS_{ASTER,Desmet}$	Slope and Catchment Area derived from ASTER GDEM V4 implemented in the method of Desmet and Govers (1996)	Karamage et al. (2017), Borrelli et al. (2017)
$LS_{ASTER,Boehner}$	Slope and Catchment Area derived from ASTER GDEM V4 implemented in the method of Böhner and Selige (2006)	-

Together with the two DEM products six realizations of the LS factor (Fig. 4.2c)) were computed. Intermediate steps such as the reprojection of the ASTER GDEM V2, DEM fill, the calculation of flow direction or flow accumulation were processed in ArcMap 10.2 (ESRI, 2012). In the calculation of LS using the method of Desmet and Govers (1996) the steps described in Panagos et al. (2015b) were followed. The use of ASTER GDEM v2 introduced strong noise in the computed LS layers that results from artifacts in the remote sensing data. Particularly, the computed soil erosion in flat areas was strongly affected by the noise signal, rendering the result as being unusable. Thus, the LS realizations using ASTER GDEM v2 in the analysis were excluded. Thus, only the three LS factor realizations that included SRTM v4.1 90m as base data were considered in the following analyses. Table 4.5 summarizes all six realizations of the LS factor. The workflow to generate the LS factor realizations are illustrated in Fig. 4.2. c)).

4.3.4 *Cover management factor C*

Vegetation cover is essential to control soil erosion (Van der Knijff et al., 2000). The management of agricultural land can mitigate or increase soil erosion (Panagos et al., 2015c). The cover management factor C subsumes the impacts of vegetation cover and land management on soil erosion (Wischmeier and Smith, 1978; Panagos et al., 2015c). The C factor relates the soil loss from land with a specific vegetation cover and where specific management practices were applied to the soil loss that would result from clean-tilled, continuous fallow land (Wischmeier and Smith, 1978; Karamage et al., 2017; Panagos et al., 2015c). For large scale studies two main approaches to compute C (Fig. 4.2d)) can be identified.

One group of methods employ vegetation indices from satellite based remote sensing products to infer C . The most relevant vegetation indices that were implemented in the literature are the Leaf Area Index (LAI) (see e.g. the implementation by Claessens et al. (2008)) and the NDVI (with multiple applications, see e.g., Karamage et al., 2017; Naipal et al., 2015; Tamene and Le, 2015; Van der Knijff et al., 2000). All recent implementations of the NDVI to infer C employ the method of Van der Knijff et al. (2000) who proposed a non linear relationship between NDVI and C :

$$C = \exp\left(-\alpha \frac{NDVI}{\beta - NDVI}\right) \quad (4.1)$$

where C is the resulting unitless C factor value, $NDVI$ is the MODIS NDVI pixel value, and α and β are shape parameters that tune the mathematical relationship. Without providing any basis, Van der Knijff et al. (2000) suggested to set $\alpha = 1$ and $\beta = 2$. These values remained to be the default values in the literature. To compute C from NDVI in this study 16 day MODIS NDVI averages (Didan, 2015) from 2000 to 2012 were acquired and aggregated to mean NDVI layers. Two different aggregations were applied, where one calculated the annual mean NDVI (see e.g., Van der Knijff et al., 2000; Tamene and Le, 2015) and the second one calculated the mean NDVI averages over the two rainy seasons March to May and October to November as proposed by Karamage et al. (2017). Both long-term mean NDVI layers were used to compute C factor realizations using Eq. 4.1.

The second group of methods to infer C that is frequently seen in the literature joins land cover classification products with agricultural statistics and C factor literature values to compile a continuous C factor layer (e.g., Borrelli et al., 2017; Panagos et al., 2015c; Bosco et al., 2015; Yang et al., 2003). To follow such type of procedure, two land cover products, the MODIS Collection 5 LC with a spatial resolution of 250 m (Channan et al., 2014; Friedl et al., 2010) and the ESA CCI LC Map v2.0.7 with a spatial resolution of 300 m (ESA, 2017) served as base layers for the join with agricultural statistics and C factor literature values. Two agricultural statistics were used that provide information on crop areas at different spatial scales. i) National agricultural surveys for Kenya on ward level (KNBS, 2015) and for Uganda on county level (UBOS, 2010) were harmonized. ii) Monfreda et al. (2008) provides global gridded crop shares of the 175

dominant crops of the world with a spatial resolution of 5'. C factor literature values from Panagos et al. (2015c) and Angima et al. (2003) were assigned to all crops found in the national agricultural surveys and the grid layers from Monfreda et al. (2008). The C factor literature values are summarized in Table 4.6. A grouping of all 175 crops listed in Monfreda et al. (2008) to the summarized crop groups in Table 4.6 can be found in Table A.3 in the Appendix. The grouping of the crops from Monfreda et al. (2008) was done according to Borrelli et al. (2017). Based on the crop shares in the administrative units of Kenya and Uganda and for the crop shares in each grid cell of Monfreda et al. (2008), weighted average C factor values were calculated as proposed in Panagos et al. (2015c):

$$C_{Crop,(x,y)} = \sum_{i=1}^n C_i \cdot fraction_{i,(x,y)} \quad (4.2)$$

where $C_{Crop,(x,y)}$ is the weighted crop C factor for the location (x, y) , C_i is the C factor of the crop i , n is the total number of crops, and $fraction_{i,(x,y)}$ is the calculated fraction of the area cultivated with crop i at the location (x, y) .

C values for non agricultural land uses of the MODIS LC were estimated according to Panagos et al. (2015c) varying the C values for forest between boundaries based on the MODIS vegetation continuous fields (VCF) tree cover product:

$$C_{nonAgri,(x,y)} = C_{LC,low} + (\max(C_{LC,high}) - \min(C_{LC,low})) \cdot (1 - VCF_{(x,y)}) \quad (4.3)$$

where $C_{nonAgri,(x,y)}$ is resulting C factor for non agricultural land uses at the location (x, y) , $C_{LC,high}$ and $C_{LC,low}$ are the upper and lower boundaries of the C factor for the respective land cover LC (see Table 4.7 for C value ranges), and $VCF_{(x,y)}$ is the MODIS VCF vegetation cover fraction in the range of 0 to 1 at the location (x, y) .

ESA CCI LC classifies the land cover as shares between different land uses (e.g. Mosaic cropland (>50%) / natural vegetation (tree, shrub, herbaceous cover) (<50%)). In this case, C values were estimated by calculating weighted averages between the calculated average C values for agricultural areas and literature values (Panagos et al., 2015c) for non agricultural land uses according to the given fractions of the land cover classes:

The calculated average C values according to the crop shares and the non agricultural land uses were superimposed with the two employed land cover products MODIS Land Cover and ESA CCI LC. The combination of the two land cover products and the two agricultural statistic products resulted in four realizations for the C factor.

$$C_{ESALC,(x,y)} = C_{Crop,(x,y)} \cdot w_{Crop,(x,y)} + C_{LC,(x,y)} \cdot w_{LC,(x,y)} \quad (4.4)$$

where $C_{ESALC,(x,y)}$ is resulting C factor for the mixed land uses according to ESA CCI-LC at the location (x, y) , $C_{Crop,(x,y)}$ is the calculated average C factor

Table 4.6: *C* factor literature values from Panagos et al. (2015c) and Angima et al. (2003) for crop groups. The values show the grouping of the 175 crops from Monfreda et al. (2008) according to Borrelli et al. (2017).

Value	Crop group	Label	C value
1	Cereal Grains	cereal	0.20
1.1	Maize	maize	0.38
1.2	Rice	rice	0.15
2	Legume Vegetables	veg_legume	0.32
3	Root and Tuber Vegetables	veg_root	0.34
4	Fruit Vegetables	veg_fruit	0.25
5	Cucurbit Vegetables	veg_cucurbit	0.25
6	Bulb Vegetables	veg_bulb	0.30
7	Leafy Vegetables	veg_leaf	0.25
7.1	Tobacco	tobacco	0.50
8.1	Mixed Legumes	for_legume	0.15
8.2	Mixed grasses	for_grass	0.10
9.1	Grapes	grape	0.35
9.2	Hops	hop	0.42
10	Oilseed Group	oilseed	0.25
10.1	Cotton	cotton	0.40
11	Fibre Crops	fibre	0.28
12	Berries Group	berry	0.15
12.1	Strawberries	strawberry	0.20
13.1	Shrubs Herbs and Spices	herb_spice	0.15
13.2	Coffee	coffee	0.20
14	Trees/Fruit Tree	tree	0.15

value for the crops at the location (x, y) based on Eq. 4.2, $C_{LC,(x,y)}$ is the *C* factor value for the non agricultural land use at the location (x, y) , and the weights $w_{Crop,(x,y)}$ and $w_{LC,(x,y)}$ are the weights of the crops and non agricultural land uses according to Table 4.8.

4.4 SOIL LOSS ESTIMATION AND ANALYSIS

4.4.1 Estimation of soil loss

In total 7, 6, 6 (3), and 6 realizations were generated for the USLE input factors R , K , LS , and C , respectively. The combination of all input factors to assemble USLE model setups resulted in 1512 realizations of the USLE model. The LS factor realizations that were generated with the ASTER GDEM V2 were however excluded from the model ensemble, as they showed large noise ratios and the number of analyzed USLE model setups was therefore halved to 756. For the overlay of the generated USLE input layers, all layers were reprojected to the grid of the SRTM v4.1 90 m DEM and the long-term mean annual soil loss A was

Table 4.7: *C* factor value ranges for non agricultural land uses from Panagos et al. (2015c) and the corresponding MODIS Collection 5 LC land cover classes.

Value	Label	C_{min}	C_{max}	w_{Crop}	w_{LC}
0	Water	-	-	0	1
1	Evergreen Needleleaf forest	0.0001	0.003	0	1
2	Evergreen Broadleaf forest	0.0001	0.003	0	1
3	Deciduous Needleleaf forest	0.0001	0.003	0	1
4	Deciduous Broadleaf forest	0.0001	0.003	0	1
5	Mixed forest	0.0001	0.003	0	1
6	Closed shrublands	0.01	0.15	0	1
7	Open shrublands	0.01	0.15	0	1
8	Woody savannas	0.01	0.15	0	1
9	Savannas	0.01	0.15	0	1
10	Grasslands	0.01	0.15	0	1
11	Permanent wetlands	-	-	0	1
12	Croplands	0	0	1	0
13	Urban built-up	-	-	0	1
14	Cropland/Natural vegetation mosaic	0.0001	0.05	0.8	0.2
15	Snow and ice	-	-	0	1
16	Barren or sparsely vegetated	0.1	0.5	0	1
254	Unclassified	-	-	0	1
255	Fill Value	-	-	0	1

calculated for all model combinations in the study region of Kenya and Uganda using Eq. 2.1.

4.4.2 Analysis of spatially distributed soil loss estimates

The ensemble of 756 spatially distributed soil loss estimates with spatial resolution of 90 m were summarized in each grid cell employing descriptive statistical measures. In each grid cell mean and median values were calculated to estimate an average soil loss from the USLE model ensemble. The range of the minimum and maximum soil loss A in a grid cell indicates the variation of the ensemble simulations in a grid cell (i.e. the disagreement between the model setups).

A common concept in the erosion literature is to relate soil loss to soil formation rates and therefore classify the soil loss as sustainable (tolerable) or non-sustainable (e.g. Blanco-Canqui and Lal, 2008; Montgomery, 2007; Van-Camp et al., 2004), or to group soil loss based on the severity of soil removal (e.g. Zachar, 1982; FAO-PNUMA-UNESCO, 1980). Suggested tolerable levels of soil loss (T) vary between 5 and 12 tons $ha^{-1} yr^{-1}$ on a global scale (Montgomery, 2007; Blanco-Canqui and Lal, 2008; Zachar, 1982). Karamage et al. (2017), Barmutaze (2015), Morgan (2009), or Lufafa et al. (2003) used 10 tons $ha^{-1} yr^{-1}$ as threshold value T for studies conducted in Eastern Africa. For soil loss levels larger than T the soil loss classification according to FAO-PNUMA-UNESCO

Table 4.8: *C* factor value values and weights for agricultural and non agricultural land uses for the use with the ESA CCI LC Map v2.0.7 together with the corresponding land cover classes from ESA CCI LC Map v2.0.7.

Value	Label	C_{LC}	w_{Crop}	w_{LC}
10	Cropland	0	1	0
11	Crop, herb cover	0.1	0.8	0.2
12	Crop, Tree, shrub cover	0.003	0.8	0.2
20	Crop irrigated or post flood	0	1	0
30	Mosaic cropland (>50 %) / natural vegetation (tree, shrub, herbaceous cover) (<50 %)	0.0265	0.75	0.25
40	Mosaic natural vegetation (tree, shrub, herbaceous cover) (>50 %) / cropland (<50 %)	0.0265	0.25	0.75
50	Tree cover, broadleaved, evergreen, closed to open (>15 %)	0.0016	0	1
60	Tree cover, broadleaved, deciduous, closed to open (>15 %)	0.0016	0	1
61	Tree cover, broadleaved, deciduous, closed (>40 %)	0.0004	0	1
62	Tree cover, broadleaved, deciduous, open (15 % – 40 %)	0.0027	0	1
70	Tree cover, needleleaved, evergreen, closed to open (>15 %)	0.0016	0	1
90	Tree cover, mixed leaf type (broadleaved and needleleaved)	0.0004	0	1
100	Mosaic tree and shrub (>50 %) / herbaceous cover (<50 %)	0.08	0	1
110	Mosaic herbaceous cover (>50 %) / tree and shrub (<50 %)	0.08	0	1
120	Shrubland	0.08	0	1
122	Deciduous shrubland	0.08	0	1
130	Grassland	0.08	0	1
150	Sparse vegetation (tree, shrub, herbaceous cover) (<15 %)	0.3	0	1
152	Sparse shrub (<15 %)	0.3	0	1
153	Sparse herbaceous cover (<15 %)	0.4	0	1
160	Tree cover, flooded, fresh or brakish water	0.003	0	1
170	Tree cover, flooded, saline water	0.003	0	1
180	Shrub or herbaceous cover, flooded, fresh/saline/brakish water	0.15	0	1
190	Urban areas	0	0	1
200	Bare areas	0.5	0	1
201	Consolidated bare areas	0.15	0	1
202	Unconsolidated bare areas	0.5	0	1

(1980) (as implemented e.g. in Hernando and Romana (2015) or Olivares et al. (2016)) were implemented, where a soil loss between 10 and 50 tons ha⁻¹ yr⁻¹ is considered to be moderate, a soil loss between 50 and 200 tons ha⁻¹ yr⁻¹ to be high, and a soil loss larger than 200 tons ha⁻¹ yr⁻¹ to be severe. In each grid cell the simulated soil losses from the 756 USLE model setups were classified into the four defined soil loss classes and calculated the frequencies for each soil loss class as follows:

$$f_{i,m,n} = \begin{cases} 0 & \text{if } A_{i,m,n} \notin [A_{class,lower}; A_{class,upper}) \\ 1 & \text{if } A_{i,m,n} \in [A_{class,lower}; A_{class,upper}) \end{cases} \quad (4.5)$$

$$f_{m,n} = \frac{\sum_{i=1}^N f_{i,m,n}}{N} \quad (4.6)$$

where $f_{m,n}$ is the frequency of models that calculated a soil loss between the defined boundaries $A_{class,lower}$ and $A_{class,upper}$ of the respective class in the grid cell (m, n) and based on the $N = 756$ USLE model setups. A step function assigns the probabilities $p_{i,m,n} = 1$ or $p_{i,m,n} = 0$ to a model i if the soil loss $A_{i,m,n}$ that was calculated with the model i for the grid cell (m, n) is included or excluded from a class interval.

4.4.3 Analysis of the USLE input factors

In each grid cell the input factors R , K , LS , and C are ranked based on their influence on the calculation of soil loss in that grid cell. Eq. 3.5 was implemented to compute the sensitivity measures for the individual model inputs and each grid cell. The resulting values for the model input sensitivity measures were ranked in descending order and the input with the strongest influence on the soil loss estimation in each pixel was determined and visualized in a map to get a spatial reference of the importance of the model inputs. The spatial patterns of the most relevant model inputs were analyzed visually.

4.4.4 Analysis of soil loss on administrative level

The soil loss on administrative levels was assessed for 27 administrative units in Uganda and Kenya. For all administrative units and all USLE model setups the mean soil loss was calculated. The distribution of the mean soil loss in each administrative units was analyzed with descriptive statistics. Employing Eq. (4.6) soil loss levels were determined for all grid cells in the respective administrative units and for all USLE model setups. The areas of each soil loss class calculated from all USLE model setups per administrative unit were summed up to compute the average share of a soil loss class for each administrative unit. Only administrative units located in the erosion prone regions that are indicated in Fig. 4.1 are analyzed in the main document below. A complete summary of the results for all counties of Kenya and districts of Uganda can be found in the Appendix section A.3.

4.4.5 Comparison of soil loss estimates to in field assessments

To provide a reference for the USLE ensemble simulations literature values of long-term mean annual soil loss from in-field assessments were used. García-Ruiz et al. (2015) compiled a comprehensive literature review for global soil loss

rates, where three sources provided values for five sites within the study area of Kenya and Uganda. All three sources, however, applied different methods to assess the soil loss and cover a wide range of spatial domains. Sutherland and Bryan (1990) estimated the soil loss from the 0.3 km² Katorin catchment located in the Lake Baringo drainage area in Kenya based on an in-stream discharge and suspended sediment sampling. Sutherland and Bryan (1990) estimated an average soil loss for the Katorin catchment of 73 tons ha⁻¹ yr⁻¹ with a range between 16 and 96 tons ha⁻¹ yr⁻¹. Kithiia (1997) reported results from soil loss monitorings in tributaries of the Athi River Basin conducted by the Kenian Ministry of Water Development. From the tributary sampling sites in the Athi River Basin the 41 km² Riara catchment with an average reported sediment load of 1474 tons yr⁻¹ (0.36 tons ha⁻¹ yr⁻¹) was selected. Bamutaze (2010) performed an erosion plot experiment in the Sinje catchment at Mt. Elgon in Uganda. Based on a two year monitoring, Bamutaze (2010) estimated a mean soil loss of 0.838 tons ha⁻¹ yr⁻¹ with a range between 0.185 and 1.761 tons ha⁻¹ yr⁻¹. De Meyer et al. (2011) assessed the soil loss from 36 farm compounds in the two villages Iguluibi and Waibale close to the northern shore of Lake Victoria in Uganda. De Meyer et al. (2011) assessed the soil loss by reconstructing the historic surface level and calculating the lost soil volume. The estimations range between 56 and 460 tons ha⁻¹ yr⁻¹ in Iguluibi and 27 and 135 tons ha⁻¹ yr⁻¹ in Waibale.

To compare the ensemble soil loss estimations from this study with literature values, mean soil losses for grid cells that cover the original study site locations were calculated. Statistical measures were aggregated for the calculated site averages and plotted against the measured soil losses acquired from the selected studies.

4.5 RESULTS

4.5.1 Soil loss from USLE ensemble simulations

Overall, the calculated soil losses by the model ensemble follow the spatial pattern indicated by the potential erosion risk from topography that was presented in Fig. 4.1a). Both, the ensemble mean (Fig. 4.3a)) and the median soil loss (Fig. 4.3b)) show increased soil losses where moderate or high erosion risks were identified based on the slope thresholds suggested by Ebisemiju (1988). Mean soil losses of larger than 50 tons ha⁻¹ yr⁻¹ were found in the south-western corner of Uganda around Lake Bunyoni and along the Rift Valley in the North-West of Kenya. Particularly, excessive soil losses that exceed 200 tons ha⁻¹ yr⁻¹ were calculated for the steep slopes around the Ruwenzori Mountains, Mt. Elgon, and Mt. Kenya with ensemble mean soil losses of up to 1865, 1663 and 1438 tons ha⁻¹ yr⁻¹, respectively. Large variations in the calculated soil losses in each grid cell in combination with highly positively skewed distributions are two reasons why the calculated mean soil losses are generally larger than the median values.

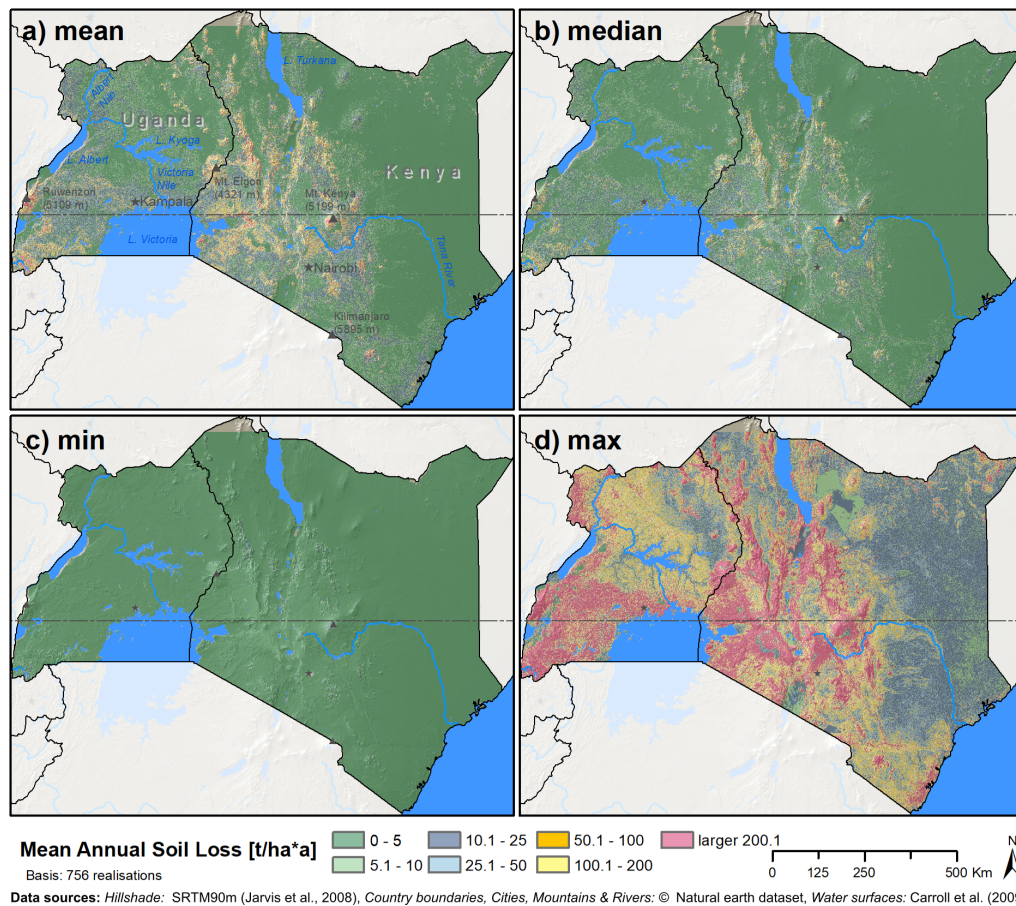


Figure 4.3: Descriptive statistics calculated for each grid cell based on the 756 USLE model realizations. Panels a) to d) show the mean, median, minimum, and maximum long-term annual soil erosion in each grid cell.

The strong discrepancy between the USLE model setups is evident from the comparison of the minimum calculated soil losses (Fig. 4.3c)) and the maximum soil losses (Fig. 4.3d)) in each grid cell. While combinations of USLE model input factors were present in the model ensemble that calculated soil losses below $10 \text{ tons ha}^{-1} \text{ yr}^{-1}$ for 99 % of the study region and soil losses below $100 \text{ tons ha}^{-1} \text{ yr}^{-1}$ for the entire study region, other input factor combinations resulted in soil losses above $200 \text{ tons ha}^{-1} \text{ yr}^{-1}$ for over 45 % of the study region and substantial soil losses of at least $50 \text{ tons ha}^{-1} \text{ yr}^{-1}$ for over 85 % of the study region.

Fig. 4.4 provides a different perspective of the same ensemble simulations. Each grid cell shows the frequency for the defined soil loss levels *tolerable*, *moderate*, *high*, and *severe* (panels a-d) respectively) that were predicted by the model members of the ULSE model ensemble. For large areas in the Northern Region of Uganda, the south of the lakes Kyoga and Albert in Uganda, and the Northeast Province and the northern parts of the Eastern Province in Kenya over 90 % (and in many cases all) of the USLE model setups calculated tolerable soil losses. In the topographically heterogeneous regions of the Uganda Plateau, the South West of Uganda and the Gregory Rift in Kenya, a substantial share

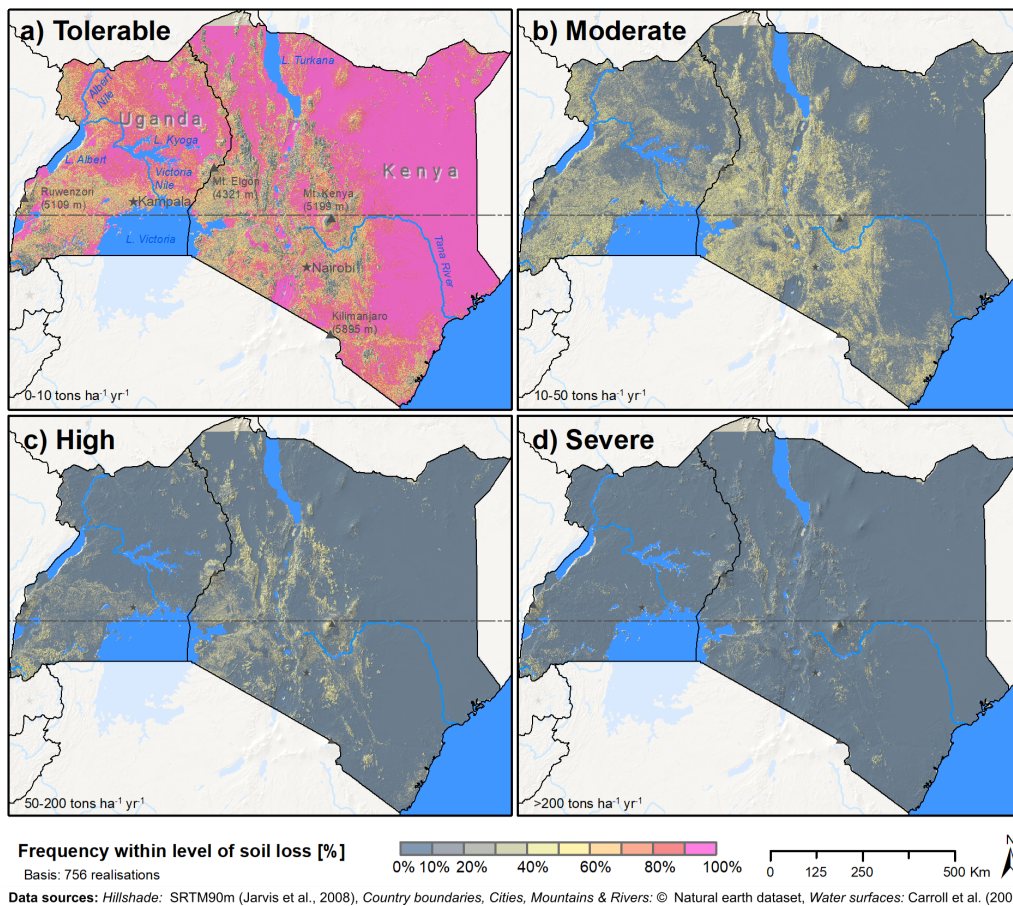


Figure 4.4: Frequency of USLE model ensemble members to predict one of the four soil loss classes tolerable (0 to 10 tons ha⁻¹ yr⁻¹) (a), moderate (10 to 50 tons ha⁻¹ yr⁻¹) (b), high (50 to 1200 tons ha⁻¹ yr⁻¹) (c), and severe (>200 tons ha⁻¹ yr⁻¹) (d), based on the soil loss classification after FAO-PNUMA-UNESCO (1980). The pixel color illustrates the percentage of models from the model ensemble that calculated a soil loss in between the respective class boundaries.

of up to 40 % of all model setups calculated a tolerable soil and the majority of model setups resulted in moderate soil losses. Only along the steep mountain ridges in the Rift Valley and the mountain massifs of Mt. Kenya, Mt. Elgon, the Ruwenzori Mountains and the region around Lake Bunyoni a substantial part of USLE model setups calculated high and severe soil losses (yellow and local red regions in Fig 4.4 c) and d)).

Fig. 4.5 combines the soil loss classification and the (un)certainties in the prediction of soil loss levels based on the USLE model ensemble into one representation. The dominant soil loss levels that a majority of model setups predicted for a grid cell are shown in green (*tolerable*), blue (*moderate*), orange (*high*), and purple (*severe*). The lightness of the colors indicates the percentage of models that calculated a soil loss within the respective soil loss classes. To highlight the complex patterns that result from the ensemble soil loss estimations in topographically heterogeneous regions, details for the regions of Mt. Elgon, Lake Bunyoni, and Mt. Kenya are illustrated in the panes b) to d) of Fig. 4.5.

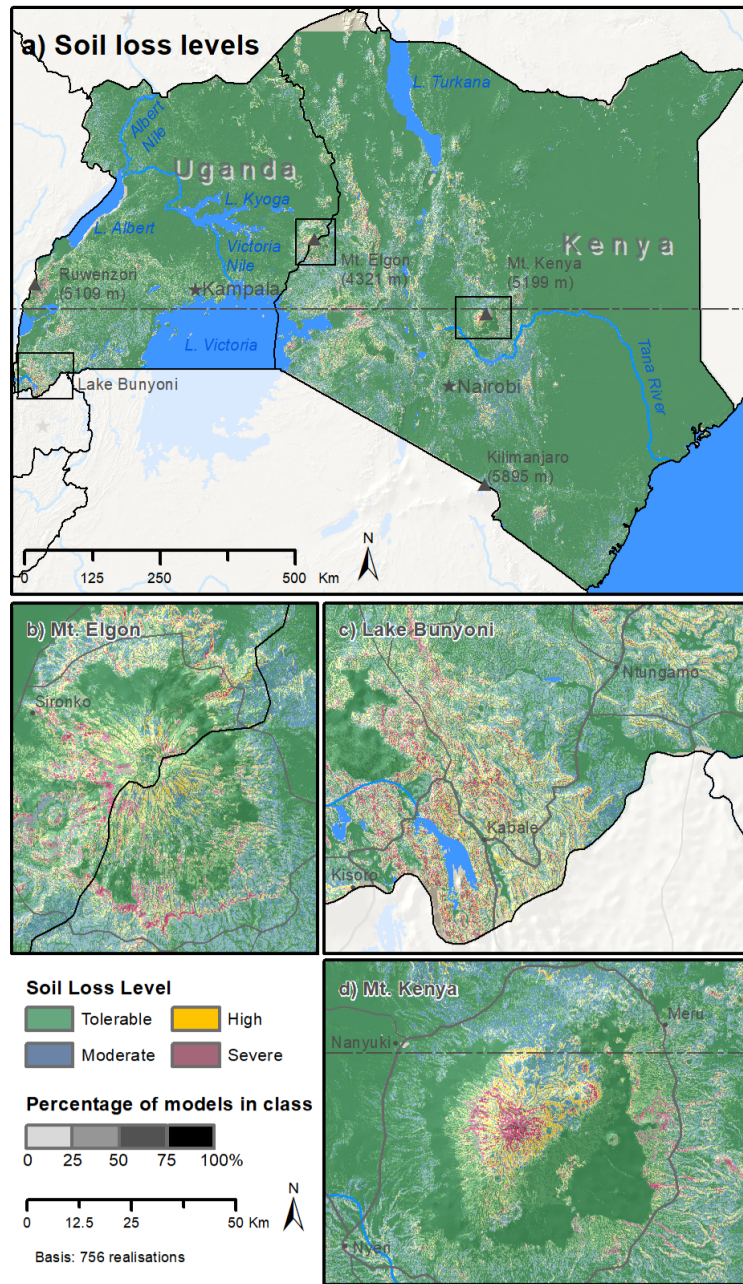


Figure 4.5: Dominant soil loss levels. The color shows the soil loss level predicted by the majority of USLE model setups. The lightness of the color indicates the percentage of models that predicted the dominant soil loss level. Panel a) shows the study area of Kenya and Uganda. The panels b), c), and d) show erosion prone areas around Mt. Elgon, Lake Bunyoni, and Mt. Kenya, respectively.

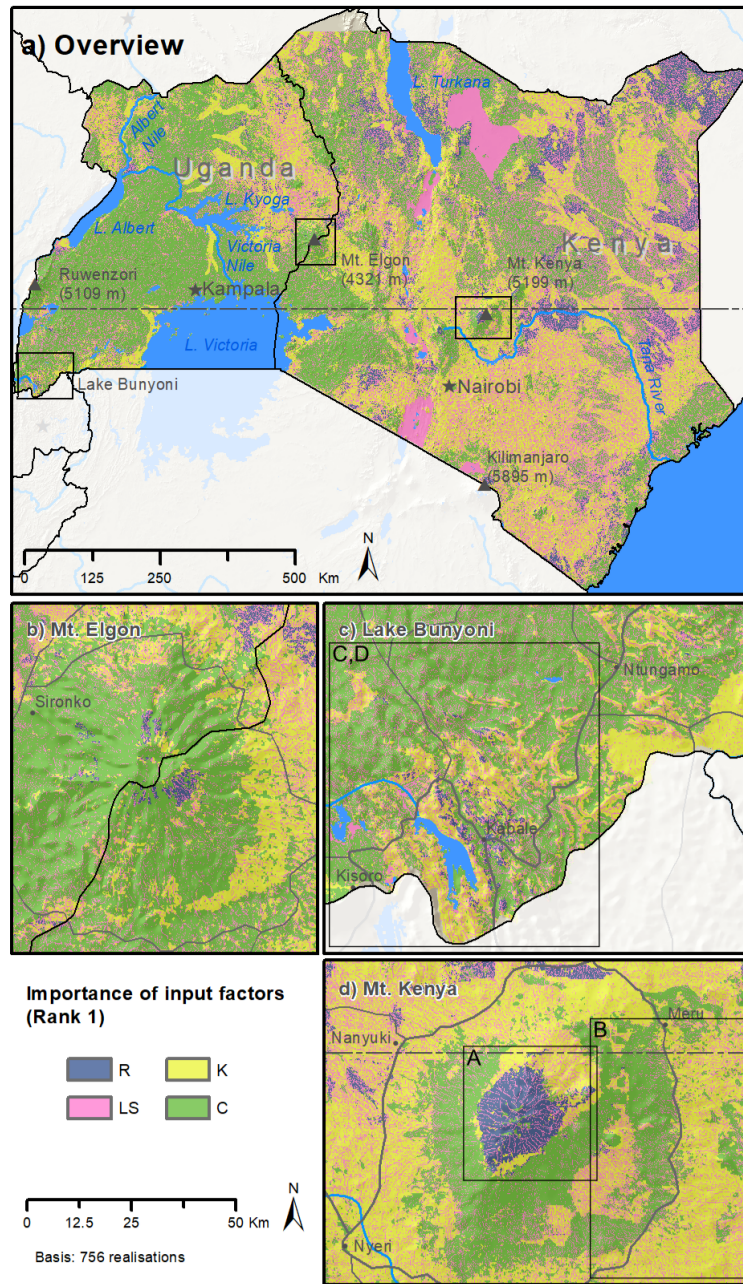
The strong agreement between the USLE model setups to calculate tolerable soil loss for the generally flat regions of Kenya and Uganda (shown in purple in Fig. 4.4 a)) is visible in dark green in Fig. 4.5 a). The soil loss level patterns in the erosion prone areas of Mt. Elgon, Lake Bunyoni, and Mt. Kenya clearly

follow the topographic patterns of these regions, with high and severe soil loss levels along the mountain ridges and tolerable to moderate soil losses in the valley bottoms. The agreement of the USLE model setups to predict the same soil loss level in such heterogeneous topographies is generally lower, showing percentages of 25 to 75 %. Only along the very steep slopes of the mountain massifs (and particularly at the top of Mt. Kenya with its steep slopes and low vegetation cover) a large majority of the USLE model ensemble predicted a severe soil loss (center of Fig. 4.5 d)). Although the entire Mt. Elgon and the Mt. Kenya massifs show moderate to steep slopes (see. Fig. 4.1 b)), a large majority of the USLE model ensemble (>75 %) calculated tolerable soil losses for the densely forested northern part of Mt. Elgon and the forest belt around Mt. Kenya.

4.5.2 Influence of USLE inputs on soil loss estimates

The range of the calculated soil loss A in a grid cell is the direct result of the different values stemming from the various input factor realizations. A large range in the values of an input factor in a grid cell has a greater impact on the resulting uncertainties of the calculated soil loss compared to input factors where the different realizations show similar values. The analysis of the strongest impact of input factors on the uncertainties of A revealed clear spatial patterns at different spatial scales (Fig. 4.6 a)). Over the whole domain, the input factors C , K , and LS were identified as the most important inputs for the uncertainties in soil loss in 34.74 %, 31.39 %, and 28.55 % of the total study area, respectively. The R factor was only locally identified as the most relevant input factor in 5.32 % of the total study area. The C factor and the K factors show large aggregated patterns in both countries. The importance of the LS factor, however, generally shows small structured, heterogeneous patterns scattered over the entire study region. Exceptions are visible in larger depressions along the Gregory Rift in zones where the slope is close to 0. Lake Magadi (100 km², an alkine lake located in an endorheic basin in the Rift Valley south of Nairobi, or a larger region in the east of Lake Turkana are the most distinct examples for large patterns of LS . Clusters of high importance of the R factor were only identified in high altitudes with generally large precipitation sums, but also in very dry regions in the northern Kenya, where the precipitation sums are close to 0.

Fig. 4.6 b)-d) provides more detail of the spatial patterns of the input factors and their importance for the calculation of the soil loss in regions around Mt. Elgon, Lake Bunyoni, and Mt. Kenya (that were also analyzed in Fig 4.5). In contrast to Fig. 4.6 a), finer-scale characteristics of input factor importance become visible. The patterns around the two mountains Mt. Elgon and Mt. Kenya show similarities. Although the R factor is spatially highly concentrated at the top of Mt. Kenya and only slightly visible on the east of Mt. Elgon, both regions show a high importance of the R factor for the calculation of A in high altitudes. High altitude areas are mostly characterised by a sparse observation network for precipitation. R is highly correlated to some, in our case spatially



Data sources: Hillshade: SRTM90m (Jarvis et al., 2008), Country boundaries, Cities, Mountains & Rivers: © Natural earth dataset, Water surfaces: Carroll et al. (2009)

Figure 4.6: Most influential USLE model input factors for the calculation of the soil loss *A*. The colours blue, yellow, pink, and green indicate whether the input factors *R*, *K*, *LS*, or *C* caused the largest range in the calculation of *A* in a grid cell. Panel a) shows the study area of Kenya and Uganda. The panels b), c), and d) show critical erosion hot spots around Mt. Elgon, Lake Bunyoni, and Mt. Kenya, respectively. The insets A) to D) indicate the extents for which the input factor realizations for *R*, *K*, *LS*, and *C* were analyzed in Fig. 4.7.

distributed, rainfall estimates. High uncertainties in rainfall records, but also in the modelling chain to derive remotely sensed precipitation explain these patterns. Moving down from the summits, belts of a high importance of the *C*

and K factor are visible. These distinct patterns result from the vertical bands of changes in vegetation in such mountainous regions and the impact of sparse and dense natural vegetation and agricultural land uses on the calculation of the C factor. The Lake Bunyoni region shows more heterogeneous patterns for the most important input factors. In the north, the calculation of A is affected by the C factor in large regions and the LS factor on very small scaled patterns. In the east and west of Lake Bunyoni, patterns for all input factors are visible that follow the terrain topography. The LS and K factor are the most relevant input factors for the calculation of A along the ridge lines, while the C factor becomes more important closer to the valley bottoms.

The importance of an input factor for the calculation of A results from the differences in the estimated input factor values for the individual input factor realizations. In Fig. 4.7 the input factor realizations of R , K , LS , and K are analyzed in the four regions A) to D) (indicated in Fig. 4.6). For the analysis only grid cells in the defined extents A) to D) were selected, which had the condition (i) that the respective input factor was the most relevant one and (ii) where the soil loss was calculated to be high to severe.

Case A) (Fig. 4.7 A)) shows the differences of R at the top of Mt. Kenya. Generally, a difference between the rainfall erosivity products derived from temporally high resolution rainfall (GloREDA (Panagos et al., 2017) and TMPA (Vrieling et al., 2014)) and the distributions of the R values obtained from long-term annual precipitation is visible. While both, GloREDA and TMPA show low R values between 1869 and 3486 $\text{MJ mm ha}^{-1} \text{h}^{-1} \text{yr}^{-1}$ and 3000 and 4602 $\text{MJ mm ha}^{-1} \text{h}^{-1} \text{yr}^{-1}$, respectively, the methods of Roose (1975), Moore (1979), Renard and Freimund (1994), and Lo et al. (1985) resulted in a wide range of R values between 4940 $\text{MJ mm ha}^{-1} \text{h}^{-1} \text{yr}^{-1}$ (minimum value with the method of Lo et al. (1985)) and 16 207 $\text{MJ mm ha}^{-1} \text{h}^{-1} \text{yr}^{-1}$ (maximum value using the method of Roose (1975)). Hence, a strong impact of the selected equation to calculate R from long-term annual precipitation is observable. Only the method of Nakil (2014) showed low R values in the same range as GloREDA and TMPA, with a range between 2590 and 3757 $\text{MJ mm ha}^{-1} \text{h}^{-1} \text{yr}^{-1}$. The method of Nakil (2014), however, generally generated very low R values (also where GloREDA and TMPA showed significantly larger R values).

Case B) (Fig. 4.7 B)) compares the K factor realizations in the south-eastern belt around Mt. Kenya. The six realizations of K show a clear pattern that is strongly affected by the methods that were employed to calculate K , while the differences between the two soil products that were used are rather insignificant. The method of Torri et al. (1997) resulted in by far the largest K values between 0.069 $\text{tons h MJ}^{-1} \text{mm}^{-1}$ and 0.088 $\text{tons h MJ}^{-1} \text{mm}^{-1}$. On average these values are three times larger than the ones calculated with the method of Williams (1995) (with a range between 0.021 $\text{tons h MJ}^{-1} \text{mm}^{-1}$ and 0.031 $\text{tons h MJ}^{-1} \text{mm}^{-1}$) and up to 13 times larger than the values calculated with the method of Wischmeier and Smith (1978) when using the SoilGrids data set (with a range between 0.011 to 0.028 $\text{tons h MJ}^{-1} \text{mm}^{-1}$).

Case C) (Fig. 4.7 C)) shows the differences between the the LS factor realizations along the ridges of the hills around Lake Bunyoni. Eventually only the

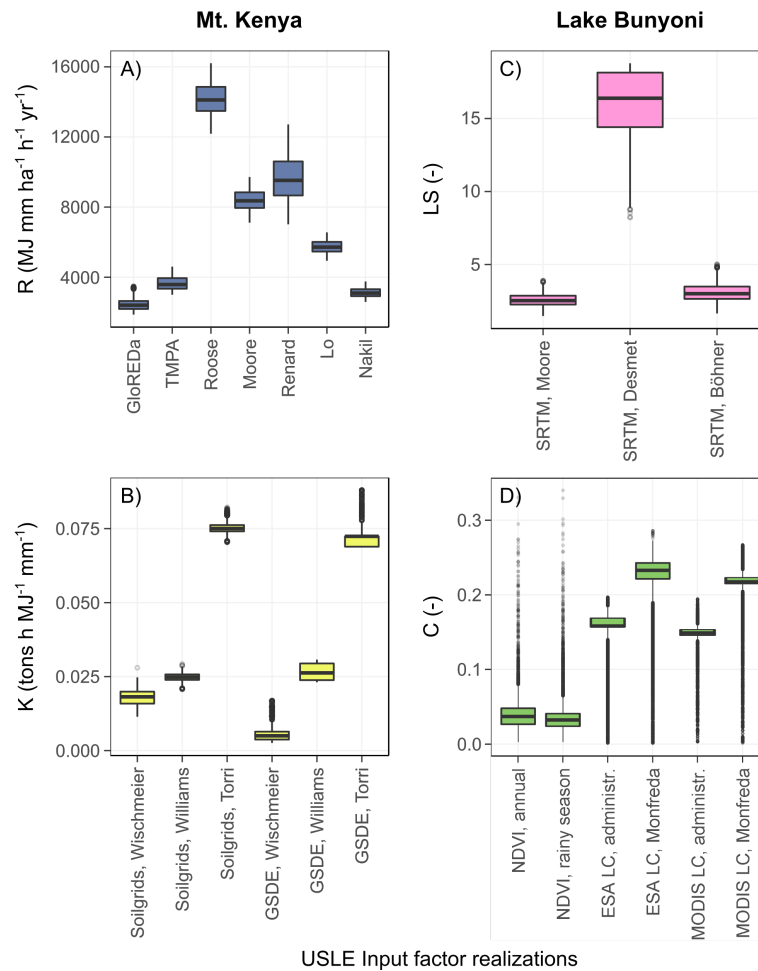


Figure 4.7: Variability between the realizations of the most important USLE model input factors. The cases A) to D) (delineated in Fig. 4.6) exemplify the differences in the distributions of the input factor R, K, LS, and C, respectively. The cases A) to D) include the values of input factor realizations for grid cells, in which the respective input factor was the most sensitive one and high to severe soil loss was predicted to be likely. Panel A) analyzes the R factor realizations at the top of Mt. Kenya, panel B) shows the differences in the K factor realizations in the belt around Mt. Kenya, and the panels C) and D) analyze the LS and C factors in the hilly topography of the Lake Bunyoni region.

SRTM 90m DEM was used as input data. Thus, Fig. 4.7 C) compares the three methods of Moore et al. (1991), Desmet and Govers (1996), and Böhner and Selige (2006). While the methods of Moore et al. (1991) and Böhner and Selige (2006) resulted in comparable values with ranges between 1.47 and 3.90 and between 1.65 and 5.03, respectively, the method of Desmet and Govers (1996) resulted in five times larger values with a range between 8.22 and 18.79.

Case D) (Fig. 4.7 D)) compares the implemented C factor realizations for the same extent around Lake Bunyoni as it was used in case C). In general two patterns are observable. A strong difference between the realizations that employ the NDVI as input and the C factor realization that were derived from land cover products and literature C factor values is visible. Further, using the

gridded crop distribution product of Monfreda et al. (2008) to derive spatially distributed mean C factor values from the literature resulted in larger values compared to the implementation of agricultural census data on the administrative unit level for Kenya and Uganda. The impact of the used land cover product (ESA LC or MODIS LC) are low. Both realizations based on NDVI (NDVI, annual and NDVI, rainy season) show mean C factor values of 0.04 and 0.03, respectively. The C values for the realizations that employed crop data from Monfreda et al. (2008) and agricultural census data were on average six times and 4.5 times larger with mean values of 0.21 and 0.15 respectively.

4.5.3 Soil loss at the administrative level

The selected administrative units in Uganda and Kenya are located in erosion prone areas (shown in Fig. 4.3 and Fig. 4.4). Averaging the soil loss for the domain of an administrative unit reduces the impact of areas with excessive soil loss. Nevertheless, the median values of mean soil loss for the selected administrative units that result from the USLE model ensemble result in a moderate (blue) soil loss in 22 of the 27 administrative units. Four administrative units show even a high (yellow) mean soil loss, while only one administrative unit resulted in a tolerable (green) soil loss (Fig. 4.8 a)). Particularly large mean soil losses were found for the administrative units Kabale and Kisoro in the Lake Bunyoni region and the administrative units Kasese and Bududa on the slopes of the Ruwenzori Mountains and Mt. Elgon, respectively. The data points shown as colored squares in Fig. 4.8 a) provide a reference to the soil loss assessment performed by Karamage et al. (2017) on district level in Uganda. The realizations of the USLE input factors developed in Karamage et al. (2017) were included in the present assessment. Thus the calculated soil loss from Karamage et al. (2017) is a member of the USLE model ensemble. In 9 of the 16 districts the soil losses calculated by Karamage et al. (2017) are lower than the 25 % quantile of soil losses that resulted from the USLE model ensemble. Only for a few districts, such as Kasese, Bundibugyo, Nebbi, or Kaabong the soil losses calculated by Karamage et al. (2017) and the ensemble means show comparable values.

For each administrative unit, the mean soil losses that resulted from the individual USLE model ensemble members show wide spreads (indicated by box plots and light gray dots in Fig. 4.8 a)). The spreads were particularly large in the administrative units with overall high soil losses. In all administrative units the mean soil loss that resulted from the individual USLE model setups are scattered over several soil loss classes (class boundaries indicated by dashed lines in Fig. 4.8 a)). Fig. 4.8 b) summarizes the numbers of model setups that predicted one of the four soil loss classes for each administrative unit. Although the median soil loss class for the majority of the administrative units is *moderate* on average 49 % (370 out of 756 models; with a range of 25.4 % to 60.4 % between the 27 administrative units) of the models from the USLE model ensemble predicted moderate soil loss, while all other model setups predicted one of the other four soil loss classes.

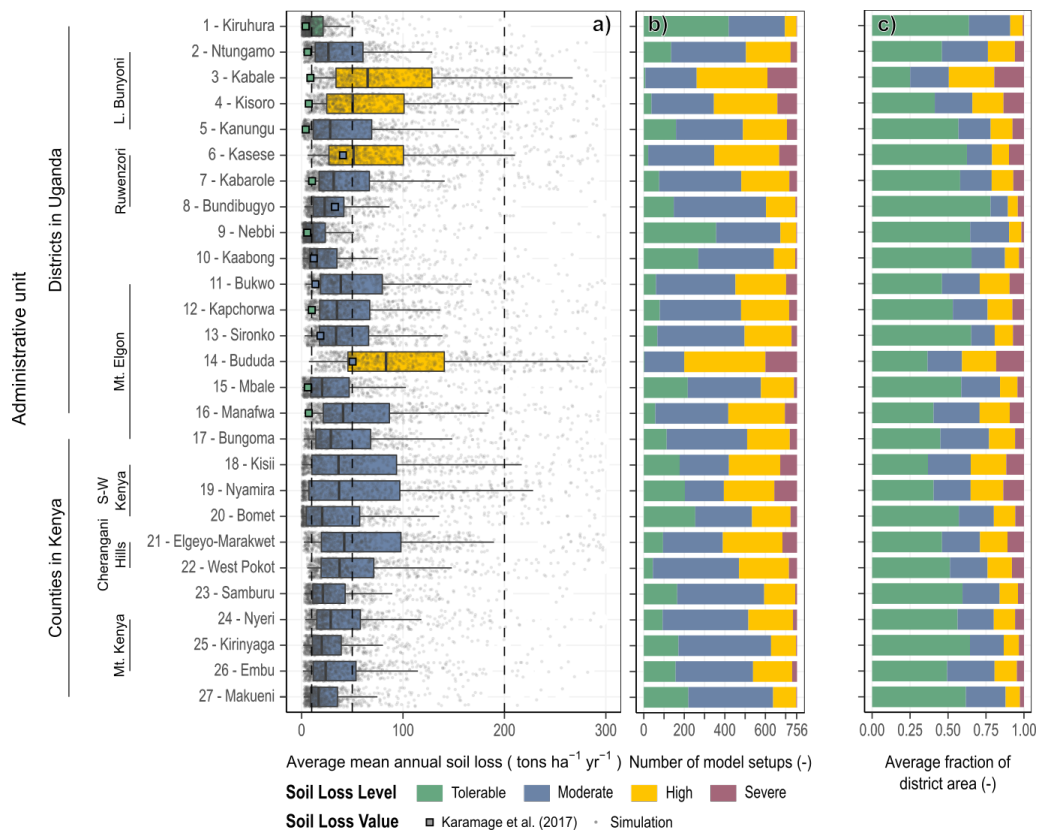


Figure 4.8: Mean soil loss in selected erosion prone administrative units of Uganda and Kenya. Panel a) shows the mean soil loss from all 756 USLE realizations in the selected administrative units with grey dots and aggregated as boxplots. The colors indicate whether the median soil loss in an administrative unit is tolerable (green), moderate (blue), high (yellow), or severe (purple). For comparison the results from Karamage et al. (2017) are plotted as colored squares. Panel b) shows the distributions of soil loss levels that were predicted by the USLE model realizations for the selected administrative units. Panel c) shows the average shares of soil loss classes for the domains of the selected administrative units.

Fig. 4.8 c) relates the soil loss classification in the selected administrative units to the average shares of the soil loss classes in the administrative unit areas. While on average only 20% of the models from the USLE model ensemble predicted a tolerable soil loss in the administrative units almost 55% of the areas of the administrative units show on average a tolerable soil loss. Areas with high and severe soil loss share only small areas in the administrative units with average fractions of 14.5% and 6.5%, respectively. Though, these areas have a strong impact on the mean soil loss in an administrative unit.

4.5.4 Comparison of soil loss estimates to in field assessments

While the total ranges of the soil loss estimates calculated for the reference sites from the USLE model ensemble cover the reference soil losses from literature values in all five cases in Fig. 4.9 the interquartile ranges for the USLE model

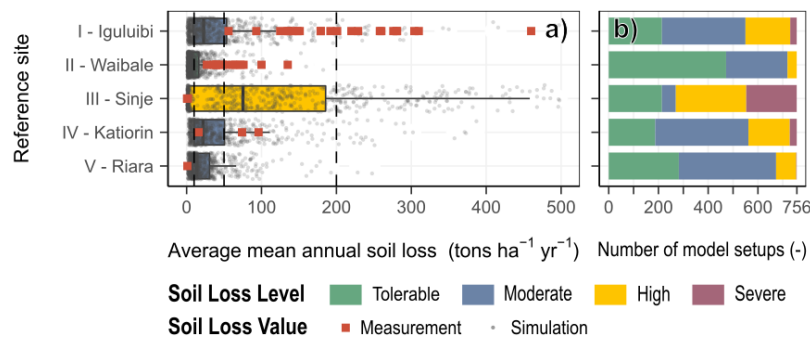


Figure 4.9: Comparison of soil loss simulations from the USLE model ensemble to in field soil loss assessments acquired from selected studies. The reference soil loss values are shown with red squares for the sites Iguluibi and Waibale (De Meyer et al., 2011), Sinje (Bamutaze, 2010), Katorin (Sutherland and Bryan, 1990), and Riara (Kithiia, 1997) in panel a). The soil loss simulations for the reference extents from all 756 USLE model realizations are shown as grey circles. Corresponding boxplots show summary statistics for the model ensembles in panel a). Panel b) summarizes the numbers of models that predicted the soil loss levels tolerable (green), moderate (blue), high (orange), and severe (purple) for the reference sites.

ensemble can strongly differ from the values that were estimated from in field experiments.

Cases I and II in Fig. 4.9 compare average soil losses for the domains of the villages Iguluibi and Waibale to soil loss assessments of small scale farm compounds. In both cases the soil losses assessed in the field exceed the interquartile ranges that result from the USLE model ensemble, with ranges of 56 to 460 tons ha⁻¹ yr⁻¹ and 8.6 to 53.4 tons ha⁻¹ yr⁻¹ in Iguluibi and 27 to 135 tons ha⁻¹ yr⁻¹ and 3.1 to 16.2 tons ha⁻¹ yr⁻¹ in Waibale.

For the Sinje test case (case III in Fig. 4.9) in the Manafwa district in Uganda Bamutaze (2010) resulted in very low soil losses between 0.185 and 1.761 tons ha⁻¹ yr⁻¹. Generally the districts along Mt. Elgon are known to be erosion prone. On average the USLE model ensemble predicted high soil loss for the location of the Sinje test catchment with a median soil loss 86.8 tons ha⁻¹ yr⁻¹ and an interquartile range between 3.9 and 212 tons ha⁻¹ yr⁻¹. Although the range of calculated soil losses is generally large, only 11 % of models from the USLE model ensemble predict soil losses that are in the range of the values reported by Bamutaze (2010).

The reported soil losses for the Katorin catchment are comparable to the soil loss estimations for the catchments extent that resulted from the USLE model ensembles (case IV in Fig. 4.9). Sutherland and Bryan (1990) reports a range of soil loss between 16 and 96 tons ha⁻¹ yr⁻¹ for the Katorin catchment and 21 % of the USLE model setups predict a soil loss in the same range. Almost 30 %, however, result in soil losses lower than 16 tons ha⁻¹ yr⁻¹.

Kithiia (1997) reports a very low soil loss of 0.36 tons ha⁻¹ yr⁻¹ for the Riara Basin. All USLE model realizations predict larger soil losses for the domain of Riara, with a minimum value of 1.6 tons ha⁻¹ yr⁻¹ and an interquartile range of 6.8 to 30.7 tons ha⁻¹ yr⁻¹.

4.6 DISCUSSION

4.6.1 *What can we learn from such an analysis*

The presented analyses illustrated how drastic the differences in the estimated soil loss magnitudes can be by selecting a method to calculate a USLE input factor. The statistical analysis of the generated USLE model ensemble (Fig. 4.3) showed that ranges of one or two magnitudes for the estimated soil loss were possible. These large ranges ultimately result from differences in the individual realizations of the USLE input factors (some realizations were over a magnitude larger than others in Fig. 4.7). These differences in the inputs propagate through the USLE equation by multiplication.

The immanent question that arises is whether it is possible to exclude any combinations of USLE input factors or individual realizations of input factors, as they fail to result in plausible soil losses and eventually reduce the ranges in estimated soil losses (Beven, 2018; Beven and Brazier, 2011). From a modellers perspective, neither the comparison to observations (Fig. 4.9), nor a plausibility check of the individual USLE model realisations generally allowed us to exclude model combinations or individual methods for the generation of USLE inputs. As a consequence, the uncertainties that result from commonly used methods to generate spatially distributed estimates of the USLE input factors and/or find additional ways to evaluate the simulated soil losses must be acknowledged (see section 4.6.2).

In the case that model setups cannot be falsified and must be considered as "fit-for-purpose" (Beven, 2018), each member of the ensemble must be treated equally as an acceptable representation of the analyzed system. In Fig. 4.4 and Fig. 4.5, and Fig. 4.8 approaches were proposed to utilize the generated USLE model ensemble and infer the severity of soil loss on different spatial levels based on a compromise of many models. From a decision makers perspective, such large ranges in soil loss imply challenges in the interpretation of the results and complicate decisions on possible measures that can be implemented. Nevertheless, the analysis of soil loss on the administrative level (Fig. 4.8) and particularly the comparison to the results from Karamage et al. (2017) should highlight an example to favor the analysis of the entire possible uncertainty range in soil loss, as opposed to accepting a single prediction of soil loss as a basis for decision making.

A possible approach to utilize the USLE ensemble predictions was presented in the combined assessment of soil loss levels that were predicted by the majority of the ensemble members and showed the fraction of models that predicted dominant soil loss levels in Fig. 4.4. Such reduction of information provided by the ensemble results enables to provide a "single" answer to the question of the severity of the soil loss to be expected and conveying the "certainty" of a prediction at the same time. Though, thresholds that define a specific soil loss as tolerable, or critical are seen as controversial (Bosco et al., 2015) and a wide range thresholds for tolerable soil loss (e.g., Karamage et al., 2017; Bosco et al., 2015; Bamutaze, 2015; Blanco-Canqui and Lal, 2008; Montgomery, 2007) and soil

loss classification schemes (e.g., Zachar, 1982; FAO-PNUMA-UNESCO, 1980) are proposed.

To illustrate the dominant soil loss level together with the frequency of models that predicted that soil loss level can strongly support the evaluation of the model results. A large share of the USLE input factor combinations, for instance, predicted low soil losses along slopes with dense forest vegetation (see e.g. dark green area in Fig. 4.5 d)). Thus, reduced soil loss in densely vegetated areas can be expected with a higher certainty based on the ensemble predictions. In contrast, areas with sparse vegetation (e.g. close to the summit of Mt. Kenya in Fig. 4.5) show increased soil loss, but lower percentages of USLE model members that predict the respective soil loss level at the same time. These are potential zones where any form of validation or plausibility check would benefit the analysis.

The analysis of the USLE input factor realizations with respect to their impact on the uncertainties of the simulated soil loss reveals patterns for the USLE inputs on different spatial scales in Fig. 4.6. These patterns can support in identifying the USLE inputs that require greater attention for the USLE model setup, based on the local conditions. Larger patterns were mainly visible for the input factors C and K , while LS showed very small scaled patterns and R showed a lower relevance for the prediction uncertainties in general. While the C is clearly the most important input factor for large regions in the densely vegetated part of Uganda and around Lake Victoria in Kenya, K is most relevant in the drier regions of Kenya. The R factor was mainly relevant in higher altitudes. The LS factor realizations were most relevant in highly variable topographies and very flat areas where the factor is close to zero and numerical issues governed the results of the sensitivity analysis.

4.6.2 *Are in-field data a valid reference for USLE model evaluation*

No clear pattern can be defined from the comparison of estimated soil losses to in-field soil loss assessments within the study domain. The selected reference studies had different specific scopes. While Sutherland and Bryan (1990), or Kithiia (1997) monitored the accumulated soil loss from river catchments, De Meyer et al. (2011) assessed the soil loss on small scales and on sites that are particularly erosion prone. While most of the selected reference studies report low to moderate soil losses for their study domains, De Meyer et al. (2011) reports high to excessive soil losses for several of the farm compounds they investigated. The methodologies that were used for the soil loss assessments strongly impacted the reported soil losses and result in wide ranges of soil loss between the selected studies.

Aforementioned limitations of the temporal and spatial representativeness of the reported soil losses from the selected reference studies are likely to be present and may have impacted the significance of the comparison to the soil loss estimates. Boardman (2006) stresses that long-term monitoring schemes and additional assessments of rills and gullies would be required to allow a comparison to soil loss estimations. Records from erosion monitoring studies are, however, usually short (Evans, 2013; Govers, 2011). The reference studies

of Sutherland and Bryan (1990) and Bamutaze (2010) for instance only covered monitoring periods of 1 and 2 years, respectively and thus are only snapshots in time that are difficult to compare with long-term assessments.

Although the soil losses reported in De Meyer et al. (2011) are based on cumulative soil losses in farm compounds over periods of 15 to 20 years, the spatial domains of the farm compounds that were analyzed do not properly reflect the spatial resolution of the grid on which the soil loss assessment with the USLE was conducted. Other reference studies, such as Sutherland and Bryan (1990) or Kithiia (1997) better meet the spatial scale of the USLE soil loss assessment. However, the presented soil yields are in-stream sediment loads. These reported loads are affected by processes, such as deposition, gully erosion, land sliding, or bank erosion that superimpose rill and inter-rill erosion (Govers, 2011). Boardman (2006) further highlights that the in-stream Sediment Delivery Ratios (SDRs) are a function of time and scale. Boardman (2006) compares the differences in the SDR of the Yellow River and British rivers that differ by a factor of 28. Such large difference in the SDR does, however, not necessarily reflect the differences in soil erosion rates.

Evans (1995) and Boardman (2006) point out that soil losses derived in plot scale experiments do not reflect erosion taking place on the landscape scale. Evans (1995) found that plot scale soil losses are larger than soil losses in the landscape by a factor of two to ten under comparable conditions. The soil losses reported in Bamutaze (2010) were however lower than the soil losses estimated by almost 90 % of all used USLE models in this study and thus show an opposite behavior.

Prasuhn et al. (2013), Warren et al. (2005), or Evans (2002), among others, demand that soil losses that were estimated by models must be supported by field based observations. Bosco et al. (2015) emphasize the limitations of in-field validation for large scale studies. Bosco et al. (2014) and Bosco et al. (2015) highlight the potential to employ new high resolution satellite imagery and Google Earth, or Google Streetview data for plausibility checks of soil loss estimates. Yet, the verification (and falsification) of the absolute magnitudes of soil loss estimates on large scales remains a challenge.

4.6.3 *Further considerations and limitations*

In this study only a selection of methods and primary data sources for the calculation of the USLE input factors was implemented. Hence, it must be recognized that the performed study does not provide a comprehensive picture of the uncertainties that are introduced by different representations of the USLE input factors. Albeit, the calculated ranges in soil loss were substantial and considering additional realizations of USLE input factors can in the worst case increase the ranges of calculated soil loss. The demonstrated procedure, however, pinpoints the central weakness of the USLE. The model can identify relative risks for soil erosion, but fails to predict exact magnitudes of soil loss. Eventually every modeller must acknowledge the limitations of the USLE (some addressed at

great length in the previous sections) and not overestimate the predictive power of the model.

Such a comprehensive analysis, as it is presented here, is very likely out of scope for most studies that employ the USLE model, as in most applications the soil loss estimation is only a small part of the entire analysis. Further, extending such analysis to larger domains or increasing the spatial resolution can be limited by available computation and storage capacities. For instance, the entire ensemble of USLE model representations in the present study comprised $11\,225 \times 14\,778 \times 1512$ ($\approx 2.5 \times 10^{11}$) pixel values required 2.13 TB distributed in SQLite data bases on four separate hard drives to allow an efficient batch-wise analysis of the model results. Nevertheless, checking the plausibility of estimated soil loss must be the minimum requirement for every study employing the USLE (see suggestion above and Bosco et al., 2015; Bosco et al., 2014).

Any analysis of the conservation support or management practice factor P was omitted in this study. For all USLE model setups the P factor was globally set to a value of 1. According to literature values, the application and maintenance of support practise measures can substantially reduce the soil erosion in erosion prone landscapes. Conservation measures, such as contour farming, strip cropping, or terracing reduces the calculated soil loss by a factor of up to 2, 4, and 10, respectively, depending on the slope on which the measure was applied (Karamage et al., 2017). Large scale estimations of P and the implementation of the P factor in large scale soil loss assessments are almost absent, as only very limited spatial data is available on soil conservation measures. Panagos et al. (2015d) generated a spatial estimate for P for entire Europe, considering the effects of contouring, stone walls, and grass margins. Panagos et al. (2015d) thereby used comprehensive spatial statistics on soil conservation based on 270 000 data points available for Europe from the LUCAS data base (LUCAS, 2012). Such detailed data is, however, not available in all regions of the world. Thus, other large scale assessments omitted the P factor and used a value of 1 globally (e.g., Borrelli et al., 2017), assigned a reduced P value globally in the study domain (Karamage et al., 2017), or assigned global values for P to specific land uses (Yang et al., 2003). Such simplifications do not reflect the spatial distributions of soil conservation measures that are actually applied in a (large scale) study domain, although their impact on large soil loss estimates can be substantial.

4.7 CONCLUSION

The USLE model, an empirical model to estimate the soil loss by water erosion is widely applied in large scale assessments and was implemented in a case study to assess the soil loss on the entire domain of Kenya and Uganda. Although the USLE has a simple model structure and is therefore easy to implement, the generation of spatially distributed estimates of the USLE input factors for the study domain poses a major challenge. Large scale (remote sensing) data products and methods to employ them for the generation of the USLE inputs greatly support soil loss assessments on large scales. In order to analyze and quantify

the impact of available data products and with methods for the calculation of USLE inputs on the uncertainties of estimated soil losses, a range of realizations for each USLE input factor was generated and combined to 756 realizations of the USLE to compute spatially distributed soil loss for Kenya and Uganda.

Overall, but particularly in erosion prone areas of the study domain, the calculated ranges of soil loss showed large values. In many cases, especially in areas with high soil losses, the calculated ranges exceeded the mean soil loss by greater than one order of magnitude. To condense the information provided by the USLE model ensemble a classification of the soil loss into the soil levels *tolerable*, *moderate*, *high*, and *severe* was proposed employing common soil loss thresholds from literature. The classification allowed to utilize the USLE ensemble predictions to analyze but consider the "certainty" of the prediction simultaneously. The employed approach enabled to identify zones with increased soil loss, but also areas where the agreement in the USLE model ensemble is low and thus suggest an evaluation and/or plausibility checks for the simulations.

A sensitivity analysis of the soil loss predictions was performed to identify the USLE input factors that introduce the strongest impact on the uncertainties of the soil loss estimates. The analysis identified clear patterns on the large scale for the input factors *C* and *K*, where the *C* factor is more relevant for areas with denser vegetation and the *K* factor showed a greater importance for the calculation of the soil loss in dry less densely vegetated areas. The *LS* factor showed very scattered patterns in complex topographies and was relevant for the uncertainties of the calculated soil loss in sloped terrain.

A validation of simulated soil loss on large scale domains, employing in-field assessments from the literature poses to be a challenge and in this study no clear conclusions can be drawn for the ensemble soil loss estimates when they were compared to soil loss observations. Thus, the comparison failed to falsify any of the generated USLE model combinations that would allow to exclude ensemble members to ultimately reduce the soil loss prediction uncertainties. Major issues for a valid comparison are the differing origins of the in-field soil loss data as well as spatial and temporal limitations of the observed data.

Although available computational and time resources will naturally limit such an analysis of soil loss predictions in most studies that employ the USLE model, the findings clearly highlight the importance to critically view and analyze single USLE model predictions, as the resulting soil loss estimates are highly sensitive to the combinations of realizations of the USLE model inputs. One must further question the aptitude of soil loss assessments based on in-stream sediment yields or small scale plot experiments to be valid data for the evaluation of soil loss estimates and want to refer to new approaches (e.g. Bosco et al., 2014) that potentially allow to check the plausibility of large scale soil loss assessments.

DISCHARGE AND NITRATE-NITROGEN LOADS UNDER CHANGE

5.1 INTRODUCTION AND OBJECTIVES

Environmental systems are under constant change. Predicting the development of natural resources in a changing system involves large uncertainties (Milly et al., 2008). Climate change, in concurrence with other dynamic processes such as population growth, land use change or economic development pose challenges to the management of water supply and water quality (Duran-Encalada et al., 2017; Yates et al., 2015). Human disturbances can exacerbate the impacts of climate and amplify consequences to water quality (Jiménez et al., 2014) on one hand. On the other hand, stakeholders in environmental systems have to respond to future changes, for instance adapting farm management practices due to changes in temperatures and precipitation patterns (Schönhart et al., 2018). Ideally, an impact assessment considers all future changes that can affect the development of the environment of interest as well as those future changes that can introduce uncertainties in the simulation of the environmental variables of interest.

As outlined in section 3.1, to describe the future development of environmental systems usually requires to make strong assumptions on their development where information is missing and deep epistemic uncertainties are present (Beven, 2018). These assumptions are typically reflected in a set of possibilities how the future development can progress, usually implemented in a discrete set of model scenarios (Montanari, 2007) that ideally cover the full range of trajectories along which the future development is plausible (Clark et al., 2016). Scenario development involves different data sources and models, which can introduce and propagate uncertainties. For example, climate scenarios have several sources of uncertainty and may include several socioeconomic scenarios (e.g. the current Representative Concentration Pathways (RCPs Moss et al., 2010; Vuuren et al., 2011)) that drive an array of Global Climate Models (GCMs) (Knutti and Sedláček, 2013). However, the GCMs also have inherent uncertainty and they provide the boundary conditions for Regional Climate Models (RCMs) (e.g. Jacob et al., 2014). Further, the downscaling (Wilby et al., 1998; Wood et al., 2004) of the RCM simulations and the bias correction (Teutschbein and Seibert, 2013; Teutschbein and Seibert, 2012) are associated with their own uncertainty and are standard procedures in climate scenario development. Eventually, it is essential to characterize the uncertainties inherent in all processes that affect the simulation of an environmental variable.

To simulate the development of hydrological variables under changing conditions, the developed scenarios are implemented as boundary conditions in hydrological models that are calibrated for historic observations. Yet, often dif-

ferent model setups and different sets of parameters in a model can perform equally well to reproduce historical observations of the variables of interest. Equifinality is a well-known issue in hydrologic modeling that has been extensively addressed in the literature (e.g. Schulz et al., 1999; Beven, 2006; Beven and Freer, 2001; Beven, 1996), where multiple model structures (e.g. Clark et al., 2008) and model parametrizations (e.g. Schulz et al., 1999) represent observations equally well and thus cannot be rejected (Beven, 2006). An adequate representation of historical data does not necessarily assure that different model setups agree when extrapolating to future conditions (Chiew and Vaze, 2015; Milly et al., 2008). Thus, differences in the model setup are a source of uncertainty in the simulation of an environmental variable under future conditions.

Altogether, an impact study comprises an abundance of combinations of trajectories of system changes and model setups to describe the future development of an environmental system. Hence, a comprehensive description of the uncertainties in the simulation of environmental variables is indispensable and UA and SA are at best a central part of any model impact study (Saltelli et al., 2008). Yet, a common procedure in impact analyses is to implement one or a few scenarios for a model input into a single calibrated "best" model setup. From an SA perspective, this approach is equivalent to a local OAT assessment of the model input sensitivity (Saltelli and Annoni, 2010; Baroni and Tarantola, 2014). A local OAT analysis however presumes linear models and non-correlated inputs which are hardly true for any environmental model application (Rosolem et al., 2012; Baroni and Tarantola, 2014). Thus, to account for interactions of model inputs and model non-linearities the application of GSA is recommended instead (Saltelli and Annoni, 2010; Saltelli and Tarantola, 2002; Baroni and Tarantola, 2014).

Chapter 3 describes at length the potentials and limitations of methods for UA and GSA to be integrated in a modeling framework with composite, uncertain model inputs. Only few studies considered such an implementation of discrete and composite model inputs in a GSA so far. With the Generalized Probabilistic Framework, Baroni and Tarantola (2014) rendered a solid basis for the implementation of correlated, non-continuous model inputs in GSA and applied the variance-based SA method of Sobol (1993) to assess the response of soil moisture, evapotranspiration, and soil water fluxes to uncertainties in meteorological input data, crop parameters, soil properties, model structure, and observation data. In a synthetic example, Dai and Ye (2015) performed model and scenario averaging to assess the impact of different model structures and scenarios of precipitation on groundwater flow and reactive transport in the soil. In a more recent study, Dai et al. (2017) employed the method of Sobol to identify the relevant system processes for groundwater flow and reactive transport represented in different model structures. Savage et al. (2016) applied GSA to identify the dominant controls in the calculation of flood inundation, to assess whether a high spatial resolution of the flood inundation model or the model parametrization is dominating the simulation. The mentioned studies illustrate the use of GSA with discrete and composite model inputs. Anderson et al. (2014) and Butler et al. (2014) highlight the importance of assessing the uncertainty of future

climate change impacts and the identification of relevant drivers and their interactions for climate policy making.

This case study demonstrates the utility of GSA and uncertainty analysis in a comprehensive setting of an environmental model impact study employing a complex eco-hydrological model to simulate discharge and nitrate-nitrogen (NO_3^- -N) loads under future change. The analyses of this case study address the following points:

- i. A comprehensive GSA is applied in two Austrian catchments to identify the dominant sources of uncertainties for the simulation of discharge and NO_3^- -N loads. The impacts of different spatial aggregations of the model setup and different model parametrizations together with the effects of changes in the land use, point source emissions, and the future climate are analyzed.
- ii. The resulting uncertainties in the simulation of the long-term monthly mean discharge and monthly sums of NO_3^- -N loads, as well as flow duration curves (FDCs) of daily discharge and daily NO_3^- -N loads visually are analyzed. Ways to visualize the discrete model inputs that provide further insights into the relationships of uncertainties in the simulations and different properties of the discrete realizations of the model inputs are presented.
- iii. Based on the GSA and the visual analysis of the simulated uncertainties conclusion on the simulation of discharge and NO_3^- -N loads as impacted by the model setup, model parametrization and the future scenarios of land use, point source emissions and climate can be drawn. These conclusions are limited to assumptions made in the model setup and in the development of the scenarios.

The chapter is structured in the following way: Section 5.2 provides an overview of the two investigated catchments. The preparation of the model input data that were used in the model setup are explained in section 5.3.2. In section 5.3.2 the setup of the SWAT model with different spatial aggregations is described and the pre-processing of the SWAT model setups that was necessary to identify the sensitive SWAT model parameters and to define non-unique parameter sets for all model setups is illustrated. The scenarios of land use, point source emissions and the climate together with the input data and pre-processing to develop the individual scenarios are specified in Section 5.4. Section 5.5 combines the SWAT model setups, the defined non-unique model parametrizations and the developed scenarios of land use, point source emissions and climate in the GSA and explains the methods that were applied to analyze the sources of uncertainties for the simulation of discharge and NO_3^- -N loads. The results of the combined GSA framework and the visual analysis are provided in section 5.6. The findings of the GSA application and the visual analysis of the simulation uncertainties for the two case studies are discussed in section 5.7 and The specific assumptions that were made during the model setup and the development of the scenarios are addressed.

5.2 STUDY SITES

The two investigated catchments (Schwechat and Raab) are representative examples for river systems in the eastern region of Austria. Both rivers have their origin in the forested foothills of the limestone Alps with a pre-alpine character and a low anthropogenic impact. The lower parts of both catchments are characterized by human activities, with primarily urban settlements and agricultural uses in the plains of the Schwechat catchment and dominant industrial activities and agricultural land uses in the valley bottom of the Raab catchment (Fig. 5.1, and Tables 5.1 and 5.2).

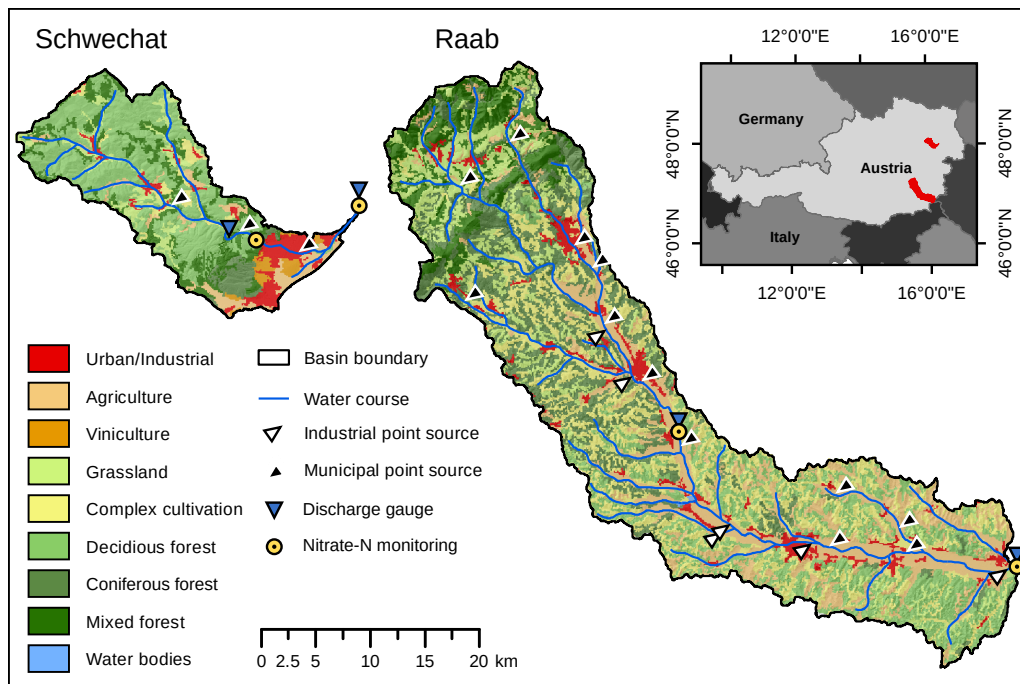


Figure 5.1: Study sites Schwechat (left) and Raab (right).

The Schwechat river has its source in the Vienna woods at the northeastern boundary of the Northern Limestone Alps with a maximum altitude of 893 m a.s.l. After a natural flow section in the narrow and dominantly forested valley of the "Helenental" (70% of the total catchment area. See Table 5.1), the Schwechat drains into the Vienna basin with flat topography and a predominance of agriculture, viniculture and settlement areas. The main agricultural crops are winter wheat and summer wheat. Larger areas in the upper part of the catchment are used as pastures ($\approx 10\%$ of the total area). The largest settlement is the city of Baden with a population of approximately 26 000 inhabitants, while smaller settlements are scattered over the catchment. All municipal waste waters are collected in three Waste Water Treatment Plants (WWTPs). These are shown as black triangles in Fig. 5.1), where the WWTP Baden is the most relevant one with a capacity of 45 000 Population Equivalents (PEs). All WWTPs perform carbon removal, nitrification, denitrification and enhanced phosphorus removal. Due to the close proximity to the city of Vienna population growth is

a likely prospect for the settlement areas in the lower part of the catchment. The part of the catchment considered in this study has its outlet next to the city of Traiskirchen at an altitude of 185 m a.s.l. and covers an area of approximately 275 km². The long term mean annual precipitation in the Vienna Basin is approximately 620 mm yr⁻¹ and the mean annual temperature is 9.9 °C

Table 5.1: Area and percentage of the land uses in the Schwechat catchment. The land use groups are the respective land uses shown in Fig. 5.1 and are derived from CORINE. The agriculture, grassland, and complex cultivation land uses are disaggregated to dominant crop classes (column 3) by employing the 2010 Austrian Agricultural Census data (Statistik Austria, 2015b). The corresponding land uses implemented in the SWAT model data base, their areas and their percentages in the catchment are listed.

Land use group	CORINE Level 3	Land use	SWAT Land use code	Area (ha)	Share (%)
Urban, Industrial	11X, 14X	Urban medium density	URMD	154.2	0.6
	11X, 14X	Urban medium/low density	URML	2388.3	8.7
	12X	Industrial	UIDU	209.5	0.8
Agriculture, Complex Cultivation	221, 222, 242	Winter wheat, winter grains	WWHT	667.6	2.4
		Spring wheat, summer grains	SWHT	317.8	1.2
		Corn, Maize	CORN	111.5	0.4
		Vegetables grouped	SGBT	74.1	0.3
		Sunflower	SUNF	30.0	0.1
		Soybean	SOYB	19.7	0.1
		Orchard, Fruit trees	ORCD	25.6	0.1
Vineyard	GRAP	699.5	2.5		
Grassland, Complex Cultivation	231, 242	Pasture, extensive use	FESC	2406.6	8.8
		Pasture, intensive use	FESI	762.9	2.8
		Alfalfa, clover, etc.	ALFA	400.7	1.5
Deciduous forest	311	Forest, deciduous	FRSD	12 941.3	47.1
Coniferous forest	312	Forest evergreen	FRSE	1152.2	4.2
Mixed forest	312	Forest, mixed	FRST	5138.4	18.7
				27 499.9	100.0

The Raab river originates at the edge of the southeastern Alps. These are characterized by low mountain ranges with a maximum altitude of 1547 m a.s.l., mostly covered by forests ($\approx 42\%$ of the total catchment area. See Table 5.2). The Raab flows through the southern part of Austria and crosses the border to Hungary close to the city of Neumarkt an der Raab at an altitude of 232 m a.s.l. The analyzed catchment of the Raab river encompasses the Austrian part of the

Raab with a catchment area of approximately 998 km². The long-stretched river valley is dominated by agricultural activities ($\approx 25\%$ of the total area), with urban areas in between. The slopes along the Raab are covered with heterogeneous patterns of forests, pasture areas and agricultural land use. The main agricultural crops are corn and oil seed pumpkins, but also wheat and vegetable production are common. While the urban areas are of similar small structure as in the Schwechat catchment, leather industries are present in the catchment that release substantial nutrient inputs into the receiving waters, which has resulted in trans-boundary conflicts (Ruzicka et al., 2009). Municipal waste waters in the Raab catchment are collected in 12 relevant WWTPs (black triangles in Fig. 5.1) that all have the same standards for wastewater treatment as in the Schwechat catchment, but have almost three times the total capacity (approximately 150 000 PE). Six relevant industrial emitters are located along the main reach of the Raab river (white triangles in Fig. 5.1) that all perform internal waste water treatment following the respective industry-specific regulations for wastewater treatment (e.g., BGBl. II Nr. 10/1999, 1999; BGBl. II Nr. 12/1999, 1999). The average annual precipitation in the Raab catchment is approximately 800 mm yr⁻¹ and the long term annual mean temperature is 9.0 °C.

5.3 THE BASELINE SWAT MODEL SETUP

This section documents the setup of the baseline SWAT models that describe the historic conditions in the Schwechat and the Raab catchments. The steps of the input data preparation, the model setup employing different model configurations (as illustrated schematically in Fig. 3.4), and the model calibration for historic observations of discharge and NO₃⁻-N loads are outlined in detail below.

5.3.1 *Model input data and preparation*

The required input data to set up a model with SWAT are a raster Digital Elevation Model (DEM) layer, a raster land use map including the parametrization of the respective land uses and the performed management operations for each land use, a raster soil map with soil physical and chemical parameters for all soil layers, and meteorological input data.

A DEM with a 10 m resolution was available for Austria from an airborne laser scan (Geoland.at, 2015). Based on the DEM three slope classes were defined with slopes of 0 to 3 %, 3 to 8 %, and >8 % in the HRU definition step.

CORINE land cover (EEA, 2015) served as the base land use map to which more detailed agricultural data was added. CORINE does not classify agricultural land uses into crop types. Therefore, tabular data of agricultural land uses at the municipal level derived from the 2010 Austrian Agricultural Census (Statistik Austria, 2015b) was superimposed onto CORINE data by randomly distributing crops according to the crops' areal share at the municipal level to CORINE pixels containing agricultural and complex cultivation land use. Typical time windows for planting, fertilizer application, tillage and harvest were derived from field experiment records for the individual crops (Land NÖ, 2015)

Table 5.2: Area and percentage of the land uses in the Raab catchment. The land use groups are the respective land uses shown in Fig. 5.1 and are derived from CORINE. The agriculture, grassland, and complex cultivation land uses are disaggregated to dominant crop classes (column 3) by employing the 2010 Austrian Agricultural Census data (Statistik Austria, 2015b). The corresponding land uses implemented in the SWAT model data base, their areas and their percentages in the catchment are listed.

Land use group	CORINE Level 3	Land use	SWAT Land use code	Area (ha)	Share (%)
Urban, Industrial	11X, 14X	Urban medium/low density	URML	11 850.8	12.0
Agriculture, Complex Cultivation	221, 222, 242	Corn, Maize	CORN	11 982.5	12.1
		Oil seed pumpkin	OELK	3171.1	3.2
		Vegetables grouped	SGBT	3035.9	3.1
		Winter wheat, winter grains	WWHT	1855.6	1.9
		Spring wheat, summer grains	WWHT	981.9	1.0
		Soybean	SOYB	445.9	0.5
		Orchard, fruit trees	ORCD	3036.1	3.1
Grassland, Complex Cultivation	231, 242	Pasture, extensive use	FESC	11 635.7	11.8
		Pasture, intensive use	FESI	8474.0	8.6
		Alfalfa, clover, etc.	ALFA	598.0	0.6
Deciduous forest	311	Forest, deciduous	FRSD	15 379.4	15.6
Coniferous forest	312	Forest evergreen	FRSE	7773.2	7.9
Mixed forest	312	Forest, mixed	FRST	18 540.2	18.8
Waterbodies	41X	Wetlands, mixed	WETL	55.4	0.1
				98 815.9	100.0

and written to the HRU management files. The management dates were randomized for all HRUs within the time windows derived for a management operation. Dates with strong rainfall or a high soil moisture potential were not used for scheduling management operations. The automated procedure to randomize and assign farm management operations was performed with the R package `SWATfarmR` Schürz (2017). With 70.0% and 42.3% forest land uses were the most dominant land uses in the Schwechat and the Raab catchments, respectively. The SWAT model setups differentiated between deciduous forests, coniferous forests and mixed forests, derived from CORINE land cover (see Tables 5.1 and 5.2). All HRUs with one of the three forest types as land use were parameterized with an initial biomass and an initial leave area index to simulate intact forests in both catchments.

To generate the raster soil layers for both catchments, the `SoilGrids250m` data base (Hengl et al., 2017) was implemented that was already implemented in the

first case study and briefly introduced in section 4.3.2. The consistent global soil information system provides soil physical and chemical parameters at a 250 m grid resolution and seven soil depths. The physical properties S_a , S_i , Cl , CRF , and the bulk density ρ_d and the chemical properties $orgC$, the cation exchange capacity of the soil CEC , and the pH were acquired for all seven soil depths. Further soil parameters that are required as input parameters for the SWAT model setup were estimated with pedo-transferfunctions provided by the R package `eupf` (Tóth et al., 2015). A detailed list of the required soil inputs for SWAT₂₀₁₂ can be found in Neitsch et al. (2011). The seven available soil depths from the SoilGrids250m data were aggregated to three soil depths (0 to 30 cm, 30 to 100 cm, and 100 to 200 cm), and the gridded data were clustered into soil classes applying `kmeans` clustering (Hartigan and Wong, 1979; R Core Team, 2017) resulting in 14 and 8 "optimum" soil classes for the rivers Schwechat and Raab respectively.

Meteorological input data was available from the INCA system developed and operated by the Central Institute for Meteorology and Geodynamics of Austria (ZAMG; Haiden et al., 2011). INCA provides reanalysis data of precipitation and temperature on 1 km grid resolution for Austria with a temporal resolution of 15 min for precipitation and 60 min for temperature in the period from 2003 to 2015. For all SWAT model setups, daily precipitation sums and daily minimum and maximum temperatures were temporally and spatially aggregated for the model subbasins.

Point source emission data was available from external emission monitoring of municipal WWTP greater than 2000 PE according to BGBI. 1996/210 (1996) for both catchments. Municipal WWTP larger than 2000 PE are responsible for 99.2% and 86.3% of municipal point source emissions in the Schwechat and the Raab catchments respectively. Thus, these data cover a substantial part of the municipal emissions. Additionally, daily and weekly internal monitoring data was available for some large WWTP schemes. In most cases however, only information on NO_3^- -N emissions was provided. A general budgeting of nitrogen emissions however showed, that the substantial share of total nitrogen is emitted in form of NO_3^- -N (87% in the Schwechat catchment and 89% in the Raab catchment). For industrial emitters monthly and annual records from internal and external monitoring agencies were available and only allowed an estimation of industrial emissions with coarse temporal resolution, while covering the annual budgets. Again, mainly data for NO_3^- -N emissions were available. Although, nitrogen is emitted in different forms the available data basis only allowed to consider NO_3^- -N loads contributed by point sources. Table 5.3 provides an overview of the model input data that was used for the SWAT model setup.

Hourly observations of discharge were available for the period from 2003 to 2015 at two gauges for the Schwechat and the Raab each (Fig. 5.1). NO_3^- -N concentration readings with varying time intervals of 5 to 15 min were available at two stations in both catchments (yellow circles in Fig. 5.1) for selected time periods resulting from monitoring campaigns at the rivers Schwechat (BMLFUW, 2013) and Raab (BMLFUW, 2015a; BMLFUW, 2015b). SWAT simulates output variables with daily time steps. To compare the observations with the modeled

Table 5.3: *Input data for the SWAT model setup, the data sources, and the data processing steps.*

Input data set	Data source	Data preparation
Topography	DEM Austria (Geoland.at, 2015)	Digital Elevation Model for Austria in 10 m resolution.
Land use	CORINE Landcover (EEA, 2015), 2010 Austrian Agricultural Census (Statistik Austria, 2015b)	Basis: CORINE Land cover, Agricultural areas re-sampled with statistical information from 2010 Austrian Agricultural Census.
Soil data	soilgrids.org (Hengl et al., 2017), euptf (Tóth et al., 2015)	Basis: SoilGrids250m 250 m resolution in 7 depths. Clustered in space and aggregated over depth. Further SWAT soil parameters derived using pedotransfer functions.
Meteorology	INCA (Haiden et al., 2011)	Precipitation and temperature data in 1 km resolution.
Agricultural practices	Statistik Austria (2015b), Land NÖ (2015)	Derive time periods and sequences of field management practices from field experiments.
Point source emissions	External monitoring, Internal records of WWTPs	Time series and point measurements of discharge and NO_3^- -N concentrations.

SWAT outputs of discharge and NO_3^- -N loads, daily NO_3^- -N loads and daily mean discharge were calculated from the observation data.

5.3.2 *Model setup, parameter selection and identification of non-unique parameter sets*

Graphical GIS user interfaces such as ArcSWAT (Winchell et al., 2015) or QSWAT (Dile et al., 2016) facilitate the setup of SWAT models. Yet, a model setup requires the modeler to define the number of subbasins as well as the number of HRUs (e.g. by removing HRUs with areas below a certain threshold from the setup and apportion their areas to the remaining HRUs). The size and the number of subbasins in a model setup can affect the process simulations and the resulting model outputs (Jha et al., 2004; Momm et al., 2017; Tripathi et al., 2006). Removing small HRUs from the model setup and allocating their areas to the remaining HRUs affects the distribution of land use, soil types, and slope classes and thus can impact the model simulations substantially (Jha et al., 2004).

The ArcSWAT plugin (Version2012.10_1.14) and ArcGIS 10.1 (ESRI, 2012) were used for the model setup. For both catchments several SWAT models were set up with different configurations. For the Schwechat and the Raab models were set up with different numbers of subbasins, whereby additionally model setups with the full number of HRUs and respective setups with a reduced number of HRUs for each number of subbasins were set up.

In total, four SWAT models, two with 3 and two with 14 subbasins for the Schwechat catchment and six models for the Raab catchments with two each of

4, 29, and 54 subbasins were set up. For the full HRU setups HRUs that resulted from the HRU overlay in ArcSWAT remained unmodified. For the model setups with a reduced number of HRUs small HRUs were eliminated, based thresholds for land use, soil, and slope classes to remove HRUs that have an area below these found thresholds. The thresholds were determined using the R package `topHRU` (Strauch et al., 2016). `topHRU` enables to find thresholds that minimize the number of HRUs of a SWAT model setup while minimizing the aggregation error (sum of changes in the areas of land uses, soils and slope classes of the reduced set of HRUs compared to the full HRU setup). To maintain a comparability between the reduced HRU setups, thresholds were selected that result in an aggregation error of maximum 5% in all reduced HRU model setups. Table 5.4 gives an overview of the final model setups for both catchments.

Table 5.4: SWAT model setups for the Schwechat and the Raab catchment including the numbers of subbasins and the number of HRUs for each setup.

Schwechat			Raab		
Setup	# Subbasin	# HRU	Setup	# Subbasin	# HRU
sw_14_full	14	1434	rb_54_full	54	5349
sw_14_thru	14	196	rb_54_thru	54	954
sw_03_full	3	606	rb_30_full	30	3516
sw_03_thru	3	64	rb_30_thru	30	584
			rb_04_full	4	755
			rb_04_thru	4	115

In a parameter screening, a GSA was applied to the simulations of discharge and NO_3^- -N loads at the catchment outlets of all SWAT model setups to identify influential model parameters. Initially, 42 model parameters were selected that are frequently calibrated in SWAT model setups to simulate discharge and NO_3^- -N loads (see e.g. Arnold et al. (2012) and Abbaspour et al. (2007) for a general overview of relevant model parameters, Mehdi et al. (2018) and Haas et al. (2016) for parameters controlling the water balance and nutrient cycles, or Haas et al. (2015) for a review on the dominant nitrogen parameters). The SWAT model setup initializes the model parameters using values obtained from the SWAT data bases (either standard values or user defined, e.g. by pedo-transferfunctions). The selected initial ranges to modify the model parameters and the selected types of parameter changes (e.g. replace parameter values globally or modify a spatially distributed parameter field by a fraction of a parameter) reflect typical procedures often found in SWAT model calibration studies. An overview of the model parameters that were identified as influential and that were further used in the model impact study is provided in Table 5.5.

The STAR VARS approach (Razavi and Gupta, 2016a; Razavi and Gupta, 2016b) was employed to screen and rank the SWAT model parameters. STAR VARS utilizes variograms along each model input dimension of the input space to infer each model inputs influence on a target variable over different scales (where short lag distances approximate the derivative based method of Morris (Morris,

1991) and long distances the method of Sobol (Sobol, 1993)). The calculation of the variograms is based on the tailored STAR sampling design where "star center" points are randomly sampled in the input space. For each center point cross sections are sampled along the input factor dimensions with an equally spaced interval. For each sampled input combination the model is evaluated and variograms along the response surface are calculated. Razavi and Gupta (2016a) proposed integrated measures of the variograms as measures of sensitivity, where the measures $IVARS_{10}$, $IVARS_{30}$, and $IVARS_{50}$ represent the integrals over 10%, 30%, and 50% of each input dimension respectively and therefore provide the sensitivity of a target variable to a model input over different scales. A detailed description of the method is provided in Razavi and Gupta (2016a) and the STAR sampling is outlined in Razavi and Gupta (2016b). The method proved to be robust and computationally efficient for high dimensional problems (e.g., Razavi and Gupta, 2016b; Haghnegahdar et al., 2017; Sheikholeslami et al., 2019; Haghnegahdar and Razavi, 2017).

STAR samples (Razavi and Gupta, 2016b) with 50 center points and ten parameter samples per parameter dimension were drawn that resulted in 18950 parameter combinations per model setup. The Nash Sutcliffe Efficiency criterion (NSE; Nash and Sutcliffe, 1970), the Kling Gupta Efficiency criterion (KGE), including its three components (Gupta et al., 2009), and a refined version of the Index of Agreement (d_r ; Willmott et al., 2012) were used to evaluate the simulated time series of daily mean discharge and daily sums NO_3^- -N loads. Additionally, the ratio of the root mean square error and standard deviation (RSR; Moriasi et al., 2007) were applied, to evaluate different segments of the FDCs of daily discharge and daily NO_3^- -N load simulations (Pfannerstill et al., 2014; Haas et al., 2016). All calculated criteria were included in the parameter sensitivity analysis as target variables. A summary of the selected criteria is given in the Appendix section A.4. A model parameter was considered to be sensitive if it showed a relative sensitivity of 10% compared to the most sensitive parameter with respect to a specific objective criterion for at least one of the employed objective criteria.

The performed GSA for the model parameters of the different model setups of the Schwechat catchment and the Raab catchment respectively showed very similar results independent of the number of subbasins and HRUs of the individual model setups (Fig. 5.2). Therefore, for the impact study the same set of model parameters was considered as influential for all model setups of the Schwechat and the Raab, respectively. In total, 19 parameters for the Schwechat and 16 parameters for the Raab were identified to be influential for the analyzed target variables (Table 5.5). The majority of parameters were identified as influential parameters in the Schwechat and the Raab model setups. The parameters $SN050COV$, $CANMX$, CDN , and $SDNCO$ were only relevant for the model setups in the Schwechat and the parameter OV_N was only influential for in the Raab. For the majority of these parameters it is a matter of the selected threshold that defines a parameter to be influential or not. The most dominant parameters were however identified as highly relevant in both catchments.

Table 5.5: Influential and non-influential SWAT model parameters for the model setups of the Schwechat and the Raab.

Parameter	Description	Influential for discharge			Influential for NO ₃ -N loads		
		Schwechat	Raab	Schwechat	Schwechat	Raab	Raab
SFTMP	Snowfall temperature (°C)	X				X	
SNOCOVMX	Minimum snow water content that corresponds to 100% snow cover	X		X		X	
SNO50COV	Snow water equivalent that corresponds to 50% snow cover	X		X		X	
SURLAG	Surface runoff lag time (h)	X	X	X		X	
GW_DELAY	Groundwater delay (d)	X	X	X		X	
GW_REVAP	Groundwater revaporation coefficient	X	X	X			
GWQMN	Threshold depth of water in shallow aquifer for return flow (mm)	X	X	X			
RCHRG_DP	Deep aquifer percolation fraction	X	X	X			
SOL_K	Saturated hydraulic conductivity (mm h ⁻¹)	X			X		
SOL_AWC	Available water capacity of the soil layer	X	X	X		X	
SLSOIL	Slope length for lateral subsurface flow (m)	X	X	X		X	
CANMX	Maximum canopy storage (mm)			X		X	
ESCO	Soil evaporation compensation factor	X	X	X			
LAT_TTIME	Lateral flow travel time	X	X	X		X	
OV_N	Manning's n-value for overland flow		X	X		X	
CN0P_til1	SCS runoff curve number for the tillage operation	X	X	X		X	
RCN	Concentration of nitrogen in rainfall			X		X	
NPERCO	Nitrogen percolation coefficient			X		X	
CDN	Denitrification exponential rate coefficient			X		X	
SDNCO	Denitrification threshold water content			X		X	

To represent the model parametrization as an input in the subsequent sensitivity and uncertainty analysis of the environmental impact study, non-unique parameter sets were identified for the Schwechat and the Raab catchments, respectively. The preceding parameter SA revealed that changes in the model parameter values influenced the simulations similarly independent of the sub-basin and HRU configurations in the Schwechat and the Raab catchment, respectively. As a consequence, but also to facilitate the separation of the effects of the model setup and the model parametrization in the analysis, parameter combinations were selected as non-unique ones that result in simulations of daily discharge and NO_3^- -N loads that fulfill certain objective criteria together with all model setups of the Schwechat and the Raab, respectively. For the respective 19 and 16 influential model parameters were randomly sampled drawing 100 000 parameter combinations. Daily discharge and NO_3^- -N loads were simulated with all model setups of the Schwechat and the Raab catchments. The simulations were evaluated with the following criteria to accept a parameter set as "fit-for-purpose": $\text{KGE} > 0.5$ for daily discharge at the catchment outlets, $\text{KGE} > 0.4$ for daily NO_3^- -N loads at the gauges with longer continuous records (in both catchments the gauging point within the catchment and not at the catchment outlet), percentage bias (pbias Gupta et al., 1999) $< 50\%$ for NO_3^- -N loads, and absolute $\text{RSR} > 1$ for different discharge and NO_3^- -N load (as shown in Pfannerstill et al., 2014; Haas et al., 2016).

In total, 43 and 52 behavioral parameter combinations were identified for the Schwechat and the Raab catchments, respectively. The ability of the selected parameter sets used with the different model setups to reproduce the observed data is illustrated in Fig. 5.3. The initial and final ranges of parameter changes are shown in Table 5.6. The 43 and 52 parameter combinations are additionally illustrated in parallel coordinate plots for the Schwechat and the Raab in Fig. 5.4 to show any clustering of individual parameters and interactions between parameters. The majority of parameters are scattered randomly and do not show any clustering or interaction with other parameters. The parameters RCN and NPERCO in the Schwechat catchment show a clear inverse relationship. This implies that the parameters compensate each other in the behavioral model setups. This finding seems plausible for the Schwechat catchment where the NO_3^- -N transport into the receiving waters is strongly groundwater driven and a surplus of NO_3^- -N input is reduced by a decrease in NO_3^- -N percolation. The parameters SLSOIL , SURLAG , and SOL_AWC show a clear bimodal pattern for the Raab catchment. The bimodal patterns of these parameters are strongly related and a compensation effect between these parameters is visible. Model setups with increased slope values (SLSOIL) and longer lag-times of the surface runoff (SURLAG) together with an increased soil available water content (SOL_AWC) resulted in behavioral model and were able to reproduce historic discharge and NO_3^- -N records, similar to the model setups where such clear relationship is not visible.

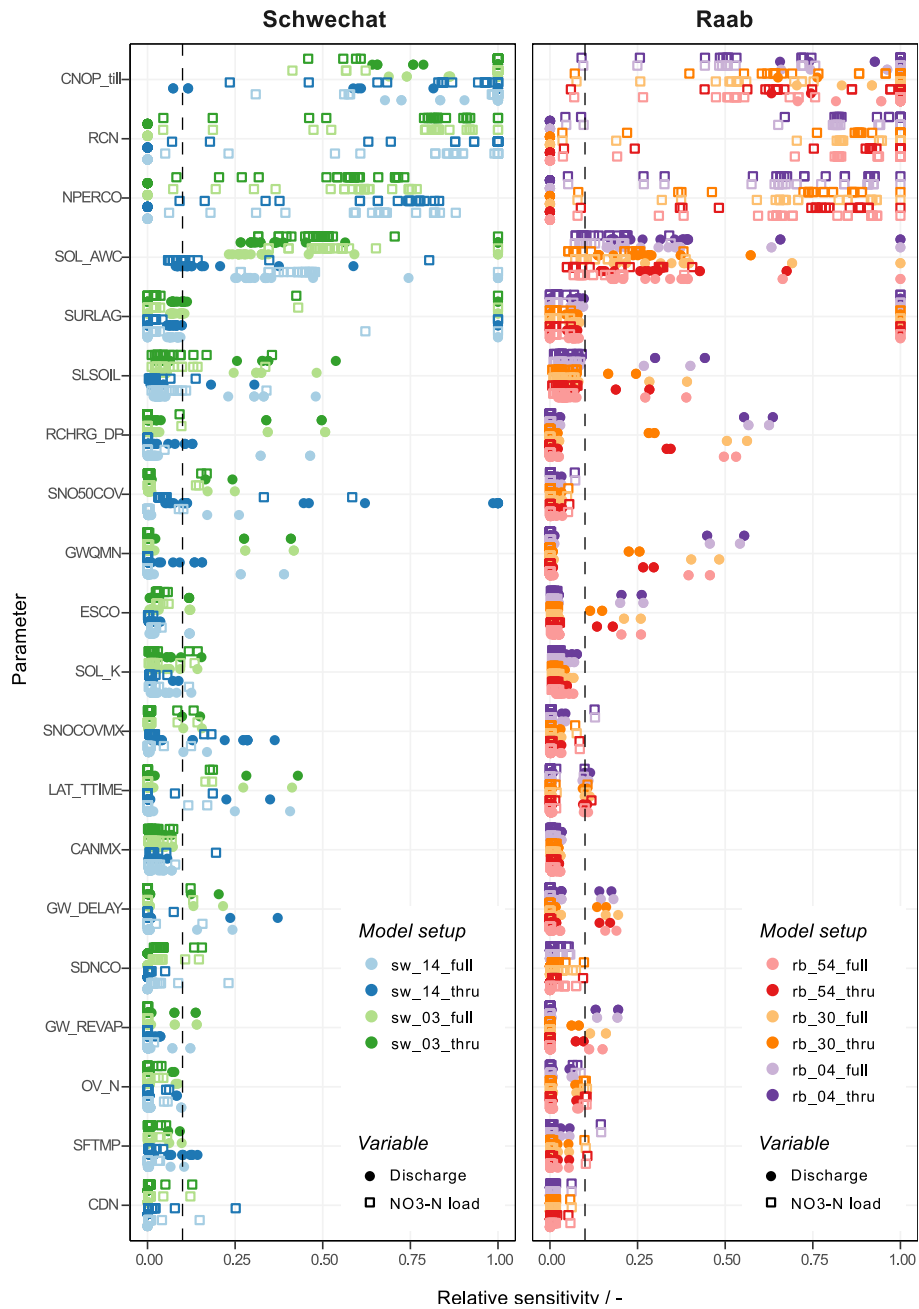


Figure 5.2: Identification of the influential SWAT model parameters for the Schwechat (left) and the Raab (right). The y-axis illustrates model parameters that showed an impact on at least one of the analyzed objective criteria. The x-axis shows the relative sensitivities of analyzed objective criteria (in relation to the most influential parameter for an objective criterion). The colors indicate the different SWAT model setups. The circles show the sensitivities for objective criteria related to discharge, while the hollow squares show parameter sensitivities for NO_3^- -N loads. The dashed line indicates the 0.1 value of relative sensitivity. A parameter is considered to be sensitive if it resulted in a relative sensitivity above this threshold for the objective criteria.

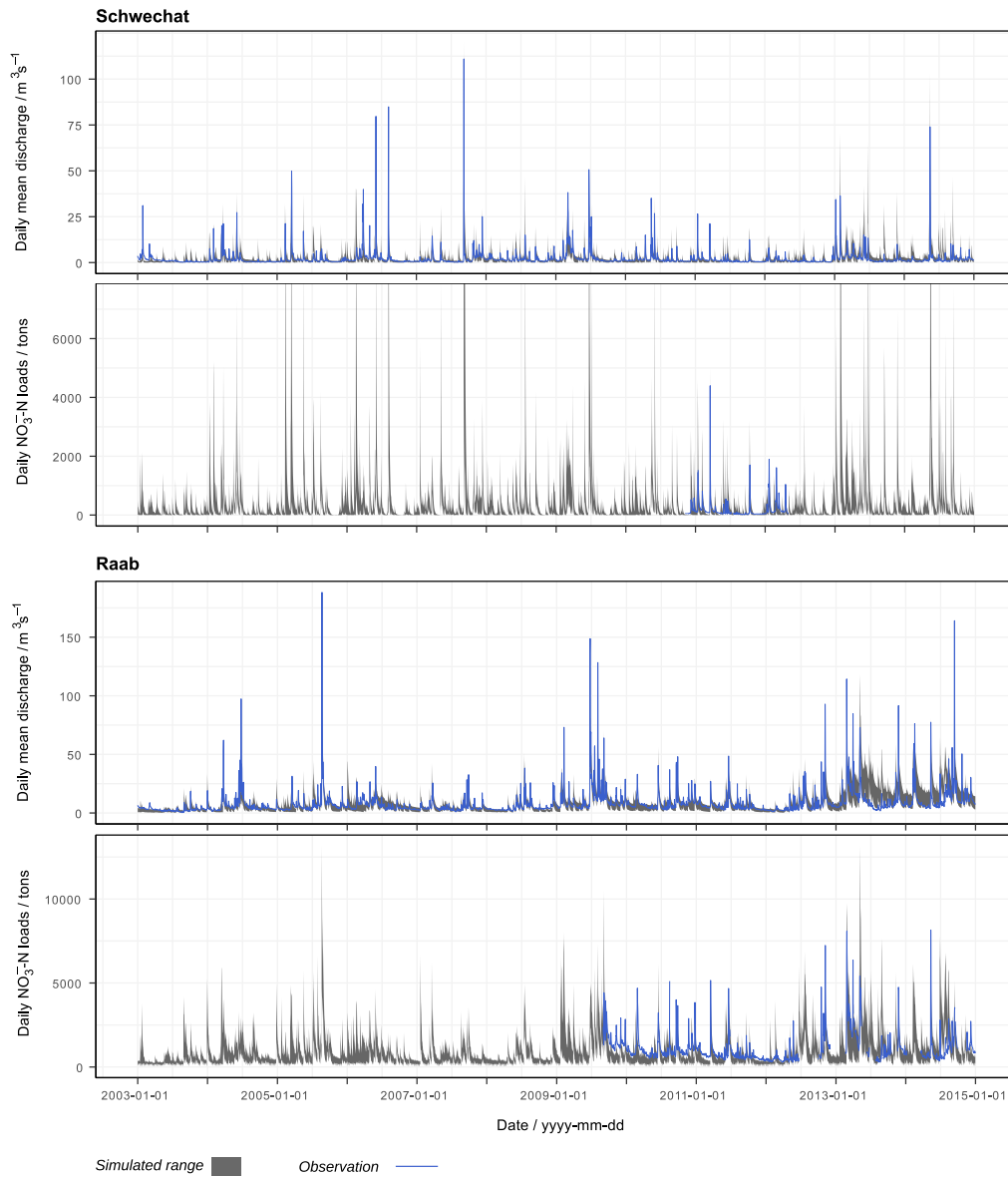


Figure 5.3: Simulated time series of daily mean discharge and daily $\text{NO}_3\text{-N}$ loads for the Schwechat (top) and the Raab (bottom) catchments for the time period 2003 to 2015. The gray bands show the ranges simulated using the selected model parameter sets with the different SWAT model setups. The blue solid lines indicate available observations of discharge and $\text{NO}_3\text{-N}$ loads for the respective time periods.

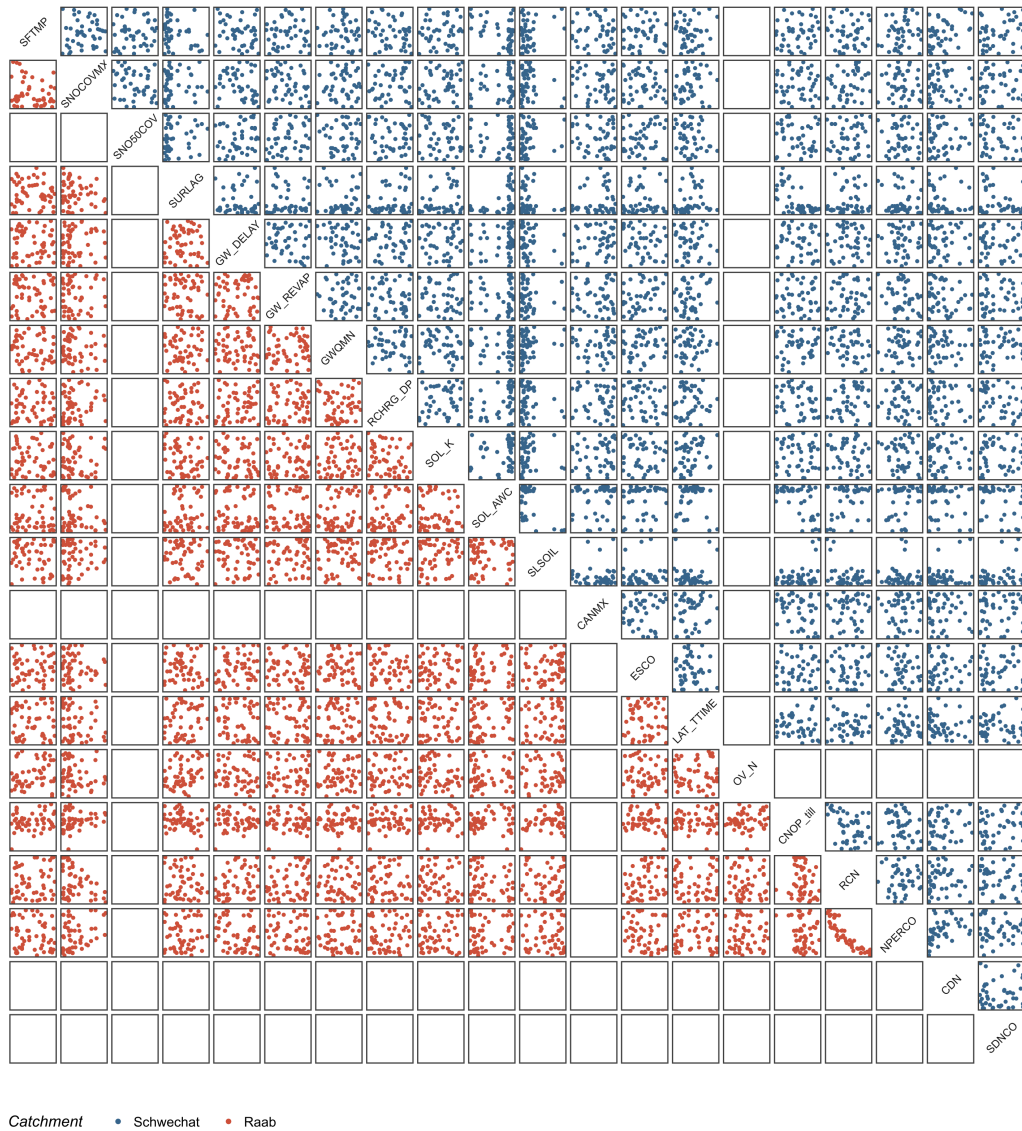


Figure 5.4: Parallel coordinate plot of the 43 and 52 behavioral SWAT model parameter combinations that were used with the model setups of the Schwechat and the Raab, respectively. Each panel illustrates the interaction of two model parameters. The parameter combinations for the Schwechat are illustrated in red (below the diagonal) and the combinations for the Raab are given in blue (above the diagonal). The x and y axes of each panel show the range of the respective parameter plotted along the x or y dimension. The corresponding parameter ranges for all illustrated parameters are provided in Table 5.6.

Table 5.6: Ranges of parameter changes for the behavioral model parameter sets. The type of change indicates whether a model parameter was replaced by absolute values, altered by adding an absolute to the initial parameter value, or changed by a relative fraction of the initial parameter value. The initial ranges of parameter changes and the ranges of parameter ranges of the behavioral parameter combinations in the model setups of the Schwechat and the Raab are shown.

Parameter	Type of change	Range of parameter change		
		Initial range	Schwechat	Raab
SFTMP	replace value	[-1.00, 1.00]	[-0.69, 0.93]	[-0.98, 0.88]
SNOCOVMX	replace value	[100.0, 500.0]	[0.9, 177.0]	[100.8, 447.5]
SNO50COV	replace value	[0.20, 0.50]	[0.21, 0.49]	
SURLAG	replace value	[0.00, 18.00]	[0.02, 0.99]	[0.01, 0.10]
GW_DELAY	replace value	[0.0, 300.0]	[5.5, 25.0]	[2.1, 283.3]
GW_REVAP	replace value	[0.02, 0.20]	[0.05, 0.15]	[0.02, 0.20]
GWQMN	replace value	[0, 3000]	[567, 2472]	[109, 2925]
RCHRG_DP	replace value	[0.01, 1.00]	[0.31, 0.69]	[0.13, 0.97]
SOL_K	relative change	[-0.90, 10.00]	[0.00, 0.97]	[-0.79, 9.76]
SOL_AWC	relative change	[-0.90, 2.00]	[-0.86, 1.49]	[0.01, 1.98]
SLSOIL	replace value	[0.0, 150.0]	[0.9, 27.6]	[14.7, 148.2]
CANMX	relative change	[-0.90, 2.50]	[0.34, 2.40]	
ESCO	replace value	[0.00, 0.90]	[0.05, 0.9]	[0.05, 0.89]
LAT_TTIME	replace value	[0.0, 180.0]	[0.8, 6.8]	[5.5, 176.3]
OV_N	absolute change	[-0.09, 0.60]		[0.07, 0.58]
CNOP_till	relative change	[-0.20, 0.10]	[-0.19, -0.06]	[-0.18, 0.01]
RCN	replace value	[2.00, 10.00]	[5.05, 9.97]	[2.30, 8.45]
NPERCO	replace value	[0.00, 1.00]	[0.24, 0.99]	[0.18, 0.7]
CDN	replace value	[0.00, 1.50]	[0.01, 1.44]	
SDNCO	replace value	[0.00, 0.50]	[0.02, 0.49]	

5.4 SCENARIO DEFINITION - PREPARATION OF DISCRETE MODEL INPUTS

The study involves future changes of the land use, point source emissions, and the climate. The uncertainties of these variables are expressed as discrete scenarios.

For the land use change scenarios, two scenario story lines (Rounsevell and Metzger, 2010) were developed for the Schwechat and the Raab catchments. A "business-as-usual" scenario extrapolates the observable trends in land use change to the future (2071 to 2100), while a second "extensive" scenario assumes an extensification of agricultural activities and other intensive land uses in both catchments (Table 5.7).

In the Schwechat catchment population growth is the strongest factor for a future change in land use (Statistik Austria, 2015a; Statistik Austria, 2016). Hence, a transformation from extensive pasture land (-35%) to urban land use and an increase of dense urban areas describe the "business-as-usual" scenario.

Table 5.7: Transformations of land uses implemented in the land use scenarios for the Schwechat and the Raab.

"business-as-usual"				"extensive"			
Land use		Change		Land use		Change	
From	To	(%)	(ha)	From	To	(%)	(ha)
Schwechat:							
Urban, light	Urban, dense	10	239	Winter wheat	Ext. pasture	27.5	184
Ext. pasture	Urban, light	15	361	Winter wheat	Legumes	27.5	184
Ext. pasture	Winter wheat	20	481				
Raab:							
Ext. pasture	Corn	75	8726	Corn	Ext. pasture	27.5	3595
Sugar beet	Corn	80	2429	Corn	Legumes	27.5	3595
Legumes	Corn	70	419				
Winter wheat	Corn	30	557				

Table 5.8: Municipal point source emissions and emission changes due to different population growth scenarios in the Schwechat and the Raab catchments.

District	Scenario BAU ¹ / BPS ²			Scenario ÖROK ³		
	Change (%)	Population	NO ₃ ⁻ -N load (kg yr ⁻¹)	Change (%)	Population	NO ₃ ⁻ -N load (kg yr ⁻¹)
Schwechat:						
Baden	0.0	32 058	39 842	32.0	42 317	52 591
Total	0.0	32 058	39 842	32.0	42 317	52 591
Raab:						
Weiz	7.7	56 982	44 918	-2.0	51 529	40 872
Südoststeiermark	2.3	32 296	16 537	-20.4	25 117	12 868
Total	5.7	89 278	61 455	-8.7	76 646	53 740

The "extensive" scenario assumes no change in population and a shift of half of the wheat producing area to extensive pastures.

Since 1970, the areas for corn production increased by 220 % in the Raab catchment, mostly for bio gas production and at the expense of sugar beets and cereals (Statistik Austria, 2017). For the "business-as-usual" scenario, an increase in the corn area by a further 100 % until the end of the century was assumed,

- 1 BAU = "business-as-usual" scenario for the districts in the Schwechat catchment that assumes no change in population numbers.
- 2 BPS = "Bevölkerungsprognose Steiermark" scenario according to "Regionale Bevölkerungsprognose Steiermark 2015/16 -Bundesland, Bezirke und Gemeinden" (Amt d. Stmk LReg, 2016)
- 3 ÖROK = "Österreichische Raumordnungskonferenz" scenario according to "ÖROK-Regionalprognosen 2014" (Statistik Austria, 2015a) and "Datenbank zur Bevölkerungsprognose 2016 - Hauptszenario" (Statistik Austria, 2016)

replacing extensive pastures (−75 %), sugar beets (−80 %), legumes (−70 %), and winter wheat (−30 %).

Groundwater protection measures lead to strict regulations for fertilizer application in the Leibnitzerfeld region adjacent to the Raab catchment (LGBl. Nr. 39/2015, 2015). Therefore, the "extensive" scenario assumes an adoption of similar nitrogen regulations in the Raab catchment. Thus, decreasing areas with intensive fertilizer application, such as corn by 50 % and transforming these areas to extensive pasture land was carried out in this scenario.

Two municipal point source emission scenarios for both catchments (Table 5.8) and two industrial point source emission scenarios for the Raab catchment (Table 5.9) were developed. The future change in municipal emissions was assumed to be directly related to the change in population. For all provinces in the Schwechat basin future scenarios predict an average population growth of 32 % (Statistik Austria, 2015a; Statistik Austria, 2016). The predictions of the population development in the provinces of the Raab are contradicting, with predicted changes between 2.3 % (Statistik Austria, 2015a) and −20.4 % (Amt d. Stmk LReg, 2016).

Table 5.9: Industrial point source emissions and implemented emission changes at the Raab due to increase in production or relocation of the dominant leather producer.

Industrial emitter	Scenario "relocation" ¹		Scenario "boom" ²	
	Change (%)	NO ₃ ⁻ -N (kg yr ⁻¹)	Change (%)	NO ₃ ⁻ -N (kg yr ⁻¹)
Agrana Fruit Austria GmbH	0.0	1029	0.0	1029
BOXMARK Leder/Feldbach	−100.0	0	30.0	88 257
BOXMARK Leder/Jennersdorf	−100.0	0	30.0	36 442
Fleischhof Raabtal GmbH	0.0	292	0.0	292
Johann Titz GmbH	0.0	3774	0.0	3774
WOLLSDORF Leder	0.0	26 572	0.0	26 572
Total	−75.20	31 667	22.6	156 366

In the Raab catchment 94 % of the industrial point source emissions stem from the leather industry and almost 70 % of the industrial point source emissions are caused by one leather manufacturing company. Thus, industrial emission scenarios were developed for that particular manufacturer. As boundaries for the production, an upper environmental boundary and a lower economical boundary were defined for the prediction of future industrial emissions. Based on an assessment of effluent dilution (ÖWAV, 2010), current environmental regulations (BGBl. II 2010/99, 2010; and BGBl. II 2006/96, 2006) allow an increase of 30 % in emissions from that leather producer, resulting in a total increase in industrial emissions of 22.6 %. Assuming a relocation of the two manufactur-

¹ The "relocation" scenario assumes a relocation of the largest leather producer of the region.

² The "boom" scenario assumes an increase in productivity of the largest leather producer within the regulatory boundaries.

ing sites of that leather producer to outside of the catchment would stop their emissions into the Raab, reducing the total industrial point emissions by 75.2 %.

Future climate change was considered with 22 downscaled and bias corrected climate change scenarios (Table 5.10). Regional climate simulations were obtained from the EU-CORDEX project (Jacob et al., 2014), providing 11 GCM-RCM simulations for the greenhouse gas concentration trajectories RCP4.5 (Smith and Wigley, 2006; Wise et al., 2009) and RCP8.5 (Riahi et al., 2007) respectively. In this study daily precipitation sums and daily minimum and maximum temperatures for the time period 2071 to 2100 were utilized. The EURO-CORDEX climate simulations are available at a spatial resolution of 12.5 km (EUR-11 Jacob et al., 2014). Statistical downscaling (Zorita and Von Storch, 1999) was applied to prepare all climate simulations at a resolution of 1 km. To correct downscaling errors (e.g. Haslinger et al., 2013; Muerth et al., 2013), bias correction (Teutschbein and Seibert, 2013) was applied to the climate simulations employing quantile mapping (Hempel et al., 2013). Downscaling and bias correction were performed for the historical period 1971 to 2000, involving the reanalysis datasets SPARTACUS (Hiebl and Frei, 2016) for minimum, mean and maximum temperature and GPARD (Hofstätter et al., 2013) for daily precipitation sums.

5.5 SIMULATIONS UNDER FUTURE CHANGE AND ANALYSIS

Table 5.11 summarizes the land use change, point source emissions, and climate change and the model setups and model parametrizations that were used for the analysis of simulated discharge and NO_3^- -N loads in the Schwechat and the Raab catchments. In total, 7000 combinations of land use, point source emissions, climate, model setups and model parametrizations were drawn for both catchments applying a quasi random sampling. The number of combinations results from previous experiments that applying the GSA method of Sobol using the sampling strategy proposed by Saltelli and Tarantola (2002) with a base sample size $N_b = 1000$ and a total sample size of $N = N_b(k + 2)$, where k is the number of model inputs that are analyzed. All sampled combinations were assembled to executable SWAT models. Daily discharge and daily NO_3^- -N loads at the outlets of the Schwechat and the Raab catchments were simulated for the period from 2071 to 2100.

The analysis of discharge and NO_3^- -N loads follows two main goals i) to identify the dominant controls on the simulation of discharge and NO_3^- -N loads in the two catchments and ii) to assess how the considered inputs control the simulation of discharge and NO_3^- -N loads.

5.5.1 Global sensitivity analysis

The GSA employs the PAWN sensitivity measure that was described in section 3.3.2. As a summary statistics the maximum statistics was implemented to com-

Table 5.10: GCM–RCM combinations implemented in the study with their long-term mean annual precipitation sums and long-term mean annual temperatures for the Schwechat and the Raab.

Model	Schwechat		Raab	
	P (mm)	T (°C)	P (mm)	T (°C)
EUR-11_CNRM-CERFACS-CNRM-CM5_RCP45_CLMcom-CCLM4-8-17	845.6	10.5	1103.0	12.4
EUR-11_CNRM-CERFACS-CNRM-CM5_RCP85_CLMcom-CCLM4-8-17	828.7	11.6	1075.6	13.7
EUR-11_CNRM-CERFACS-CNRM-CM5_RCP45_SMHI-RCA4	911.9	10.9	1118.0	12.6
EUR-11_CNRM-CERFACS-CNRM-CM5_RCP85_SMHI-RCA4	943.8	12.4	1091.0	14.4
EUR-11_ICHEC-EC-EARTH_RCP45_CLMcom-CCLM4-8-17	813.3	10.6	967.0	12.5
EUR-11_ICHEC-EC-EARTH_RCP85_CLMcom-CCLM4-8-17	809.2	12.1	941.5	14.4
EUR-11_ICHEC-EC-EARTH_RCP45_SMHI-RCA4	915.8	11.2	1018.4	12.9
EUR-11_ICHEC-EC-EARTH_RCP85_SMHI-RCA4	939.7	12.9	1036.1	15.1
EUR-11_ICHEC-EC-EARTH_RCP45_KNMI-RACMO22E	772.7	10.9	965.0	12.6
EUR-11_ICHEC-EC-EARTH_RCP85_KNMI-RACMO22E	779.0	12.6	925.6	14.6
EUR-11_ICHEC-EC-EARTH_RCP45_DMI-HIRHAM5	925.8	10.4	962.8	12.4
EUR-11_ICHEC-EC-EARTH_RCP85_DMI-HIRHAM5	912.9	12.1	976.8	14.4
EUR-11_IPSL-IPSL-CM5A-MR_RCP45_IPSL-INERIS-WRF331F	907.2	10.2	1046.7	13.0
EUR-11_IPSL-IPSL-CM5A-MR_RCP85_IPSL-INERIS-WRF331F	996.2	11.6	1202.2	14.6
EUR-11_IPSL-IPSL-CM5A-MR_RCP45_SMHI-RCA4	899.8	11.7	1076.8	13.7
EUR-11_IPSL-IPSL-CM5A-MR_RCP85_SMHI-RCA4	934.6	13.5	1217.3	15.9
EUR-11_MPI-M-MPI-ESM-LR_RCP45_CLMcom-CCLM4-8-17	839.1	11.5	960.5	13.6
EUR-11_MPI-M-MPI-ESM-LR_RCP85_CLMcom-CCLM4-8-17	867.9	13.3	913.2	15.7
EUR-11_MOHC-HadGEM2-ES_RCP45_SMHI-RCA4	974.4	11.6	1108.5	13.6
EUR-11_MOHC-HadGEM2-ES_RCP85_SMHI-RCA4	945.0	13.6	1117.4	15.9
EUR-11_MOHC-HadGEM2-ES_RCP45_SMHI-RCA4	781.1	10.2	940.3	12.2
EUR-11_MOHC-HadGEM2-ES_RCP85_SMHI-RCA4	813.2	12.0	1021.4	14.3

pute the PAWN sensitivity index T_i for the input x_i . Eq. 3.7 can therefore be written as follows:

$$T_i = \max_{x_i = x_i^1, \dots, x_i^{n_i}} (KS_j(x_i^j)) \quad (5.1)$$

where the values $x_i = x_i^1, \dots, x_i^j, \dots, x_i^{n_i}$ are the n_i discrete realizations of the input x_i , and $KS_j(x_i^j)$ is the Kolmogorov-Smirnov distance calculated for the

realization j of the input x_i . The calculation of the maximum statistics provides information on the maximum impact that a model input x_i has on the simulation of a target variable y_i . The maximum statistics is less sensitive to large differences in the numbers of realizations which is particularly relevant in the present case study, where the numbers of realizations range between 2 and 53. Further, the distribution of the resulting Kolmogorov-Smirnov distances can be highly skewed (e.g. the majority of discrete realizations has a low impact, while a few realizations strongly influence the simulation). Therefore, the significance of a median sensitivity of a target variable y_i to a model input x_i is questionable and provides an additional argument for the analysis of the maximum impact of a model input x_i on a target variable y_i .

Table 5.11: SWAT model inputs and their numbers of realizations that were implemented in the sensitivity analyses for the Schwechat and the Raab.

Input	Nr. of Realizations		Details on realizations
	Schwechat	Raab	
Land use scenario	2	2	one "extensive", one "business-as-usual"
Point source scenario	2	4	Population growth: optimistic/pessimistic , Industry Raab: "relocation" / "boom"
Climate scenario	22	22	11 RCP4.5, 11 RCP8.5, period: 2071 to 2100
Model setup	4	6	Raab: 54, 30, 4 subbasins with/without HRU reduction, Schwechat: 14, 3 subbasins with/without HRU reduction
Parametrization	43	52	Discharge: KGE >0.5, NO ₃ ⁻ -N loads: KGE >0.4, pbias <50 %

To account for the effect of different numbers of discrete realizations of the analyzed inputs, but also to assess whether the number of drawn samples of input combinations ($N = 7000$) was sufficient to perform a GSA with PAWN, confidence intervals were calculated for the PAWN indices applying bootstrapping (Hinkley, 1988; Efron, 1987) using the R package *boot* (Canty and Ripley, 2017). To calculate the bootstrap mean and the 95% confidence intervals, 1000 bootstrap replicates were drawn (as demonstrated in Sarrazin et al. (2016)).

Signature measures of discharge and NO₃⁻-N loads were used as target variables y . Signature measures are measures that describe specific characteristics of simulated time series (Euser et al., 2013) (in this case of daily mean discharge and daily sums of NO₃⁻-N loads). Quantile values (0.01, 0.05, 0.20, 0.70, 0.95, and 0.99) of daily discharge and daily NO₃⁻-N loads, long-term mean discharges and long-term mean sums of NO₃⁻-N loads on an annual basis and for the meteorological seasons spring, summer, autumn, and winter, and mean NO₃⁻-N concentrations for different ranges of discharge quantiles (very high discharge (above 0.95 quantile), high discharge (0.95 to 0.70 quantile), medium discharge (0.70 to 0.20 quantile), low discharge (0.20 to 0.05 quantile), and very low discharge (below 0.05 quantile)) were calculated.

5.5.2 Visual analysis of the simulation uncertainties

To investigate how the inputs of land use change, changes in point source emissions, climate change, the model setup or the model parametrization control the simulation of discharge and NO_3^- -N loads, the simulation outputs and their associated uncertainties were visually analyzed. The 7000 assembled combinations of model inputs, model setups and parametrizations resulted in ranges of simulated discharge and NO_3^- -N loads. All executed model setups represent plausible realizations of the future conditions in both catchments to simulate future discharge and NO_3^- -N loads. Thus, the overall simulation uncertainties of simulated discharge and NO_3^- -N loads comprise all 7000 simulations of the Schwechat and the Raab catchments, respectively.

The uncertainty bands (no thresholds were set) of the simulations of the long-term mean monthly specific discharge, the long-term mean monthly sums of NO_3^- -N loads and the FDCs of daily discharge and daily NO_3^- -N loads were visually analyzed. These variables are related to a wide range of the signature measures that were analyzed in the GSA and thus allow a comparison of the GSA results with the results of the visual uncertainty analysis.

The low number of possible values taken by each input allowed a more detailed analysis of their effect on the simulated uncertainties, by subsetting the uncertainty bands of the discharge and NO_3^- -N load simulations with respect to the individual realizations of the analyzed model input. The separated simulation uncertainty bands were additionally colored with respect to the specific properties of an input, such as the temperature or precipitation anomalies of each climate scenario compared to historical records. These color ranges greatly facilitated identifying the dominant controls of the simulation.

5.6 RESULTS

5.6.1 Identification of the most influential model inputs

Fig. 5.5 summarizes the influence of the implemented land use, point source emission, climate scenarios, the different model setups and the model parametrizations for the simulation of future discharge and Loads in the Schwechat (left) and the Raab (right) catchments. Each plot panel shows the calculated PAWN indices for the analyzed target variables for one model input in a catchment. Related target variables are grouped by colors to support the interpretability (e.g. to identify changes in sensitivity from high to low discharge). In its entirety each panel provides a general overview of the importance of an input for the simulation of discharge and NO_3^- -N loads. Individual PAWN indices (a single bar in a plot panel) highlight the importance of an input for the simulation of specific characteristics of the time series of discharge and NO_3^- -N loads.

The white boxes on top of each bar show the bootstrap means and the 95% confidence intervals (CIs) of each PAWN index and therefore provides an indicator for the adequacy of the sample size that was used to perform the analysis and the impact of differing numbers of discrete values of the analyzed input

variables. In general the bootstrapping resulted in narrow confidence intervals (maximum 0.05 and -0.08) for all analyzed model inputs and all signature measures providing high confidence in the resulting sensitivities. Although the numbers of discrete realizations of the analyzed model inputs (e.g. only 2 land use scenarios, but 43 and 52 model parametrizations) differ strongly and therefore result in different subset sizes to calculate the PAWN indices, no substantial differences in the confidence intervals is visible.

The land use scenarios applied to SWAT demonstrated a rather negligible impact on all signature measures, with mean PAWN indices below 0.05 to 0.07 and confidence intervals in the same range for the Schwechat and Raab respectively (first row Fig. 5.5). The point source scenarios, in contrast, showed a considerable influence on the signature measures of NO_3^- -N loads and concentrations in the Raab catchment, while the impacts of the point sources in the Schwechat catchment were negligibly low (second row Fig. 5.5). Thus, based on the implemented point source emission scenarios, industrial emitters in the Raab catchment are relevant for the development of in-stream NO_3^- -N loads and concentrations, particularly for low discharges and low NO_3^- -N loads. The importance of the industrial point sources in SWAT increases when higher NO_3^- -N load quantiles (low NO_3^- -N loads, from dark yellow to light yellow in Fig. 5.5) and NO_3^- -N concentrations for low discharges (from dark red to light red in Fig. 5.5) are simulated, which is evident from an increase in the mean PAWN index from 0.11 to 0.49 and 0.22 to 0.43, respectively. The climate scenarios and the model parametrizations show respective decreases in their importance for the simulation of low NO_3^- -N loads and NO_3^- -N concentrations for low discharges (with decreases in the mean PAWN index from 0.71 to 0.28 for the climate scenarios' influence on NO_3^- -N loads and from 0.79 to 0.36 for model parametrization's influence on NO_3^- -N concentrations).

The implemented climate scenarios showed large impacts on all calculated signature measures of discharge and NO_3^- -N loads (third row Fig. 5.5). The mean PAWN indices range between 0.25 to 0.90 and 0.25 to 0.96 for the Schwechat and the Raab, respectively. The climate scenarios were the most relevant inputs for the simulation of seasonal mean discharges and seasonal sums of NO_3^- -N loads. For the simulation of low discharge quantiles (large daily discharges) climate scenarios showed the highest relevance. For the simulation of low discharges however, the importance of the climate scenarios decreases, while the model parametrization becomes more relevant (from dark green to light green in Fig. 5.5). The mean PAWN indices of climate scenarios drop from 0.74 to 0.47 in the Schwechat catchment and from 0.82 to 0.51 for the simulation of lower discharges, while the mean PAWN indices for the model parametrization show respective increases from 0.43 to 0.87 and 0.44 to 0.80.

In general, the model parametrization was highly influential for all calculated signature measures and is comparable to that of the climate scenarios, with mean PAWN indices ranging between 0.43 to 0.90 in the Schwechat and 0.36 to 0.80 in the Raab (fifth row Fig. 5.5). Particularly, for the simulation of NO_3^- -N concentrations the model parametrization was the most dominant control of the variable simulated. In contrast to the large impact of the model parametrization,

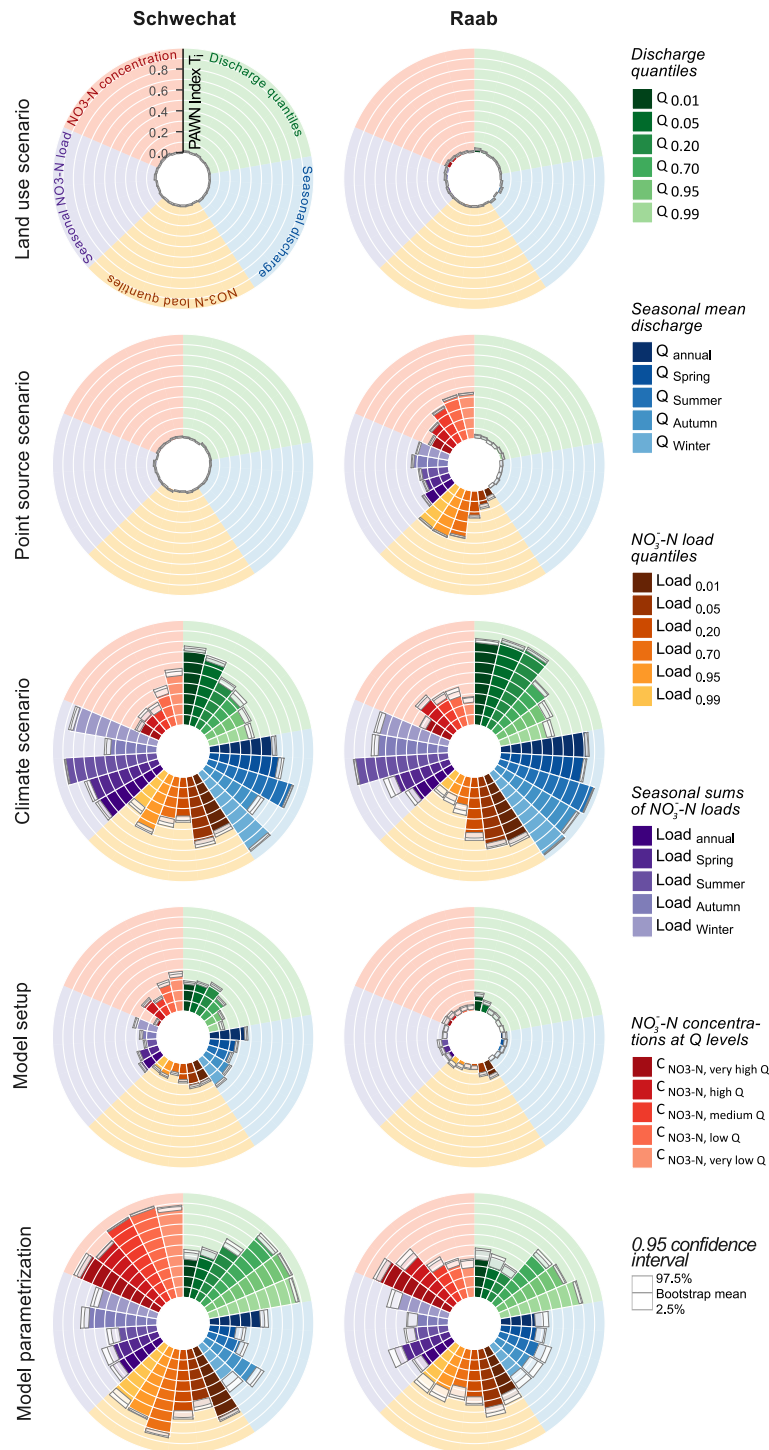


Figure 5.5: Influence of discrete SWAT inputs on simulated signature measures of discharge and NO_3^- -N loads in the Schwechat (left) and the Raab (right) catchment. Row-wise the panels illustrate the impacts of the model inputs land use scenarios, point source scenarios, climate scenarios, the model setup, and the model parametrization. Each circle plot shows the set of PAWN indices calculated for the respective catchment and model inputs. PAWN indices are illustrated in colored groups and clockwise order for discharge quantiles (green), seasonal long-term mean discharges (blue), quantiles of NO_3^- -N loads (yellow), seasonal sums of NO_3^- -N loads (purple), and mean NO_3^- -N concentrations for discharge quantiles (red). The white boxes represent the bootstrap mean and the 95% confidence intervals for the calculated PAWN indices.

the relevance of the model setup was much lower for the simulation of discharge and NO_3^- -N loads and concentrations. Overall, values of the PAWN index for the choice of the model setup did not exceed 0.37, and were much smaller (two to five times) compared to the model parametrization. The model setups yielded insignificantly low PAWN indices for the majority of signature measures with values below 0.1 in the Raab catchment (2.5% CI almost 0 for many signature measures), indicating that the model setup had a low influence on most of the analyzed processes. Only for high discharges and large NO_3^- -N loads a mean value for the PAWN index above 0.1 is visible.

5.6.2 Simulation uncertainties of discharge and NO_3^- -N loads

Using all 7000 combinations of land use, point source emissions, climate, model setups, and model parametrizations, the simulated discharges and NO_3^- -N loads deviated by up to 350% (grey bands in Fig. 5.6) from the simulations of discharge and NO_3^- -N loads in the reference period 2003 to 2015 (dashed line in Fig. 5.6). In the Schwechat (left column in Fig. 5.6) wider uncertainty bands are visible for the spring and early summer months. The results for the Raab catchment (right column) show wider uncertainty bands emerged for summer as well as for winter/early spring. A notable difference between the two catchments is how the simulations of long term monthly discharges and NO_3^- -N loads in the reference period compare to the ranges of future simulations. While the majority of model combinations for the Schwechat simulated larger discharges and NO_3^- -N loads for all months in the future, for the Raab catchment the simulations of discharge and especially NO_3^- -N loads are lower in comparison to the reference period.

The analyses of the uncertainty bands with respect to the implemented land use scenarios and the point source scenarios fully confirm the results from the SAs (Fig. 5.7). The attributed uncertainty bands for the two land use scenarios almost entirely overlap and show only minor deviations. A similar result is illustrated for the two point source scenarios in the Schwechat catchment. The scenarios in the Raab catchment involved industrial point source emissions. The grouped uncertainty bands that include scenarios with an increase in industrial production (red) and the uncertainty bands that include a decrease in industrial production (blue) show similar patterns. Yet, the blue and red uncertainty bands show a clear shift to each other. On average the scenarios with an increase in industrial production show long-term monthly sums of NO_3^- -N loads that are 15 tons higher compared to the scenarios with a decrease in industrial production. The same scenarios show larger amplitudes for medium and low NO_3^- -N loads, while large NO_3^- -N loads remain uninfluenced by the two scenarios for the development of the leather industry.

The GSA identified the climate scenarios to have a great influence on all signature measures of the simulated variables. Attributing the uncertainty bands to the individual GCM-RCM combinations unveils diverse outcomes for the future flow regime, the distribution and amplitude of monthly NO_3^- -N loads, as well as the appearance of high and low discharges and NO_3^- -N loads (Fig. 5.8). A visual

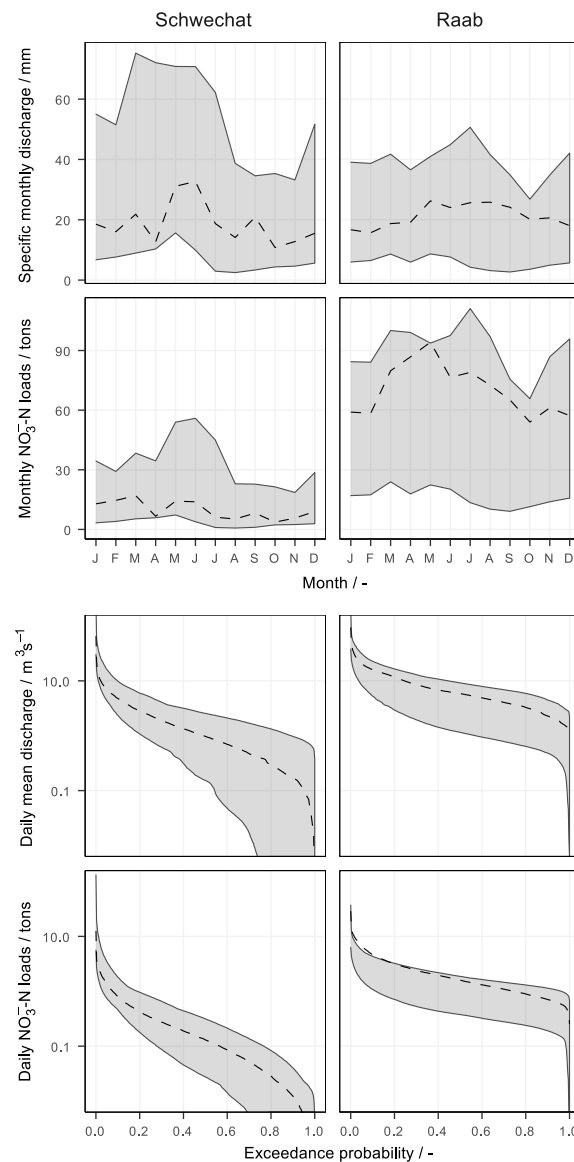


Figure 5.6: Simulated uncertainties resulting from the 7000 combinations of realizations of the influencing variables for the Schwechat (left) and the Raab (right). The grey bands illustrate the absolute ranges of simulated long-term mean monthly specific discharge (first row), long-term monthly sums of NO_3^- -N loads (second row), FDCs of mean daily discharges (third row), and FDCs for daily sums of NO_3^- -N loads (fourth row). The dashed lines show the best simulation of the historical reference period.

analysis of the separated uncertainty bands identifies the mean annual precipitation anomalies of the GCM-RCM combinations to have a strong impact on the simulation of discharge and NO_3^- -N loads. In comparison to the reference period (dashed line), wetter future climate scenarios (blue) simulated larger discharge and NO_3^- -N loads, while dryer future conditions lead to a drastic reduction in discharge and NO_3^- -N loads.

Half of the 22 implemented GCM-RCM combinations simulated an increase of more than 75 mm (dark blue) and for two GCM-RCM combinations, an increase

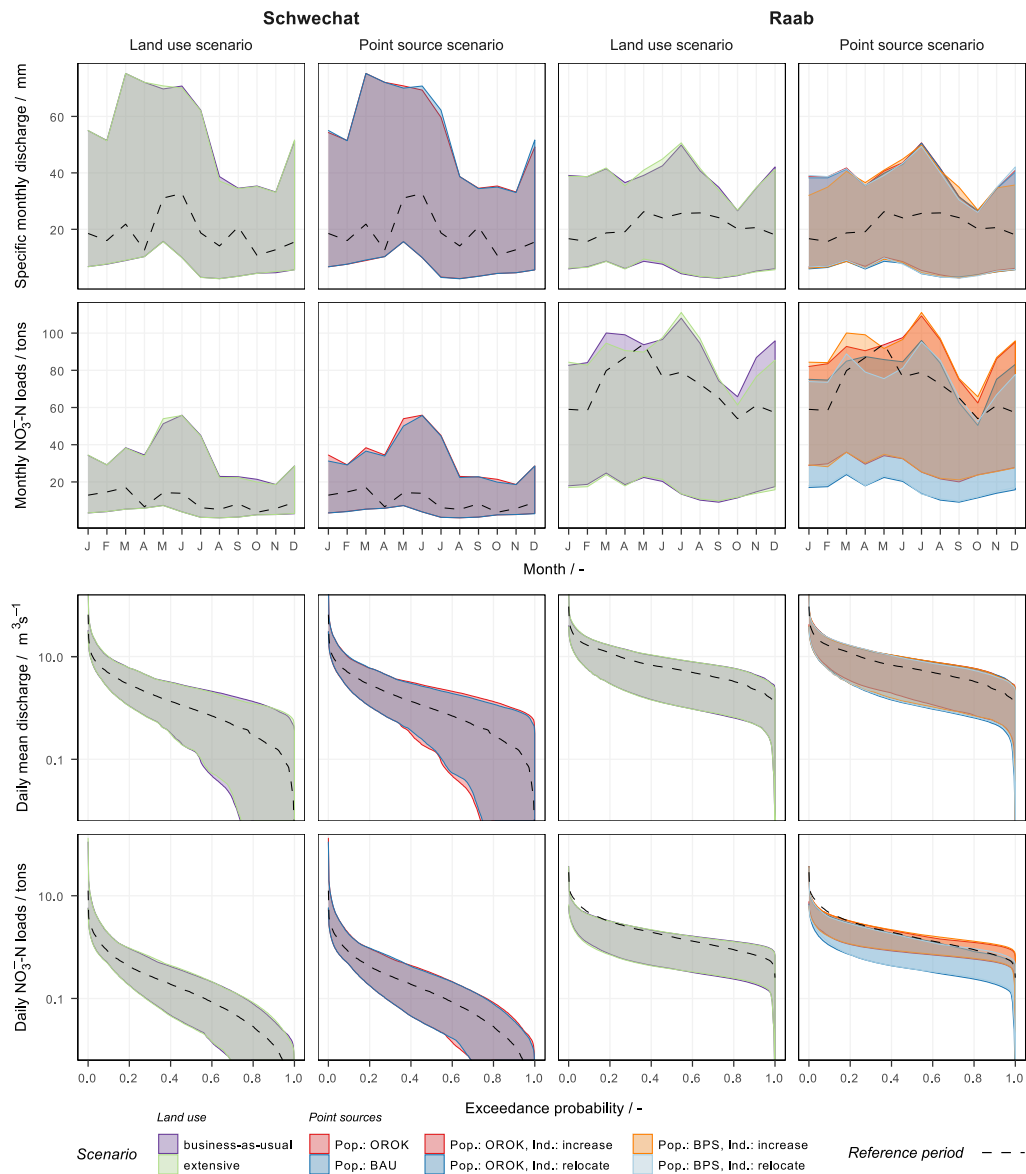


Figure 5.7: The influence of land use change and the development of point source emissions on the uncertainties resulting from the 7000 combinations of realizations of the influencing variables for the Schwechat (left) and the Raab (right). The uncertainties are illustrated for simulated long-term mean monthly specific discharge (first row), long-term monthly sums of $\text{NO}_3\text{-N}$ loads (second row), FDCs of mean daily discharges (third row), and FDCs for daily sums of $\text{NO}_3\text{-N}$ loads (fourth row). The uncertainty bands are attributed to the implemented land use scenarios (left panels per catchment) and the point emission scenarios (right panels). The colors of the grouped uncertainty bands indicate the different scenarios. The dashed lines show the best simulation of the historical reference period. The corresponding land use changes are provided in Table 5.7. The corresponding population growth scenarios (Pop. in the legend) are listed in Table 5.8 and the corresponding industrial emission scenarios in the Raab catchment (Ind. in the legend) are listed in Table 5.9.

of more than 25 mm (light blue) of precipitation for the Schwechat catchment was simulated. In contrast, for the Raab nine and four GCM-RCM combinations simulated a decrease in precipitation of more than 75 mm (dark red) and 25 mm

(light red), respectively. Consequently, a decrease in discharge and NO_3^- -N loads due to a decrease in precipitation is pronounced in the Raab catchment, while the majority of simulations of the Schwechat catchment show an increase in discharge and NO_3^- -N loads.

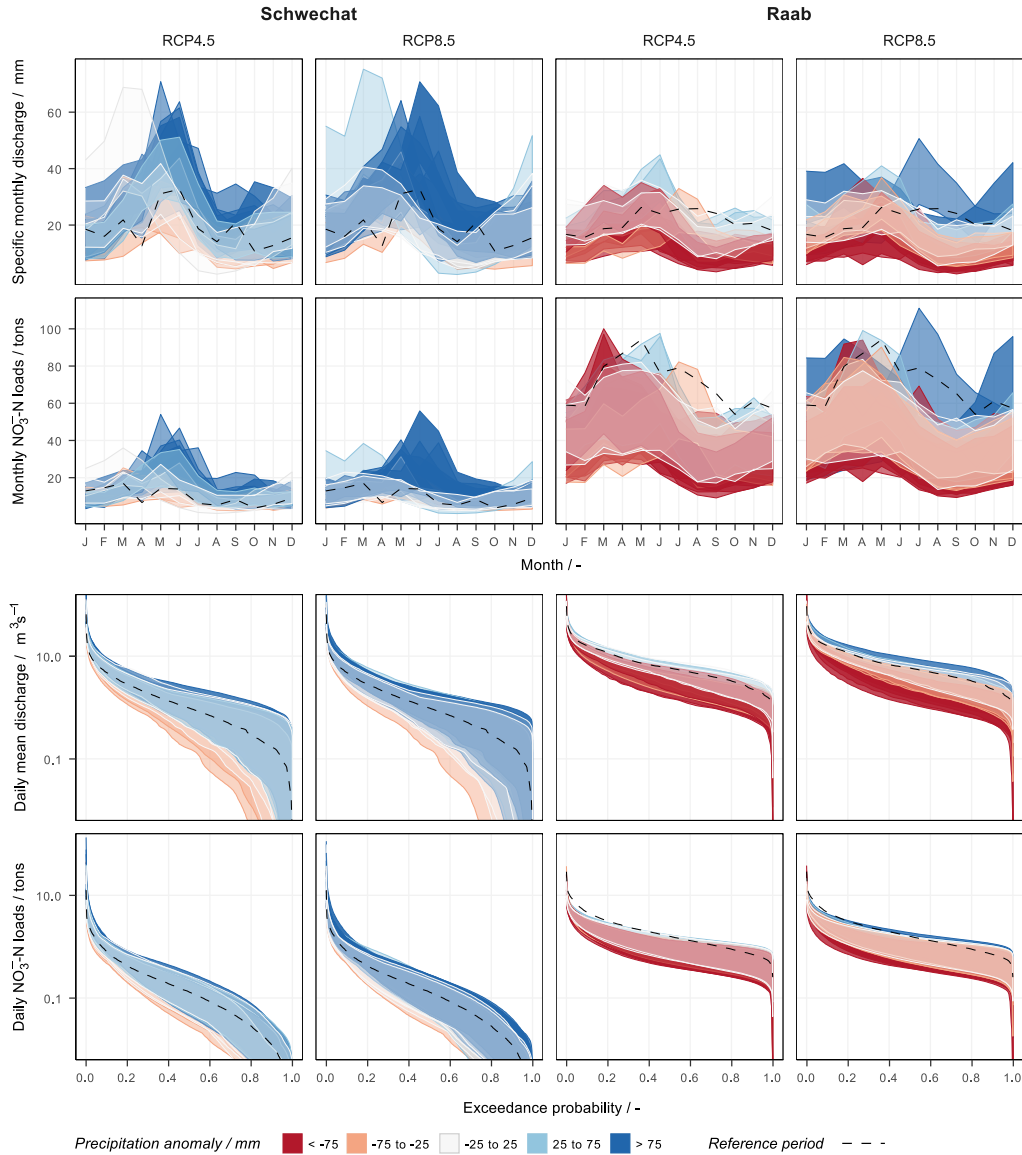


Figure 5.8: The influence of deviations in precipitation on the uncertainties resulting from the 7000 combinations of realizations of the influencing variables for the Schwechat (left) and the Raab (right). The uncertainties are illustrated for simulated long-term mean monthly specific discharge (first row), long-term monthly sums of NO_3^- -N loads (second row), FDCs of mean daily discharges (third row), and FDCs for daily sums of NO_3^- -N loads (fourth row). The uncertainty bands are attributed to the individual implemented climate scenarios. The colors of the uncertainty bands show the anomalies in long-term mean annual precipitation of each climate scenario, where blue represents wetter conditions compared to the reference period and red dryer conditions. The dashed lines show the best simulation of the historical reference period.

While a grouping of the individual climate scenarios with respect to their temperature anomalies shows a more indefinite picture, all climate scenarios

simulated an increase in temperature. Nevertheless, the expectation that an increase in annual mean temperature increases evapotranspiration and thus reduces discharge and NO_3^- -N loads is not met in Fig. 5.9. A clear separation of warmer and cooler climate scenarios, as it is observable for precipitation is not the case with temperature. Consequently, the differences in precipitation predominantly account for the influence of the climate scenarios, rather than the differences in temperature.

Although the influence of the model setups was much lower compared to the influence of the climate scenarios or the model parametrization, the analysis of the uncertainty bands for the different model setups provides interesting insights (Fig. 5.10). The uncertainty bands do overlap to a great extent, which confirms a low impact of the use of different model setups in the simulation of discharge and NO_3^- -N loads. Noteworthy is, that model setups that use the full set of HRUs agree much stronger in their simulations compared to the model setups where the number of HRUs was reduced. The difference between the full HRU and the reduced HRU model setups is distinct in the Schwechat catchment. The uncertainty bands of the two full HRU model setups almost completely overlap, although their numbers of subbasins are different (4 and 14 subbasins). The two model setups with a reduced number of HRUs (but also with 4 and 14 subbasins) show differences of up to 15 mm in the simulated monthly specific discharge and up to 7 tons in the monthly NO_3^- -N loads ($\approx 20\%$ of the uncertainty bandwidth).

The model parametrizations were relevant for all signature measures of discharge and NO_3^- -N loads and were most dominant for medium and low flows. The most dominant model parameters in both catchments were the parameters `CNOP_till` and `SOL_AWC`. Both parameters control the water retention and thus the immanent contribution of rainfall to the river discharge. Large values of `CNOP_till` and small values of `SOL_AWC` reduce the water retention capacity and increase the amplitude of medium and low discharges (third row in Fig. 5.11). A similar but inverse behavior is visible with medium NO_3^- -N loads (last row in Fig. 5.11), where a higher water retention results in an increase of NO_3^- -N loads. For the long-term monthly mean discharges and sums of NO_3^- -N loads two effects are observable in Fig. 5.11. First, smaller values of `CNOP_till` and larger values of `SOL_AWC` decrease the upper boundary of the uncertainty bands. Second, selected model parametrizations with large values of `CNOP_till` and small values of `SOL_AWC` cause considerably larger discharges in spring and a strongly reduced runoff in the autumn months in the Schwechat catchment.

5.7 DISCUSSION

5.7.1 *What can we as modelers learn from such analysis*

The illustrated modeling studies for the Schwechat and the Raab catchments emphasized the necessity to characterize, identify and explicitly communicate the uncertainties in a modeling chain, particularly for future simulations of environmental variables where large uncertainties are inherent in several modeling

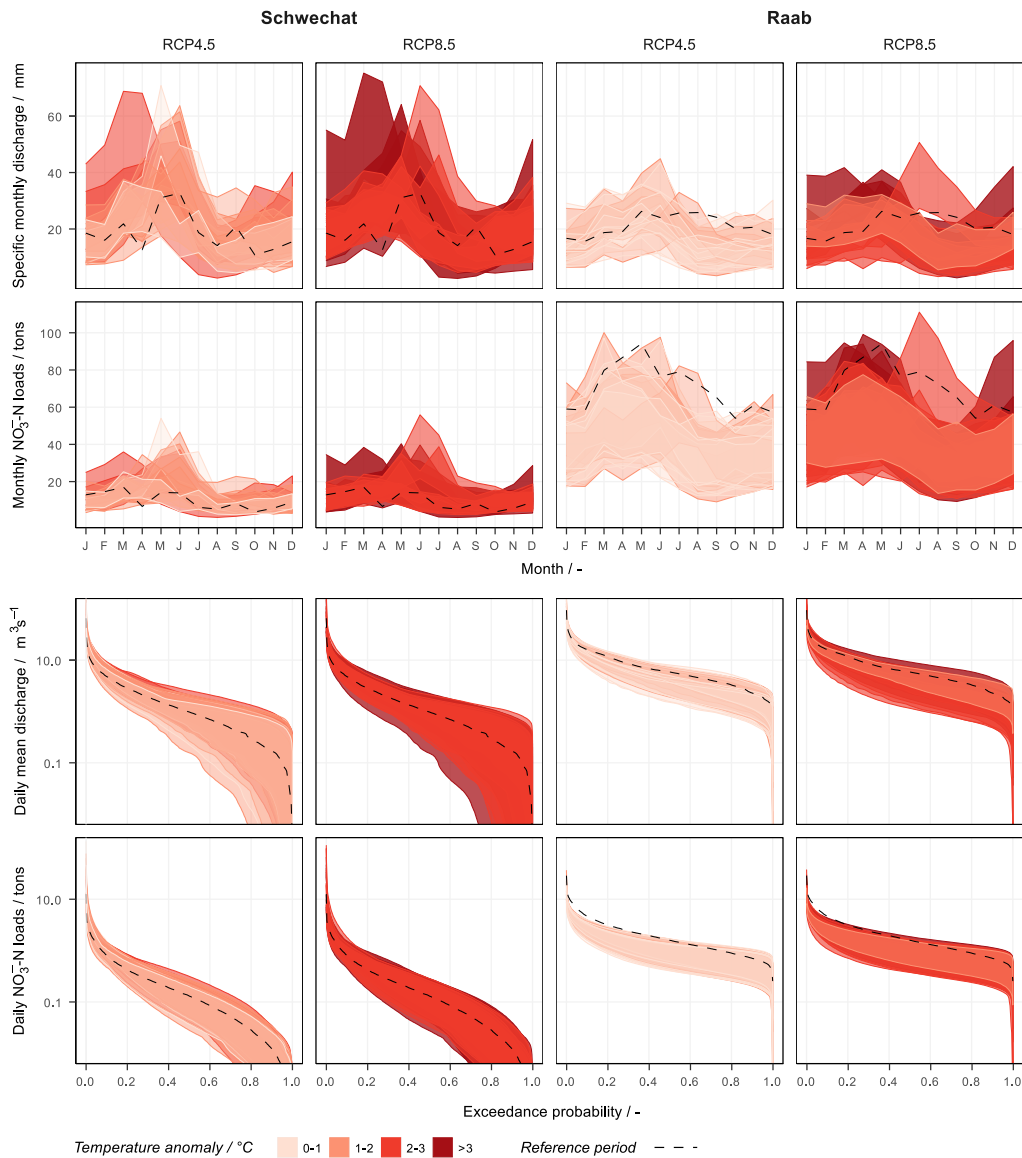


Figure 5.9: The influence of deviations in air temperature on the uncertainties resulting from the 7000 combinations of realizations of the influencing variables for the Schwechat (left) and the Raab (right). The uncertainties are illustrated for simulated long-term mean monthly specific discharge (first row), long-term monthly sums of $\text{NO}_3\text{-N}$ loads (second row), FDCs of mean daily discharges (third row), and FDCs for daily sums of $\text{NO}_3\text{-N}$ loads (fourth row). The uncertainty bands are attributed to the individual implemented climate scenarios. The colors of the uncertainty bands show the anomalies in long-term mean annual air temperature of each climate scenario, where a darker red represents hotter conditions compared to the reference period. The dashed lines show the best simulation of the historical reference period.

inputs. While the sensitivity analysis of signature measures related to discharge, $\text{NO}_3\text{-N}$ loads and $\text{NO}_3\text{-N}$ concentrations provided a comprehensive overview of the dominant influencing inputs on specific modeled variables, the analysis of the uncertainty bands for the simulation of the modeled variables provided insights into which properties of the model inputs (e.g. mean annual precipitation or mean air temperature of a climate scenario) control the uncertainties

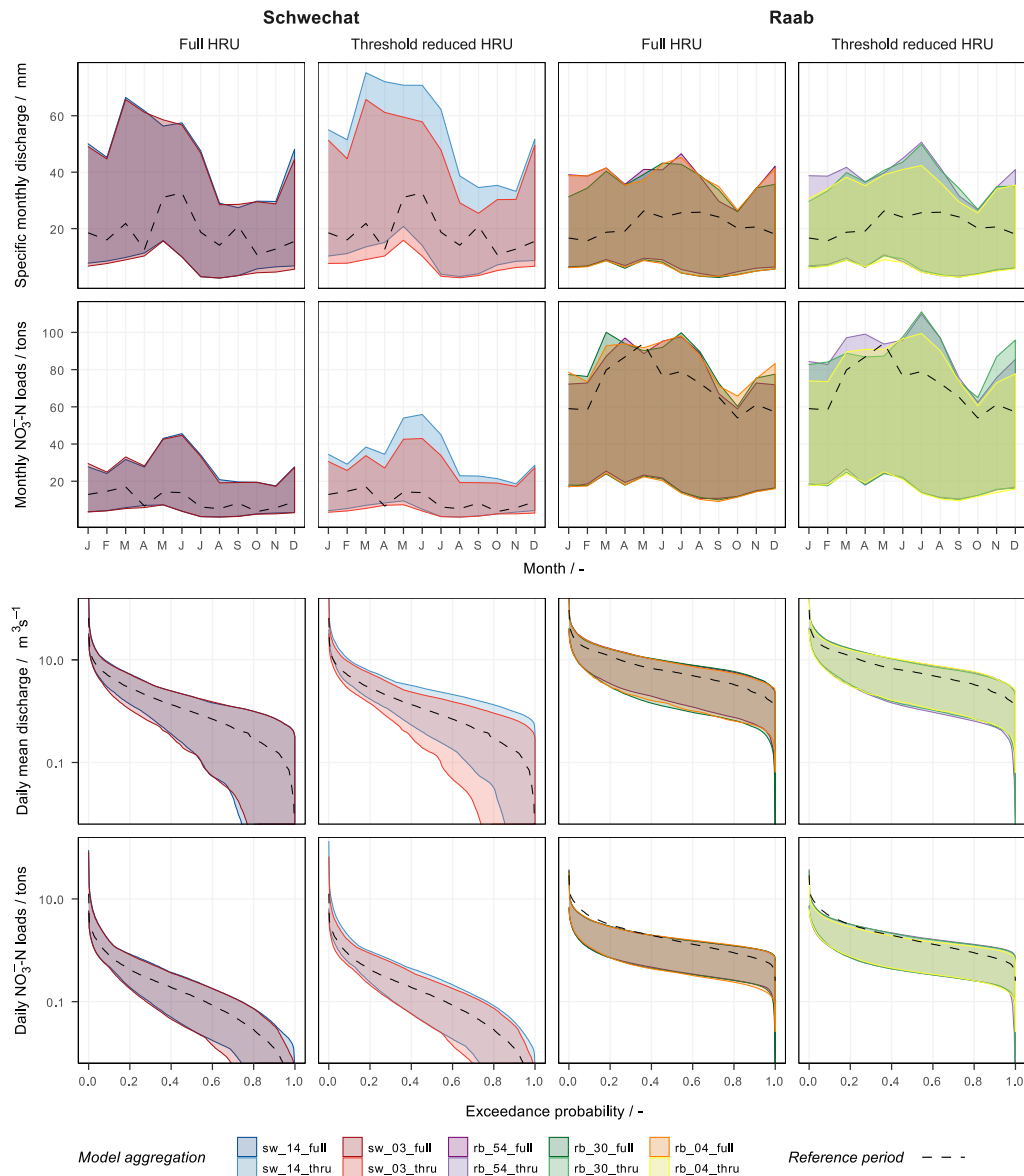


Figure 5.10: The influence of the model setup on the uncertainties resulting from the 7000 combinations of realizations of the influencing variables for the Schwechat (left) and the Raab (right). The uncertainties are illustrated for simulated long-term mean monthly specific discharge (first row), long-term monthly sums of $\text{NO}_3\text{-N}$ loads (second row), FDCs of mean daily discharges (third row), and FDCs for daily sums of $\text{NO}_3\text{-N}$ loads (fourth row). The uncertainty bands are attributed to the individual SWAT model setups. The results are separated for model setups where the full set of HRUs was used (left panels per catchment) and for setups with a reduced set of HRUs (right panels). The colors of the uncertainty bands show the different model setups with varying numbers of subbasins. The dashed lines show the best simulation of the historical reference period.

and how these control the simulation. The analyses allow to draw conclusions that are beneficial to consecutive steps of an impact study, for instance to refine the impact study setup and to focus on the most influential components and ultimately to reduce the uncertainties in the modeling simulation chain.

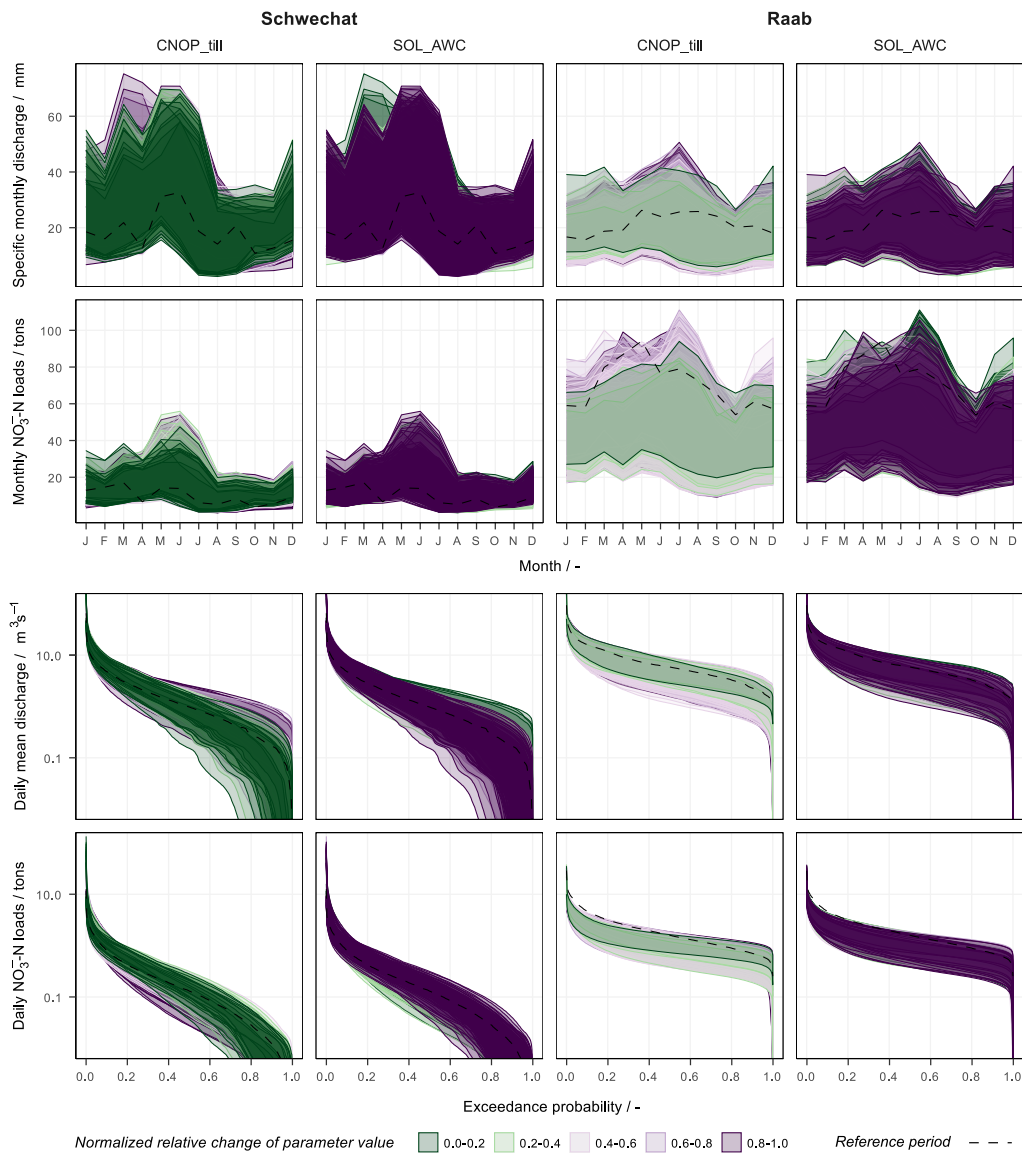


Figure 5.11: The influence of model parametrization on the uncertainties resulting from the 7000 combinations of realizations of the influencing variables for the Schwechat (left) and the Raab (right). The uncertainties are illustrated for simulated long-term mean monthly specific discharge (first row), long-term monthly sums of NO_3^- -N loads (second row), FDCs of mean daily discharges (third row), and FDCs for daily sums of NO_3^- -N loads (fourth row). The uncertainty bands are attributed to the individual "behavioral" SWAT model parameter sets. The effect of the two dominant model parameters CNOP_till (left panels for each catchment) and SOL_AWC (right panels) is shown. The subsetting uncertainty bands are colored with respect to the changes of the parameter values, shown as normalized values for comparability. The dashed lines show the best simulation of the historical reference period.

The land use scenarios showed an almost negligible impact on the simulation of discharge and NO_3^- -N loads. The discharge and the NO_3^- -N loads at the catchment are however integrated signals for the entire catchment and changes in land use may have a greater importance for particular points in a catchment. Many case studies have applied the SWAT model to assess the impact of land

use change on different variables of the water cycle (Wagner et al., 2017; Mehdi et al., 2015b), water quality (Guse et al., 2015; Mehdi et al., 2015a; Teshager et al., 2016), or sediment yield (Bieger et al., 2013). Bieger et al. (2013) found very low land use change induced increases in discharge for a catchment in China. Only an assumed strong intensification of the agriculture led to a 4% increase in discharge. At the same time however, a strong increase in sediment yield of up to 450% for the summer months was simulated due to the intensification of agriculture. Guse et al. (2015) also found only small changes in simulated discharge caused by future land use change in a German lowland catchment. In absolute numbers the simulated future NO_3^- -N loads showed small differences between the baseline scenario and the two applied methods of land use change presented by Guse et al. (2015). Yet, the temporal patterns in NO_3^- -N loads caused by the different approaches of changing the land use were the major observable difference. Mehdi et al. (2015b) however found that including agricultural land use change into the impact assessment of a southern German watershed strongly increased the NO_3^- -N and total phosphorus loads. Teshager et al. (2016) support the findings of Mehdi et al. (2015b) and also found that corn intensive scenarios lead to an increase in discharge and significant water quality problems while an extensive scenario where mainly switchgrass is planted lead to water quality improvements under future climate change. Consequently, the low impact of land use change found in the present study seems reasonable with respect to other literature, particularly as no extreme scenarios were implemented. This does however not generally imply a low importance of land use change in environmental impact assessments. Land use change or changes in the management can be the most relevant input, particularly when strong future changes, such as possible bans of emittents are considered (Honti et al., 2017).

Industrial emitters were the main cause for the impact of point sources on medium to low NO_3^- -N loads. The future scenarios of the development of industrial emitters were however highly uncertain. The developed scenarios are based on expert knowledge. Yet, there is no reliable basis available on status of the industrial emitters by the end of the century. Therefore, the developed scenarios should be noted as feasible futures, rather than e.g. politically realizable futures (Godet and Roubelat, 1996). To set a feasible range as boundaries for the future development of industrial emitters can lead to an overestimation of their impact in comparison to other influencing variables. Nevertheless, the visualization of the NO_3^- -N FDC of the Raab case study highlights the effect of the industrial emissions for medium and small NO_3^- -N loads. Large NO_3^- -N loads however, are hardly affected by the implemented scenarios, indicating that large NO_3^- -N emissions are mainly driven by agricultural activities.

The selection of climate scenarios had a strong influence on the simulation of discharge and NO_3^- -N loads in both catchments. The analysis of the uncertainties bands identified the differences in precipitation between the GCM-RCM combinations as being the main control, while the differences in air temperature had a low impact on the simulation outcome. This finding stands in contrast to other studies. Milly and Dunne (2011) and Sheffield et al. (2012) for example,

identified empirical approaches for the calculation of evapotranspiration as the main source for overestimation of the climate's influence on hydrological processes, particularly when evapotranspiration is a function of air temperature (Clark et al., 2016; Shaw and Riha, 2011; Roderick et al., 2014). In the climate scenarios used in this study, the impact of large differences in mean annual precipitation on the simulated outputs exceeded the impact of the differences in air temperature.

The effect of the model setup, with different watershed subdivisions, on the simulation of discharge or water quality variables has been investigated in various studies (e.g. Jha et al., 2004; Momm et al., 2017; Pignotti et al., 2017). Jha et al. (2004) emphasize the greater impact of changes during the HRU definition over the defined number of subbasins, as a consequent change in the distribution of land use, soil, or topography strongly affect runoff and the nutrient budget in a catchment. The analysis of the uncertainties bands with respect to the different model setups clearly confirmed the study by Jha et al. (2004), especially in the case of the Schwechat. Nevertheless, the impact of the model setup was lower than the effect of the model parametrization by a factor of up to five in the Schwechat study and up to eight in the Raab catchment. Yet, the model setup strongly affects the computation time. In the present case, where aggregated discharge and NO_3^- -N loads at the catchment outlets were the variables of interest a strong focus on the model parametrization is of higher priority than the spatial distribution of the model setup. Therefore, to maintain short computation times (and at the same time to maintain the distributions of land use, soil, or topography) a model setup with a low number of subbasins without any reduction of the number of HRUs is beneficial.

The impact of parameter non-uniqueness on the simulation of hydrological and water quality variables has been demonstrated previously (e.g.; Wilby, 2005; Mehdi et al., 2018). The importance of the model parametrization for the simulation of discharge and NO_3^- -N loads was confirmed in the present study as well. Large sensitivities of all signature measures of discharge and NO_3^- -N loads to the different model parametrizations were identified. Although all selected parameter sets represented historical observations of discharge and NO_3^- -N loads with a certain goodness of fit (based on defined objective criteria), the colored grouping of the uncertainty bands illustrated that the selected model parameter sets control the simulation of future discharge and NO_3^- -N loads in different ways. Thus, the large impact of the model parametrization and the distinctive patterns identified in the uncertainty bands suggest a great potential to further refine the model parametrization and consequently reduce simulation uncertainties with a more intensive model calibration. Additional information on the time series of observations can help to constrain the model parameters and adequately describe the relevant processes (e.g. Hrachowitz et al., 2014; Pfannerstill et al., 2017).

5.7.2 *How to attribute subjectivity inherent in the scenarios*

Scenarios always reflect subjective assumptions made by the modeler. Assumptions that are made in the scenario development however, can strongly influence a simulation and thus affects a comparison of different model inputs and their impacts on the simulation. All steps in a scenario development involve subjective assumptions and can lack plausibility (Mahmoud et al., 2009; Vuuren et al., 2012), regardless of whether the process involves expert knowledge, the input of stakeholders in an participatory process, or an exploratory approach that extrapolates trends, these practices potentially introduce uncertainties in the definition of scenarios. Technical aspects such as how the scenario is represented in the model are also strongly biased by the modelers decision and represent an additional source of uncertainty (Mahmoud et al., 2009). The communication of the potential uncertainties inherent in the developed scenarios and the boundaries of the explanatory power of an scenario ensemble is essential for the integrity of any impact study (Mahmoud et al., 2009; Jones et al., 2014).

In the present study, several assumptions were made in the development of scenarios that are highly subjective, such as the extrapolated gradient of future land use changes, the drastic changes in future industrial emissions, and also the selection of objective criteria that define a behavioral SWAT model setup. Scenarios must cover a broad range of possible futures and have to be adequately represented in the model setup. An explicit delineation of the implemented scenarios and their limitations is essential to clearly illustrate the limitations of an impact study's conclusions. An immanent risk in any impact study is that the model representation of a future change, or the uncertainties in a model input fail to reproduce the response of a simulated variable that would have taken place in the real environmental system. Hence, a detailed analysis of the simulation uncertainties perfectly complements a SA to identify possible shortcomings in the study setup. Attributing the uncertainty bands resulting from the simulation of an environmental variable to individual model inputs prove to be a useful visual analysis tool that gives the power to illustrate the uncertainties in a transparent way. Furthermore, the colored differentiation provides a visual guidance to judge the impacts of different implemented scenarios.

5.7.3 *Sensitivity analysis or hydrologic storylines*

The presented approach implements large samples combining scenarios for different model inputs and different model setups and parametrizations in a GSA to identify the dominant contributors of uncertainties in the simulated outputs. The utilization of SA with large sample sizes however, raises the following issues: i) compared to a standard approach to perform an impact assessment, where a few different future scenarios are implemented into a model, the computational demand of a GSA requiring hundreds or thousands of model executions is larger by several orders of magnitude. Thus, a practical implementation of the presented procedure in impact studies is questionable and a strong coop-

eration between research and the practitioners is essential. ii) scenarios of different model inputs are often interrelated (Mahmoud et al., 2009). A change in one model input therefore for example expects the change of another model input into one direction and makes a change into another direction unlikely. While the implementation of input dependencies, although challenging is feasible for continuous model inputs, for instance by a transformation of the input space (e.g., Tarantola and Mara, 2017; Mara and Tarantola, 2012), or the determination of input distribution functions (Hart and Gremaud, 2018), the dependencies of composite model inputs are usually difficult to express mathematically. To identify the dependencies between composite model inputs, expert knowledge is required to properly constrain the model input combinations and therefore complicates the implementation in approaches, such as the presented one.

Clark et al. (2016) therefore suggest to identify consistent hydrologic story lines that result in least severe, most likely, and most severe responses of the modeled system. Such an approach would tremendously reduce the number of necessary model evaluations, but also establish consistency between the considered influencing variables. Nevertheless, the feasible combinations of influencing variables that lead to extreme or likely responses of the modeled system are hardly known a priori. Consequently, a sensitivity analysis with a constrained sampling space, to avoid infeasible combinations of influencing variables might be a pragmatic compromise.

5.8 CONCLUSION

This study utilized methods for GSA in environmental impact studies to identify the dominant sources of uncertainties for the simulation of environmental variables under future changing conditions. In the two Austrian catchments of the rivers Schwechat and Raab, the river discharge and the NO_3^- -N loads were simulated under the condition of future changes in climate, land use, and emissions from urban and industrial point sources implementing different SWAT model setups with various model parametrizations.

Both analyses for the Schwechat and the Raab identified climate change and the model parametrization to be the most important (influential) model inputs for the simulation of discharge and NO_3^- -N loads, based on performing a GSA and on the resulting analysis of signature measures of discharge and NO_3^- -N loads (quantiles of discharge and NO_3^- -N loads, seasonal mean discharge and seasonal sums of NO_3^- -N loads and NO_3^- -N concentrations for discharge quantiles). The impact of the model setup on simulated variables of discharge and NO_3^- -N loads was found to be considerably lower than the impact of the model parametrization for the Schwechat and even more distinct for the Raab. The impact of the implemented scenarios for land use and municipal point source emissions were negligible for all analyzed signature measures. Because of a large leather industry in the Raab catchment, the future development of industrial emission in the Raab catchment was found to be relevant for low NO_3^- -N loads and NO_3^- -N concentrations during low discharge.

Accompanying the GSA, a detailed analysis of the simulation uncertainties provided additional insights on how the uncertainties in the model inputs control simulated discharge and NO_3^- -N loads. The visualizations that were developed supported the identification of the relevant properties of the model inputs that control the simulation uncertainties and provide insight how individual realizations of a model input can affect the simulations. In the climate simulations, the precipitation was found to dominate the simulation outputs, rather than changes in air temperature. Although the impact of the model setup on the simulation of discharge and NO_3^- -N loads was low, the visual analysis of the uncertainty bands illustrated that the HRU definition is an important step in the model setup. The use of the full set of HRUs was identified as the preferred setup in the two simulated catchments. In contrast the effect of using different numbers of subbasins in the model setup was low for the simulation of discharge and NO_3^- -N loads at the catchment outlets.

The drawn conclusions are the result of specific conditions and the assumptions made for each individual catchment analyzed in this case study. The conclusions cannot be extrapolated with ease to other catchments. Nevertheless, the presented work provides an approach to identify and analyze the dominant sources of simulation uncertainties in environmental impact studies that can easily be generalized and that can act as a template for further impact studies. The analyses advocate for a stronger focus on the communication of uncertainties in model simulation and their sources in environmental impact studies. Although a variety of tools to perform SA are available for different programming languages (e.g., Pianosi and Wagener, 2015; Reusser, 2015; Iooss et al., 2018; Houska et al., 2015), the main constraint for a practical application remains the development of a comprehensive set of discrete input realizations, the computational costs of such analysis, and the lack of straight forward methods to implement composite inputs into SA. This might detain the practical application of such methods. To facilitate the implementation of composite model inputs in SA, procedures and tools for uncertainty and sensitivity analysis and visualization and communication must be available in order to promote such analyses in the modeling communities.

Part III

SYNTHESIS

Information is the resolution of uncertainty.
— Claude Shannon

SYNTHESIS AND CONCLUSIONS

6.1 SCIENTIFIC CONTEXT

More than ever, the assessment of the future development of our changing environment is critical to water resources planning (even the IAHS dedicated the current Scientific Decade to this issue (Montanari et al., 2013)). The systems we analyze are highly dynamic and affected by multiple system changes at the same time (Srinivasan et al., 2017; Montanari et al., 2013; Merz et al., 2011). Thus, a stationary perception of the systems we analyze is simply insufficient (Wilby, 2010; Milly et al., 2008). Eco-hydrological modeling plays a key role in the evaluation of our changing environmental systems, as to depict the interaction and co-evolution of changing environmental systems and the dynamics in anthropogenic activities (Sivapalan et al., 2012). Yet, to adequately depict complex interactions between the changing environments and the dynamic anthropogenic influences with the available well established eco-hydrological modeling approaches is limited. This is particularly relevant when strongly generalized empirical model concepts are implemented, or when models that fit historic data well are implemented to extrapolate future events under change (discussed at length in this thesis and well documented by e.g. Hrachowitz and Clark, 2017; Merz et al., 2011; Blöschl and Montanari, 2010; Kirchner, 2006; Favis-Mortlock, 1998).

Both, limitations in an adequate system representation by a model, as well as the implementation of future system changes are likely to introduce substantial uncertainties in the simulation of environmental variables (Blöschl and Montanari, 2010). Although environmental modeling studies usually account for uncertainties that are present in the projections we make on future system changes, such as climate change (e.g. Clark et al., 2016; Mehdi et al., 2015b; Merz et al., 2011), or land cover change (e.g. Wagner et al., 2017; Teshager et al., 2016; Guse et al., 2015; Mehdi et al., 2015b; Bieger et al., 2013), model uncertainties that may be introduced by an inadequate model structure, or the model parameterizations, or the process representation are hardly considered. Although the attention for uncertainty analysis in eco-hydrological modeling is increasing (Pappenberger and Beven, 2006), overall, the uncertainty of environmental model simulations is likely to be underestimated, due to an incomplete comprehension of present sources of uncertainties in a study setting (Bosshard et al., 2013; Blöschl and Montanari, 2010; Wilby, 2010). A profound understanding of the simulation uncertainties requires a comprehensive picture of the dominant sources of uncertainties in the inputs and components that describe an analyzed system. Comprehensive uncertainty (UA) and model sensitivity analysis (SA) are, however, computationally expensive and labor intensive. System changes and different system representations are typically represented by discrete sets

of scenarios or a discrete number of model setups. Their implementation additionally impedes an execution of comprehensive UA. Thus, comprehensive eco-hydrological studies that aim to cover a wide realistic range of simulation uncertainties and to identify the dominant sources of uncertainties are rare (see e.g. Estrada-Carmona et al., 2017; Dai et al., 2017; Savage et al., 2016; Dai and Ye, 2015; Baroni and Tarantola, 2014).

There is a need to make UA and SA more accessible for comprehensive analyses in environmental impact studies. The work presented in this thesis is motivated by meeting this need and introduces a comprehensive UA and SA framework to implement discrete composite model inputs in eco-hydrological modeling workflows and to facilitate an analysis of the entire chain of uncertainties in eco-hydrological studies. The applicability of the UA and SA framework is illustrated in two diverse case studies with differing scopes and different complex eco-hydrological model applications that employ two of the most frequently implemented eco-hydrological models. In summary, a systematic procedure for comprehensive model diagnostics can be delineated from the case study results and general conclusions can be drawn that contribute to a wider understanding of the potentials and limitations of comprehensive UA and SA with discrete model inputs.

6.2 GENERALIZED UNCERTAINTY AND SENSITIVITY ANALYSIS FRAMEWORK

The general framework concept of the developed framework was based on the limited body of literature that was available at the time of the framework development. Authors such as Baroni and Tarantola (2014) or Dai and Ye (2015) presented first concepts to employ GSAs with discrete sets of realizations of uncertain inputs to perform a comprehensive UAs and to identify the most dominant sources of uncertainties implementing VBAs using the Sobol (1993) sensitivity index. Baroni and Tarantola (2014) and Dai and Ye (2015) both followed a probabilistic approach, where the uncertain inputs were treated as variables with a most likely value and a distribution from which discrete realizations were sampled.

A central scope for the developed framework presented in this thesis was to follow a possibilistic perspective on the uncertain inputs. As emphasized at several points in this thesis uncertain inputs in eco-hydrological modeling studies are typically expressed as discrete, nominal variables. A most likely value and a distribution to sample from simply do not exist for such types of variables. Hence, all discrete realizations of an input that are developed and considered in an analysis are treated as equally possible options. Although the implemented methods for UA and SA allow for any specific sampling design, the members of each set of realizations for each input are all equally likely (referring to a probabilistic terminology, see also Fig. 3.4). The discrete, nominal input structure determined specific requirements for the selection and the design of the UA and SA methods that are eventually implemented in a modeling workflow. The requirements can be summarized as: i) a capability to analyze the entire input space (GSA), ii) applicability with nominal discrete inputs, iii) robustness for input sets

that strongly differ in their numbers of realizations, iv) moment-independence concerning the output distributions, and v) computational efficiency.

The two presented case studies differed in the complexity of the eco-hydrological models that were implemented. Particularly, the model structures of the two implemented models required diverging decisions in the selection of the SA methods for both studies. While the USLEs model allows an analytical analysis of the outputs' uncertainty and its sensitivity to uncertainties in the model inputs, the more complex SWAT model required the implementation of numerical methods that approximate the output uncertainties and sensitivities. In both cases global methods were selected for the performance of an SA. While for the USLE a global analytical solution was implemented, the SWAT model application employed the PAWN sensitivity index as proposed by Pianosi and Wagener (2018). PAWN (Pianosi and Wagener, 2018) allows the application of any generic input sampling to be employed in the approximation of the PAWN sensitivity index. Yet, an extension of the method specifically for the use with discrete model inputs and model input sets that strongly differed in their numbers of realizations was required. The methodological extension was outlined and presented in this thesis. In order to attain a robust measure of sensitivity for discrete model inputs with different numbers of input realizations, in both cases the maximum influence of an input on the simulated output was calculated. Unlike the median (which was also suggested by Pianosi and Wagener (2015) as a summary statistics to compute the PAWN sensitivity index) the maximum statistics is less sensitive to the influence of a large number of similar input realizations, but provides an information of the total impact on the simulation of an output variable that is achievable by the given set of input realizations. The analytical analysis of the USLE simulation results allowed a highly computationally efficient analysis of all possible input combinations. In the case of the SWAT application, the input space was substantially larger and an analysis of all input combinations was infeasible. Thus, a sampling of a subset of the possible input combinations was required. Yet, the computation of the PAWN index for the reduced subset was tested by employing bootstrapping and was found to be sufficiently robust. Overall, a computationally efficient solution for the analyses in both case studies was achieved.

Generally, the presented UA and SA framework allows for a high flexibility in terms of the goal of a study, the analyzed inputs, or the eco-hydrological model that is implemented. Yet, the major challenge lies in the translation of the formulated specifications of an input change into an appropriate model representation by modifying all model components that represent that system change in the model. The inputs of the USLE are linearly combined to formulate the model equation. Thus, the separation of the model components was easily achievable in the USLE model application (setting aside possible correlations between the inputs due to the primary input data that is required for the computation of the USLE inputs). For a SWAT model application, however, the translation of the of the input realizations into the model components requires thorough considerations that all model components that are affected by an input are modified accordingly. Further, modifications that result from one input

may also affect the structure of how changes in other inputs are implemented. An example observable in the presented case study is the implementation of different realizations of the inputs of precipitation and air temperature, that subsume the input "climate change". The implemented climate data was provided in a gridded format with a spatial resolution of 1 km by 1 km. A SWAT₂₀₁₂ model setup requires to define the weather inputs for each subbasin that is generated in a model setup. The gridded weather data was spatially averaged for the defined subbasins accordingly. The analysis framework, however, also included the model structure and therefore different numbers of subbasins as an input. Thus, the number of subbasins affects the spatial aggregation of the weather inputs for the input "climate change". Additionally, the weather affects farm management practices, such as the date of seeding. Different realizations of weather inputs require a specific definition of farm management practices in the model setups. These eventually affect the land use component in the model setups, that was again considered as an input in the analyses. The simple example of the implementation of weather inputs affects multiple model components and clearly illustrates the challenges of the setup of the UA and SA framework. Thus, although the framework can be formulated in a very general manner every implementation in a case study setting requires to draft a thorough design of the analyses.

6.3 COMPREHENSIVE UNCERTAINTY ANALYSIS, OVERLOOKED NECESSITY?

As already addressed by several other authors before, there is a tendency to underestimate the uncertainties in the predictions we make in environmental impact studies (Bosshard et al., 2013; Merz et al., 2011; Wilby, 2010; Blöschl and Montanari, 2010). Central causes for an underestimation of the total prediction uncertainties, such as the limitations of an appropriate sub-processes representation that are present in a system, a static perception of changing systems, or by simply neglecting parameter equifinality were addressed in this thesis. A central issue in environmental impact studies is that single models (equifinality issue) that appropriately fit historic observations (static perception), such as discharge observations at the catchment outlet (neglecting sub-process representation) are typically employed to analyze systems under changed conditions. Thus, even if comprehensive sets of realizations of the system changes are accounted for in the simulation uncertainties, the aforementioned sources of uncertainties are present in any assessment and, yet, are usually neglected.

The results of the two presented case studies make very clear, that the system representation by a model can pose a substantial source of uncertainties. The SA results for the influence of five input factors on different signature measures of daily simulated discharge and NO_3^- -N loads (Fig. 5.5) identified the model parameterization to be highly influential. Particularly, for the simulation of medium and low discharges as well as NO_3^- -N concentrations at different discharge levels the model parameterization was by far the most influential input, in both catchments that were investigated. The study presented in Chapter 4 assessed the soil loss under present conditions and did not perform any analyses

under changed conditions. Thus, this study does not allow for a comparison of the influence of other potential sources of uncertainties for the prediction of soil loss. Yet, the soil loss estimates that resulted from 756 representations of the USLE model showed substantial simulation uncertainties. In several locations of the study area of Kenya and Uganda ranges in soil loss that resulted from the USLE model ensemble exceeded the ensemble mean values by over an order of magnitude. The limitations of a "single model" approach to simulate soil loss with the USLE becomes particularly evident from a comparison to the results in Karamage et al. (2017) that were illustrated in Fig. 4.8. For the compared districts of Uganda, Karamage et al. (2017) predicted a comparably low mean soil loss. Although several of the model predictions from the USLE model ensemble predicted extreme (implausible?) soil losses, as well as, lower values than the ones that are observable in Karamage et al. (2017) for the same districts, a large majority of the model realizations of the USLE model ensemble still resulted in substantially larger soil losses compared to Karamage et al. (2017). In 9 of the 16 analyzed districts the soil losses calculated by Karamage et al. (2017) were lower than the 25% quantile of soil losses that resulted from the USLE model ensemble.

In order to create a realistic picture of the prediction uncertainties of a study, based on the case study results, comprehensive UA and SA appears to be an indispensable part of environmental impact analyses, rather than being a modeler's burden. Overall, the simulation uncertainties as well as the apportionment of the uncertainties to the uncertain inputs must be treated as valuable information, even if it means to accept extreme uncertainties as illustrated in the presented case study examples. Overall, as a modeling community we have to start to uncover how methodological choices in modeling affect the conclusions we draw from environmental modeling studies.

6.4 COMPREHENSIVE UNCERTAINTY ANALYSIS, AN UNCERTAIN AFFAIR?

"[U]ncertain information is definitely more useful than a wrong certainty" (Blöschl and Montanari, 2010). The tendency to underestimate the uncertainties in the simulations of environmental model simulations likely result from an incomplete delineation of the uncertainty sources (Bosshard et al., 2013; Wilby, 2010). The delineation of uncertainties itself is, however, an uncertain procedure. Future system changes are typically expressed by a set of discrete scenarios that delineate how a system component can evolve from historic conditions (Refsgaard et al., 2007). Yet, the representation of the future evolution of a system component is constrained by the assumptions that were made on the development of a system component and the concepts and models that are implemented to propagate the development of that system component (Clark et al., 2016). A concrete example are future climate change simulations that are usually implemented in environmental modeling studies. The current climate simulations are based on socioeconomic Representative Concentration Pathways (RCPs), which reflect a concrete set of assumptions on a change in the radiative forcing. These RCP scenarios drive a set of GCMs. Although this

modeling chain likely results in wide ranges for the projections of the climatic variables, the discrete set of scenarios and the implemented global circulation models constrain the uncertainties and may not consider other equally possible futures that cannot be identified because, for example, limits to our knowledge are present (Rounsevell and Metzger, 2010). This circumstance is well reflected by Donald Rumsfeld's statement in 2002 who was the US Secretary of State for Defense at that time, that "[t]here are known knowns. These are things we know that we know. There are known unknowns. That is to say, there are things that we know we don't know. But there are also unknown unknowns. There are things we don't know we don't know." In research we typically investigate the known knowns while UA reflects the known unknowns (Logan, 2009). Thus, future scenarios usually fail to represent unexpected events or surprises that can as well lead to possible futures (Beven, 2018). The same ideas apply to the system representation by the eco-hydrological model. As already discussed in the Introduction of this thesis, our current eco-hydrological models are limited to appropriately depict all system processes. Model ensembles are an approach to depict these limitations. A by far greater challenge is to comprehend how a future change alters the processes in a system. How to account for these changes in the model realizations is usually poorly, if at all, considered in the implemented model setups. Hence, a very likely chance exists that an entire model ensemble fails to depict the processes that control the systems' behavior under future change.

Both case studies that were presented in this thesis employed discrete sets of realizations for the analyzed inputs. In both studies constraints in the development of the input realizations are evident. The limitations in the description of climate change as it was described above was present in the SWAT model application. Also, the analyzed sets of SWAT model setups and SWAT model parametrizations were very limited by their numbers of configurations and only proved to be sufficient representations of historical observations. Thus, none of the implemented model setups can guarantee an appropriate representation of the modeled catchments under future changes.

In practice however, trivial factors can eventually constrain the comprehensiveness of an UA and SA analysis. Scenario development is simply labor intensive. Additionally, the computational costs for analyses of large sets of realizations for several inputs can easily become a limiting factor. Thus, comprehensiveness of an UA always comes with finding a compromise depicting the uncertainties of only a few (or one) inputs with great detail, or to analyze multiple sources of uncertainties with limited resources for the input realization development for each individual input. Both case studies generally followed the latter approach. Thus, most inputs were represented by a low number of realizations. A low number of input realizations to represent the feasible range of that input does not necessarily constrain the significance of an UA and SA analysis. If the relationship between a process and the changes of an input is fairly well understood a low number of inputs can properly delineate the input uncertainties and the resulting output uncertainties (Rounsevell and Metzger, 2010).

In the UA and SA analysis of the SWAT model applications the implementation of a reduced set of input realizations was therefore feasible for the land use scenarios. Specific land uses (and the resulting model parametrizations) directly cause extreme effects on specific output variables, such as the contribution to the total nutrient loads, or the generation of fast surface runoff. Hence, the implementation of a few land use input realizations that define the extreme boundaries of any land use change impact might be sufficient to describe the possible changes in the output variables that are induced by land use change. Although even if in theory the impact of land use changes on the analyzed output variables seems to be clear, their implementation in a SWAT model setup posed to be a major cause for concern as discussed in section 5.7.1.

The UA and SA of the USLE model application was also constrained by computational resources, primarily due to the storage requirements of the processed data. Therefore, only small sets of input factor realizations were included in the analysis. Thus, the input uncertainties that were depicted by the sets of input realizations are very likely incomprehensive. One of the major constraints was the implementation of very limited primary input data. For the computation of R factor realizations, for example, only one large scale precipitation product was implemented, even though multiple global rainfall products exist. Although several relationships between long-term precipitation products and the rainfall erosivity were included in the input realizations, the developed R factor realizations do not reflect any uncertainty that would be introduced by different precipitation products. Apparently, the decision to include one potential source of uncertainties at the cost of other sources of uncertainties is a subjective one that will eventually affect the analysis results.

In summary many constraints for a comprehensive definition of input uncertainties can be identified in both case studies. This is particularly dissatisfactory for modeling studies in which comprehensiveness of the UA and SA was the main aim. Nonetheless, the performed UA and SA greatly contributed to the system understanding in both case studies which clearly emphasizes that uncertainty is an additional attribute of information that must be acknowledged. Ultimately, the introductory quote of this section should be extended to: *"Although a comprehensive understanding of the inherent uncertainties is hardly achievable, limited uncertain information is definitely more useful than a wrong certainty"*. For any comprehensive UA a clear definition of the included sources of uncertainty in the input realization development and the limitations of an analysis are essential to communicate the limits of the explanatory power of a study.

6.5 SIGNIFICANCE OF ENVIRONMENTAL IMPACT STUDIES, A CHIMERA?

A common goal in environmental modeling studies is to identify significant trends of environmental variables due to trends in one or several inputs. Yet, the question arises if any plausible changes can be delineated taking into account the full range of uncertainties that is actually present in an assessment. There is a body of literature available that strongly question the capability to identify significant changes of environmental variables due to system changes with the

data that is available and the methods that are employed. Hall et al. (2014) and Blöschl et al. (2015), for instance, assessed changes in flood risk for European river basins. One conclusion was that clear trends that can be delineated from short discharge records risk to not to be supported by longer records. Future projections in flood risk are substantial and are often not appropriately communicated. Schulz and Bernhardt (2016) illustrated in a minimalistic synthetic example based on long-term discharge records at the river Danube that the estimation of trends typically performed in impact assessments greatly fails and is even incapable of identifying whether a trend is negative or positive. Merz et al. (2011) simulated the discharge from 273 Austrian catchments with an HBV-type model (Bergström, 1995) that were calibrated for a 5 year historic period and were then implemented to reproduce observed trends in discharge for later time periods. Merz et al. (2011) concluded that overall the models failed to simulate "future" discharge and generally underestimated high flows. Duethmann et al. (2020) very recently updated the study setting of Merz et al. (2011) and tested additional hypothesis, with the conclusion that overall the model failed to simulate discharge under climate change.

These few examples indicate that any trends that are identified (or missed) by modeling impact assessments have to be critically evaluated, particularly when the uncertainties are not well communicated. An opposite perspective raises the question whether trends and changes in the data can be identified at all, when the study results include extremely large uncertainties. Overall, the two presented case studies would answer this question definitely with a yes. Even further, not only can patterns (temporally/spatially) be identified, but the comprehensive UAs and SAs further provide information under which assumptions which study outcome would be more likely. The results of the SWAT model applications illustrated in the Fig. 5.7 – 5.11 greatly support that statement. The model ensemble simulations for the Raab and the Schwechat catchments in Fig. 5.6 indicate that there is a strong tendency for an increase in discharge and NO_3^- -N loads leaving the Schwechat catchment, while discharge and especially the NO_3^- -N tend to decrease in the Raab catchment. A detailed analysis on the input factor level revealed that these identified trends mainly result from the assumption that future annual precipitation sums in the Schwechat catchment increase, while they tend to decrease in the Raab catchment. Although the soil loss study presented in this thesis does not attempt to make predictions under changed conditions, the evaluation of the spatial patterns also support the statement above. Indeed, the simulated uncertainties of the soil loss predictions are extremely high. Though, the study allows an analysis of the spatial patterns of soil loss, as well as, the identification of erosion prone areas. Further, the model ensemble provides information on the confidence of a soil loss estimation in a certain location. A key message from these results is that it is essential to focus more on why an impact study simulates a trend and what assumptions lead to that trend, rather than focusing too much on the absolute magnitudes that resulted from a simulation as already postulated by Blöschl and Montanari (2010) in a similar context.

Such extreme uncertainties as the ones that were communicated in the two presented case studies raise the question whether options exist to reduce the uncertainties in the inputs (or input combinations) and eventually reduce the simulation uncertainties. Clark et al. (2016) rendered a blueprint procedure for the characterization and reduction of uncertainties in climate change studies. Clark et al. (2016) propose several options, such as assigning weights to input realizations based on the confidence in the quality of an input realizations (e.g. better/poor performing climate models), or model rejection based on certain criteria. Although the presented case studies in this thesis proposed some procedures for uncertainty reduction and tested a few of them, no procedure was identified in the two studies that allowed an uncertainty reduction with acceptable confidence. Eventually, both studies suggested to follow the more conservative approach to accept the present uncertainties, when the evaluation cannot clearly support any reduction in the uncertainties.

OUTLOOK AND POTENTIAL RESEARCH

Given the importance of an appropriate consideration and communication of uncertainties in environmental modeling studies, a central future goal is to raise the acceptance and awareness for comprehensive UA and SA in the eco-hydrological modeling communities. Still, common arguments, such as the difficulty of an UA application, a difficulty of uncertainty communication in decision making, or difficulties in the interpretation of UA results by policy makers hinder the application of UA and the communication of uncertainties (Pappenberger and Beven, 2006). Yet, a slow but steady change is observable in the society that the perception on the uncertainties of projections and forecasts change. A good example are weather forecasts, where over the last years uncertainty bands become more and more common in the forecasts that are broadcasted in the national television. Studies even confirm that people prefer uncertain information and show greater confidence in forecasts that illustrate the uncertainties in the prognosis (Morss et al., 2008). Pappenberger and Beven (2006) suggest that the main problem is rather an ineffective communication of uncertainties, rather than a lack of understanding. There is hope that a progressing wide acceptance of communicated uncertainty eventually make UA and the communication of uncertainties a requisite in environmental studies. Ultimately, we as a modeling community have to come up with best practice examples to evaluate and communicate uncertainties (see e.g. Frias et al., 2018; Goerlandt and Reniers, 2016; Pianosi et al., 2016; Morss et al., 2008).

The two presented case studies clearly illustrated that comprehensive UA and SA are labor intensive and computationally expensive. Eventually, a constrain in time and computing resources will be the limiting factor for a wide application in environmental impact studies. Yet, although there is potentially a great acceptance of uncertainty communication, there has to be a great acceptance of UA within the environmental modeling communities as well. Thus, increasing the efficiency of UA methods and an increase in automatization have the potential to promote the acceptance of UA. Several published tools are available that support the user in the implementation of UA and SA (e.g., Pianosi and Wagener, 2015; Reusser, 2015; Iooss et al., 2018; Houska et al., 2015; Frias et al., 2018). The implementation of these methods into straight forward workflows (e.g. an automatization of the framework proposed in this thesis) could greatly benefit future analyses. To tremendously decrease the computational costs, Clark et al. (2016) for example propose to the development of consistent storylines rather than to simulate all combinations of possible input combinations. A thorough investigation and the comparison of strengths and weaknesses of the different modeling strategies can be relevant.

This thesis only presents two studies that highlight the potentials of comprehensive UA and SA in environmental modeling studies and eventually adds

insights to a still very limited body of literature on that topic. Ultimately, further studies are required that implement such UA and SA frameworks or concepts that were proposed by Baroni and Tarantola (2014) or Dai and Ye (2015) to gain knowledge on comprehensive UA and SA in environmental modeling and to draw general conclusions on input factor importance.

The two case studies implemented a very reduced set of methods for SA to evaluate the importance of model inputs for the simulation of the respective output variables. More importantly, this thesis and the accompanying publications only report results that employed the maximum statistics to compute sensitivity measures. Preceding experiments employed different methods for SA, such as the method of Sobol (1993), or a modified version of the STAR VARS method (Razavi and Gupta, 2016a; Razavi and Gupta, 2016b), as well as other summary statistics in the computation of sensitivity measures. Yet, first results showed differences in the resulting sensitivities and input importance a detailed analysis and methods comparison of SA with discrete model inputs with differently large sets of realizations is still missing.

As outlined above, the delineation of input uncertainties is highly subjective and strongly biased by the assumptions we make, the implemented methods for the development of the respective input realizations, or the primary input data that is used for the computation of the input realizations. Thus, it is of interest how sensitive the result of a comprehensive UA and SA workflow is to initial decisions on any of the mentioned biases.

APPENDIX

A.1 USED SOFTWARE

The majority of the analyses that were performed in both case studies and that are presented in this work were conducted in the R computing environment (R Core Team, 2019). Analyses in R benefit from the use of R packages that were developed by the R community. Below an overview of the used packages, but also other software that were used in the analyses is given.

The entire calculation of the USLE model realizations, most part of the input factor generation and the entire analysis of the simulation results were performed in the R. Spatial tasks and analyses were performed using the spatial R packages `raster` (Hijmans, 2019), `sf` (Pebesma, 2018), `rgdal` (Bivand et al., 2019), and `fasterize` (Ross, 2018). Data handling with SQLite data bases was managed through interfacing with the `RSQLite` (Müller et al., 2018) and `dbplyr` (Wickham and Ruiz, 2019) packages. Parallel computing to run some analyses was performed with the R packages `foreach` (Microsoft Corporation and Weston, 2017b), `doSNOW` (Microsoft Corporation and Weston, 2017a), and `parallel` (R Core Team, 2019). LS factor realizations were generated with the LS Module in SAGA GIS (Conrad et al., 2015). Spatial maps were prepared in ArcGIS (ESRI, 2012).

All SWAT simulations were performed by executing SWAT model setups from the R environment. Simulation results were returned to the R environment and analyzed there. The handling of the SWAT projects in R was done using earlier versions and code that are now implemented in the R package `SWATplusR` (Schürz, 2020b). Overview maps of the catchments were prepared in ArcGIS.

Data analyses in both case studies employed the R packages `dplyr` (Wickham et al., 2019b), `forcats` (Wickham, 2019), `lubridate` (Grolemund and Wickham, 2011), `purrr` (Henry and Wickham, 2019), `tibble` (Müller and Wickham, 2019), and `tidyr` (Wickham and Henry, 2019). Apart from map visualizations all figures were plotted in R using the `ggplot2` package (Wickham et al., 2019a). Schematic figures were prepared using the open source vector drawing software `inkscape` (project, 2019).

A.2 SUPPLEMENTARY MATERIALS FOR THE USLE INPUT GENERATION

The information on soil structure s and soil permeability p were assembled based on information given in Panagos et al. (2014), Borrelli et al. (2017), and (Baruth et al., 2006). The Tables A.1 and A.2 summarize the parameter values for p and s that were used in the case study in Chapter 4.

Table A.1: Lookup table to derive the soil permeability p from the USDA soil texture classification.

Value	USDA texture class	Permeability class p
1	Clay	6
2	Silty Clay	6
3	Sandy Clay	5
4	Silty Clay Loam	5
5	Clay Loam	4
6	Sandy Clay Loam	4
7	Silt	3
8	Silty Loam	3
9	Loam	3
10	Sandy Loam	2
11	Loamy Sand	2
12	Sand	1

Table A.2: Lookup table to derive the soil structure s from the soil taxonomy classification according to the WRB

WRB	Soil name	Qualifier	Soil group	Structure class s
1	Haplic Acrisols	Haplic	AC	2
2	Haplic Acrisols (Alumic)	Haplic	AC	2
3	Haplic Acrisols (Ferric)	Haplic	AC	2
4	Haplic Acrisols (Humic)	Haplic	AC	4
5	Plinthic Acrisols	Plinthic	AC	2
6	Vetic Acrisols	Vetic	AC	2
7	Haplic Albeluvisols	Haplic	AB	2
8	Histic Albeluvisols	Histic	AB	2
9	Umbric Albeluvisols	Umbric	AB	2
10	Cutanic Alisols	Cutanic	AL	2
11	Haplic Alisols	Haplic	AL	2
12	Aluandic Andosols	Aluandic	AN	1
13	Haplic Andosols	Haplic	AN	1
14	Vitric Andosols	Vitric	AN	1
15	Albic Arenosols	Albic	AR	2
16	Ferralic Arenosols	Ferralic	AR	2
17	Haplic Arenosols	Haplic	AR	2
18	Haplic Arenosols (Calcaric)	Haplic	AR	2
19	Hypoluvic Arenosols	Hypoluvic	AR	2
20	Protic Arenosols	Protic	AR	2
21	Haplic Calcisols	Haplic	CL	2
22	Haplic Calcisols (Sodic)	Haplic	CL	2
23	Luvic Calcisols	Luvic	CL	2
24	Petric Calcisols	Petric	CL	2

Table A.2 continued ...

WRB	Soil name	Qualifier	Soil group	Structure class s
25	Endogleyic Cambisols	Endogleyic	CM	4
26	Ferralic Cambisols	Ferralic	CM	2
27	Haplic Cambisols	Haplic	CM	2
28	Haplic Cambisols (Calcaric)	Haplic	CM	1
29	Haplic Cambisols (Chromic)	Haplic	CM	1
30	Haplic Cambisols (Dystric)	Haplic	CM	1
31	Haplic Cambisols (Eutric)	Haplic	CM	1
32	Haplic Cambisols (Humic)	Haplic	CM	4
33	Haplic Cambisols (Sodic)	Haplic	CM	1
34	Leptic Cambisols	Leptic	CM	1
35	Vertic Cambisols	Vertic	CM	1
36	Calcic Chernozems	Calcic	CH	2
37	Haplic Chernozems	Haplic	CH	2
38	Luvic Chernozems	Luvic	CH	2
39	Haplic Cryosols	Haplic	CR	2
40	Turbic Cryosols	Turbic	CR	2
41	Vitric Cryosols	Vitric	CR	2
42	Petric Durisols	Petric	DU	2
43	Acric Ferralsols	Acric	FR	2
44	Haplic Ferralsols	Haplic	FR	2
45	Haplic Ferralsols (Rhodic)	Haplic	FR	2
46	Haplic Ferralsols (Xanthic)	Haplic	FR	2
47	Umbric Ferralsols	Umbric	FR	2
48	Haplic Fluvisols	Haplic	FL	2
49	Haplic Fluvisols (Arenic)	Haplic	FL	2
50	Haplic Fluvisols (Calcaric)	Haplic	FL	2
51	Haplic Fluvisols (Dystric)	Haplic	FL	2
52	Haplic Fluvisols (Eutric)	Haplic	FL	2
53	Calcic Gleysols	Calcic	GL	2
54	Haplic Gleysols	Haplic	GL	2
55	Haplic Gleysols (Dystric)	Haplic	GL	2
56	Haplic Gleysols (Eutric)	Haplic	GL	2
57	Mollic Gleysols	Mollic	GL	4
58	Umbric Gleysols	Umbric	GL	2
59	Calcic Gypsisols	Calcic	GY	2
60	Haplic Gypsisols	Haplic	GY	2
61	Calcic Histosols	Calcic	HS	4
62	Cryic Histosols	Cryic	HS	4
63	Fibric Histosols	Fibric	HS	4
64	Hemic Histosols	Hemic	HS	4
65	Sapric Histosols	Sapric	HS	4
66	Calcic Kastanozems	Calcic	KS	2

Table A.2 continued ...

WRB	Soil name	Qualifier	Soil group	Structure class s
67	Haplic Kastanozems	Haplic	KS	2
68	Haplic Leptosols	Haplic	LP	2
69	Haplic Leptosols (Eutric)	Haplic	LP	2
70	Lithic Leptosols	Lithic	LP	2
71	Mollic Leptosols	Mollic	LP	2
72	Rendzic Leptosols	Rendzic	LP	4
73	Haplic Lixisols	Haplic	LX	2
74	Haplic Lixisols (Chromic)	Haplic	LX	2
75	Haplic Lixisols (Ferric)	Haplic	LX	2
76	Albic Luvisols	Albic	LV	2
77	Calcic Luvisols	Calcic	LV	2
78	Gleyic Luvisols	Gleyic	LV	2
79	Haplic Luvisols	Haplic	LV	2
80	Haplic Luvisols (Chromic)	Haplic	LV	2
81	Haplic Luvisols (Ferric)	Haplic	LV	2
82	Leptic Luvisols	Leptic	LV	2
83	Stagnic Luvisols	Stagnic	LV	2
84	Vertic Luvisols	Vertic	LV	2
85	Alic Nitisols	Alic	NT	2
86	Haplic Nitisols (Rhodic)	Haplic	NT	1
87	Haplic Phaeozems	Haplic	PH	1
88	Leptic Phaeozems	Leptic	PH	2
89	Luvic Phaeozems	Luvic	PH	4
90	Endogleyic Planosols	Endogleyic	PL	2
91	Haplic Planosols (Dystric)	Haplic	PL	2
92	Haplic Planosols (Eutric)	Haplic	PL	2
93	Luvic Planosols	Luvic	PL	2
94	Solodic Planosols	Solodic	PL	2
95	Acric Plinthosols	Acric	PT	2
96	Lixic Plinthosols	Lixic	PT	2
97	Gleyic Podzols	Gleyic	PZ	2
98	Haplic Podzols	Haplic	PZ	2
99	Aric Regosols	Aric	RG	2
100	Calcaric Regosols	Calcaric	RG	2
101	Haplic Regosols (Dystric)	Haplic	RG	2
102	Haplic Regosols (Eutric)	Haplic	RG	2
103	Haplic Regosols (Sodic)	Haplic	RG	2
104	Leptic Regosols	Leptic	RG	2
105	Gypsic Solonchaks	Gypsic	SC	2
106	Haplic Solonchaks	Haplic	SC	2
107	Haplic Solonchaks (Sodic)	Haplic	SC	2
108	Calcic Solonetz	Calcic	SN	2

Table A.2 continued ...

WRB	Soil name	Qualifier	Soil group	Structure class s
109	Gleyic Solonetz	Gleyic	SN	2
110	Haplic Solonetz	Haplic	SN	2
111	Mollic Solonetz	Mollic	SN	1
112	Luvic Stagnosols	Luvic	ST	4
113	Haplic Umbrisols	Haplic	UM	4
114	Leptic Umbrisols	Leptic	UM	1
115	Calcic Vertisols	Calcic	VR	2
116	Haplic Vertisols	Haplic	VR	2
117	Haplic Vertisols (Eutric)	Haplic	VR	2
118	Mollic Vertisols	Mollic	VR	2

The method of Borrelli et al. (2017) to implement crop data from Monfreda et al. (2008) to compute C values requires a grouping of all crops that are provided by Monfreda et al. (2008) and to assign C factor literature values. The Table A.3 provides all crops that are available in Monfreda et al. (2008) and the respective classes into which all crops were classified. The respective C values for the crop classes are shown in Table 4.6.

Table A.3: Grouping of crops available from Monfreda et al. (2008) based on Borrelli et al. (2017).

Value	Crop	Label
11	Manila fibre (abaca)	abaca
11	Agave fibres nes	agave
8.2	Forage and silage, alfalfa	alfalfa
14	Almonds, with shell	almond
7	Anise, badian, fennel, coriander	aniseetc
14	Apples	apple
14	Apricots	apricot
14	Areca nuts	areca
4	Artichokes	artichoke
6	Asparagus	asparagus
14	Avocados	avocado
2	Bambara beans	bambara
14	Bananas	banana
1	Barley	barley
2	Beans, dry	bean
3	Beets for fodder	beetfor
12	Berries nes	berrynes
12	Blueberries	blueberry
14	Brazil nuts, with shell	brazil
2	Broad beans, horse beans, dry	broadbean
1	Buckwheat	buckwheat
7	Cabbages and other brassicas	cabbage

Table A.3 continued ...

Value	Crop	Label
7	Cabbage for fodder	cabbagefor
10	Canary seed	canaryseed
14	Carobs	carob
3	Carrots and turnips	carrot
3	Carrots for fodder	carrotfor
14	Cashew nuts, with shell	cashew
14	Cashew apple	cashewapple
3	Cassava	cassava
10	Castor oil seed	castor
7	Cauliflowers and broccoli	cauliflower
1	Cereals, nes	cerealnes
14	Cherries	cherry
14	Chestnut	chestnut
2	Chick peas	chickpea
3	Chicory roots	chicory
4	Chillies and peppers, green	chilleetc
13.1	Cinnamon (canella)	cinnamon
14	Fruit, citrus nes	citrusnes
13.1	Cloves	clove
8.1	Forage and silage, clover	clover
14	Cocoa, beans	cocoa
14	Coconuts	coconut
13.2	Coffee, green	coffee
11	Coir	coir
10.1	Seed cotton	cotton
2	Cow peas, dry	cowpea
12	Cranberries	cranberry
5	Cucumbers and gherkins	cucumberetc
12	Currants	currant
14	Dates	date
4	Eggplants (aubergines)	eggplant
11	Fibre crops nes	fibrenes
14	Figs	fig
11	Flax fibre and tow	flax
1	Fonio	fonio
8.2	Forage products	fornes
14	Fruit, fresh nes	fruitnes
6	Garlic	garlic
3	Ginger	ginger
12	Gooseberries	gooseberry
9.1	Grapes	grape
14	Grapefruit (inc. pomelos)	grapefruitetc

Table A.3 continued . . .

Value	Crop	Label
8.1	Forage and silage, grasses nes	grassnes
2	Beans, green	greenbean
2	Leguminous vegetables, nes	greenbroadbean
1.1	Maize, green	greencorn
6	Onions, shallots, green	greenonion
2	Peas, green	greenpea
2	Groundnuts, with shell	groundnut
14	Gums	gums
14	Hazelnuts, with shell	hazelnut
13.1	Hemp tow waste	hemp
13.1	Hempseed	hempseed
9.2	Hops	hop
11	Jute	jute
11	Bastfibres, other	jutelikefiber
11	Kapok fibre	kapokfiber
14	Kapok fruit	kapokseed
14	Karite nuts (sheanuts)	karite
14	Kiwi fruit	kiwi
14	Kola nuts	kolanut
8.1	Forage and silage, legumes	legumenes
14	Lemons and limes	lemonlime
2	Lentils	lentil
7	Lettuce and chicory	lettuce
10	Linseed	linseed
2	Lupins	lupin
1.1	Maize	maize
8.1	Forage and silage, maize	maizefor
14	Mangoes, mangosteens, guavas	mango
13.1	Mate	mate
5	Melons, other (inc.cantaloupes)	melonetc
5	Melonseed	melonseed
1	Millet	millet
1	Mixed grain	mixedgrain
10	Mustard seed	mustard
13.1	Nutmeg, mace and cardamoms	nutmeg
14	Nuts, nes	nutnes
1	Oats	oats
14	Oil, palm fruit	oilpalm
8.2	Forage and silage, green oilseeds	oilseedfor
10	Oilseeds nes	oilseednes
4	Okra	okra
14	Olives	olive

Table A.3 continued . . .

Value	Crop	Label
6	Onions, dry	onion
14	Oranges	orange
14	Papayas	papaya
2	Peas, dry	pea
14	Peaches and nectarines	peachetc
14	Pears	pear
4	Pepper (piper spp.)	pepper
13.1	Peppermint	peppermint
14	Persimmons	persimmon
2	Pigeon peas	pigeonpea
4	Chillies and peppers, dry	pimento
14	Pineapples	pineapple
14	Pistachios	pistachio
14	Plantains	plantain
14	Plums and sloes	plum
1.1	Popcorn	popcorn
10	Poppy seed	poppy
3	Potatoes	potato
2	Pulses, nes	pulsenes
5	Pumpkins, squash and gourds	pumpkinetc
13.1	Pyrethrum, dried	pyrethrum
14	Quinces	quince
7	Quinoa	quinoa
13.1	Ramie	ramie
10	Rapeseed	rapeseed
12	Raspberries	rasberry
1.2	Rice, paddy	rice
3	Roots and tubers, nes	rootnes
14	Rubber, natural	rubber
1	Rye	rye
8.2	Forage and silage, rye grass	ryefor
10	Safflower seed	safflower
10	Sesame seed	sesame
11	Sisal	sisal
1	Sorghum	sorghum
8.2	Forage and silage, sorghum	sorghumfor
14	Cherry sour	sourcherry
2	Soybeans	soybean
13.1	Spices, nes	spicenes
7	Spinach	spinach
14	Fruit, stone nes	stonefruitnes
12.1	Strawberries	strawberry

Table A.3 continued ...

Value	Crop	Label
2	String beans	stringbean
3	Sugar beet	sugarbeet
13.1	Sugar cane	sugarcane
13.1	Sugar crops, nes	sugarnes
10	Sunflower seed	sunflower
3	Swedes for fodder	swedefor
3	Sweet potatoes	sweetpotato
14	Tangerines, mandarins, clementines, satsumas	tangetc
3	Taro (cocoyam)	taro
13.1	Tea	tea
7.1	Tobacco, unmanufactured	tobacco
4	Tomatoes	tomato
1	Triticale	triticale
14	Fruit, tropical fresh nes	tropicalnes
14	Tung nuts	tung
3	Turnips for fodder	turnipfor
13.1	Vanilla	vanilla
7	Vegetables, fresh nes	vegetablenes
3	Vegetables and roots fodder	vegfor
2	Vetches	vetch
14	Walnuts, with shell	walnut
5	Watermelons	watermelon
1	Wheat	wheat
3	Yams	yam
3	Yautia (cocoyam)	yautia
8.2	Mixed grass	mixedgrass
4	Mushrooms	mushroom

A.3 USLE RESULTS FOR ADMINISTRATIVE UNITS IN KENYA AND UGANDA

The detailed analysis on administrative level in Section 4.5.3 cover only selected erosion prone districts. The following supplementary results summarize the soil loss estimates for all districts of Kenya (Table A.4) and Uganda (Table A.5).

Table A.4: Quantiles of mean soil loss estimates for all Kenyan counties based on the 756 USLE model setups in tons ha⁻¹ yr⁻¹.

County	A_{min}	$A_{0.025}$	$A_{0.25}$	A_{median}	A_{mean}	$A_{0.75}$	$A_{0.975}$	A_{max}
Baringo	3.80	6.37	14.23	28.50	45.16	52.81	191.96	419.07
Bomet	0.28	0.74	4.66	20.95	46.71	59.13	243.26	535.72
Bungoma	2.24	4.02	14.23	29.40	53.83	68.77	253.74	478.27
Busia	0.14	0.37	2.13	5.76	13.27	14.42	84.66	176.16
Busia	0.42	1.01	5.98	16.68	34.26	46.30	187.06	326.36

Table A.4 continued ...

County	A_{min}	$A_{0.025}$	$A_{0.25}$	A_{median}	A_{mean}	$A_{0.75}$	$A_{0.975}$	A_{max}
Elgeyo-Marakwet	2.21	4.15	20.54	47.21	85.20	110.60	381.12	797.47
Embu	1.43	3.49	11.85	24.30	45.26	55.41	216.03	398.70
Garissa	0.04	0.09	0.29	0.62	1.22	1.43	6.07	13.26
Homa Bay	1.27	2.96	12.98	25.40	49.39	64.17	241.87	460.75
Isiolo	0.31	0.46	1.35	2.70	5.11	5.79	24.15	58.87
Kajiado	1.03	1.47	3.89	7.68	12.98	15.60	55.57	138.84
Kakamega	0.57	1.32	7.71	20.23	42.55	53.18	229.32	423.42
Kericho	0.77	1.75	11.35	40.34	85.99	112.63	445.07	880.44
Kiambu	1.62	3.10	8.47	17.06	33.22	41.06	148.06	374.20
Kilifi	0.71	1.10	2.59	5.21	8.55	9.96	37.07	76.14
Kirinyaga	1.70	3.44	10.73	19.94	32.15	39.14	130.04	311.77
Kisii	0.45	1.40	11.03	41.69	87.38	112.13	478.90	855.23
Kisumu	0.77	1.67	8.20	18.87	36.78	48.58	179.19	312.46
Kitui	1.13	1.82	4.82	8.97	15.76	20.05	77.05	120.30
Kwale	1.08	1.74	4.26	8.38	14.26	16.58	65.69	131.82
Laikipia	1.67	2.70	5.78	12.16	19.15	22.38	77.39	154.36
Lamu	0.16	0.27	0.67	1.28	2.21	2.65	10.33	28.36
Machakos	2.21	3.27	8.91	17.72	29.72	36.16	140.89	268.93
Makueni	2.18	3.42	8.82	16.80	28.63	35.40	135.48	257.18
Mandera	0.15	0.28	0.89	1.98	4.08	4.67	18.59	52.47
Marsabit	0.24	0.44	1.39	3.23	6.21	6.98	28.61	77.57
Meru	4.35	6.23	15.49	29.60	47.43	55.31	208.95	381.88
Migori	0.72	1.83	8.79	20.35	40.86	52.09	207.99	401.34
Mombasa	0.24	0.53	2.85	5.82	11.92	14.11	56.94	144.75
Murang'a	0.91	2.40	13.75	32.42	64.47	74.91	298.77	736.36
Nairobi	0.60	0.99	2.49	4.96	8.19	9.67	30.22	62.62
Nakuru	1.98	3.55	10.32	19.15	34.75	42.17	137.92	327.17
Nandi	0.80	1.67	10.92	44.57	95.42	123.65	501.74	1044.62
Narok	1.94	3.80	9.94	18.79	31.77	38.16	122.35	278.61
Nithi	0.88	2.12	9.61	21.72	41.55	50.02	216.83	401.98
Nyamira	0.36	1.01	7.94	46.09	100.58	129.21	553.75	1049.56
Nyandarua	1.55	2.96	10.19	20.41	37.28	44.56	161.21	421.70
Nyeri	3.75	4.91	15.23	28.99	49.03	58.68	200.25	509.01
Samburu	2.93	4.28	11.13	21.12	35.95	43.86	149.83	364.36
Siaya	0.42	0.93	5.42	14.69	30.40	38.90	161.58	289.34
Taita Taveta	1.22	1.85	4.32	8.38	13.90	17.05	53.06	98.17
Tana River	0.12	0.20	0.57	1.14	2.21	2.55	10.38	26.09
Trans-Nzoia	1.06	2.24	8.36	17.34	32.72	41.69	135.38	317.96
Turkana	0.63	1.16	4.21	8.84	17.56	20.10	87.18	235.97
Uasin Gishu	0.45	1.32	5.04	11.16	20.91	26.36	92.86	194.55
Vihiga	1.01	2.43	14.82	42.74	90.58	116.79	490.03	894.40
Wajir	0.05	0.10	0.36	0.84	1.70	2.01	7.96	22.51

Table A.4 continued ...

County	A_{min}	$A_{0.025}$	$A_{0.25}$	A_{median}	A_{mean}	$A_{0.75}$	$A_{0.975}$	A_{max}
West Pokot	5.70	8.19	19.57	38.27	62.83	74.23	282.83	658.77

Table A.5: Quantiles of mean soil loss estimates for all Ugandan districts based on the 756 USLE model setups in $\text{tons ha}^{-1} \text{yr}^{-1}$.

District	A_{min}	$A_{0.025}$	$A_{0.25}$	A_{median}	A_{mean}	$A_{0.75}$	$A_{0.975}$	A_{max}
Abim	0.45	0.87	3.77	9.32	19.57	20.93	111.83	266.39
Adjumani	0.17	0.40	1.39	3.54	8.27	8.56	51.30	135.02
Amolatar	0.14	0.32	1.00	1.96	3.81	4.45	20.53	47.31
Amuria	0.32	0.48	1.34	2.74	4.60	5.56	20.97	47.91
Amuru	0.25	0.61	2.15	4.73	9.51	11.26	51.36	125.75
Apac	0.11	0.25	1.10	2.45	5.38	6.17	32.21	71.53
Arua	0.52	1.09	3.48	7.76	15.51	18.14	87.64	218.54
Budaka	0.26	0.51	1.53	3.46	6.72	7.55	36.10	83.14
Bududa	7.20	16.99	48.59	90.69	138.78	173.71	544.75	1080.05
Bugiri	0.18	0.44	2.18	5.80	12.62	15.63	72.79	144.78
Bukedea	0.29	0.40	1.07	2.54	4.65	5.62	24.03	57.89
Bukwo	4.01	6.71	18.91	40.58	71.78	83.36	346.17	862.47
Buliisa	0.34	0.69	1.80	3.63	6.62	7.74	32.80	81.80
Bundibugyo	2.77	4.81	11.56	22.82	35.20	42.36	149.53	351.58
Bushenyi	0.83	1.62	8.15	21.92	45.47	55.09	234.39	581.16
Busia	0.14	0.37	2.13	5.76	13.27	14.42	84.66	176.16
Busia	0.42	1.01	5.98	16.68	34.26	46.30	187.06	326.36
Butaleja	0.09	0.22	1.05	2.32	4.94	5.46	26.27	70.94
Dokolo	0.23	0.49	1.65	3.26	6.56	7.63	36.51	82.59
Gulu	0.17	0.43	1.56	3.66	7.27	8.25	43.18	94.47
Hoima	0.38	0.86	3.58	8.73	18.36	20.30	107.23	263.87
Ibanda	0.56	1.18	7.30	22.89	48.91	61.11	255.55	638.36
Iganga	0.10	0.25	1.47	4.19	10.02	10.68	58.44	141.16
Isingiro	1.31	2.96	10.81	21.64	39.31	48.51	176.13	440.66
Jinja	0.35	0.77	3.83	10.23	21.65	25.05	122.20	260.94
Kaabong	1.35	2.08	7.90	15.31	30.26	35.03	140.63	417.29
Kabale	6.33	11.42	38.18	75.16	139.47	168.40	591.69	1528.61
Kabarole	3.51	5.83	17.44	31.97	58.40	71.15	252.52	679.17
Kaberamaido	0.15	0.34	1.37	2.65	5.67	6.57	32.23	72.59
Kalangala	0.44	0.83	2.37	4.56	7.47	9.24	29.94	77.59
Kaliro	0.19	0.43	1.59	3.09	6.62	7.83	37.97	76.33
Kampala	0.36	0.90	2.84	5.78	10.47	12.18	48.75	134.17
Kamuli	0.13	0.31	1.32	3.13	6.88	7.94	38.47	94.85
Kamwenge	0.24	0.52	3.37	11.81	26.91	34.51	142.76	362.28
Kanungu	1.03	2.17	11.96	29.16	58.95	72.99	281.56	716.80
Kapchorwa	3.73	5.72	18.18	35.99	59.51	69.22	273.16	683.50

Table A.5 continued . . .

District	A_{min}	$A_{0.025}$	$A_{0.25}$	A_{median}	A_{mean}	$A_{0.75}$	$A_{0.975}$	A_{max}
Kasese	5.87	9.70	28.24	54.78	100.06	116.50	462.94	1456.00
Katakwi	0.15	0.31	0.84	1.73	2.85	3.37	12.85	31.60
Kayunga	0.06	0.14	0.75	2.66	6.36	7.38	36.85	95.09
Kibaale	0.12	0.27	1.84	12.02	27.74	34.26	154.96	440.75
Kiboga	0.11	0.25	1.79	7.42	16.46	21.55	85.20	184.72
Kiruhura	0.28	0.60	3.51	7.98	17.86	21.22	93.63	219.21
Kisoro	4.17	7.66	26.40	55.33	104.63	123.90	502.82	1176.19
Kitgum	0.35	0.63	2.10	5.31	11.36	12.15	66.64	175.60
Koboko	0.50	1.14	4.08	8.58	17.76	21.09	96.81	255.96
Kotido	0.26	0.43	1.30	2.44	4.67	5.45	20.23	54.87
Kumi	0.38	0.49	1.39	3.16	5.50	6.76	26.77	61.62
Kyenjojo	0.08	0.21	1.53	12.67	29.33	37.14	156.18	408.83
Lira	0.25	0.58	2.01	3.76	7.04	8.96	33.35	68.17
Luwero	0.05	0.10	0.65	4.44	10.47	12.61	61.59	143.92
Lyantonde	0.45	1.05	4.76	10.64	21.62	24.96	113.22	280.43
Manafwa	2.82	6.27	21.94	43.16	75.25	92.97	334.56	784.16
Masaka	0.43	0.90	4.40	10.18	20.53	24.71	100.07	222.03
Masindi	0.11	0.28	1.56	4.62	10.04	12.67	54.43	118.38
Mayuge	0.24	0.60	2.76	7.64	16.94	19.90	96.49	224.54
Mbale	0.80	1.86	8.88	20.37	39.45	47.56	192.09	491.53
Mbarara	1.17	2.40	10.83	22.35	44.29	53.06	216.08	537.82
Mityana	0.11	0.24	1.38	13.11	29.60	37.63	163.10	421.42
Moroto	0.34	0.54	2.61	6.22	12.15	14.50	54.41	143.37
Moyo	0.75	1.54	5.00	11.57	23.45	25.48	128.32	348.41
Mpigi	0.17	0.40	2.48	9.51	21.05	26.32	117.76	266.30
Mubende	0.13	0.32	2.34	14.12	32.39	40.82	179.79	483.67
Mukono	0.25	0.57	2.87	9.73	22.68	27.35	135.69	283.77
Nakapiripirit	0.61	1.18	3.43	6.65	12.36	15.37	53.39	131.04
Nakaseke	0.08	0.16	1.00	3.06	6.69	8.38	37.50	82.68
Nakasongola	0.11	0.18	0.59	1.34	2.93	3.24	14.96	49.23
Namutumba	0.19	0.42	1.60	3.61	7.82	8.27	46.96	98.26
Nebbi	0.72	1.42	4.41	10.73	21.97	23.54	130.48	320.27
Ntungamo	1.55	3.24	13.54	27.23	51.78	63.08	233.03	589.40
Nyadri	0.69	1.33	4.36	9.50	17.84	20.65	89.71	245.90
Oyam	0.10	0.22	1.19	2.95	6.65	7.86	36.78	85.58
Pader	0.16	0.32	1.23	3.19	6.52	6.50	40.92	91.25
Pallisa	0.25	0.51	1.56	3.25	6.15	7.10	31.89	75.11
Rakai	0.83	1.59	6.37	13.15	25.60	30.50	127.61	289.09
Rukungiri	0.87	1.70	9.16	23.16	47.04	56.62	226.57	555.65
Sironko	3.02	5.88	17.71	34.32	54.44	68.44	214.86	512.23
Soroti	0.27	0.43	1.23	2.96	5.43	6.18	31.19	67.77
Ssembabule	0.18	0.45	2.94	7.78	16.82	19.53	89.37	226.69

Table A.5 continued . . .

District	A_{min}	$A_{0.025}$	$A_{0.25}$	A_{median}	A_{mean}	$A_{0.75}$	$A_{0.975}$	A_{max}
Tororo	0.30	0.49	1.61	4.46	10.21	10.28	69.82	152.00
Wakiso	0.36	0.75	3.77	9.96	22.18	25.48	128.60	283.77
Yumbe	0.26	0.64	2.12	4.44	8.68	10.26	43.56	129.48

A.4 EFFICIENCY CRITERIA AND SIGNATURE MEASURES

The case study in Chapter 5 employed several widely applied efficiency criteria and signature measures to evaluate the model parameterizations of the model setups in the model calibration phase. Signature measures were additionally implemented to compute the influences of the model model input factors on the simulation of these signatures. In the following the employed efficiency criteria and signature measures are listed:

Nash Sutcliffe Efficiency (NSE, Nash and Sutcliffe, 1970)

The *NSE* is defined by the quotient of the mean squared error of simulations and observations to the observation variance (Gupta et al., 2009) and can be written as:

$$NSE = 1 - \frac{\sum_{i=1}^n (s_i - o_i)^2}{\sum_{i=1}^n (o_i - \bar{o})^2} \quad (\text{A.1})$$

where s_i and o_i are the simulated and observed values at the step i and \bar{o} is the mean value of the n observed values. The *NSE* can vary in the range between $(-\infty, 1]$ where 1 indicates a complete fit between simulations and observations, 0 and negative values indicate that on average the model predictions are as good or worse than the mean value of the observations.

Kling Gupta Efficiency (KGE, Gupta et al., 2009)

The *KGE* computes the Euclidean distance of the Pearson correlation coefficient r , the ratio simulation and observation means α , and the ratio of simulation and observation standard deviations β . The three individual components can be written as follows (Gupta et al., 2009):

$$r = \frac{\text{cov}(s, o)}{\sigma_s \sigma_o} \quad (\text{A.2})$$

where $\text{cov}(s, o)$ is the covariance of the simulations and observations and σ_s and σ_o are the standard deviations of the simulations and observations,

$$\alpha = \frac{\sigma_s}{\sigma_o} \quad (\text{A.3})$$

where σ_s and σ_o are the standard deviations of the simulations and observations, and

$$\beta = \frac{\mu_s}{\mu_o} \quad (\text{A.4})$$

where μ_s and μ_o are the mean values of the simulations and observations. The *KGE* is computed as follows:

$$KGE = 1 - \sqrt{(r - 1)^2 + (\alpha - 1)^2 + (\beta - 1)^2} \quad (\text{A.5})$$

The *KGE* can vary in the range between $(-\infty, 1]$. All three *KGE* components r , α , and β result in the value 1 for a perfect fit between simulations and observations and thus result in a $KGE = 1$. Deviations between simulations and observations in any of the three components result in value smaller than 1.

The refined index of agreement (d_r , Willmott et al., 2012)

Unlike the *NSE* and the *KGE* the index of agreement d_r employs mean absolute differences rather than squared differences between simulations and observations, to reduce the impact of large values in the calculation of the criterion. A further advantage of d_r is that it is bounded on the upper and the lower limits. d_r is defined as:

$$d_r = \begin{cases} 1 - \frac{\sum_{i=1}^n |s_i - o_i|}{2 \sum_{i=1}^n |o_i - \bar{o}|} & \text{if } \sum_{i=1}^n |s_i - o_i| \leq \sum_{i=1}^n |o_i - \bar{o}| \\ \frac{2 \sum_{i=1}^n |o_i - \bar{o}|}{\sum_{i=1}^n |s_i - o_i|} - 1 & \text{if } \sum_{i=1}^n |s_i - o_i| > \sum_{i=1}^n |o_i - \bar{o}| \end{cases} \quad (\text{A.6})$$

where s_i and o_i are the simulated and observed values at the step i and \bar{o} is the mean value of the n observed values. d_r can vary in the range between $[-1, 1]$. d_r compares the sum of absolute deviations between simulations and observations to the absolute deviations that the observation data show to the mean of the observations. Thus, $d_r = 1$ indicates that no deviations between simulations and observations are given in the data. Values of 0.5 and -0.5 indicate that the deviations of the simulations to the observations are half and twice the

deviations of the observations to the mean of the observations, respectively (Willmott et al., 2012).

Ratio of root-mean-square error and standard deviation (RSR, Moriasi et al., 2007)

The *RSR* employs the quotient of the root-mean-square error of the simulations to the observations to the standard deviation of the observations as a criterion of model efficiency. The *RSR* is defined as:

$$RSR = \frac{\sqrt{\sum_{i=1}^n (s_i - o_i)^2}}{\sqrt{\sum_{i=1}^n (o_i - \bar{o})^2}} \quad (\text{A.7})$$

where s_i and o_i are the simulated and observed values at the step i and \bar{o} is the mean value of the n observed values. The *RSR* can vary in the range between $(-\infty, 0]$, where 0 indicates that no deviation between simulations and observations are present and larger values indicate larger errors between simulation and observation.

Flow Duration Curve (FDC, e.g., Yilmaz et al., 2008; Vogel and Fennessey, 1994)

An FDC provides information on the magnitudes and their respective frequency of a variable and is the complement of a CDF (Vogel and Fennessey, 1994). The value of the variable x for a certain exceedance probability p is defined by specific quantile value x_p (see Fig. A.1)

FDCs were implemented as signatures to evaluate model parameterizations, by computing the *RSR* for the 5 FDC segments illustrated in Fig. A.1. In the sensitivity analysis that analyzed the discrete composite model inputs 6 quantile values for discharge and $\text{NO}_3\text{-N}$ loads for the exceedance probabilities were implemented with $p = (0.01, 0.05, 0.20, 0.70, 0.95, 0.99)$.

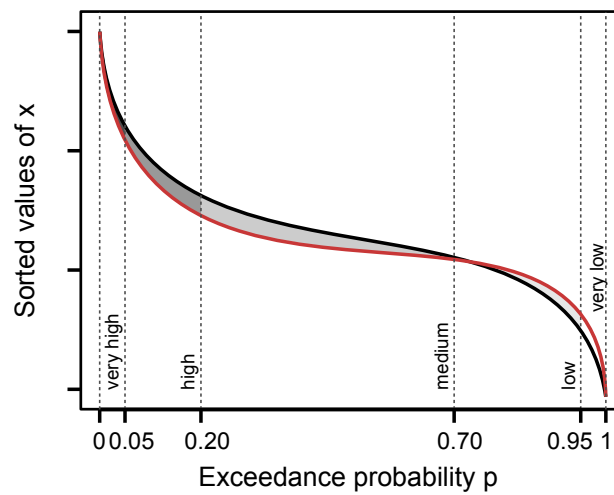


Figure A.1: Schematic example of a Flow Duration Curve (FDC). The red and black solid lines exemplify simulated and observed flow duration curves. The dashed lines separate the FDCs into segments of very high to very low values of x (in this case as shown in Pfannerstill et al. (2014)). The gray shaded areas enclosed between simulated and observed FDC indicate the areas that are used to compute the differences between simulated and observed discharge/ NO_3^- -N load segments (according to Pfannerstill et al. (2014) and Haas et al. (2016)).

BIBLIOGRAPHY

- Abbaspour, K. C. (2015). *SWAT-CUP: SWAT Calibration and Uncertainty Programs - A User Manual*. Tech. rep. Department of Systems Analysis, Integrated Assessment, Modelling (SIAM), Eawag, Swiss Federal Institute of Aquatic Science, and Technology, p. 100 (cit. on pp. 14, 21).
- Abbaspour, K. C., J. Yang, I. Maximov, R. Siber, K. Bogner, J. Mieleitner, J. Zobrist, and R. Srinivasan (2007). "Modelling hydrology and water quality in the pre-alpine/alpine Thur watershed using SWAT." In: *Journal of Hydrology* 333.2-4, pp. 413-430. DOI: 10.1016/j.jhydrol.2006.09.014 (cit. on p. 82).
- Alewel, C., P. Borrelli, K. Meusburger, and P. Panagos (2019). "Using the USLE: Chances, challenges and limitations of soil erosion modelling." In: *International Soil and Water Conservation Research* 7.3, pp. 203-225. DOI: <https://doi.org/10.1016/j.iswcr.2019.05.004> (cit. on pp. 14, 15, 40).
- Ammann, L., F. Fenicia, and P. Reichert (2019). "A likelihood framework for deterministic hydrological models and the importance of non-stationary autocorrelation." In: *Hydrology and Earth System Sciences* 23.4, pp. 2147-2172. DOI: 10.5194/hess-23-2147-2019 (cit. on p. 20).
- Amt d. Stmk LReg (2016). *Regionale Bevölkerungsprognose Steiermark 2015/16 -Bundesland, Bezirke und Gemeinden*. Tech. rep. Graz, Austria. URL: <http://docplayer.org/32447223-Regionale-bevoelkerungsprognose-steiermark-2015-16-bundesland-bezirke-und-gemeinden.html> (cit. on pp. 90, 91).
- Anderson, B., E. Borgonovo, M. Galeotti, and R. Roson (2014). "Uncertainty in climate change modeling: can global sensitivity analysis be of help?" In: *Risk analysis* 34.2, pp. 271-293. DOI: 10.1111/risa.12117 (cit. on pp. 22, 74).
- Angima, S. D., D. E. Stott, M. K. O'Neill, C. K. Ong, and G. A. Weesies (2003). "Soil erosion prediction using RUSLE for central Kenyan highland conditions." In: *Agriculture, Ecosystems and Environment* 97.1-3, pp. 295-308. DOI: 10.1016/S0167-8809(03)00011-2 (cit. on pp. 14, 15, 52, 53).
- Arnold, J. G., P. M. Allen, M. Volk, J. R. Williams, and D. D. Bosch (2010). "Assessment of Different Representations of Spatial Variability on SWAT Model Performance." In: *Transactions of the ASABE* 53, pp. 1433-1443. ISSN: 2151-0040. DOI: 10.13031/2013.34913 (cit. on p. 13).
- Arnold, J. G. and N. Fohrer (2005). "SWAT2000: current capabilities and research opportunities in applied watershed modelling." In: *Hydrological Processes* 19.3, pp. 563-572. DOI: 10.1002/hyp.5611 (cit. on p. 16).
- Arnold, J. G., D. N. Moriasi, P. W. Gassman, K. C. Abbaspour, M. J. White, R. Srinivasan, C. Santhi, R. D. Harmel, a. V. Griensven, M. W. VanLiew, N. Kannan, and M. K. Jha (2012). "Swat: Model Use, Calibration, and Validation." In: *Asabe* 55.4, pp. 1491-1508 (cit. on p. 82).
- Arnold, J. G., R. Srinivasan, R. S. Muttiah, and P. M. Allen (1999). "Continental scale simulation of the hydrologic balance." In: *Journal of the American Water Resources Association* 35.5, pp. 1037-1051. DOI: 10.1111/j.1752-1688.1999.tb04192.x (cit. on p. 16).
- Arnold, J. G., R. Srinivasan, R. S. Muttiah, and J. R. Williams (1998). "Large area hydrologic modeling and assessment part I: model development." In: *Journal of the American Water Resources Association* 34.1, pp. 73-89. DOI: 10.1111/j.1752-1688.1998.tb05961.x (cit. on pp. 12, 16).
- Bai, Z. G., D. L. Dent, L. Olsson, and M. E. Schaepman (2008). "Proxy global assessment of land degradation." In: *Soil Use and Management* 24.3, pp. 223-234. DOI: 10.1111/j.1475-2743.2008.00169.x (cit. on p. 42).
- Bamutaze, Y. (2010). "Patterns of water erosion and sediment loading in Manafwa in catchment on Mt. Elgon, Eastern Uganda." PhD thesis. Department of Geography, Geo-information and Climatic Science, Makerere University, Kampala, Uganda (cit. on pp. 57, 67, 70).
- Bamutaze, Y. (June 2015). "Revisiting socio-ecological resilience and sustainability in the coupled mountain landscapes in Eastern Africa." In: *Current Opinion in Environmental Sustainability* 14, pp. 257-265. DOI: 10.1016/j.cosust.2015.06.010 (cit. on pp. 54, 68).

- Baroni, G. and S. Tarantola (2014). "A General Probabilistic Framework for uncertainty and global sensitivity analysis of deterministic models: A hydrological case study." In: *Environmental Modelling & Software* 51, pp. 26–34. DOI: 10.1016/j.envsoft.2013.09.022 (cit. on pp. 4, 22, 74, 114, 124).
- "Pedo-transfer rule 5 (PTR05): top soil structure class (STS)" (2006). In: *New soil information for the MARS Crop Yield Forecasting System*. Ed. by B. Baruth, G. Genovese, and L. Montanarella. European Commission, Joint Research Centre (EC JRC). Chap. Annex 4.5. URL: https://esdac.jrc.ec.europa.eu/Projects/SINF0/pdf/annex4_5.pdf (cit. on pp. 48, 125).
- Beasley, D., L. Huggins, and a. Monke (1980). "ANSWERS: A model for watershed planning." In: *Transactions of the ASAE* 23.4, pp. 938–944. DOI: 10.13031/2013.34692 (cit. on p. 12).
- Benavidez, R., B. Jackson, D. Maxwell, and K. Norton (2018). "A review of the (Revised) Universal Soil Loss Equation ((R)USLE): with a view to increasing its global applicability and improving soil loss estimates." In: *Hydrology and Earth System Sciences* 22.11, pp. 6059–6086. DOI: 10.5194/hess-22-6059-2018 (cit. on pp. 15, 40).
- Bergström, S. (1995). "The HBV model." In: *Computer Models of Watershed Hydrology*. Ed. by V. P. Singh. Highlands Ranch, CO, USA: Water Resources Publications, pp. 443–476. ISBN: 0918334918, 9780918334916 (cit. on p. 120).
- Beven, K. J. (1989). "Changing ideas in hydrology — The case of physically-based models." In: *Journal of Hydrology* 105.1, pp. 157–172. DOI: 10.1016/0022-1694(89)90101-7 (cit. on pp. 1, 2).
- Beven, K. J. (1996). "The limits of splitting: Hydrology." In: *Science of the Total Environment* 183.1-2, pp. 89–97. DOI: 10.1016/0048-9697(95)04964-9 (cit. on pp. 3, 21, 74).
- Beven, K. J. (2000). "Uniqueness of place and process representations in hydrological modelling." In: *Hydrology and Earth System Sciences* 4.2, pp. 203–213. DOI: 10.5194/hess-4-203-2000 (cit. on pp. 1, 2).
- Beven, K. J. (2001). "On hypothesis testing in hydrology." In: *Hydrological Processes* 15, pp. 1655–1657. DOI: 10.1002/hyp.436 (cit. on p. 2).
- Beven, K. J. (2006). "A manifesto for the equifinality thesis." In: *Journal of Hydrology* 320.1-2, pp. 18–36. DOI: 10.1016/j.jhydrol.2005.07.007 (cit. on pp. 1, 74).
- Beven, K. J. (2007). "Towards integrated environmental models of everywhere: uncertainty, data and modelling as a learning process." In: *Hydrology and Earth System Sciences* 11.1, pp. 460–467. DOI: 10.5194/hess-11-460-2007 (cit. on p. 3).
- Beven, K. J. (2016). "Facets of uncertainty: epistemic uncertainty, non-stationarity, likelihood, hypothesis testing, and communication." In: *Hydrological Sciences Journal* 61.9, pp. 1652–1665. DOI: 10.1080/02626667.2015.1031761 (cit. on p. 20).
- Beven, K. J. (2018). "On hypothesis testing in hydrology: Why falsification of models is still a really good idea." In: *Wiley Interdisciplinary Reviews: Water* 5.3, e1278. DOI: 10.1002/wat2.1278 (cit. on pp. 6, 68, 73, 118).
- Beven, K. J. (2019). "Towards a methodology for testing models as hypotheses in the inexact sciences." In: *Proceedings of the Royal Society A: Mathematical, Physical and Engineering Sciences* 475.2224, p. 20180862. DOI: 10.1098/rspa.2018.0862 (cit. on pp. 1, 3).
- Beven, K. J., S. Almeida, W. P. Aspinall, P. D. Bates, S. Blazkova, E. Borgomeo, J. Freer, K. Goda, J. W. Hall, J. C. Phillips, M. Simpson, P. J. Smith, D. B. Stephenson, T. Wagener, M. Watson, and K. L. Wilkins (2018). "Epistemic uncertainties and natural hazard risk assessment – Part 1: A review of different natural hazard areas." In: *Natural Hazards and Earth System Sciences* 18.10, pp. 2741–2768. DOI: 10.5194/nhess-18-2741-2018 (cit. on pp. 5, 20).
- Beven, K. J. and A. Binley (1992). "The future of distributed models: Model calibration and uncertainty prediction." In: *Hydrological Processes* 6.3, pp. 279–298. DOI: 10.1002/hyp.3360060305 (cit. on pp. 2, 19, 26).
- Beven, K. J. and R. E. Brazier (2011). "Dealing with Uncertainty in Erosion Model Predictions." In: *Handbook of Erosion Modelling*. Ed. by R. P. C. Morgan and M. A. Nearing. Wiley Online Library. Chap. 4, pp. 52–79 (cit. on pp. 2, 29, 39, 68).
- Beven, K. J., H. Cloke, F. Pappenberger, R. Lamb, and N. Hunter (2015). "Hyperresolution information and hyperresolution ignorance in modelling the hydrology of the land surface." In: *Science China Earth Sciences* 58.1, pp. 25–35. DOI: 10.1007/s11430-014-5003-4 (cit. on p. 1).
- Beven, K. J. and J. Freer (2001). "Equifinality, data assimilation, and uncertainty estimation in mechanistic modelling of complex environmental systems using the GLUE methodology."

- In: *Journal of Hydrology* 249.1, pp. 11–29. DOI: [https://doi.org/10.1016/S0022-1694\(01\)00421-8](https://doi.org/10.1016/S0022-1694(01)00421-8) (cit. on p. 74).
- Beven, K. J. and P. C. Young (2013). “A guide to good practice in modeling semantics for authors and referees.” In: *Water Resources Research* 49, pp. 5092–5098. DOI: 10.1002/wrcr.20393 (cit. on p. 40).
- BGBI. 1996/210 (1996). *Verordnung des Bundesministers für Land- und Forstwirtschaft über die Begrenzung von Abwasseremissionen aus Abwasserreinigungsanlagen für Siedlungsgebiete (1. AEV für kommunales Abwasser)* (cit. on p. 80).
- BGBI. II 2006/96 (2006). *Qualitätszielverordnung Chemie Oberflächen-gewässer (QZV Chemie OG)* (cit. on p. 91).
- BGBI. II 2010/99 (2010). *Qualitätszielverordnung Ökologie Oberflächen-gewässer (QZV Ökologie OG)* (cit. on p. 91).
- BGBI. II Nr. 10/1999 (1999). *Verordnung des Bundesministers für Land- und Forstwirtschaft über die Begrenzung von Abwasseremissionen aus Gerbereien, Lederfabriken und Pelzzurichtereien (AEV Gerberei)* (cit. on p. 78).
- BGBI. II Nr. 12/1999 (1999). *Verordnung des Bundesministers für Land- und Forstwirtschaft über die Begrenzung von Abwasseremissionen aus der Schlachtung und Fleischverarbeitung (AEV Fleischwirtschaft)* (cit. on p. 78).
- Bicknell, B. R., J. C. Imhoff, J. L. Kittle Jr, A. S. Donigian Jr, and R. C. Johanson (1993). *Hydrologic simulation program-FORTRAN (HSPF): User’s Manual for Release 10, Rep. No. EPA/600/R-93*. Tech. rep. U.S. EPA, Environmental Research Laboratory, Athens, GA. Bingner, R.L., Darden, R.W., Theurer, (cit. on p. 12).
- Bieger, K., J. G. Arnold, H. Rathjens, M. J. White, D. D. Bosch, P. M. Allen, M. Volk, and R. Srinivasan (2017). “Introduction to SWAT+, A Completely Restructured Version of the Soil and Water Assessment Tool.” In: *JAWRA Journal of the American Water Resources Association* 53.1, pp. 115–130. DOI: 10.1111/1752-1688.12482 (cit. on p. 13).
- Bieger, K., G. Hörmann, and N. Fohrer (2013). “The impact of land use change in the Xiangxi Catchment (China) on water balance and sediment transport.” In: *Regional Environmental Change* 15.3, pp. 485–498. DOI: 10.1007/s10113-013-0429-3 (cit. on pp. 106, 113).
- Bingner, R. L., F. D. Theurer, and Y. Yuan (Jan. 2017). *AnnAGNPS TECHNICAL PROCESSES, Documentation Version 5.0*. Tech. rep. USDA-ARS, National Sedimentation Laboratory (cit. on p. 12).
- Bivand, R., T. Keitt, and B. Rowlingson (2019). *rgdal: Bindings for the ‘Geospatial’ Data Abstraction Library*. R package version 1.4-3. URL: <https://CRAN.R-project.org/package=rgdal> (visited on 03/11/2019) (cit. on p. 125).
- Blanco-Canqui, H. and R. Lal (2008). *Principles of soil conservation and management*. Springer Science & Business Media (cit. on pp. 54, 68).
- Blöschl, G., L. Gaál, J. Hall, A. Kiss, J. Komma, T. Nester, J. Parajka, R. A. P. Perdigão, L. Plavcová, M. Rogger, J. L. Salinas, and A. Viglione (2015). “Increasing river floods: fiction or reality?” In: *WIREs Water* 2.4, pp. 329–344. DOI: 10.1002/wat2.1079 (cit. on p. 120).
- Blöschl, G. and A. Montanari (2010). “Climate change impacts—throwing the dice?” In: *Hydrological Processes: An International Journal* 24.3, pp. 374–381. DOI: 10.1002/hyp.7574 (cit. on pp. 1–3, 5, 19, 113, 116, 117, 120).
- Blöschl, G. and E. Zehe (2005). “On hydrological predictability.” In: *Hydrological Processes* 19.19, pp. 3923–3929. DOI: 10.1002/hyp.6075 (cit. on p. 2).
- BMLFUW (Feb. 2013). *IMW3: Integrierte Betrachtung eines Gewässerabschnitts auf Basis kontinuierlicher und validierter Langzeitmessreihen [Integrated Monitoring of a river section on the basis of continuous and validated long measurement time series] (In German)*. Tech. rep. Vienna: Bundesministerium für Land- und Forstwirtschaft, Umwelt und Wasserwirtschaft, Sektion VII Wasser, p. 265 (cit. on p. 80).
- BMLFUW (2015a). *Online monitoring at the Station Neumarkt/Raab at the River Raab. Operated by the TU Wien, Institut für Gewässergüte, Ressourcenmanagement und Abfallwirtschaft*. (Visited on 07/08/2015) (cit. on p. 80).
- BMLFUW (2015b). *Online monitoring at the Station St.Margarethen/Takern II at the River Raab. Operated by TBS Water Consult*. (Visited on 11/02/2015) (cit. on p. 80).

- Boardman, J. (1996). "Soil erosion by water: problems and prospects for research." In: *Advances in Hillslope Processes*. Ed. by M. G. Anderson and S. M. Brooks. Wiley, Chichester, UK, pp. 489–505 (cit. on p. 39).
- Boardman, J. (2006). "Soil erosion science: Reflections on the limitations of current approaches." In: *CATENA* 68.2-3, pp. 73–86. DOI: 10.1016/j.catena.2006.03.007 (cit. on pp. 39, 40, 69, 70).
- Böhner, J. and T. Selige (2006). "Spatial Prediction of Soil Attributes Using Terrain Analysis and Climate Regionalisation." In: *'SAGA - Analysis and Modelling Applications'*. Ed. by J. Böhner, K. McCloy, and J. Strobl. Göttinger Geographische Abhandlungen, Göttingen, 13-28 (cit. on pp. 50, 64).
- Bollinne, A. (1985). "Adjusting the universal soil loss equation to use in Western Europe." In: *Soil Erosion and Conservation*. Ed. by S. El-Swaify, W. Moldenhauer, and L. A. Soil Conservation Society of America, Ankeny, Iowa, pp. 206–213 (cit. on pp. 15, 39).
- Borah, D. and M. Bera (2003). "Watershed-scale hydrologic and nonpoint-source pollution models: Review of mathematical bases." In: *Transactions of the ASAE* 46.6, p. 1553. DOI: 10.13031/2013.15644 (cit. on pp. 11–13).
- Borgonovo, E., X. Lu, E. Plischke, O. Rakovec, and M. C. Hill (2017). "Making the most out of a hydrological model data set: Sensitivity analyses to open the model black-box." In: *Water Resources Research*, pp. 7933–7950. DOI: 10.1002/2017WR020767 (cit. on p. 19).
- Borgonovo, E. (2007). "A new uncertainty importance measure." In: *Reliability Engineering & System Safety* 92.6, pp. 771–784. DOI: 10.1016/j.res.s.2006.04.015 (cit. on p. 27).
- Borrelli, P., D. A. Robinson, L. R. Fleischer, E. Lugato, C. Ballabio, C. Alewell, K. Meusburger, S. Modugno, B. Schütt, V. Ferro, V. Bagarello, K. V. Oost, L. Montanarella, and P. Panagos (2017). "An assessment of the global impact of 21st century land use change on soil erosion." In: *Nature Communications* 8.1. DOI: 10.1038/s41467-017-02142-7 (cit. on pp. 14, 40, 41, 45, 48–53, 71, 125, 129).
- Bosco, C., D. De Rigo, O. Dewitte, J. Poesen, and P. Panagos (2015). "Modelling soil erosion at European scale: Towards harmonization and reproducibility." In: *Natural Hazards and Earth System Sciences* 15.2, pp. 225–245. DOI: 10.5194/nhess-15-225-2015 (cit. on pp. 2, 39, 40, 50, 51, 68, 70, 71).
- Bosco, C., D. D. Rigo, and O. Dewitte (2014). "Visual Validation of the e-RUSLE Model Applied at the Pan-European Scale." In: *Scientific Topics Focus 1*. MRI-11a13. Notes on Transdisciplinary Modelling for Environment, Maeutike Research Initiative. DOI: 10.6084/m9.figshare.844627.v5 (cit. on pp. 70–72).
- Bosshard, T., M. Carambia, K. Goergen, S. Kotlarski, P. Krahe, M. Zappa, and C. Schär (2013). "Quantifying uncertainty sources in an ensemble of hydrological climate-impact projections." In: *Water Resources Research* 49.3, pp. 1523–1536. DOI: 10.1029/2011WR011533 (cit. on pp. 113, 116, 117).
- Box, G. E. P. (1976). "Science and statistics." In: *Journal of the American Statistical Association* 71.356, pp. 791–799 (cit. on p. 1).
- Box, G. E. P. (1979). "Robustness in the strategy of scientific model building." In: *Robustness in statistics*. Ed. by P. L. Launer and G. N. Wilkinson. Elsevier, pp. 201–236 (cit. on pp. 1, 9).
- Breiman, L., J. Friedman, R. Olshen, and C. Stone (1984). *Classification and regression trees*. Wadsworth Int. Group (cit. on p. 25).
- Browning, G. M., C. L. Parish, and J. A. Glass (1947). "A method for determining the use of limitations of rotation and conservation practices in the control of soil erosion in Iowa." In: *Journal of the American Society of Agronomy* 39, pp. 65–73 (cit. on p. 14).
- Butler, M. P., P. M. Reed, K. Fisher-Vanden, K. Keller, and T. Wagener (2014). "Identifying parametric controls and dependencies in integrated assessment models using global sensitivity analysis." In: *Environmental modelling & software* 59, pp. 10–29. DOI: 10.1016/j.envsoft.2014.05.001 (cit. on pp. 22, 74).
- Campolongo, F., A. Saltelli, T. Sørensen, and S. Tarantola (2009). "Hitchhiker's Guide to Sensitivity Analysis." In: *Sensitivity Analysis*. Ed. by A. Saltelli, K. Chan, and E. M. Scott. Chichester, West Sussex, UK: John Wiley & Sons, Ltd. Chap. 2, pp. 15–47. ISBN: 978-0-470-74382-9 (cit. on p. 22).
- Canty, A. and B. D. Ripley (2017). *boot: Bootstrap R (S-Plus) Functions*. R package version 1.3-20 (cit. on p. 94).

- Channan, S., K. Collins, and W. R. Emanuel (2014). *Global mosaics of the standard MODIS land cover type data*. College Park, Maryland, USA (cit. on p. 51).
- Chiew, F. H. and J. Vaze (2015). "Hydrologic nonstationarity and extrapolating models to predict the future: Overview of session and proceeding." In: *IAHS-AISH Proceedings and Reports*. Vol. 371. 10, pp. 17–21. DOI: 10.5194/piahs-371-17-2015 (cit. on p. 74).
- Chun, M.-H., S.-J. Han, and N.-I. Tak (2000). "An uncertainty importance measure using a distance metric for the change in a cumulative distribution function." In: *Reliability Engineering & System Safety* 70.3, pp. 313–321. DOI: 10.1016/S0951-8320(00)00068-5 (cit. on p. 27).
- Claessens, L., P. Van Breugel, A. Notenbaert, M. Herrero, and J. Van De Steeg (2008). "Mapping potential soil erosion in East Africa using the Universal Soil Loss Equation and secondary data." In: *IAHS publication* 325, p. 398 (cit. on p. 51).
- Clark, M. P., R. L. Wilby, E. D. Gutmann, J. A. Vano, S. Gangopadhyay, A. W. Wood, H. J. Fowler, C. Prudhomme, J. R. Arnold, and L. D. Brekke (2016). "Characterizing Uncertainty of the Hydrologic Impacts of Climate Change." In: *Current Climate Change Reports* 2, pp. 55–64. DOI: 10.1007/s40641-016-0034-x (cit. on pp. 3, 5, 22, 73, 107, 109, 113, 117, 121, 123).
- Clark, M. P., A. G. Slater, D. E. Rupp, R. A. Woods, J. A. Vrugt, H. V. Gupta, T. Wagener, and L. E. Hay (2008). "Framework for Understanding Structural Errors (FUSE): A modular framework to diagnose differences between hydrological models." In: *Water Resources Research* 44.12. DOI: 10.1029/2007WR006735 (cit. on pp. 21, 74).
- Conrad, O., B. Bechtel, M. Bock, H. Dietrich, E. Fischer, L. Gerlitz, J. Wehberg, V. Wichmann, and J. Böhner (2015). "System for Automated Geoscientific Analyses (SAGA) v. 2.1.4." In: *Geoscientific Model Development* 8.7, pp. 1991–2007. DOI: 10.5194/gmd-8-1991-2015 (cit. on pp. 50, 125).
- Cukier, R. I., C. M. Fortuin, K. E. Shuler, A. G. Petschek, and J. H. Schaibly (1973). "Study of the sensitivity of coupled reaction systems to uncertainties in rate coefficients. I Theory." In: *The Journal of Chemical Physics* 59.8, pp. 3873–3878. DOI: 10.1063/1.1680571 (cit. on p. 26).
- Cuntz, M., J. Mai, M. Zink, S. Thober, R. Kumar, D. Schäfer, M. Schrön, J. Craven, O. Rakovec, D. Spieler, V. Prykhodko, G. Dalmasso, J. Musuuza, B. Langenberg, S. Attinger, and L. Samaniego (2015). "Computationally inexpensive identification of noninformative model parameters by sequential screening." In: *Water Resources Research* 51.8, pp. 6417–6441. DOI: 10.1002/2015WR016907 (cit. on p. 25).
- Dai, H. and M. Ye (2015). "Variance-based global sensitivity analysis for multiple scenarios and models with implementation using sparse grid collocation." In: *Journal of Hydrology* 528, pp. 286–300. DOI: 10.1016/j.jhydrol.2015.06.034 (cit. on pp. 22, 74, 114, 124).
- Dai, H., M. Ye, A. P. Walker, and X. Chen (2017). "A new process sensitivity index to identify important system processes under process model and parametric uncertainty." In: *Water Resources Research* 53.4, pp. 3476–3490. ISSN: 19447973. DOI: 10.1002/2016WR019715 (cit. on pp. 22, 74, 114).
- De Meyer, A., J. Poesen, M. Isabirye, J. Deckers, and D. Raes (2011). "Soil erosion rates in tropical villages: A case study from Lake Victoria Basin, Uganda." In: *CATENA* 84.3, pp. 89–98. DOI: 10.1016/j.catena.2010.10.001 (cit. on pp. 57, 67, 69, 70).
- Desmet, P. and G. Govers (1996). "A GIS procedure for automatically calculating the USLE LS factor on topographically complex landscape units." In: *Journal of soil and water conservation* 51.5, pp. 427–433 (cit. on pp. 50, 64).
- Didan, K. (2015). "MOD13Q1 MODIS/Terra vegetation indices 16-day L3 global 250m SIN grid V006." In: *NASA EOSDIS Land Processes DAAC*. DOI: 10.5067/MODIS/MOD13Q1.006 (cit. on pp. 43, 51).
- Dile, Y. T., P. Daggupati, C. George, R. Srinivasan, and J. Arnold (2016). "Introducing a new open source GIS user interface for the SWAT model." In: *Environmental modelling & software* 85, pp. 129–138. DOI: 10.1016/j.envsoft.2016.08.004 (cit. on pp. 16, 81).
- Dissmeyer, G. and G. Foster (1980). *A guide for predicting sheet and rill erosion on forest land*. Technical Publication SA-TP-11, USDA Forest Service-State and Private Forestry Southeastern Area (cit. on p. 15).
- Dubus, I. G. and C. D. Brown (2002). "Sensitivity and first-step uncertainty analyses for the preferential flow model MACRO." In: *Journal of Environmental Quality* 31.1, pp. 227–240 (cit. on pp. xvi, 24).

- Duethmann, D., G. Blöschl, and J. Parajka (2020). "Why does a conceptual hydrological model fail to predict discharge changes in response to climate change?" In: *Hydrology and Earth System Sciences Discussions* 2020, pp. 1–28. DOI: 10.5194/hess-2019-652 (cit. on p. 120).
- Duran-Encalada, J. A., A. Paucar-Caceres, E. R. Bandala, and G. H. Wright (2017). "The impact of global climate change on water quantity and quality: A system dynamics approach to the US–Mexican transborder region." In: *European Journal of Operational Research* 256.2, pp. 567–581. DOI: 10.1016/j.ejor.2016.06.016 (cit. on p. 73).
- Ebisemijew, F. (1988). "Gully morphometric controls in a laterite terrain, Guyana." In: *Geo Eco Trop* 12, pp. 41–59 (cit. on pp. 42, 43, 57).
- EEA (2015). *CORINE Land Cover 2006 raster data. Version 17 (12/2013)*. URL: <http://www.eea.europa.eu/data-and-maps/data/corine-land-cover-2006-raster-3> (visited on 02/06/2015) (cit. on pp. 78, 81).
- Efron, B. (1987). "Better bootstrap confidence intervals." In: *Journal of the American statistical Association* 82.397, pp. 171–185. DOI: 10.2307/2289144 (cit. on p. 94).
- ESA (2017). *ESA Land Cover Climate Change Initiative (ESA LC CCI) data: ESACCI-LC-L4-LCCS-Map-300m-P1Y-1992_2015-v2.0.7.tif via Centre for Environmental Data Analysis*. URL: <http://maps.elie.ucl.ac.be/CCI> (cit. on p. 51).
- ESRI (2012). *ArcGIS Desktop: Release 10.1*. Redlands, CA (cit. on pp. 50, 81, 125).
- Estrada-Carmona, N., E. B. Harper, F. DeClerck, and A. K. Fremier (2017). "Quantifying model uncertainty to improve watershed-level ecosystem service quantification: a global sensitivity analysis of the RUSLE." In: *International Journal of Biodiversity Science, Ecosystem Services & Management* 13.1, pp. 40–50. DOI: 10.1080/21513732.2016.1237383 (cit. on p. 114).
- Euser, T., H. C. Winsemius, M. Hrachowitz, F. Fenicia, S. Uhlenbrook, and H. H. Savenije (2013). "A framework to assess the realism of model structures using hydrological signatures." In: *Hydrology and Earth System Sciences* 17.5, pp. 1893–1912. DOI: 10.5194/hess-17-1893-2013 (cit. on p. 94).
- Evans, R. (2002). "An alternative way to assess water erosion of cultivated land – field-based measurements: and analysis of some results." In: *Applied Geography* 22.2, pp. 187–207. DOI: 10.1016/S0143-6228(02)00004-8 (cit. on p. 70).
- Evans, R. (1995). "Some methods of directly assessing water erosion of cultivated land - a comparison of measurements made on plots and in fields." In: *Progress in Physical Geography* 19, pp. 115–129. DOI: 10.1177/030913339501900106 (cit. on pp. 39, 70).
- Evans, R. (2013). "Assessment and monitoring of accelerated water erosion of cultivated land - when will reality be acknowledged?" In: *Soil Use and Management* 29, pp. 105–118. DOI: 10.1111/sum.12010 (cit. on pp. 40, 69).
- Evans, R. and J. Boardman (2016a). "A reply to panagos et al., 2016 (Environmental science & policy 59 (2016) 53–57)." In: *Environmental science & policy* 60, pp. 63–68. DOI: 10.1016/j.envsci.2016.03.004 (cit. on p. 39).
- Evans, R. and J. Boardman (2016b). "The new assessment of soil loss by water erosion in Europe. Panagos P. et al., 2015 Environmental Science & Policy 54, 438–447—A response." In: *Environmental Science & Policy* 58, pp. 11–15. DOI: 10.1016/j.envsci.2015.12.013 (cit. on p. 39).
- FAO-PNUMA-UNESCO (1980). *Metodología provisional para la evaluación de la degradación de los suelos*. Tech. rep. Organización de las Naciones Unidas para el Desarrollo de la Agricultura y la Alimentación (FAO), Programa de las Naciones Unidas para el Medio Ambiente (PNUMA), Organización de las Naciones Unidas para el Medio Ambiente (UNESCO), Roma, Italia (In Spanish) (cit. on pp. 54, 59, 69).
- Favis-Mortlock, D. (1998). "Validation of Field-Scale Soil Erosion Models Using Common Datasets." In: *Modelling Soil Erosion by Water, NATO ASI Series book series (volume 55)*. Ed. by J. Boardman and D. Favis-Mortlock. Springer Berlin Heidelberg. Chap. 9, pp. 89–127. DOI: 10.1007/978-3-642-58913-3_9 (cit. on pp. 2, 15, 39, 113).
- Ferro, V., G. Giordano, and M. Iovino (1991). "Isoerosivity and erosion risk map for sicily." In: *Hydrological Sciences Journal* 36.6, pp. 549–564. DOI: 10.1080/02626669109492543 (cit. on p. 47).
- Fick, S. E. and R. J. Hijmans (2017). "WorldClim 2: new 1-km spatial resolution climate surfaces for global land areas." In: *International Journal of Climatology* 37.12, pp. 4302–4315. DOI: 10.1002/joc.5086 (cit. on pp. 43, 45).

- Frias, M. D., M. Iturbide, R. Manzanas, J. Bedia, J. Fernandez, S. Herrera, A. S. Cofino, and J. M. Gutierrez (2018). "An R package to visualize and communicate uncertainty in seasonal climate prediction." In: *Environmental Modelling & Software* 99, pp. 101–110. DOI: 10.1016/j.envsoft.2017.09.008 (cit. on p. 123).
- Friedl, M. A., D. Sulla-Menashe, B. Tan, A. Schneider, N. Ramankutty, A. Sibley, and X. Huang (2010). *MODIS Collection 5 global land cover: Algorithm refinements and characterization of new datasets, 2001–2012, Collection 5.1 IGBP Land Cover*. Boston, MA, USA. URL: <http://glcf.umd.edu/data/lc/> (visited on 06/19/2018) (cit. on p. 51).
- García-Ruiz, J. M., S. Beguería, E. Nadal-Romero, J. C. González-Hidalgo, N. Lana-Renault, and Y. Sanjuán (2015). "A meta-analysis of soil erosion rates across the world." In: *Geomorphology* 239, pp. 160–173. DOI: 10.1016/j.geomorph.2015.03.008 (cit. on p. 56).
- Gassman, P. W., M. R. Reyes, C. H. Green, and J. G. Arnold (2007). "The Soil and Water Assessment Tool: Historical development, applications, and future research directions." In: *Transactions of the ASABE* 50.4, pp. 1211–1250 (cit. on pp. 14, 16).
- Geoland.at (2015). *Digitales Geländemodell (DGM) Österreich*. URL: <https://www.data.gv.at/katalog/dataset/b5de6975-417b-4320-afdb-eb2a9e2a1dbf> (visited on 11/19/2015) (cit. on pp. 78, 81).
- Godet, M. and F. Roubelat (1996). "Creating the future : The use and misuse of scenarios." In: *Long Range Planning* 29.2, pp. 164–171. DOI: 10.1016/0024-6301(96)00004-0 (cit. on p. 106).
- Goerlandt, F. and G. Reniers (2016). "On the assessment of uncertainty in risk diagrams." In: *Safety Science* 84, pp. 67–77. DOI: 10.1016/j.ssci.2015.12.001 (cit. on p. 123).
- Govers, G. (2011). "Misapplications and Misconceptions of Erosion Models." In: *Handbook of Erosion Modelling*. Ed. by R. P. C. Morgan and M. A. Nearing. Blackwell Publishing Ltd. Chap. 7, pp. 117–134 (cit. on pp. 15, 39, 40, 69, 70).
- Grayson, R. and G. Blöschl (2000). "Summary of pattern comparison and concluding remarks." In: *Spatial Patterns in Catchment Hydrology: Observations and Modelling*. Ed. by R. Grayson and G. Blöschl. Cambridge University Press: Cambridge, UK. Chap. 14, pp. 355–367. ISBN: 0-521-63316-8 (cit. on pp. 1, 2).
- Griensven, A. van, T. Meixner, S. Grunwald, T. Bishop, M. Diluzio, and R. Srinivasan (2006). "A global sensitivity analysis tool for the parameters of multi-variable catchment models." In: *Journal of hydrology* 324, pp. 10–23. DOI: 10.1016/j.jhydrol.2005.09.008 (cit. on p. 24).
- Grolemund, G. and H. Wickham (2011). "Dates and Times Made Easy with lubridate." In: *Journal of Statistical Software* 40.3, pp. 1–25. DOI: 10.18637/jss.v040.i03 (cit. on p. 125).
- Gupta, H. V., C. Perrin, G. Blöschl, A. Montanari, R. Kumar, M. Clark, and V. Andréassian (2014). "Large-sample hydrology: a need to balance depth with breadth." In: *Hydrology and Earth System Sciences* 18.2, pp. 463–477. DOI: 10.5194/hess-18-463-2014. URL: <https://www.hydro1-earth-syst-sci.net/18/463/2014/> (cit. on pp. 1, 2).
- Gupta, H. and S. Razavi (2017). "Challenges and Future Outlook of Sensitivity Analysis." In: *Sensitivity Analysis in Earth Observation Modelling*. Ed. by G. P. Petropoulos and P. K. Srivastava. 1st ed. Elsevier. Chap. 20, pp. 397–415. DOI: 10.1016/B978-0-12-803011-0.00020-3 (cit. on p. 23).
- Gupta, H. V., H. Kling, K. K. Yilmaz, and G. F. Martinez (2009). "Decomposition of the mean squared error and NSE performance criteria: Implications for improving hydrological modelling." In: *Journal of Hydrology* 377.1-2, pp. 80–91. DOI: 10.1016/j.jhydrol.2009.08.003 (cit. on pp. xvi, 83, 137).
- Gupta, H. V. and G. S. Nearing (2014). "Debates—the future of hydrological sciences: A (common) path forward? Using models and data to learn: A systems theoretic perspective on the future of hydrological science." In: *Water Resources Research* 50.6, pp. 5351–5359. DOI: 10.1002/2013WR015096 (cit. on p. 20).
- Gupta, H. V. and S. Razavi (2018). "Revisiting the Basis of Sensitivity Analysis for Dynamical Earth System Models." In: *Water Resources Research* 54.11, pp. 8692–8717. DOI: 10.1029/2018wr022668 (cit. on p. 21).
- Gupta, H. V., S. Sorooshian, and P. O. Yapo (1999). "Status of Automatic Calibration for Hydrologic Models: Comparison with Multilevel Expert Calibration." In: *Journal of Hydrologic Engineering* 4.2, pp. 135–143. DOI: 10.1061/(ASCE)1084-0699(1999)4:2(135) (cit. on pp. xvii, 85).

- Guse, B., M. Pfannerstill, and N. Fohrer (2015). "Dynamic Modelling of Land Use Change Impacts on Nitrate Loads in Rivers." In: *Environmental Processes* 2.4, pp. 575–592. DOI: 10.1007/s40710-015-0099-x (cit. on pp. 106, 113).
- Guse, B., M. Pfannerstill, M. Strauch, D. E. Reusser, S. Lüdtke, M. Volk, H. Gupta, and N. Fohrer (2016). "On characterizing the temporal dominance patterns of model parameters and processes." In: *Hydrological Processes* 30.13, pp. 2255–2270. DOI: 10.1002/hyp.10764 (cit. on p. 23).
- Haas, M. B., B. Guse, M. Pfannerstill, and N. Fohrer (2015). "Detection of dominant nitrate processes in ecohydrological modeling with temporal parameter sensitivity analysis." In: *Ecological Modelling* 314, pp. 62–72. DOI: 10.1016/j.ecolmodel.2015.07.009 (cit. on p. 82).
- Haas, M. B., B. Guse, M. Pfannerstill, and N. Fohrer (2016). "A joined multi-metric calibration of river discharge and nitrate loads with different performance measures." In: *Journal of Hydrology* 536, pp. 534–545. DOI: 10.1016/j.jhydro.2016.03.001 (cit. on pp. 82, 83, 85, 140).
- Haghnegahdar, A. and S. Razavi (2017). "Insights into sensitivity analysis of earth and environmental systems models: On the impact of parameter perturbation scale." In: *Environmental Modelling & Software* 95, pp. 115–131. DOI: 10.1016/j.envsoft.2017.03.031 (cit. on pp. 26, 83).
- Haghnegahdar, A., S. Razavi, F. Yassin, and H. Wheeler (2017). "Multi-criteria sensitivity analysis as a diagnostic tool for understanding model behavior and characterizing model uncertainty." In: *Hydrological Processes* 31.25, pp. 4462–4476. DOI: 10.1002/hyp.11358 (cit. on pp. 23, 26, 83).
- Haiden, T., A. Kann, C. Wittmann, G. Pistotnik, B. Bica, and C. Gruber (2011). "The Integrated Nowcasting through Comprehensive Analysis (INCA) System and Its Validation over the Eastern Alpine Region." In: *Weather and Forecasting* 26.2, pp. 166–183. DOI: 10.1175/2010WAF2222451.1 (cit. on pp. 80, 81).
- Haith, D. A. and L. L. Shoemaker (1987). "Generalized Watershed Loading Functions for Stream Flow Nutrients." In: *Journal of the American Water Resources Association* 23.3, pp. 471–478. DOI: 10.1111/j.1752-1688.1987.tb00825.x (cit. on p. 12).
- Hall, J., B. Arheimer, M. Borga, R. Brázdil, P. Claps, A. Kiss, T. R. Kjeldsen, J. Kriaučiūnienė, Z. W. Kundzewicz, M. Lang, M. C. Llasat, N. Macdonald, N. McIntyre, L. Mediero, B. Merz, R. Merz, P. Molnar, A. Montanari, C. Neuhold, J. Parajka, R. A. P. Perdigão, L. Plavcová, M. Rogger, J. L. Salinas, E. Sauquet, C. Schär, J. Szolgay, A. Viglione, and G. Blöschl (2014). "Understanding flood regime changes in Europe: a state-of-the-art assessment." In: *Hydrology and Earth System Sciences* 18.7, pp. 2735–2772. DOI: 10.5194/hess-18-2735-2014 (cit. on p. 120).
- Hart, J. and P. Gremaud (2018). "Robustness of the Sobol' indices to distributional uncertainty." In: *arXiv preprint arXiv:1803.11249v3* (cit. on p. 109).
- Hartigan, J. A. and M. A. Wong (1979). "Algorithm AS 136: A K-Means Clustering Algorithm." In: *Applied Statistics* 28.1, p. 100. DOI: 10.2307/2346830 (cit. on p. 80).
- Haslinger, K., I. Anders, and M. Hofstätter (2013). "Regional climate modelling over complex terrain: an evaluation study of COSMO-CLM hindcast model runs for the Greater Alpine Region." In: *Climate Dynamics* 40.1-2, pp. 511–529. DOI: 10.1007/s00382-012-1452-7 (cit. on p. 92).
- Hempel, S., K. Frieler, L. Warszawski, J. Schewe, and F. Piontek (2013). "A trend-preserving bias correction - The ISI-MIP approach." In: *Earth System Dynamics* 4.2, pp. 219–236. DOI: 10.5194/esd-4-219-2013 (cit. on p. 92).
- Hengl, T., J. M. De Jesus, G. B. Heuvelink, M. R. Gonzalez, M. Kilibarda, A. Blagotić, W. Shangguan, M. N. Wright, X. Geng, B. Bauer-Marschallinger, M. A. Guevara, R. Vargas, R. A. MacMillan, N. H. Batjes, J. G. Leenaars, E. Ribeiro, I. Wheeler, S. Mantel, and B. Kempen (2017). "SoilGrids250m: Global gridded soil information based on machine learning." In: *PLoS one* 12.2, pp. 1–40. DOI: 10.1371/journal.pone.0169748 (cit. on pp. 47, 79, 81).
- Henry, L. and H. Wickham (2019). *purrr: Functional Programming Tools*. R package version 0.3.2. URL: <https://CRAN.R-project.org/package=purrr> (visited on 03/15/2019) (cit. on p. 125).
- Hernando, D. and M. G. Romana (June 2015). "Development of a Soil Erosion Classification System for Cut and Fill Slopes." In: *Transportation Infrastructure Geotechnology* 2.4, pp. 155–166. DOI: 10.1007/s40515-015-0024-9 (cit. on p. 55).

- Hiebl, J. and C. Frei (2016). "Daily temperature grids for Austria since 1961—concept, creation and applicability." In: *Theoretical and Applied Climatology* 124.1-2, pp. 161–178. DOI: 10.1007/s00704-015-1411-4 (cit. on p. 92).
- Hijmans, R. J. (2019). *raster: Geographic Data Analysis and Modeling*. R package version 2.9-5. URL: <https://CRAN.R-project.org/package=raster> (visited on 05/14/2019) (cit. on p. 125).
- Hinkley, D. V. (1988). "Bootstrap methods." In: *Journal of the Royal Statistical Society. Series B (Methodological)*, pp. 321–337 (cit. on p. 94).
- Hofstätter, M., M. Ganekind, and J. Hiebl (2013). "GPARD-6: A new 60-year gridded precipitation dataset for Austria based on daily rain gauge measurements." In: *DACH 2013 - Deutsch-Österreichisch-Schweizerische Meteorologen-Tagung*. Innsbruck, Austria (cit. on p. 92).
- Homma, T. and A. Saltelli (1996). "Importance measures in global sensitivity analysis of nonlinear models." In: *Reliability Engineering & System Safety* 52.1, pp. 1–17. DOI: 10.1016/0951-8320(96)00002-6 (cit. on p. 26).
- Honti, M., N. Schuwirth, J. Rieckermann, and C. Stamm (2017). "Can integrative catchment management mitigate future water quality issues caused by climate change and socio-economic development?" In: *Hydrology and Earth System Sciences* 21.3, pp. 1593–1609. DOI: 10.5194/hess-21-1593-2017 (cit. on p. 106).
- Hosseini, S. M., B. Ataie-Ashtiani, and C. T. Simmons (2017). "Spring hydrograph simulation of karstic aquifers: Impacts of variable recharge area, intermediate storage and memory effects." In: *Journal of hydrology* 552, pp. 225–240. DOI: 10.1016/j.jhydro.2017.06.018 (cit. on p. 30).
- Houska, T., P. Kraft, A. Chamorro-Chavez, and L. Breuer (2015). "SPOTting model parameters using a ready-made python package." In: *PloS one* 10.12, e0145180. DOI: 10.1371/journal.pone.0145180 (cit. on pp. 110, 123).
- Hrachowitz, M. and M. P. Clark (2017). "HESS Opinions: The complementary merits of competing modelling philosophies in hydrology." In: *Hydrology and Earth System Sciences* 21.8, pp. 3953–3973. DOI: 10.5194/hess-21-3953-2017 (cit. on pp. 1–4, 13, 113).
- Hrachowitz, M., O. Fovet, L. Ruiz, T. Euser, S. Gharari, R. Nijzink, J. Freer, H. H. Savenije, and C. Gascuel-Oudou (2014). "Process consistency in models: The importance of system signatures, expert knowledge, and process complexity." In: *Water Resources Research* 50.9, pp. 7445–7469. DOI: 10.1002/2014WR015484 (cit. on p. 107).
- Huffman, G. J., D. T. Bolvin, E. J. Nelkin, D. B. Wolff, R. F. Adler, G. Gu, Y. Hong, K. P. Bowman, and E. F. Stocker (Feb. 2007). "The TRMM Multisatellite Precipitation Analysis (TMPA): Quasi-Global, Multiyear, Combined-Sensor Precipitation Estimates at Fine Scales." In: *Journal of Hydrometeorology* 8.1, pp. 38–55. DOI: 10.1175/jhm560.1 (cit. on p. 45).
- Iooss, B., A. Janon, G. Pujol, with contributions from Khalid Boumhaout, S. D. Veiga, T. Delage, J. Fruth, L. Gilquin, J. Guillaume, L. Le Gratiet, P. Lemaitre, B. L. Nelson, F. Monari, R. Oomen, B. Ramos, O. Roustant, E. Song, J. Staum, R. Sueur, T. Touati, and F. Weber (2018). *sensitivity: Global Sensitivity Analysis of Model Outputs*. R package version 1.15.1. URL: <https://CRAN.R-project.org/package=sensitivity> (cit. on pp. 110, 123).
- Jacob, D., J. Petersen, B. Eggert, A. Alias, O. B. Christensen, L. M. Bouwer, A. Braun, A. Colette, M. Déqué, G. Georgievski, E. Georgopoulou, A. Gobiet, L. Menut, G. Nikulin, A. Haensler, N. Hempelmann, C. Jones, K. Keuler, S. Kovats, N. Kröner, S. Kotlarski, A. Kriegsmann, E. Martin, E. van Meijgaard, C. Moseley, S. Pfeifer, S. Preuschmann, C. Radermacher, K. Radtke, D. Rechid, M. Rounsevell, P. Samuelsson, S. Somot, J.-F. Soussana, C. Teichmann, R. Valentini, R. Vautard, B. Weber, and P. Yiou (2014). "EURO-CORDEX: new high-resolution climate change projections for European impact research." In: *Regional Environmental Change* 14.2, pp. 563–578. DOI: 10.1007/s10113-013-0499-2 (cit. on pp. 73, 92).
- Jansen, M. J. W. (1999). "Analysis of variance designs for model output." In: *Computer Physics Communications* 117, pp. 35–43. DOI: 10.1016/S0010-4655(98)00154-4 (cit. on pp. 24, 27).
- Jarvis, A., H. I. Reuter, A. Nelson, and E. Guevara (2008). *Hole-filled SRTM for the globe Version 4*. available from the CGIAR-CSI SRTM 90m Database. URL: <https://cgiarcsi.community/data/srtm-90m-digital-elevation-database-v4-1/> (cit. on pp. 44, 50).
- Jetten, V. and D. Favis-Mortlock (2006). "Modelling Soil Erosion in Europe." In: *Soil Erosion in Europe*. Ed. by J. Boardman and J. Poesen. John Wiley & Sons, Ltd. Chap. 50, pp. 695–716. DOI: 10.1002/0470859202.ch50 (cit. on pp. 13, 39).

- Jha, M., P. W. Gassman, S. Secchi, R. Gu, and J. Arnold (2004). "Effect of Watershed Subdivision on SWAT Flow, Sediment, and Nutrient Predictions." In: *Journal of the American Water Resources Association* 40.3, pp. 811–825. DOI: 10.1111/j.1752-1688.2004.tb04460.x (cit. on pp. 81, 107).
- Jiménez, B. E., T. Oki, N. W. Arnell, G. Benito, J. G. Cogley, P. Döll, T. Jiang, and S. S. Mwakilila (2014). "Freshwater Resources." In: *Climate Change 2014: Impacts, Adaptation, and Vulnerability. Part A: Global and Sectoral Aspects. Contribution of Working Group II to the Fifth Assessment Report of the Intergovernmental Panel on Climate Change*. Ed. by C. Field, V. Barros, D. Dokken, K. Mach, M. Mastrandrea, T. Bilir, M. Chatterjee, K. Ebi, Y. Estrada, R. Genova, B. Girma, E. Kissel, A. Levy, S. MacCracken, P. Mastrandrea, and L. White. Cambridge, United Kingdom and New York, NY, USA: Cambridge University Press, pp. 229–269 (cit. on p. 73).
- Jones, A., H. Breuning-Madsen, M. Brossard, A. Dampha, J. Deckers, O. Dewitte, T. Gallali, S. Hallett, R. Jones, M. Kilasara, P. Le Roux, E. Micheli, O. Spaargaren, L. Thombiano, E. Van Ranst, M. Yemefack, and R. Zougmore, eds. (2013). *Soil Atlas of Africa*. European Union Joint Research Centre, p. 176. ISBN: 978-92-79-26715-4 (cit. on p. 42).
- Jones, R., A. Patwardhan, S. Cohen, S. Dessai, A. Lammel, R. Lempert, M. Mirza, and H. von Storch (2014). "Foundations for Decision Making." In: *Climate Change 2014: Impacts, Adaptation, and Vulnerability. Part A: Global and Sectoral Aspects. Contribution of Working Group II to the Fifth Assessment Report of the Intergovernmental Panel on Climate Change*. Ed. by C. Field, V. Barros, D. Dokken, K. Mach, M. Mastrandrea, T. Bilir, M. Chatterjee, K. Ebi, Y. Estrada, R. Genova, B. Girma, E. Kissel, A. Levy, S. MacCracken, P. Mastrandrea, and L. White. Cambridge, United Kingdom and New York, NY, USA: Cambridge University Press, pp. 195–228. DOI: 10.1017/CB09781107415379.007 (cit. on p. 108).
- Karamage, F., C. Zhang, T. Liu, A. Maganda, and A. Isabwe (2017). "Soil erosion risk assessment in Uganda." In: *Forests* 8.2, p. 52. DOI: 10.3390/f8020052 (cit. on pp. 14, 41, 45, 47, 48, 50, 51, 54, 65, 66, 68, 71, 117).
- Kinnell, P. (2010). "Event soil loss, runoff and the Universal Soil Loss Equation family of models: A review." In: *Journal of Hydrology* 385.1, pp. 384–397. DOI: 10.1016/j.jhydrol.2010.01.024 (cit. on pp. 12, 14, 15, 39, 47, 49).
- Kirchner, J. W. (2006). "Getting the right answers for the right reasons: Linking measurements, analyses, and models to advance the science of hydrology." In: *Water Resources Research* 42.3, W03S04. DOI: 10.1029/2005WR004362 (cit. on pp. 1–3, 113).
- Kithiia, S. M. (1997). "Land use changes and their effects on sediment transport and soil erosion within the Athi drainage basin, Kenya." In: *Human Impact on Erosion and Sedimentation (Proceedings of Rabat Symposium 56, April 1997)*, IAHS Publ. no. 245. Ed. by D. E. Walling and J.-L. Probst. International Association of Hydrological Sciences, pp. 145–150. ISBN: 901502-30-9 (cit. on pp. 57, 67, 69, 70).
- Kiureghian, A. D. and O. Ditlevsen (2009). "Aleatory or epistemic? Does it matter?" In: *Structural Safety* 31.2. Risk Acceptance and Risk Communication, pp. 105–112. DOI: 10.1016/j.strusafe.2008.06.020 (cit. on p. 20).
- Kleijnen, J. P. C. and J. C. Helton (1999). "Statistical analyses of scatterplots to identify important factors in large-scale simulations, 1: Review and comparison of techniques." In: *Reliability Engineering & System Safety* 65.2, pp. 147–185. DOI: 10.1016/S0951-8320(98)00091-X (cit. on p. 25).
- Klemeš, V. (1986). "Dilettantism in hydrology: Transition or destiny?" In: *Water Resources Research* 22.9S, 177S–188S. DOI: 10.1029/WR022i09Sp0177S (cit. on pp. 1, 3, 37).
- KNBS (2015). "Section agriculture." In: *County Statistical Abstracts*. Nairobi, Kenya: Kenya National Bureau of Statistics (cit. on p. 51).
- Knisel, W. G. (1980). *CREAMS: A field scale model for chemicals, runoff, and erosion from agricultural management systems*. US Department of Agriculture, Conservation Research Report 26, pp. 643 (cit. on p. 16).
- Knutti, R. and J. Sedláček (2013). "Robustness and uncertainties in the new CMIP5 climate model projections." In: *Nature Climate Change* 3.4, pp. 369–373. DOI: 10.1038/nclimate1716 (cit. on p. 73).
- Kratzert, F., D. Klotz, C. Brenner, K. Schulz, and M. Herrnegger (2018). "Rainfall-runoff modelling using Long Short-Term Memory (LSTM) networks." In: *Hydrology and Earth System*

- Sciences* 22.11, pp. 6005–6022. DOI: 10.5194/hess-22-6005-2018. URL: <https://www.hydrology-earth-syst-sci.net/22/6005/2018/> (cit. on p. 1).
- Kratzert, F., D. Klotz, G. Shalev, G. Klambauer, S. Hochreiter, and G. Nearing (2019). "Towards learning universal, regional, and local hydrological behaviors via machine learning applied to large-sample datasets." In: *Hydrology and Earth System Sciences* 23.12, pp. 5089–5110. DOI: 10.5194/hess-23-5089-2019 (cit. on p. 1).
- Krysanova, V. and J. G. Arnold (2008). "Advances in ecohydrological modelling with SWAT—a review." In: *Hydrological Sciences Journal* 53.5, pp. 939–947. DOI: 10.1623/hysj.53.5.939 (cit. on p. 16).
- Kuczera, G. and E. Parent (1998). "Monte Carlo assessment of parameter uncertainty in conceptual catchment models: the Metropolis algorithm." In: *Journal of Hydrology* 211.1, pp. 69–85. DOI: 10.1016/S0022-1694(98)00198-X (cit. on p. 19).
- Lafren, J. M., W. J. Elliot, D. C. Flanagan, C. R. Meyer, and M. A. Nearing (1997). "WEPP—predicting water erosion using a process-based model." In: *Journal of Soil and Water Conservation* 52.2, pp. 96–102 (cit. on p. 12).
- Land NÖ (2015). *Landwirtschaftliche Bildung in NÖ - Versuche*. URL: <http://www.lako.at/de/versuche/?lang=de%7B%5C%7Da=179%7B%5C%7Da%7B%5C%7Durlname=versuche%7B%5C%7Dversuche%7B%5C%7Da=1> (visited on 11/19/2015) (cit. on pp. 78, 81).
- Leonard, R. A., W. G. Knisel, and D. A. Still (1987). "GLEAMS: Groundwater Loading Effects of Agricultural Management Systems." In: *Transactions of the ASAE* 30.5, pp. 1403–1418. DOI: 10.13031/2013.30578 (cit. on pp. 12, 16).
- LGBL Nr. 39/2015 (2015). *Verordnung des Landeshauptmannes von Steiermark vom 20. Mai 2015, mit der ein Regionalprogramm zum Schutz der Grundwasserkörper Grazer Feld, Leibnitzer Feld und Unteres Murtal erlassen und Schongebiete bestimmt werden (Grundwasserschutzprogramm Graz bis B* (cit. on p. 91).
- Liu, H., W. Chen, and A. Sudjianto (2006). "Relative Entropy Based Method for Probabilistic Sensitivity Analysis in Engineering Design." In: *Journal of Mechanical Design* 128, p. 326. DOI: 10.1115/1.2159025 (cit. on p. 27).
- Lo, A., S. A. El-Swaify, E. W. Dangler, and L. Shinshiro (1985). "Effectiveness of EI₃₀ as an erosivity index in Hawaii." In: *Soil Erosion and Conservation*. Ed. by S. A. El-Swaify, W. C. Moldenhauer, and A. Lo. Ankeny, IA, USA: Soil Conservation Society of America, pp. 384–392 (cit. on pp. 45, 47, 63).
- Logan, D. C. (2009). "Known knowns, known unknowns, unknown unknowns and the propagation of scientific enquiry." In: *Journal of Experimental Botany* 60.3, pp. 712–714. DOI: 10.1093/jxb/erp043 (cit. on p. 118).
- LUCAS (2012). *Land Use/Cover Area Frame Statistical Survey Database*. URL: http://epp.eurostat.ec.europa.eu/portal/page/portal/lucas/data/LUCAS_primary_data/2012 (cit. on p. 71).
- Lufafa, A., M. Tenywa, M. Isabirye, M. Majaliwa, and P. Woomer (June 2003). "Prediction of soil erosion in a Lake Victoria basin catchment using a GIS-based Universal Soil Loss model." In: *Agricultural Systems* 76.3, pp. 883–894. DOI: 10.1016/S0308-521X(02)00012-4 (cit. on p. 54).
- Mahmoud, M., Y. Liu, H. Hartmann, S. Stewart, T. Wagener, D. Semmens, R. Stewart, H. Gupta, D. Dominguez, F. Dominguez, D. Hulse, R. Letcher, B. Rashleigh, C. Smith, R. Street, J. Ticehurst, M. Twery, H. van Delden, R. Waldick, D. White, and L. Winter (2009). "A formal framework for scenario development in support of environmental decision-making." In: *Environmental Modelling and Software* 24.7, pp. 798–808. DOI: 10.1016/j.envsoft.2008.11.010 (cit. on pp. 108, 109).
- Malagó, A., F. Bouraoui, O. Vigiak, B. Grizzetti, and M. Pastori (2017). "Modelling water and nutrient fluxes in the Danube River Basin with SWAT." In: *Science of The Total Environment* 603-604, pp. 196–218. DOI: <https://doi.org/10.1016/j.scitotenv.2017.05.242> (cit. on p. 14).
- Mannschatz, T., T. Wolf, and S. Hülsmann (2016). "Nexus Tools Platform: Web-based comparison of modelling tools for analysis of water-soil-waste nexus." In: *Environmental Modelling & Software* 76, pp. 137–153. DOI: 10.1016/j.envsoft.2015.10.031 (cit. on pp. 11, 16).
- Mantovan, P. and E. Todini (2006). "Hydrological forecasting uncertainty assessment: Incoherence of the GLUE methodology." In: *Journal of Hydrology* 330.1, pp. 368–381. DOI: 10.1016/j.jhydro.2006.04.046 (cit. on p. 20).

- Mara, T. A. and S. Tarantola (2012). "Variance-based sensitivity indices for models with dependent inputs." In: *Reliability Engineering & System Safety* 107, pp. 115–121. DOI: 10.1016/j.res.s.2011.08.008 (cit. on p. 109).
- Massmann, C. and H. Holzmann (2015). "Analysing the Sub-processes of a Conceptual Rainfall-Runoff Model Using Information About the Parameter Sensitivity and Variance." In: *Environmental Modeling and Assessment* 20.1, pp. 41–53. DOI: 10.1007/s10666-014-9414-6 (cit. on p. 23).
- McInerney, D., D. Kavetski, M. Thyer, J. Lerat, and G. Kuczera (2019). "Benefits of Explicit Treatment of Zero Flows in Probabilistic Hydrological Modeling of Ephemeral Catchments." In: *Water Resources Research* 55.12, pp. 11035–11060. DOI: 10.1029/2018WR024148 (cit. on p. 20).
- Mehdi, B., B. Lehner, C. Gombault, A. Michaud, I. Beaudin, M.-F. Sottile, and A. Blondlot (2015a). "Simulated impacts of climate change and agricultural land use change on surface water quality with and without adaptation management strategies." In: *Agriculture, Ecosystems & Environment* 213, pp. 47–60. DOI: 10.1016/j.agee.2015.07.019 (cit. on p. 106).
- Mehdi, B., R. Ludwig, and B. Lehner (2015b). "Evaluating the impacts of climate change and crop land use change on streamflow, nitrates and phosphorus: A modeling study in Bavaria." In: *Journal of Hydrology: Regional Studies* 4, pp. 60–90. DOI: 10.1016/j.ejrh.2015.04.009 (cit. on pp. 106, 113).
- Mehdi, B., K. Schulz, R. Ludwig, F. Ferber, and B. Lehner (2018). "Evaluating the Importance of Non-Unique Behavioural Parameter Sets on Surface Water Quality Variables under Climate Change Conditions in a Mesoscale Agricultural Watershed." In: *Water Resources Management* 32.2, pp. 619–639. DOI: 10.1007/s11269-017-1830-3 (cit. on pp. 82, 107).
- Merritt, W., R. Letcher, and A. Jakeman (2003). "A review of erosion and sediment transport models." In: *Environmental Modelling & Software* 18.8-9, pp. 761–799. DOI: 10.1016/s1364-8152(03)00078-1 (cit. on pp. 11, 12).
- Merz, R., J. Parajka, and G. Blöschl (2011). "Time stability of catchment model parameters: Implications for climate impact analyses." In: *Water Resources Research* 47.2, W02531. DOI: 10.1029/2010WR009505 (cit. on pp. 3, 6, 113, 116, 120).
- Microsoft Corporation and S. Weston (2017a). *doSNOW: Foreach Parallel Adaptor for the 'snow' Package*. R package version 1.0.16. URL: <https://CRAN.R-project.org/package=doSNOW> (visited on 10/23/2018) (cit. on p. 125).
- Microsoft Corporation and S. Weston (2017b). *foreach: Provides Foreach Looping Construct for R*. R package version 1.4.4. URL: <https://CRAN.R-project.org/package=foreach> (visited on 10/23/2018) (cit. on p. 125).
- Milly, P. C. D., J. Betancourt, M. Falkenmark, R. M. Hirsch, Z. W. Kundzewicz, D. P. Lettenmaier, and R. J. Stouffer (2008). "Climate change. Stationarity is dead: whither water management?" In: *Science* 319.5863, pp. 573–574. DOI: 10.1126/science.1151915 (cit. on pp. 73, 74, 113).
- Milly, P. C. D. and K. A. Dunne (2011). "On the hydrologic adjustment of climate-model projections: The potential pitfall of potential evapotranspiration." In: *Earth Interactions* 15.1, pp. 1–14. DOI: 10.1175/2010EI363.1 (cit. on p. 106).
- Mockus, V. (1964). *Estimation of direct runoff from storm rainfall*. National Engineering Handbook, Section 4: Hydrology. Tech. rep. Washington, D.C.: USDA Soil Conservation Service (cit. on p. 13).
- Momm, H. G., R. L. Bingner, R. Emilaire, J. Garbrecht, R. R. Wells, and R. A. Kuhnle (2017). "Automated watershed subdivision for simulations using multi-objective optimization." In: *Hydrological Sciences Journal* 62.10, pp. 1564–1582. DOI: 10.1080/02626667.2017.1346794 (cit. on pp. 81, 107).
- Monfreda, C., N. Ramankutty, and J. A. Foley (2008). "Farming the planet: 2. Geographic distribution of crop areas, yields, physiological types, and net primary production in the year 2000." In: *Global Biogeochemical Cycles* 22.1, pp. 1–19. DOI: 10.1029/2007GB002947 (cit. on pp. 51–53, 65, 129).
- Montanari, A., G. Young, H. Savenije, D. Hughes, T. Wagener, L. Ren, D. Koutsoyiannis, C. Cudennec, E. Toth, S. Grimaldi, G. Blöschl, M. Sivapalan, K. Beven, H. Gupta, M. Hipsey, B. Schaefli, B. Arheimer, E. Boegh, S. Schymanski, G. D. Baldassarre, B. Yu, P. Hubert, Y. Huang, A. Schumann, D. Post, V. Srinivasan, C. Harman, S. Thompson, M. Rogger, A. Viglione, H. McMillan, G. Characklis, Z. Pang, and V. Belyaev (2013). "'Panta Rhei—Everything Flows":

- Change in hydrology and society—The IAHS Scientific Decade 2013–2022.” In: *Hydrological Sciences Journal* 58.6, pp. 1256–1275. DOI: 10.1080/02626667.2013.809088 (cit. on p. 113).
- Montanari, A. (2007). “What do we mean by ‘uncertainty’? The need for a consistent wording about uncertainty assessment in hydrology.” In: *Hydrological Processes* 21.6, pp. 841–845. DOI: 10.1002/hyp.6623 (cit. on pp. 20, 21, 73).
- Montgomery, D. R. (Aug. 2007). “Soil erosion and agricultural sustainability.” In: *Proceedings of the National Academy of Sciences* 104.33, pp. 13268–13272. DOI: 10.1073/pnas.0611508104 (cit. on pp. 54, 68).
- Moore, I. D., R. B. Grayson, and A. R. Ladson (1991). “Digital terrain modelling: A review of hydrological, geomorphological, and biological applications.” In: *Hydrological Processes* 5.1, pp. 3–30. DOI: 10.1002/hyp.3360050103 (cit. on pp. 50, 64).
- Moore, T. R. (1979). “Rainfall Erosivity in East Africa.” In: *Geografiska Annaler. Series A, Physical Geography* 61.3/4, pp. 147–156. DOI: 10.2307/520909 (cit. on pp. 15, 41, 45, 47, 63).
- Mora, E. B., J. Spelling, and A. H. van der Weijde (2019). “Benchmarking the PAWN distribution-based method against the variance-based method in global sensitivity analysis: Empirical results.” In: *Environmental Modelling & Software* 122, p. 104556. DOI: 10.1016/j.envsoft.2019.104556 (cit. on pp. 27, 30).
- Morgan, R. P. C. (2009). *Soil erosion and conservation*. John Wiley & Sons (cit. on pp. 47, 54).
- Moriasi, D., J. Arnold, M. Van Liew, R. Binger, R. Harmel, and T. Veith (2007). “Model evaluation guidelines for systematic quantification of accuracy in watershed simulations.” In: *Transactions of the ASABE* 50.3, pp. 885–900. DOI: 10.13031/2013.23153 (cit. on pp. xvii, 83, 139).
- Morris, M. D. (1991). “Factorial sampling plans for preliminary computational experiments.” In: *Technometrics* 33.2, pp. 161–174 (cit. on pp. 24, 82).
- Morss, R. E., J. L. Demuth, and J. K. Lazo (2008). “Communicating Uncertainty in Weather Forecasts: A Survey of the U.S. Public.” In: *Weather and Forecasting* 23.5, pp. 974–991. DOI: 10.1175/2008WAF2007088.1 (cit. on p. 123).
- Moss, R. H., J. A. Edmonds, K. A. Hibbard, M. R. Manning, S. K. Rose, D. P. Van Vuuren, T. R. Carter, S. Emori, M. Kainuma, T. Kram, G. A. Meehl, J. F. Mitchell, N. Nakicenovic, K. Riahi, S. J. Smith, R. J. Stouffer, A. M. Thomson, J. P. Weyant, and T. J. Wilbanks (2010). “The next generation of scenarios for climate change research and assessment.” In: *Nature* 463.7282, pp. 747–756. DOI: 10.1038/nature08823 (cit. on p. 73).
- Muerth, M. J., B. Gauvin St-Denis, S. Ricard, J. A. Velázquez, J. Schmid, M. Minville, D. Caya, D. Chaumont, R. Ludwig, and R. Turcotte (2013). “On the need for bias correction in regional climate scenarios to assess climate change impacts on river runoff.” In: *Hydrology and Earth System Sciences* 17.3, pp. 1189–1204. DOI: 10.5194/hess-17-1189-2013 (cit. on p. 92).
- Müller, K. and H. Wickham (2019). *tibble: Simple Data Frames*. R package version 2.1.3. URL: <https://CRAN.R-project.org/package=tibble> (visited on 06/06/2019) (cit. on p. 125).
- Müller, K., H. Wickham, D. A. James, and S. Falcon (2018). *RSQLite: ‘SQLite’ Interface for R*. R package version 2.1.1. URL: <https://CRAN.R-project.org/package=RSQLite> (visited on 04/24/2019) (cit. on p. 125).
- Murphy, J. M., D. M. H. Sexton, D. N. Barnett, G. S. Jones, M. J. Webb, M. Collins, and D. A. Stainforth (2004). “Quantification of modelling uncertainties in a large ensemble of climate change simulations.” In: *Nature* 430, pp. 768–772. DOI: 10.1038/nature02771 (cit. on p. 23).
- Musgrave, G. W. (1947). “The quantitative evaluation of factors in water erosion, a first approximation.” In: *Journal of Soil and Water Conservation* 2, pp. 133–138 (cit. on p. 14).
- Naipal, V., C. Reick, J. Pongratz, and K. Van Oost (2015). “Improving the global applicability of the RUSLE model - Adjustment of the topographical and rainfall erosivity factors.” In: *Geoscientific Model Development* 8.9, pp. 2893–2913. ISSN: 19919603. DOI: 10.5194/gmd-8-2893-2015 (cit. on pp. 40, 45, 47, 48, 51).
- Nakil, M. (2014). “Analysis of parameters causing water induced soil erosion.” In: *Unpublished Fifth Annual Progress Seminar, Indian Institute of Technology, Bombay* (cit. on pp. 45, 47, 63).
- NASA/METI/AIST/Japan SpaceSystems, and US/Japan ASTER Science Team (2009). *ASTER Global Digital Elevation Model*. DOI: 10.5067/ASTER/ASTGTM.002 (cit. on p. 50).
- Nash, J. E. and J. V. Sutcliffe (1970). “River flow forecasting through conceptual models part I - A discussion of principles.” In: *Journal of Hydrology* 10.3, pp. 282–290. DOI: 10.1016/0022-1694(70)90255-6 (cit. on pp. xvi, 83, 137).

- Nearing, G. S. (2013). "Diagnostics and Generalizations for Parametric State Estimation." PhD thesis. Department of Hydrology and Water Resources, The University of Arizona, Tucson, AZ, USA (cit. on p. 20).
- Nearing, G., F. Kratzert, A. K. Sampson, C. S. Pelissier, D. Klotz, J. Frame, and H. Gupta (Feb. 2020). "What Role Does Hydrological Science Play in the Age of Machine Learning?" In: *EarthArXiv*. DOI: 10.31223/osf.io/3sx6g (cit. on p. 1).
- Neitsch, S., J. Arnold, J. Kiniry, and J. Williams (2011). *Soil and Water Assessment Tool Theoretical Documentation Version 2009*. Tech. rep. Temple, Texas: Texas Water Resources Institute (cit. on pp. 13, 16, 17, 80).
- Norton, J. (2015). "An introduction to sensitivity assessment of simulation models." In: *Environmental Modelling & Software* 69, pp. 166–174. ISSN: 1364-8152. DOI: 10.1016/j.envsoft.2015.03.020 (cit. on p. 23).
- Olivares, R. U., A. D. M. Bulos, and E. Z. Sombrito (Feb. 2016). "Environmental assessment of soil erosion in Inabanga watershed (Bohol, Philippines)." In: *Energy, Ecology and Environment* 1.2, pp. 98–108. DOI: 10.1007/s40974-016-0012-0 (cit. on p. 55).
- ÖWAV (2010). *ÖWAV-Regelblatt 25: Abwasserentsorgung in dünn besiedelten Gebieten, 2. vollständig überarbeitete Auflage* (cit. on p. 91).
- Panagos, P., C. Ballabio, P. Borrelli, K. Meusburger, A. Klik, S. Rousseva, M. P. Tadić, S. Michaelides, M. Hrabalíková, P. Olsen, J. Aalto, M. Lakatos, A. Rymaszewicz, A. Dumitrescu, S. Begueria, and C. Alewell (2015a). "Rainfall erosivity in Europe." In: *Science of the Total Environment* 511, pp. 801–814. DOI: 10.1016/j.scitotenv.2015.01.008 (cit. on pp. 40, 45).
- Panagos, P., P. Borrelli, and K. Meusburger (2015b). "A New European Slope Length and Steepness Factor (LS-Factor) for Modeling Soil Erosion by Water." In: *Geosciences* 5.2, pp. 117–126. DOI: 10.3390/geosciences5020117 (cit. on pp. 40, 49, 50).
- Panagos, P., P. Borrelli, K. Meusburger, C. Alewell, E. Lugato, and L. Montanarella (2015c). "Estimating the soil erosion cover-management factor at the European scale." In: *Land Use Policy* 48, pp. 38–50. DOI: 10.1016/j.landusepol.2015.05.021 (cit. on pp. 40, 51–54).
- Panagos, P., P. Borrelli, K. Meusburger, B. Yu, A. Klik, K. Jae Lim, J. E. Yang, J. Ni, C. Miao, N. Chattopadhyay, S. H. Sadeghi, Z. Hazbavi, M. Zabihi, G. A. Larionov, S. F. Krasnov, A. V. Gorobets, Y. Levi, G. Erpul, C. Birkel, N. Hoyos, V. Naipal, P. T. S. Oliveira, C. A. Bonilla, M. Meddi, W. Nel, H. Al Dashti, M. Boni, N. Diodato, K. Van Oost, M. Nearing, and C. Ballabio (2017). "Global rainfall erosivity assessment based on high-temporal resolution rainfall records." In: *Scientific Reports* 7.1, p. 4175. DOI: 10.1038/s41598-017-04282-8 (cit. on pp. 40, 45, 47, 63).
- Panagos, P., P. Borrelli, K. Meusburger, E. H. van der Zanden, J. Poesen, and C. Alewell (2015d). "Modelling the effect of support practices (P-factor) on the reduction of soil erosion by water at European scale." In: *Environmental Science and Policy* 51, pp. 23–34. DOI: 10.1016/j.envsci.2015.03.012 (cit. on p. 71).
- Panagos, P., P. Borrelli, J. Poesen, C. Ballabio, E. Lugato, K. Meusburger, L. Montanarella, and C. Alewell (2015e). "The new assessment of soil loss by water erosion in Europe." In: *Environmental Science and Policy* 54, pp. 438–447. DOI: 10.1016/j.envsci.2015.08.012 (cit. on pp. 14, 39, 40, 48).
- Panagos, P., P. Borrelli, J. Poesen, K. Meusburger, C. Ballabio, E. Lugato, L. Montanarella, and C. Alewell (2016). "Reply to "The new assessment of soil loss by water erosion in Europe. Panagos P. et al., 2015 Environ. Sci. Policy 54, 438–447—A response" by Evans and Boardman [Environ. Sci. Policy 58, 11–15]." In: *Environmental Science & Policy* 59, pp. 53–57. DOI: 10.1016/j.envsci.2016.02.010 (cit. on p. 39).
- Panagos, P., K. Meusburger, C. Ballabio, P. Borrelli, and C. Alewell (2014). "Soil erodibility in Europe: A high-resolution dataset based on LUCAS." In: *Science of the Total Environment* 479-480.1, pp. 189–200. DOI: 10.1016/j.scitotenv.2014.02.010 (cit. on pp. 45, 48, 125).
- Pandey, A., S. K. Himanshu, S. Mishra, and V. P. Singh (2016). "Physically based soil erosion and sediment yield models revisited." In: *CATENA* 147, pp. 595–620. DOI: 10.1016/j.catena.2016.08.002 (cit. on pp. 11–14).
- Pappenberg, F. and K. J. Beven (2006). "Ignorance is bliss: Or seven reasons not to use uncertainty analysis." In: *Water Resources Research* 42.5, W05302. DOI: 10.1029/2005WR004820 (cit. on pp. 4, 113, 123).

- Pappenberger, F., K. J. Beven, M. Ratto, and P. Matgen (2008). "Multi-method global sensitivity analysis of flood inundation models." In: *Advances in water resources* 31.1, pp. 1–14. DOI: 10.1016/j.advwatres.2007.04.009 (cit. on p. 19).
- Park, C. K. and K.-I. Ahn (1994). "A new approach for measuring uncertainty importance and distributional sensitivity in probabilistic safety assessment." In: *Reliability Engineering & System Safety* 46.3, pp. 253–261. DOI: 10.1016/0951-8320(94)90119-8 (cit. on p. 27).
- Pebesma, E. (2018). "Simple Features for R: Standardized Support for Spatial Vector Data." In: *The R Journal* 10.1, pp. 439–446. DOI: 10.32614/RJ-2018-009 (cit. on p. 125).
- Pfannerstill, M., K. Bieger, B. Guse, D. D. Bosch, N. Fohrer, and J. G. Arnold (2017). "How to Constrain Multi-Objective Calibrations of the SWAT Model Using Water Balance Components." In: *Journal of the American Water Resources Association* 53.3, pp. 532–546. DOI: 10.1111/1752-1688.12524 (cit. on p. 107).
- Pfannerstill, M., B. Guse, and N. Fohrer (2014). "Smart low flow signature metrics for an improved overall performance evaluation of hydrological models." In: *Journal of Hydrology* 510, pp. 447–458. DOI: 10.1016/j.jhydrol.2013.12.044 (cit. on pp. 83, 85, 140).
- Pianosi, F., K. J. Beven, J. Freer, J. W. Hall, J. Rougier, D. B. Stephenson, and T. Wagener (2016). "Sensitivity analysis of environmental models: A systematic review with practical workflow." In: *Environmental Modelling & Software* 79, pp. 214–232. ISSN: 13648152. DOI: 10.1016/j.envsoft.2016.02.008 (cit. on pp. 19, 22–27, 123).
- Pianosi, F. and T. Wagener (2015). "A simple and efficient method for global sensitivity analysis based on cumulative distribution functions." In: *Environmental Modelling & Software* 67, pp. 1–11. DOI: 10.1016/j.envsoft.2015.01.004 (cit. on pp. xvii, 22, 23, 27, 30–32, 110, 115, 123).
- Pianosi, F. and T. Wagener (2018). "Distribution-based sensitivity analysis from a generic input-output sample." In: *Environmental Modelling & Software* 108, pp. 197–207. DOI: 10.1016/j.envsoft.2018.07.019 (cit. on pp. 19, 27, 32, 115).
- Pignotti, G., H. Rathjens, R. Cibin, I. Chaubey, and M. Crawford (2017). "Comparative analysis of HRU and grid-based SWAT models." In: *Water* 9.4, p. 272. DOI: 10.3390/w9040272 (cit. on p. 107).
- Prasuhn, V., H. Liniger, S. Gisler, K. Herweg, A. Candinas, and J.-P. Clément (2013). "A high-resolution soil erosion risk map of Switzerland as strategic policy support system." In: *Land Use Policy* 32, pp. 281–291. DOI: 10.1016/j.landusepol.2012.11.006 (cit. on p. 70).
- project, I. (2019). *Inkscape: Release 0.92.4*. URL: <https://www.inkscape.org> (visited on 01/14/2019) (cit. on p. 125).
- Puy, A., S. Lo Piano, and A. Saltelli (July 2019). "A sensitivity analysis of the PAWN sensitivity index." In: *arXiv e-prints*, arXiv:1904.04488v2. URL: <https://arxiv.org/abs/1904.04488v2> (cit. on p. 30).
- Quilbé, R., A. N. Rousseau, P. Lafrance, J. Leclerc, and M. Amrani (2006). "Selecting a Pesticide Fate Model at the Watershed Scale Using a Multi-criteria Analysis." In: *Water Quality Research Journal* 41.3, pp. 283–295. DOI: 10.2166/wqrj.2006.032 (cit. on p. 13).
- R Core Team (2017). *R: A language and environment for statistical computing*. Vienna, Austria. URL: <https://www.r-project.org/> (cit. on p. 80).
- R Core Team (2019). *R: A language and environment for statistical computing*. Vienna, Austria. URL: <https://www.r-project.org/> (visited on 03/05/2019) (cit. on p. 125).
- Rakovec, O., M. C. Hill, M. P. Clark, A. H. Weerts, A. J. Teuling, and R. Uijlenhoet (2014). "Distributed Evaluation of Local Sensitivity Analysis (DELSA), with application to hydrologic models." In: *Water Resour. Res* 50, pp. 409–426. DOI: 10.1002/2013WR014063 (cit. on pp. 23, 24).
- Rathjens, H., N. Oppelt, D. D. Bosch, J. G. Arnold, and M. Volk (2015). "Development of a grid-based version of the SWAT landscape model." In: *Hydrological Processes* 29.6, pp. 900–914. DOI: 10.1002/hyp.10197 (cit. on p. 13).
- Ratto, M., S. Tarantola, and A. Saltelli (2001). "Sensitivity analysis in model calibration: GSA-GLUE approach." In: *Computer Physics Communications* 136.3, pp. 212–224. DOI: 10.1016/S0010-4655(01)00159-X (cit. on pp. 19, 23, 26).
- Razavi, S. and H. V. Gupta (2015). "What do we mean by sensitivity analysis? The need for comprehensive characterization of "global" sensitivity in Earth and Environmental systems

- models." In: *Water Resources Research* 51.5, pp. 3070–3092. DOI: 10.1002/2014WR016527 (cit. on pp. 4, 22, 23).
- Razavi, S. and H. V. Gupta (2016a). "A new framework for comprehensive, robust, and efficient global sensitivity analysis: 1. Theory." In: *Water Resources Research* 52.1, pp. 423–439. DOI: 10.1002/2015WR017558 (cit. on pp. xvi, xviii, 27, 82, 83, 124).
- Razavi, S. and H. V. Gupta (2016b). "A new framework for comprehensive, robust, and efficient global sensitivity analysis: 2. Application." In: *Water Resources Research* 52.1, pp. 440–455. DOI: 10.1002/2015WR017559 (cit. on pp. xviii, 22, 23, 26, 27, 82, 83, 124).
- Refsgaard, J. C. and B. Storm (1995). "MIKE SHE." In: *Computer Models of Watershed Hydrology*. Ed. by V. P. Singh. Water Resources Publication. Chap. 23 (cit. on p. 12).
- Refsgaard, J. C., J. P. van der Sluijs, A. L. Højberg, and P. A. Vanrolleghem (2007). "Uncertainty in the environmental modelling process – A framework and guidance." In: *Environmental Modelling & Software* 22, pp. 1543–1556. DOI: 10.1016/j.envsoft.2007.02.004 (cit. on pp. 20, 21, 117).
- Reichert, P. (2006). "A standard interface between simulation programs and systems analysis software." In: *Water Science and Technology* 53.1, pp. 267–275. DOI: 10.2166/wst.2006.029 (cit. on p. 20).
- Renard, K. G., D. C. Yoder, D. T. Lightle, and S. M. Dabney (2011). "Universal Soil Loss Equation and Revised Universal Soil Loss Equation." In: *Handbook of Erosion Modelling*. Ed. by R. P. C. Morgan and M. A. Nearing. Wiley Online Library. Chap. 8, pp. 137–167 (cit. on p. 15).
- Renard, K. G. and J. R. Freimund (1994). "Using monthly precipitation data to estimate the R-factor in the revised USLE." In: *Journal of Hydrology* 157.1–4, pp. 287–306. DOI: 10.1016/0022-1694(94)90110-4 (cit. on pp. 45, 47, 63).
- Renard, K. G., G. R. Foster, G. Weesies, D. McCool, and D. Yoder (1997). *Predicting soil erosion by water: a guide to conservation planning with the Revised Universal Soil Loss Equation (RUSLE)*. Washington, DC: US Department of Agriculture, Agriculture Handbook No.703, pp. 404 (cit. on p. 15).
- Renard, K. G., G. R. Foster, G. A. Weesies, and J. P. Porter (1991). "RUSLE: Revised universal soil loss equation." In: *Journal of Soil and Water Conservation* 46.1, pp. 30–33 (cit. on p. 15).
- Renschler, C. S. (2003). "Designing geo-spatial interfaces to scale process models: the GeoWEPP approach." In: *Hydrological Processes* 17.5, pp. 1005–1017. DOI: 10.1002/hyp.1177 (cit. on p. 12).
- Reusser, D. (2015). *fast: Implementation of the Fourier Amplitude Sensitivity Test (FAST)*. R package version 0.64. URL: <https://CRAN.R-project.org/package=fast> (cit. on pp. 110, 123).
- Riahi, K., A. Grübler, and N. Nakicenovic (2007). "Scenarios of long-term socio-economic and environmental development under climate stabilization." In: *Technological Forecasting and Social Change* 74.7, pp. 887–935. DOI: 10.1016/j.techfore.2006.05.026 (cit. on p. 92).
- Richards, L. A. (1931). "CAPILLARY CONDUCTION OF LIQUIDS THROUGH POROUS MEDIA." In: *Physics* 1.5, pp. 318–333. DOI: 10.1063/1.1745010 (cit. on p. 13).
- Risse, L. M., M. A. Nearing, J. M. Laflen, and A. D. Nicks (1993). "Error Assessment in the Universal Soil Loss Equation." In: *Soil Science Society of America Journal* 57.3, p. 825. DOI: 10.2136/sssaj1993.03615995005700030032x (cit. on p. 39).
- Roderick, M. L., F. Sun, W. H. Lim, and G. D. Farquhar (2014). "A general framework for understanding the response of the water cycle to global warming over land and ocean." In: *Hydrology and Earth System Sciences* 18.5, pp. 1575–1589. DOI: 10.5194/hess-18-1575-2014 (cit. on p. 107).
- Roose, E. J. (1975). *Erosion et ruissellement en Afrique de l'Ouest : vingt années de mesures en petites parcelles expérimentales*. Tech. rep. Office de la scientifique et Technique Outre-Mer, Centre D'Adiopo-doumé, Côte d'Ivoire (cit. on pp. 15, 45, 47, 63).
- Rosolem, R., H. V. Gupta, W. J. Shuttleworth, X. Zeng, and L. G. G. De Gonçalves (2012). "A fully multiple-criteria implementation of the Sobol method for parameter sensitivity analysis." In: *Journal of Geophysical Research: Atmospheres* 117. DOI: 10.1029/2011JD016355 (cit. on p. 74).
- Ross, N. (2018). *fasterize: Fast Polygon to Raster Conversion*. R package version 1.0.0. URL: <https://CRAN.R-project.org/package=fasterize> (visited on 05/18/2019) (cit. on p. 125).
- Rouholahnejad, E., K. C. Abbaspour, R. Srinivasan, V. Bacu, and A. Lehmann (2014). "Water resources of the Black Sea Basin at high spatial and temporal resolution." In: *Water Resources Research* 50.7, pp. 5866–5885. DOI: 10.1002/2013WR014132 (cit. on p. 14).

- Rounsevell, M. D. and M. J. Metzger (2010). *Developing qualitative scenario storylines for environmental change assessment*. DOI: 10.1002/wcc.63 (cit. on pp. 89, 118).
- Ruzicka, K., O. Gabriel, U. Bletterie, S. Winkler, and M. Zessner (2009). "Cause and effect relationship between foam formation and treated wastewater effluents in a transboundary river." In: *Physics and Chemistry of the Earth. Advances in Sustainable Management of Water Quality on Catchment Scale* 34.8-9, pp. 565-573. DOI: 10.1016/j.pce.2009.01.002 (cit. on p. 78).
- Saltelli, A. (2002). "Making best use of model evaluations to compute sensitivity indices." In: *Computer physics communications* 145.2, pp. 280-297. DOI: 10.1016/S0010-4655(02)00280-1 (cit. on p. 27).
- Saltelli, A. (2009). "What is Sensitivity Analysis." In: *Sensitivity Analysis*. Ed. by A. Saltelli, K. Chan, and E. M. Scott. Chichester, West Sussex, UK: John Wiley & Sons, Ltd. Chap. 1, pp. 3-13. ISBN: 978-0-470-74382-9 (cit. on p. 21).
- Saltelli, A., K. Aleksankina, W. Becker, P. Fennell, F. Ferretti, N. Holst, S. Li, and Q. Wu (2019). "Why so many published sensitivity analyses are false: A systematic review of sensitivity analysis practices." In: *Environmental Modelling & Software* 114, pp. 29-39. DOI: 10.1016/j.envsoft.2019.01.012 (cit. on p. 4).
- Saltelli, A. and P. Annoni (2010). "How to avoid a perfunctory sensitivity analysis." In: *Environmental Modelling & Software* 25.12, pp. 1508-1517. DOI: 10.1016/j.envsoft.2010.04.012 (cit. on pp. 24, 74).
- Saltelli, A., P. Annoni, I. Azzini, F. Campolongo, M. Ratto, and S. Tarantola (2010). "Variance based sensitivity analysis of model output. Design and estimator for the total sensitivity index." In: *Computer Physics Communications* 181, pp. 259-270. DOI: 10.1016/j.cpc.2009.09.018 (cit. on pp. 26, 27).
- Saltelli, A., M. Ratto, T. Andres, F. Campolongo, J. Cariboni, D. Getelli, M. Saisana, and S. Tarantola (2008). *Global Sensitivity Analysis. The Primer*. Chichester, West Sussex, UK: John Wiley & Sons Ltd. 306 pp. ISBN: 0470059974 (cit. on pp. 19, 21-26, 74).
- Saltelli, A. and S. Tarantola (2002). "On the Relative Importance of Input Factors in Mathematical Models." In: *Journal of the American Statistical Association* 97.459, pp. 702-709. DOI: 10.1198/016214502388618447 (cit. on pp. 74, 92).
- Saltelli, A., S. Tarantola, F. Campolongo, and M. Ratto (2004). *Sensitivity analysis in practice: A guide to assessing scientific models*. 1st ed. Vol. 91. 10-11. Chichester, West Sussex, UK: John Wiley & Sons Ltd, p. 219. ISBN: 0-470-87093-1 (cit. on pp. 19, 22, 23).
- Saltelli, A., S. Tarantola, and K. P.-S. Chan (1999). "A quantitative model-independent method for global sensitivity analysis of model output." In: *Technometrics* 41.1, pp. 39-56. DOI: 10.1080/00401706.1999.10485594 (cit. on p. 27).
- Sarrazin, F., F. Pianosi, and T. Wagener (2016). "Global Sensitivity Analysis of environmental models: Convergence and validation." In: *Environmental Modelling & Software* 79, pp. 135-152. DOI: 10.1016/j.envsoft.2016.02.005 (cit. on pp. 22, 23, 26, 94).
- Savage, J. T. S., F. Pianosi, P. Bates, J. Freer, and T. Wagener (2016). "Quantifying the importance of spatial resolution and other factors through global sensitivity analysis of a flood inundation model." In: *Water Resources Research* 52.11, pp. 9146-9163. DOI: 10.1002/2015WR018198 (cit. on pp. 22, 74, 114).
- Savenije, H. H. G. (2009). "HESS Opinions "The art of hydrology"*." In: *Hydrology and Earth System Sciences* 13.2, pp. 157-161. DOI: 10.5194/hess-13-157-2009. URL: <https://www.hydrology-earth-syst-sci.net/13/157/2009/> (cit. on p. 3).
- Schönhart, M., H. Trautvetter, J. Parajka, A. P. Blaschke, G. Hepp, M. Kirchner, H. Mitter, E. Schmid, B. Strenn, and M. Zessner (2018). "Modelled impacts of policies and climate change on land use and water quality in Austria." In: *Land Use Policy* 76, pp. 500-514. DOI: 10.1016/j.landusepol.2018.02.031 (cit. on p. 73).
- Schulz, K. and M. Bernhardt (2016). "The end of trend estimation for extreme floods under climate change?" In: *Hydrological Processes* 30.11, pp. 1804-1808. DOI: 10.1002/hyp.10816 (cit. on p. 120).
- Schulz, K., K. J. Beven, and B. Huwe (1999). "Equifinality and the problem of robust calibration in nitrogen budget simulations." In: *Soil Science Society of America Journal* 63.6, pp. 1934-1941. DOI: 10.2136/sssaj1999.6361934x (cit. on pp. 26, 74).

- Schürz, C. (2017). *SWATfarmR: Simple rule based scheduling of management operations in SWAT2012*. R package version 0.2.2. URL: <https://github.com/chrisschuerz/SWATfarmR> (visited on 06/14/2017) (cit. on p. 79).
- Schürz, C. (2020a). *soilgridr: Working with Soilgrids data in R*. R package version 0.2.0. URL: <https://github.com/chrisschuerz/soilgridr> (visited on 02/10/2020) (cit. on p. 48).
- Schürz, C. (2020b). *SWATplusR: Running SWAT2012 and SWAT+ Projects in R*. R package version 0.2.8. DOI: 10.5281/zenodo.3373859. URL: <https://github.com/chrisschuerz/SWATplusR> (visited on 02/10/2020) (cit. on p. 125).
- Schürz, C., B. Hollosi, C. Matulla, A. Pressl, T. Ertl, K. Schulz, and B. Mehdi (2019). "A comprehensive sensitivity and uncertainty analysis for discharge and nitrate-nitrogen loads involving multiple discrete model inputs under future changing conditions." In: *Hydrology and Earth System Sciences* 23.3, pp. 1211–1244. DOI: 10.5194/hess-23-1211-2019 (cit. on p. 22).
- Schwarz, G. E., A. B. Hoos, R. B. Alexander, and R. A. Smith (2006). *The SPARROW Surface Water-Quality Model: Theory, Application and User Documentation*. Tech. rep. U.S. Geological Survey techniques and methods report, Vol. 6/10, p. 248 (cit. on p. 13).
- Shangguan, W., Y. Dai, Q. Duan, B. Liu, and H. Yuan (2014). "A global soil data set for earth system modeling." In: *Journal of Advances in Modeling Earth Systems* 6, pp. 249–263. DOI: 10.1002/2013MS000293 (cit. on p. 47).
- Shaw, S. B. and S. J. Riha (2011). "Assessing temperature-based PET equations under a changing climate in temperate, deciduous forests." In: *Hydrological Processes* 25.9, pp. 1466–1478. DOI: 10.1002/hyp.7913 (cit. on p. 107).
- Sheffield, J., E. F. Wood, and M. L. Roderick (2012). "Little change in global drought over the past 60 years." In: *Nature* 491.7424, pp. 435–438. DOI: 10.1038/nature11575 (cit. on p. 106).
- Sheikholeslami, R., S. Razavi, H. V. Gupta, W. Becker, and A. Haghnegahdar (2019). "Global sensitivity analysis for high-dimensional problems: How to objectively group factors and measure robustness and convergence while reducing computational cost." In: *Environmental Modelling & Software* 111, pp. 282–299. DOI: doi.org/10.1016/j.envsoft.2018.09.002 (cit. on pp. 26, 83).
- Shen, C., E. Laloy, A. Elshorbagy, A. Albert, J. Bales, F.-J. Chang, S. Ganguly, K.-L. Hsu, D. Kifer, Z. Fang, K. Fang, D. Li, X. Li, and W.-P. Tsai (2018). "HESS Opinions: Incubating deep-learning-powered hydrologic science advances as a community." In: *Hydrology and Earth System Sciences* 22.11, pp. 5639–5656. DOI: 10.5194/hess-22-5639-2018 (cit. on p. 1).
- Shen, C. (2018). "A Transdisciplinary Review of Deep Learning Research and Its Relevance for Water Resources Scientists." In: *Water Resources Research* 54.11, pp. 8558–8593. DOI: 10.1029/2018WR022643 (cit. on p. 1).
- Singh, R., T. Wagener, R. Crane, M. E. Mann, and L. Ning (2014). "A vulnerability driven approach to identify adverse climate and land use change combinations for critical hydrologic indicator thresholds: Application to a watershed in Pennsylvania, USA." In: *Water Resources Research* 50.4, pp. 3409–3427. DOI: 10.1002/2013WR014988 (cit. on p. 25).
- Singh, V. P. and D. A. Woolhiser (2002). "Mathematical Modeling of Watershed Hydrology." In: *Journal of Hydrologic Engineering* 7.4, pp. 270–292. DOI: 10.1061/(asce)1084-0699(2002)7:4(270) (cit. on pp. 11, 12, 14).
- Sivapalan, M., H. H. G. Savenije, and G. Blöschl (2012). "Socio-hydrology: A new science of people and water." In: *Hydrological Processes* 26.8, pp. 1270–1276. DOI: 10.1002/hyp.8426 (cit. on p. 113).
- Smith, D. D. (1941). "Interpretation of soil conservation data for field use." In: *Agricultural Engineering* 22, pp. 173–175 (cit. on p. 14).
- Smith, R. A., G. E. Schwarz, and R. B. Alexander (1997). "Regional interpretation of water-quality monitoring data." In: *Water Resources Research* 33.12, pp. 2781–2798. DOI: 10.1029/97WR02171 (cit. on p. 12).
- Smith, S. J. and T. M. Wigley (2006). "Multi-gas forcing stabilization with minicam." In: *Energy Journal* 27.SPEC. ISS. NOV. Pp. 373–391. DOI: 10.5547/ISSN0195-6574-EJ-VolSI2006-NoSI3-19 (cit. on p. 92).
- Sobol, I. M. (1993). "Sensitivity analysis for nonlinear mathematical models." In: *Mathematical Modelling and Computational Experiments* 4.1, pp. 407–414. DOI: 10.18287/0134-2452-2015-39-4-459-461. (cit. on pp. 19, 26, 74, 83, 114, 124).

- Spaeth, K. E., F. B. Pierson, M. A. Weltz, and W. H. Blackburn (2003). "Evaluation of USLE and RUSLE Estimated Soil Loss on Rangeland." In: *Journal of Range Management* 56.3, pp. 234–246. DOI: 10.2307/4003812 (cit. on p. 15).
- Spear, R. C. and G. M. Hornberger (1980). "Eutrophication in peel inlet—II. Identification of critical uncertainties via generalized sensitivity analysis." In: *Water Research* 14.1, pp. 43–49. DOI: 10.1016/0043-1354(80)90040-8 (cit. on pp. 25, 26).
- Srinivasan, V., M. Sanderson, M. Garcia, M. Konar, G. Blöschl, and M. Sivapalan (2017). "Prediction in a socio-hydrological world." In: *Hydrological Sciences Journal* 62.3, pp. 338–345. DOI: 10.1080/02626667.2016.1253844 (cit. on p. 113).
- Statistik Austria (2015a). *ÖROK-Regionalprognosen 2014 - Bevölkerung, Ausführliche Tabellen zur kleinräumigen ÖROK-Prognose 2014*. URL: <http://www.oerok.gv.at/> (visited on 11/15/2016) (cit. on pp. 89–91).
- Statistik Austria (2015b). *STATCube - Statistical Data base of the Statistik Austria: Agricultural census - Land use (not openly accessible)*. URL: <http://statcube.at/statistik.at/ext/statcube> (visited on 06/03/2015) (cit. on pp. 77–79, 81).
- Statistik Austria (2016). *Datenbank zur Bevölkerungsprognose 2016 - Hauptszenario*. URL: <https://www.statistik.at/> (visited on 10/14/2016) (cit. on pp. 89–91).
- Statistik Austria (2017). *STATCube - Statistical Data base of the Statistik Austria: Agricultural and forestry holdings with arable land and their cultivated land area (not openly accessible)*. URL: [data.%20http://statcube.at/statistik.at/ext/statcube](data:%20http://statcube.at/statistik.at/ext/statcube) (visited on 05/22/2017) (cit. on p. 90).
- Stevens, S. S. (1946). "On the Theory of Scales of Measurement." In: *Science* 103.2684, pp. 677–680. DOI: 10.1126/science.103.2684.677 (cit. on p. 28).
- Strauch, M., R. Schwappe, and C. Schürz (2016). *TopHRU: Threshold optimization for HRUs in SWAT*. DOI: 10.5281/zenodo.154379. URL: <https://github.com/michstrauch/TopHRU/tree/v1.2> (cit. on p. 82).
- Sutherland, R. A. and K. B. Bryan (1990). "Runoff and erosion from a small semiarid catchment, Baringo district, Kenya." In: *Applied Geography* 10.2, pp. 91–109. ISSN: 0143-6228. DOI: 10.1016/0143-6228(90)90046-R (cit. on pp. 57, 67, 69, 70).
- Tamene, L. and Q. B. Le (2015). "Estimating soil erosion in sub-Saharan Africa based on landscape similarity mapping and using the revised universal soil loss equation (RUSLE)." In: *Nutrient Cycling in Agroecosystems* 102.1, pp. 17–31. DOI: 10.1007/s10705-015-9674-9 (cit. on pp. 48, 49, 51).
- Tarantola, S. and T. A. Mara (2017). "Variance-based sensitivity indices of computer models with dependent inputs: The Fourier Amplitude Sensitivity Test." In: *International Journal for Uncertainty Quantification* 7.6. DOI: 10.1615/Int.J.UncertaintyQuantification.2017020291 (cit. on p. 109).
- Teshager, A. D., P. W. Gassman, J. T. Schoof, and S. Secchi (2016). "Assessment of impacts of agricultural and climate change scenarios on watershed water quantity and quality, and crop production." In: *Hydrology and Earth System Sciences* 20.8, pp. 3325–3342. DOI: 10.5194/hess-20-3325-2016 (cit. on pp. 106, 113).
- Teutschbein, C. and J. Seibert (2013). "Is bias correction of regional climate model (RCM) simulations possible for non-stationary conditions." In: *Hydrology and Earth System Sciences* 17.12, pp. 5061–5077. DOI: 10.5194/hess-17-5061-2013 (cit. on pp. 73, 92).
- Teutschbein, C. and J. Seibert (2012). "Bias correction of regional climate model simulations for hydrological climate-change impact studies: Review and evaluation of different methods." In: *Journal of Hydrology* 456-457, pp. 12–29. DOI: 10.1016/j.jhydro.2012.05.052 (cit. on p. 73).
- Tiwari, A. K., L. M. Risse, and M. A. Nearing (2000). "Evaluation of WEPP and its comparison with USLE and RUSLE." In: *Transactions of the ASAE* 43.5, pp. 1129–1135. DOI: 10.13031/2013.3005 (cit. on p. 39).
- Torri, D., J. W. A. Poesen, and L. Borselli (1997). "Predictability and uncertainty of the soil erodibility factor using a global dataset." In: *CATENA* 31, pp. 1–22. DOI: [https://doi.org/10.1016/S0341-8162\(97\)00036-2](https://doi.org/10.1016/S0341-8162(97)00036-2) (cit. on pp. 48, 49, 63).
- Tóth, B., M. Weynants, A. Nemes, A. Makó, G. Bilas, and G. Tóth (2015). "New generation of hydraulic pedotransfer functions for Europe." In: *European Journal of Soil Science* 66.1, pp. 226–238. DOI: 10.1111/ejss.12192 (cit. on pp. 80, 81).

- Tripathi, M. P., N. S. Raghuwanshi, and G. P. Rao (2006). "Effect of watershed subdivision on simulation of water balance components." In: *Hydrological Processes* 20.5, pp. 1137–1156. DOI: 10.1002/hyp.5927 (cit. on p. 81).
- Tuo, Y., G. Chiogna, and M. Disse (2015). "A Multi-Criteria Model Selection Protocol for Practical Applications to Nutrient Transport at the Catchment Scale." In: *Water* 7, pp. 2851–2880. ISSN: 2073-4441. DOI: 10.3390/w7062851 (cit. on pp. 11, 13).
- UBOS (2010). "Volume IV: Crop Area and Production Report." In: *Uganda Census of Agriculture 2008/2009*. Kampala, Uganda: Uganda Bureau of Statistics, p. 178 (cit. on p. 51).
- Van der Knijff, J., R. Jones, and L. Montanarella (2000). *Soil Erosion Risk Assessment in Europe, EUR 19044 EN*. Tech. rep. European Soil Bureau, European Commission, 34 pp. (Cit. on pp. 39–41, 51).
- Van-Camp, L., B. Bujarrabal, A. R. Gentile, R. J. Jones, L. Montanarella, C. Olazabal, and S.-K. Selvaradjou (2004). *Reports of the Technical Working Groups Established under the Thematic Strategy for Soil Protection. EUR 21319 EN/6, 872 pp*. Tech. rep. Office for Official Publications of the European Communities, Luxembourg (cit. on p. 54).
- Venohr, M., U. Hirt, J. Hofmann, D. Opitz, A. Gericke, A. Wetzig, S. Natho, F. Neumann, J. Hürdler, M. Matranga, J. Mahnkopf, M. Gadegast, and H. Behrendt (2011). "Modelling of Nutrient Emissions in River Systems – MONERIS – Methods and Background." In: *International Review of Hydrobiology* 96.5, pp. 435–483. DOI: 10.1002/iroh.201111331 (cit. on pp. 12, 13).
- Vogel, R. M. and N. M. Fennessey (1994). "Flow Duration Curves. I: New Interpretation and Confidence Intervals." In: *Journal of Water Resources Planning and Management* 120.4, pp. 485–504. DOI: 10.1061/(ASCE)0733-9496(1994)120:4(485) (cit. on p. 139).
- Vrieling, A., J. C. B. Hoedjes, and M. van der Velde (2014). "Towards large-scale monitoring of soil erosion in Africa: Accounting for the dynamics of rainfall erosivity." In: *Global and Planetary Change* 115, pp. 33–43. DOI: 10.1016/j.gloplacha.2014.01.009 (cit. on pp. 45, 47, 63).
- Vrieling, A., G. Sterk, and S. M. de Jong (2010). "Satellite-based estimation of rainfall erosivity for Africa." In: *Journal of Hydrology* 395, pp. 235–241. ISSN: 0022-1694. DOI: 10.1016/j.jhydrol.2010.10.035 (cit. on pp. 40, 41).
- Vrugt, J. A., C. J. F. ter Braak, M. P. Clark, J. M. Hyman, and B. A. Robinson (2008). "Treatment of input uncertainty in hydrologic modeling: Doing hydrology backward with Markov chain Monte Carlo simulation." In: *Water Resources Research* 44.12, W00B09. DOI: 10.1029/2007WR006720 (cit. on pp. xv, 19).
- Vrugt, J. A., C. Ter Braak, C. Diks, B. A. Robinson, J. M. Hyman, and D. Higdon (2009). "Accelerating Markov chain Monte Carlo simulation by differential evolution with self-adaptive randomized subspace sampling." In: *International Journal of Nonlinear Sciences and Numerical Simulation* 10.3, pp. 273–290. DOI: 10.1515/IJNSNS.2009.10.3.273 (cit. on p. 19).
- Vuuren, D. P. van, J. Edmonds, M. Kainuma, K. Riahi, A. Thomson, K. Hibbard, G. C. Hurtt, T. Kram, V. Krey, J. F. Lamarque, T. Masui, M. Meinshausen, N. Nakicenovic, S. J. Smith, and S. K. Rose (2011). "The representative concentration pathways: An overview." In: *Climatic Change* 109.1, pp. 5–31. DOI: 10.1007/s10584-011-0148-z (cit. on p. 73).
- Vuuren, D. P. van, M. T. Kok, B. Girod, P. L. Lucas, and B. de Vries (2012). "Scenarios in Global Environmental Assessments: Key characteristics and lessons for future use." In: *Global Environmental Change* 22.4, pp. 884–895. DOI: 10.1016/j.gloenvcha.2012.06.001 (cit. on p. 108).
- Wagner, P. D., S. M. Bhallamudi, B. Narasimhan, S. Kumar, N. Fohrer, and P. Fiener (2017). "Comparing the effects of dynamic versus static representations of land use change in hydrologic impact assessments." In: *Environmental Modelling and Software*, pp. 1–9. DOI: 10.1016/j.envsoft.2017.06.023 (cit. on pp. 106, 113).
- Warren, S. D., H. Mitsova, M. G. Hohmann, S. Landsberger, F. Y. Iskander, T. S. Ruzycski, and G. M. Senseman (2005). "Validation of a 3-D enhancement of the Universal Soil Loss Equation for prediction of soil erosion and sediment deposition." In: *CATENA* 64, pp. 281–296. DOI: 10.1016/j.catena.2005.08.010 (cit. on p. 70).
- Welles, J. (1984). "The survival advantage of stupidity." In: *Speculations in Science and Technology* 17.1, pp. 17–21 (cit. on p. 37).

- Weltz, M. A., M. R. Kidwell, and H. D. Fox (1998). "Influence of abiotic and biotic factors in measuring and modeling soil erosion on rangelands: state of knowledge." In: *Rangeland Ecology & Management/Journal of Range Management Archives* 51.5, pp. 482–495 (cit. on p. 15).
- Wickham, H. (2019). *forcats: Tools for Working with Categorical Variables (Factors)*. R package version 0.4.0. URL: <https://CRAN.R-project.org/package=forcats> (visited on 02/17/2019) (cit. on p. 125).
- Wickham, H., W. Chang, L. Henry, T. L. Pedersen, K. Takahashi, C. Wilke, K. Woo, and H. Yutani (2019a). *ggplot2: Create Elegant Data Visualisations Using the Grammar of Graphics*. R package version 3.1.1. URL: <http://ggplot2.tidyverse.org> (visited on 04/11/2019) (cit. on p. 125).
- Wickham, H., R. François, L. Henry, and K. Müller (2019b). *dplyr: A Grammar of Data Manipulation*. R package version 0.8.1. URL: <https://CRAN.R-project.org/package=dplyr> (visited on 05/17/2019) (cit. on p. 125).
- Wickham, H. and L. Henry (2019). *tidyr: Easily Tidy Data with 'spread()' and 'gather()' Functions*. R package version 0.8.3. URL: <https://CRAN.R-project.org/package=tidyr> (visited on 03/02/2019) (cit. on p. 125).
- Wickham, H. and E. Ruiz (2019). *dbplyr: A 'dplyr' Back End for Databases*. R package version 1.4.0. URL: <https://CRAN.R-project.org/package=dbplyr> (visited on 04/24/2019) (cit. on p. 125).
- Wilby, R. L., T. M. L. Wigley, D. Conway, P. D. Jones, B. C. Hewitson, J. Main, and D. S. Wilks (1998). "Statistical downscaling of general circulation model output: A comparison of methods." In: *Water Resour. Res.* 34.11, pp. 2995–3008. DOI: 10.1029/98wr02577 (cit. on p. 73).
- Wilby, R. L. (2010). "Evaluating climate model outputs for hydrological applications." In: *Hydrological Sciences Journal* 55.7, pp. 1090–1093. DOI: 10.1080/02626667.2010.513212 (cit. on pp. 113, 116, 117).
- Wilby, R. L. (2005). "Uncertainty in water resource model parameters used for climate change impact assessment." In: *Hydrological Processes* 19.16, pp. 3201–3219. DOI: 10.1002/hyp.5819 (cit. on p. 107).
- Williams, J. R. (1995). "The EPIC model - Soil Erosion." In: *Computer Models of Watershed Hydrology*. Ed. by V. P. Singh. Highlands Ranch, CO, USA: Water Resources Publications, pp. 909–1000. ISBN: 0918334918, 9780918334916 (cit. on pp. 15, 16, 48, 49, 63).
- Williams, J. R., J. G. Arnold, J. R. Kiniry, P. W. Gassman, and C. H. Green (2008). "History of model development at Temple, Texas." In: *Hydrological Sciences Journal* 53.5, pp. 948–960. DOI: 10.1623/hysj.53.5.948 (cit. on p. 16).
- Williams, J. R., A. D. Nicks, and J. G. Arnold (1985). "Simulator for Water Resources in Rural Basins." In: *Journal of Hydraulic Engineering* 111.6, pp. 970–986. DOI: 10.1061/(asce)0733-9429(1985)111:6(970) (cit. on p. 16).
- Williams, J. R., K. G. Renard, and P. T. Dyke (1983). "EPIC: A new method for assessing erosion's effect on soil productivity." In: *Journal of Soil and Water Conservation* 38.5, pp. 381–383 (cit. on p. 16).
- Williams, J. R. and R. C. Izaurralde (2006). "The APEX Model." In: *Watershed Models*. Ed. by V. P. Singh and D. K. Frevert. Taylor & Francis Group. Chap. 18, pp. 437–481. ISBN: 978-1-4200-3743-2 (cit. on p. 12).
- Willmott, C. J., S. M. Robeson, and K. Matsuura (2012). "A refined index of model performance." In: *International Journal of Climatology* 32.13, pp. 2088–2094. DOI: 10.1002/joc.2419 (cit. on pp. xv, 83, 138, 139).
- Winchell, M., R. Srinivasan, M. Di Luzio, and J. G. Arnold (2015). *ArcSWAT 2012.10.19 Interface for SWAT2012*. Temple, Texas. URL: <http://swat.tamu.edu/software/arcswat/> (cit. on pp. 16, 81).
- Wischmeier, W. H. and D. D. Smith (1965). *Predicting rainfall-erosion losses from cropland east of the Rocky Mountains*. Washington, DC: US Department of Agriculture, Agricultural Handbook No. 282, pp. 58 (cit. on pp. 14, 15, 41).
- Wischmeier, W. H. and D. D. Smith (1978). *Predicting rainfall erosion losses - a guide to conservation planning*. Hyattsville, Maryland: US Department of Agriculture, Agricultural Handbook No. 537, pp. 58 (cit. on pp. xvii, 2, 12, 14, 15, 45, 48, 49, 51, 63).
- Wise, M., K. Calvin, A. Thomson, L. Clarke, B. Bond-Lamberty, R. Sands, S. J. Smith, A. Janetos, and J. Edmonds (2009). "Implications of Limiting CO₂ Concentrations for Land Use and Energy." In: *Science* 324.5931, pp. 1183–1186. DOI: 10.1126/science.1168475 (cit. on p. 92).

- Wood, A. W., L. R. Leung, V. Sridhar, and D. P. Lettenmaier (2004). "Hydrologic implications of dynamical and statistical approaches to downscaling climate model outputs." In: *Climatic Change* 62.1-3, pp. 189–216. DOI: 10.1023/B:CLIM.0000013685.99609.9e (cit. on p. 73).
- Yang, D., S. Kanae, T. Oki, T. Koike, and K. Musiak (2003). "Global potential soil erosion with reference to land use and climate changes." In: *Hydrological Processes* 17.14, pp. 2913–2928. DOI: 10.1002/hyp.1441 (cit. on pp. 14, 40, 44, 45, 47, 48, 51, 71).
- Yang, J., P. Reichert, K. C. Abbaspour, and H. Yang (2007). "Hydrological modelling of the Chaohe Basin in China: Statistical model formulation and Bayesian inference." In: *Journal of Hydrology* 340.3, pp. 167–182. DOI: 10.1016/j.jhydro.2007.04.006 (cit. on p. 20).
- Yates, D. N., K. A. Miller, R. L. Wilby, and L. Kaatz (2015). "Decision-centric adaptation appraisal for water management across Colorado's Continental Divide." In: *Climate Risk Management* 10, pp. 35–50. DOI: 10.1016/j.crm.2015.06.001 (cit. on p. 73).
- Yilmaz, K. K., H. V. Gupta, and T. Wagener (2008). "A process-based diagnostic approach to model evaluation: Application to the NWS distributed hydrologic model." In: *Water Resources Research* 44.9, W09417. DOI: 10.1029/2007WR006716 (cit. on p. 139).
- Young, P. C. (2001). "Data-based Mechanistic Modelling and Validation of Rainfall-Flow Processes." In: *Model Validation: Perspectives in Hydrological Science*. Ed. by M. G. Anderson and P. Bates. John Wiley, Chichester, pp. 117–161 (cit. on p. 40).
- Young, R. A., C. A. Onstad, D. D. Bosch, and W. P. Anderson (1989). "AGNPS: A nonpoint-source pollution model for evaluating agricultural watersheds." In: *Journal of Soil and Water Conservation* 44.2, pp. 168–173 (cit. on p. 12).
- Yu, B. and C. Rosewell (1996). "A robust estimators of the R-factor for the Universal Soil Loss Equation." In: *American Society of Agricultural Engineers* 39.2, pp. 559–561. DOI: <https://doi.org/10.13031/2013.27535> (cit. on p. 47).
- Yuan, Y., Y. Khare, X. Wang, P. B. Parajuli, I. Kisekka, and S. Finsterle (2015). "Hydrologic and Water Quality Models: Sensitivity." In: *Transactions of the ASABE* 58.6, pp. 1721–1744. DOI: 10.13031/trans.58.10611 (cit. on p. 24).
- Zachar, D. (1982). *Soil Erosion (Developments in Soil Science 10)*. Elsevier Scientific Publishing Company, Amsterdam (cit. on pp. 54, 69).
- Zadeh, F. K., J. Nossent, F. Sarrazin, F. Pianosi, A. van Griensven, T. Wagener, and W. Bauwens (2017). "Comparison of variance-based and moment-independent global sensitivity analysis approaches by application to the SWAT model." In: *Environmental Modelling and Software* 91, pp. 210–222. DOI: 10.1016/j.envsoft.2017.02.001 (cit. on p. 30).
- Zadeh, L. A. (2005). "Toward a generalized theory of uncertainty (GTU)—an outline." In: *Information Sciences* 172.1, pp. 1–40. DOI: 10.1016/j.ins.2005.01.017 (cit. on p. 19).
- Zalewski, M., G. Janauer, and G. Jolankai (1997). *Ecohydrology. A new paradigm for the sustainable use of aquatic resources. International Hydrological Programme*. Tech. rep. SC-97/WS/12. UNESCO, Paris (cit. on p. 11).
- Zalewski, M. (2013). "Ecohydrology: process-oriented thinking towards sustainable river basins." In: *Ecohydrology & Hydrobiology* 13.2, pp. 97–103. DOI: 10.1016/j.ecohyd.2013.06.001 (cit. on pp. 1, 11).
- Zingg, A. W. (1940). "Degree and length of land slope as it affects soil loss in run-off." In: *Agricultural Engineering* 21, pp. 59–64 (cit. on p. 14).
- Zorita, E. and H. Von Storch (1999). "The analog method as a simple statistical downscaling technique: Comparison with more complicated methods." In: *Journal of Climate* 12.8 PART 2, pp. 2474–2489. DOI: 10.1175/1520-0442(1999)012<2474:TAMAAS>2.0.CO;2 (cit. on p. 92).

DECLARATION

This work consists of two major parts, a frame that sets the theoretical foundation of this thesis and outlines the contribution to the body of scientific literature focusing on uncertainty and sensitivity with discrete model inputs and a case study section that employs the theoretical framework in eco-hydrological model applications.

I hereby declare that I am the sole author of the thesis frame including the introduction in Section 1, the outline of the general framework in Part I, and the synthesis of this thesis in Part III. No assistance other than that which is permitted has been used to compile the theoretical framework of this thesis. Ideas and quotes taken directly or indirectly from other sources are identified as such.

Part II presents edited versions of two scientific articles that were submitted to the peer reviewed journal Hydrology and Earth System Sciences (HESS). My personal scientific contribution and the contributions of all co-authors can be summarized as follows:

Article 1 presented in Chapter 4:

Schürz, C., B. Mehdi, J. Kiesel, K. Schulz, and M. Herrnegger (*in review*, 2019) *A systematic assessment of uncertainties in large scale soil loss estimation from different representations of USLE input factors - A case study for Kenya and Uganda*, In: Hydrol. Earth Syst. Sci. Discuss., doi: 10.5194/hess-2019-602

I developed the conceptual idea of the study. Together with Mathew Herrnegger I designed the study and acquired and processed the input data . All simulations and analyses that were presented in the study were performed by myself. Mathew Herrnegger and I prepared all the figures that are presented in this study. Karsten Schulz and Jens Kiesel provided input to the theoretical framework to increase the scientific quality of this study. Large parts of the manuscript were compiled by myself with contributions of all other co-authors Bano Mehdi, Jens Kiesel, Karsten Schulz, and Mathew Herrnegger.

Article 2 presented in Chapter 5:

Schürz, C., B. Hollosi, C. Matulla, A. Pressl, T. Ertl, K. Schulz, and B. Mehdi (2019) *A comprehensive sensitivity and uncertainty analysis for discharge and nitrate-nitrogen loads involving multiple discrete model inputs under future changing conditions*, In: *Hydrol. Earth Syst. Sci.*, 23, 1211–1244, doi: 10.5194/hess-23-1211-2019 Part II covers two case studies

The general conceptual idea for this study stems from a project proposal developed by Karsten Schulz with contributions of Bano Mehdi and Christoph Matulla. I developed the methodological framework that was employed in this study and designed and performed all analyses illustrated. Bano Mehdi and Christoph Schürz acquired all SWAT model input data, set up the models, and developed the land use change scenarios, Brigitta Hollosi and Christoph Matulla developed the future climate change scenarios, and Alexander Pressl and Thomas Ertl calculated present wastewater emissions and developed the future municipal and industrial emission scenarios that were assembled to the presented comprehensive uncertainty framework by myself.

Vienna, April 2020

A handwritten signature in black ink, reading 'Christoph Schürz'. The signature is written in a cursive style with a horizontal line underneath it.

Christoph Schürz

Final Version as of April 20, 2020.

